AD_____

Award Number: DAMD17-97-1-7174

TITLE: Novel and Selective Inactivators for Matrix Metalloproteases Involved in Breast Cancer Metastasis

PRINCIPAL INVESTIGATOR: Shahriar Mobashery, Ph.D.

CONTRACTING ORGANIZATION: Wayne State University
Detroit, Michigan 48202

REPORT DATE: **July 2001**

TYPE OF REPORT: Final

PREPARED FOR: U.S. Army Medical Research and Materiel Command
Fort Detrick, Maryland 21702-5012

REPORT DOCUMENTATION PAGE

Form Approved
OMB No. 074-0188

1. AGENCY USE ONLY (Leave blank)	2. REPORT DATE	3. REPORT TYPE AND DATES COVERED
	July 2001	Final (13 Jun 97 - 13 Jun 01)

4. TITLE AND SUBTITLE
Novel and Selective Inactivators for Matrix Metalloproteases Involved in Breast Cancer Metastasis

5. FUNDING NUMBERS
DAMD17-97-1-7174

6. AUTHOR(S)
Shahriar Mobashery, Ph.D.

7. PERFORMING ORGANIZATION NAME(S) AND ADDRESS(ES)
Wayne State University
Detroit, Michigan 48202

E-MAIL:
som@ chem.wayne.edu

8. PERFORMING ORGANIZATION REPORT NUMBER

9. SPONSORING / MONITORING AGENCY NAME(S) AND ADDRESS(ES)
U.S. Army Medical Research and Materiel Command
Fort Detrick, Maryland 21702-5012

10. SPONSORING / MONITORING AGENCY REPORT NUMBER

11. SUPPLEMENTARY NOTES
This report contains colored photos

12a. DISTRIBUTION / AVAILABILITY STATEMENT
Approved for public release; distribution unlimited

12b. DISTRIBUTION CODE

13. ABSTRACT *(Maximum 200 Words)*
The research was a multidisciplinary and multifaceted endeavor on matix metalloproteases (MMPs) as target for intervention of cancer. The specific targets were gelatinases, MMP-2 and MMP-9, two members of the MMP family We generated three-dimensional computational models for gelatinases (and other MMPs) that have been made available to the scientific community. The structural knowledge and sequence information were used collectively to address the issue of evolution of MMPs and their diversification of function. Furthermore, we investigated the issues of inhibition (binding) of MMPs by tissue protein inhibitors, the TIMPs, in an extensive investigation with homogeneous preparations of the proteins. This knowledge was used in *de novo* design of synthetic inhibitors for gelatinases that are highly specific for these enzymes over the other related MMPs. One synthetic inhibitor proved to be highly potent and selective inhibitor for gelatinases. This is the first mechanism-based inhibitor for targeting of MMPs, and it shows a number of features (discussed herein) that sets it apart from the known MMP inhibitors.

14. SUBJECT TERMS	15. NUMBER OF PAGES
Breast Cancer, Idea Award	90
	16. PRICE CODE

17. SECURITY CLASSIFICATION OF REPORT	18. SECURITY CLASSIFICATION OF THIS PAGE	19. SECURITY CLASSIFICATION OF ABSTRACT	20. LIMITATION OF ABSTRACT
Unclassified	Unclassified	Unclassified	Unlimited

NSN 7540-01-280-5500

Standard Form 298 (Rev. 2-89)
Prescribed by ANSI Std. Z39-18
298-102

Table of Contents

Introduction

Tumor metastasis is the major cause of treatment failure in breast cancer patients. Numerous studies have shown that metastasis depends on the ability of the tumor cells to invade basement membranes and connective tissue matrices in a process involving a specialized group of enzymes capable of degrading extracellular matrix components.[1,2] Matrix metalloproteases (MMPs) belong to a large family of zinc-dependent proteinases capable of degrading extracellular matrix[1,2] and are known to be involved in many physiological and pathological processes. To date, the MMP family of enzymes comprises 26 known enzymes of human source. It is predicted that there may be as many as 100 such enzymes in humans, for which the genomic sequence may provide additional details. These enzymes are produced in inactive proenzyme ("latent") forms, which are activated in a set of complex proteolytic activation process, which is being understood only recently. The activation process is a critical event in regulation of MMP activity and is essential for extracellular matrix degradation during tumor cell invasion. The MMPs have two zinc and two calcium ions in their structures. One zinc ion is located in the active site and is required for enzymic activity. These enzymes are often multidomain proteins, which have in common a catalytic domain, which is highly homologous among all MMPs. Within the catalytic domain, a zinc-binding motif, a β-sheet core and peripheral helices are conserved structural elements. Of particular importance in tumor cell invasion and angiogenesis are MMP-2 and MMP-9 (gelatinases A and B, respectively) due to their ability to cleave basement membrane type IV collagen. Indeed, expression of MMP-2 and MMP-9 is elevated in many human tumors,[3,4] including breast cancer tumors.[5-9] Hence, inhibition of these enzymes is highly sought as the means for adjuvant chemotherapy of breast cancer. Studies with the natural tissue inhibitors of metalloproteases (TIMPs) and reversible synthetic MMP inhibitors have shown promising results in prevention of tumor growth, invasion and angiogenesis. However, the therapeutic use of the TIMP proteins is limited. While there are existing reversible inhibitors for MMPs with high affinities for the active sites of these enzymes, in a few cases that inhibition of different MMPs has been studied with a given inhibitor, often selectivity is lacking.[10-12] Inhibition of many (or all) MMPs would be undesirable because of the myriad of important functions that these enzymes play in the normal physiology of the cell; such inhibitors that lack selectivity may prove to be toxic because of this reason. We proposed to prepare novel and selective mechanism-based inactivators for gelatinases A and B in a rational drug design program as potential anti-breast-cancer agents.

Body

I. Computer-Generated Models for Gelatinases A and B and Evolution of Function. When we embarked on this research, a handful of crystal structures, and one NMR structure, for the catalytic domains of two collagenases and one stromelysin had been made available through the Brookhaven Protein Data Bank. The availability of these structural coordinates presented us with an opportunity to study them, and use them in our computer-aided design of inhibitor. Based on sequence similarities, the structures of the catalytic domains of all MMPs were believed to be highly similar, though not identical. Because of the documented central importance of gelatinases to breast cancer, we were interested in the structures for gelatinases, which were not available. We used the program COMPOSER to predict the gelatinase structures for their catalytic domains. The program utilizes the existing structural information (crystal or NMR) in predicting the folding patterns of the related proteins of unknown structures. The structures of the catalytic domains of gelatinases A and B were generated and they were submitted to dynamics simulations, and subsequently, energy-minimization protocols to produce three-dimensional folds for these proteins (see the manuscript in Appendices for details).[13] We were struck by the similarity of the structures of collagenases, stromelysin, and gelatinases.[13] This is a factor that would make *selective inhibition* of the individual MMPs a challenging task by conventional inhibitor design strategies, as will be discussed below. We also predicted the full

structure for gelatinases in a subsequent effort (data unpublished). The X-ray structure for the full-length gelatinase A (MMP-2) was published late in 1999. When the coordinates became available several months ago, the similarity of that structure to the computational model that we predicted was striking. The two structures were superimposible, and the differences were only present in the location of two to three loops, which are believed to be mobile surface elements. So, the computational model that we generated and used in the design of the inhibitors was a good one, a fact that enabled us to design and prepare highly specific inhibitors for gelatinases. These models serve as the centerpieces of the design work. We hasten to add that we have made available to the scientific community these models and others at our group Web site (http://sun2.science.wayne.edu/~somgroup/). Our Web site has had just under 2700 visitors since late in October of 1998, when we started recording the number of visitors. These visitors often connect to our Web site to download the coordinates for our models.

In an aspect of our modeling of these enzymes, we have looked at the diversity of the sequences, and by consequence diversity of functions of MMPs. In the most extensive study of its kind, we reported on both sequence analysis and modeling effort to understand function of the structures of over 60 MMPs (see the manuscript in Appendices for details).[14] These studies indicated that the accepted dogma for MMPs, that the multiple domains of these proteins assembled to give diversity of function was not valid. The results indicated that assembly of the domains was indeed a very early event in evolution of these enzymes, and diversification of function took place after such initial assembly.[14] Furthermore, we have discovered four distinct motifs for metal binding in MMPs (see the manuscript in Appendices for details).[15] It is interesting that the three-dimensional structures are strictly conserved, despite the diversity in motifs.[15] These indicate that after assembly of domains, nature went in many different evolutionary tangents to realize distinct functions for the various MMPs. These findings bolster our view that the original proposal by us, that selective inhibition of these enzymes is possible, was indeed valid.

II. Kinetic Analysis for the Binding of the Latent and Active Forms of the Human Matrix metalloprotease-2 and -9 to TIMP-1 and TIMP-2. The availability of homogeneous preparations of MMP2 and MMP-9 (both latent and active forms) and those for TIMP-1 and TIMP-2 to us presented the opportunity for a systematic evaluation of the interactions of these proteins (see the manuscript in Appendices for details).[16] The dissociation constants (K_d) of TIMP-1 and TIMP-2 for the active and latent forms of MMP-2 and MMP-9 were evaluated using surface plasmon resonance (SPR) and enzyme inhibition studies. SPR analysis shows biphasic kinetics with high- (nM) and low- (μM) affinity binding sites of TIMP-2 and TIMP-1 for MMP-2 (72- and 62-kDa species) and MMP-9 (92- and 82-kDa species), respectively. In contrast, binding data of TIMP-2 to a MMP-2 45-kDa active form lacking the C-terminal domain and to a MMP-2 C-terminal domain (CTD) fragment displays monophasic kinetics with K_d values of 315 and 60 nM, respectively. This suggests that the CTD contains the high-affinity binding site while the catalytic domain contains the low-affinity site. Also, binding of TIMP-2 to proMMP-2 is stronger at both the high- and low-affinity sites than the corresponding binding of TIMP-2 to the MMP-2 62-kDa form demonstrating the importance of the N-terminal prodomain. In addition, the K_d value of TIMP-1 for the MMP-2 62-kDa species is 28.6 nM at the high affinity site yet, neither the MMP-2 45-kDa species nor the CTD interacts with TIMP-1. Enzyme inhibition studies demonstrate that TIMPs are slow-binding inhibitors with monophasic inhibition kinetics. This suggests that a single binding event results in enzyme inhibition. The kinetic parameters for the onset of inhibition are fast ($k_{on} \sim 10^5$ M^{-1} s^{-1}) with slow off rates ($k_{off} \sim 10^{-3}$ s^{-1}). The inhibition constants (K_i) are in the 10^{-7} - 10^{-9} M range and correlate with the values determined by SPR.[16] This extensive investigation revealed for the first time that the interactions of these protein inhibitors with the MMPs was in a slow-binding manner, for which the kinetic parameters were evaluated. Furthermore, the mechanistic bases for the effective functions of the TIMPs as inhibitors of MMPs was revealed due to a very rapid

association with gelatinases and slow dissociation of the complex to the individual proteins (see the manuscript in Appendices for details).

III. Mechanism-Based Inactivators for Gelatinases as Potential Anti-Breast-Cancer Agents. Considerable interest has been generated in the past several years in mechanism-based irreversible enzyme inactivators (also know as "k_{cat} inhibitors" or "suicide substrates"). In this type of inactivation, the targeted enzyme uses a portion of its catalytic mechanism to generate—from an otherwise chemically unreactive group in a substrate analogue—a functionality reactive for covalent and irreversible modification of residues in the enzyme active site. Since the reactive species is formed only within the active site of the targeted enzyme, these inactivators have great promise for high *in vivo* selectivity. The potential high specificity for a targeted enzyme with these inactivators arises predominantly from three factors. (i) A mechanism-based inactivator has to satisfy the binding specificity requirements at the active site. In this respect these molecules are not any different than conventional reversible inhibitors or affinity inactivators. (ii) Furthermore, the structural requirements must be satisfied in the molecule so that it may undergo the requisite chemical activation by the enzyme to generate the inactivating species within the active site. It is this activation step that is responsible for the onset of the enzyme inactivation process. (iii) Finally, there must be a nucleophilic amino-acid residue present in the active site in the proper orientation, which may be trapped by the inactivating species in a covalent manner, resulting in *irreversible* enzyme inactivation. **It is known that small changes in the structure of this type of inactivator would alter its ability to interact with the targeted enzyme dramatically (i.e., criteria ii and iii are primarily affected). A corollary to this statement would be that minute changes in the structures of the active sites of the targeted enzymes (as in functionally related enzymes, such as in the family of MMPs) may impart increased selectivity and specificity to the inactivator for a given enzyme**. This is an aspect of this type of enzyme inactivator that is of great interest for the design of inactivators for MMPs since their active sites (catalytic domains) are highly similar in structure.[13] To drive this point home, an example will be informative here. We had designed two custom-made mechanism-based inactivators, one for carboxypeptidase A and another for carboxypeptidase B—both enzymes are metalloproteases that have virtually identical three-dimensional structures. These compounds show as much as 20,000-fold preference (in terms of k_{inact}/K_i) for the individual enzyme for which they were designed (unpublished results). At this juncture, we should state that our group has carried out the pioneering work in design and evaluation of mechanism-based inactivators for metalloproteases,[17-22] which put us in a good position to do the same task successfully for the MMPs. The targeted molecules would be the first mechanism-based inactivators for MMPs, which we expected would not suffer the shortcomings of the existing reversible competitive inhibitors in having a lack of specificity in targeting for these important enzymes.

As described earlier, we decided to target gelatinases (MMP-2 and MMP-9) for inactivation by our strategies for mechanism-based inactivation. The design process went through a number of iterations and several dozens of compounds were prepared in the process. As outlined in the annual reports for years 1 and 2 of the research, these compounds either did not work as they were intended, or they did so poorly. We prepared both peptidic and non-peptidic analogues among these initial sets of compounds. The problem rested with their relative poor affinity for the enzyme. We had to increase the affinity, if these strategies were to be successful. We went back to the computational models for inhibition of gelatinases and have designed new structural motifs for the inhibitors that we hoped would show the mechanism-based inhibition characteristic, as well as high affinity.

Our efforts ultimately paid off in our development of the first mechanism-based inhibitor for matrix metalloproteinases (MMPs) recently (see the manuscript in Appendices for details).[23] The inhibitor, (4-phenoxyphenylsulfonyl)methylthiirane (**1**), was designed to bind the active site of gelatinases, MMP-2 and MMP-9, specifically and the thiirane moiety was expected to coordinate to the active-site zinc ion. Our strategy for mechanism-based inhibition of MMPs by compound **1** is depicted in Scheme 1. The strategy envisions that coordination of the thiirane with the active-site zinc ion would activate it for modification by a nucleophile in the enzyme active site. The biphenyl moiety in compounds **1-6** would fit in the P_1, subsite of gelatinases, which is a deep hydrophobic pocket.[13] Energy-minimized complexes of MMP-2 and MMP-9 with compound **1** indicated that the biphenyl group would fit in the active site analogously to the same group in reversible inhibitors of MMP-2 and MMP-9. This binding mode would bring the sulfur of the thiirane in **1** into the coordination sphere of the zinc ion. The models indicated that the thiirane moiety in compounds **2** and **3**, with longer carbon backbones, would not be able to coordinate with the zinc ion, but would fit in an extended conformation in the active site.

Scheme 1

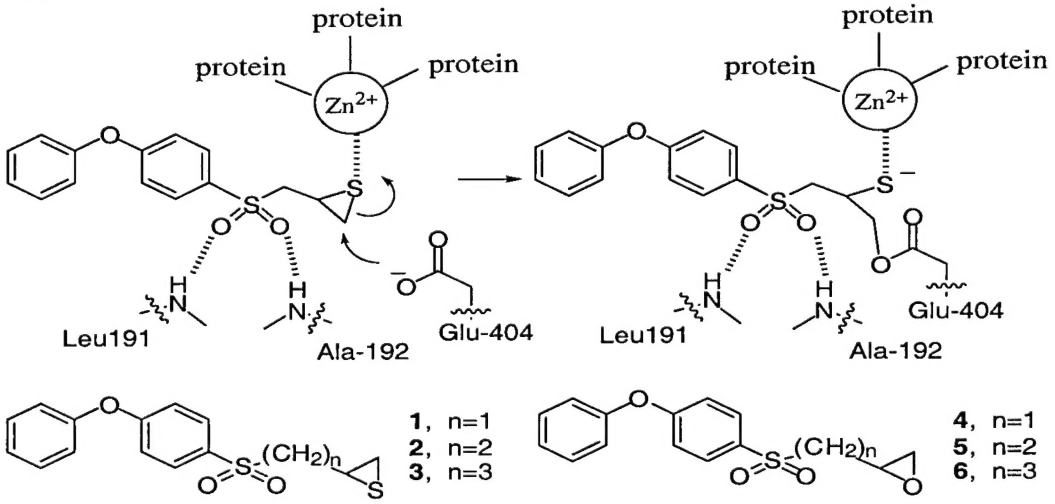

Scheme 2 shows the synthetic route for compounds **1-6**. 4-Phenoxythiophenol **10** was prepared from the commercially available 4-phenoxyphenol **7** via a three-step procedure. Subsequent alkylation of **10** with allyl bromide, 4-bromo-1-butene and 5-bromo-1-pentene, respectively, led to the sulfanyl compounds **11-13** in good yields. Epoxidation of **12** and **13** with mCPBA proceeded in 2-3 days, but that for **11** took 7 days and required an excess of mCPBA. Finally, conversion of the epoxides **4-6** to their corresponding thiirane derivatives **1-3**, respectively, was accomplished by the treatment of each epoxide with ammonium thiocyanate. Although the thiiranes **2** and **3** were isolated in high yields (93 and 85%, respectively), thiirane **1** could only be recovered in a poor 14% yield.

Scheme 2

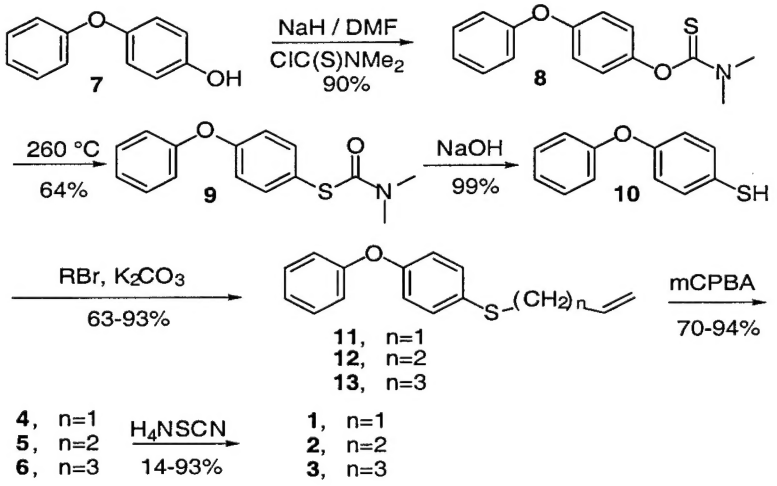

Compounds **1-6** were evaluated with purified homogeneous preparations of MMPs (see the manuscript in Appendices for details). Whereas inhibitors **2-6** showed either no inhibition or relatively poor inhibition of the MMPs (K_i values of micromolar at best), the behavior of inhibitor **1** was different. Inhibitor **1** showed a dual behavior. It served as a mechanism-based inhibitor with a partition ratio of 79 $\pm$ 10 (i.e. k_{cat}/k_{inact}) for MMP-2 and of 416 $\pm$ 63 for MMP-9. Furthermore, it also behaved as a slow-binding inhibitor, for which the rate constants for the onset of inhibition (k_{on}) and recovery of activity from inhibition (k_{off}) were evaluated (Table 1). It would appear that coordination of the thiirane with the zinc ion (as seen in the energy-minimized computational models; Scheme 1) would set in motion a conformational change, which is presumed from the slow-binding kinetic behavior. The kinetic data fit the model for slow-binding inhibition. Covalent modification of the enzymes ensued this conformational change. We incubated inhibitor **1** with MMP-2 to the point that less than 5% activity remained. This inhibitor-enzyme complex was dialyzed over three days, which resulted in recovery of approximately 50% of the activity. This observation is consistent with modification of the active site Glu-404, via the formation of an ester bond, which is a relatively labile covalent linkage. The time-dependent loss of activity is not merely due to the slow-binding behavior. For instance, for a k_{off} of 2 x 10^{-3} s^{-1} (the values are not very different from one another in Table 1) the half time for recovery of activity ($t_{1/2}$) is calculated at just under 6 min. The fact that 50% of activity still did not recover after dialysis over three days strongly argues for the covalency of enzyme modification.

We observe selectivity in inhibition of gelatinases by inhibitor **1**. The K_i values are 13.9 $\pm$ 0.4 nM and 600 $\pm$ 200 nM for MMP-2 and MMP-9, respectively. In contrast, the corresponding K_i values for the other MMPs tested, including MMP-3, which does show the slow-binding mechanism- based inhibition profile, are in the micromolar range. Interestingly, the values for k_{on} are 611- and 78-fold larger for MMP-2 and MMP-9, respectively, than that for MMP-3. Collectively, these kinetic parameters make inhibitor **1** a potent and selective inhibitor for both MMP-2 and MMP-9, more so for MMP-2. We have determined previously that two molecules of either TIMP-1 or TIMP-2 bind to activated MMP-2 and MMP-9.[16] One binding event is high affinity and would appear physiologically relevant, whereas the second binding event takes place with relatively lower affinity (micromolar).[16] Inhibition of MMP-2 and MMP-9 by TIMP-2 and TIMP-1, respectively, also follows slow-binding kinetics. The kinetic parameters for these

interactions at the high affinity site are listed in Table 1. We find it noteworthy that the kinetic parameters for the slow-binding component of inhibition of MMP-2 and MMP–9 by inhibitor **1** (k_{on} and k_{off}) approach closely the same parameters for those of the TIMPs.[16]

Table 1. Kinetic parameters for inhibition of MMPs by the synthetic inhibitors.

	k_{on} ($M^{-1}s^{-1}$) x 10^{-4}	k_{off} (s^{-1}) x 10^{3}	K_i (μM)
Inhibitor 1			
MMP-2	11 ± 1	1.8 ± 0.1	0.0139 ± 0.0004
MMP-9	1.4 ± 0.3	7.1 ± 0.5	0.6 ± 0.2
MMP-3	0.018 ± 0.004	5.5 ± 0.4	15 ± 6
MMP-7			96 ± 41
MMP-1			206 ± 60
TIMP-1			
MMP-2	4.4 ± 0.1	1.3 ± 0.2	0.029 ± 0.005
MMP-9	5.2 ± 0.1	1.2 ± 0.2	0.024 ± 0.004
TIMP-2			
MMP-2	3.3 ± 0.1	0.8 ± 0.1	0.023 ± 0.004
MMP-9	2.2 ± 0.1	1.3 ± 0.2	0.058 ± 0.007

IV. Effect of Synthetic Inhibitors for MMPs on Activation of MMP-2. The results presented in a manuscript that we just submitted (see the manuscript in Appendices for details)[24] demonstrate that pro-MMP-2 activation by MT1-MMP at the cell surface is the results of a highly regulated enzymatic process that involves two independent events, which under certain conditions may work synergistically to enhance MT1-MMP-dependent activation of pro-MMP-2. For example, for pro-MMP-2 our data show that a short (5 min) exposure to TIMP-2 followed by a 15-min incubation with pro-MMP-2 was sufficient to rapidly activate pro-MMP-2 without detectable accumulation of active (57 kDa) MT1-MMP. The reason for the lack of detection of active enzyme under this conditions is unclear, but may be related to the detection method (immunoblotting), rapid enzyme turnover and/or to the internalization and turnover of the MT1-MMP (57 kDa)-TIMP-2 complex. Under conditions of sub-stoichiometric TIMP-2 molar concentrations relative to MT1-MMP, the efficient binding of TIMP-2 results in optimal pro-MMP-2 activation.[24] Thus, while rapid bursts of TIMP-2 expression will be sufficient to generate ternary complex and consequently activate pro-MMP-2 in the absence of a significant and detectable accumulation of active MT1-MMP, chronic exposure to TIMP-2 or broad-spectrum MMP inhibitors would maintain a steady level of MT1-MMP on the cell surface. For other MT1-MMP substrates, such as extracellular matrix components, which do not require ternary complex formation to be hydrolyzed by MT1-MMP, sustained TIMP-2 expression and/or presence of synthetic inhibitors may indirectly enhance catalytic activity, as demonstrated in our manuscript using pro-MMP-2 as a substrate (see the manuscript in Appendices for details).[24]

Recent accomplishments in drug design have resulted in the generation of a variety of novel MMP inhibitors with effective anti-tumor and anti-angiogenic activities in animal models of cancer, as discussed earlier. These encouraging results have brought some of these compounds, such as Marimastat and Batimastat, to human clinical trials. The majority of the compounds undergoing testing in humans, however, lack specificity towards the various MMP families. The hydroxamates, for instance, inhibit a wide spectrum of MMPs, including MT1-MMP, as herein demonstrated, often with similar affinities. The complex outcome of MT1-MMP inhibition on catalytic activity demonstrated in a recent manuscript by us[24] raises important issues regarding

the potential consequences of inhibiting MT1-MMP. The autocatalytic turnover of MT1-MMP on the cell surface may represent an important regulatory step aimed at controlling pericellular proteolysis, a process that is likely to be favored by lateral diffusion and clustering of MT1-MMP molecules in specialized cell surface structures. Thus, reversible inhibition of MT1-MMP activity would play a role in preventing excessive enzyme clearance from the cell surface and indirectly favor proteolysis. Such an effect by MMP inhibitors would depend on the spectrum of activity (K_i values) elicited by each particular inhibitor against the different members of the MMP family and on their pharmacokinetics. The reversible MMP inhibitors tested in our publication (Marimastant and Batimastat) exhibit different K_i values for the catalytic domain of MT1-MMP, which correlated well with their efficacy in promoting pro-MMP-2 activation with TIMP-2. In contrast, the mechanism-based inhibitor **1** is a highly selective inhibitor of MMP-2[23] over MT1-MMP,[24] and is substantially less effective for MT1-MMP inhibition.

Our inhibitor **1** is highly specific for inhibition of gelatinases, enzymes that are inhibited covalently by this inhibitor. The inhibitor did not pursue the metal-chelation strategy for its inhibition, in contrast to the case of the existing inhibitors. We have shown in the manuscript that this inhibitor is substantially less effective in inhibition of MT1-MMP, for which it was not designed (see the manuscript in Appendices for details). Furthermore, in contrast to the case of gelatinases, it simply behaves as a linear competitive inhibitor for MT1-MMP. Again in contrast to Marimastat and Batimastat, this inhibitor did not show any ability to stimulate activation of MMP-2. Hence, the inhibitor should not have the unexpected drawback that we have demonstrated for the metal chelators Marimastat and Batimastat. This example underscores the need for development of novel strategy in inhibition of MMPs by entirely different mechanisms, such as was the case for inhibitor **1**.

We have conducted in collaboration with Dr. Irit Sagi of the Weitzman Institute in Israel the X-ray absorption spectroscopy (XAS) of the full-length human MMP-2 in its latent, active, and inhibited states and report the structural changes at the zinc ion site upon enzyme activation and inhibition. We have also examined the molecular structure of MMP-2 in complex with inhibitor **1**. It is shown that **1** directly binds the catalytic zinc ion of MMP-2. Interestingly, the novel mode of binding of the inhibitor to the catalytic zinc reconstructs the conformational environment around the active site metal ion back to that of the pro-enzyme.

We have outlined in this report a novel example for potent inhibition of human gelatinases by the small-molecule inhibitor **1**, which follows both slow-binding and mechanism-based inhibition in its kinetic profile. This compound appears to behave similarly to TIMP-2 and TIMP-1 in the slow-binding component of inhibition. Furthermore, the inhibitor also exhibits a covalent mechanism-based behavior in inhibition of these enzymes. The selectivity that inhibitor **1** displays (both in affinities and the modes of inhibition) among the other structurally similar MMPs is noteworthy.

In summary, this compound was shown to be a potent mechanism-based inhibitor for gelatinase, but its kinetic behavior was complicated by the fact that incubation of the enzymes with **1** indicated a kinetic profile for slow-binding inhibition, which was characterized. The kinetic parameters for the slow-binding component of inhibition of gelatinases by **1** approached closely the same parameters measured for inhibition of these enzymes by the TIMPs, which was an important finding. The slow-binding inhibition was followed by covalent modification of the enzyme and the attendant time-dependent loss of activity. The collective results indicated high selectivity for inhibition of gelatinases over other members of the MMP family. This observation on selectivity of inhibition for gelatinases among the other structurally similar MMPs is noteworthy and should serve as a paradigm in the design of inhibitors for other closely related enzymes.

V. Technical objectives 1-3. The three tasks that were outlined in the original applications are reproduced verbatim below. We have meet each task and then we have exceeded each in scope. For example, the iterative design process went considerably beyond "second-generation" inactivators in arriving at inhibitor **1** (Task 3). We made many compounds and not just two, as proposed in Task 1. Task 2 has been accomplished with five enzymes rather than four. The computational models, study of evolution of function of MMPs, and analyses of the kinetics of TIMP inhibition of gelatinases all assisted us in understanding the process of inhibition by synthetic compounds. These accomplishments were in addition to what was proposed under the three tasks.

Task 1: Years 1-2: Synthesize the two prototypic gelatinase inactivators. The initial synthetic work is the major effort in this project, and we expect that it would take the longest to accomplish.

Task 2: Year 3: The *in vitro* kinetic experiments to assess mechanistic expectations with four enzymes. We anticipate that full analysis for each compound would require 2-3 weeks.

Task 3: Year 3: Design, synthesis and kinetic evaluation of the second-generation gelatinase inactivators. During years 1-2 the syntheses of building blocks will be completed for the preparation of the two prototypes. To prepare the second-generation molecules we would merely use these building blocks in chemical assembly with various amino acids, which would require a few months, and is considerably less labor-intensive that the initial synthetic effort.

Key Research Accomplishments

* Generated computational models for the three-dimensional structures for gelatinases A and B. The coordinates were made available to the scientific community. These structures were used in the design aspect of the inhibitor development.
* We performed a structure-based sequence homology analysis to address the issue of evolution and diversification of the family of MMPs. We proposed that diversification of MMPs took place after the initial assembly of the full complements of the various domains into the primordial enzyme.
* With the structural information at hand, we provided insights into the metal binding motifs outside the active site. It would appear that there are at least three distinct motifs for the non-catalytic zinc ion in the MMPs.
* We described an extensive analysis of the kinetics of binding of TIMPs to gelatinates (latent and active forms). The analysis revealed that two TIMP molecules bind to each MMP, for which the details of the kinetic interactions were reported.
* We designed, synthesized, and characterized the first mechanism-based inactivator for gelatinases. The compounds afforded potent and selective inhibition of gelatinases.
* The best of these inhibitors is being studied in rodant models for human breast cancer metastasis in collaboration with Drs. Ralph Parchment and Fred Miller.

Reportable Outcomes

* Eight manuscripts in top journals.
* The database for sequence analyses for MMPs, and the coordinates for their models, are provided to the public in our group Web site.

* The US patent for the inhibitor has been filed.
* Several abstracts on the work have been presented in various scientific meetings, including the Gordon Conferences and the Era of Hope meeting in Atlanta (2000).
* The work on the inhibitor was the subject of a press conference at the Era of Hope meeting in Atlanta (2000).
* The American Chemical Society issued a press release on the inhibitor work in June 2000, the text of which is provided in the Appendices.
* The work on the inhibitor has received news coverage by reports in *Nature*, *Chemical & Engineering News*, *Modern Drug Design*, and *ReutersMD*.
* The following trainees received partial or full support from the grant: Dr. Yasuhiro Tanaka has joined the Ajinomoto Company (Tokyo, Japan) as a Senior Scientist; Dr. Zhi-Hong Li is currently a Senior Scientist with the Coulter Pharmaceutical Company (South San Francisco, CA); Dr. Steven Brown is currently a member of the group; Dr. Irina Massova has joined the Roche Pharmaceutical Company; Dr. Lakshmi Kotra has joined the faculty of Pharmacy at the University of Toronto. Mr. Cosimo Fuda is currently a student in the lab.

Conclusions

The research was a multidisciplinary and multifaceted endeavor. We generated three-dimensional computational models for gelatinases (and other MMPs) that have been made available to the scientific community. The structural knowledge and sequence information were used collectively to address the issue of evolution of MMPs and their diversification of function. Furthermore, we studied the issues of inhibition (binding) of MMPs by tissue protein inhibitors, the TIMPs, in an extensive investigation with homogeneous preparations of the proteins. We have synthesized a highly potent and selective inhibitor for gelatinases, which are being evaluated in rodant models for human cancer metastasis..

References

(1) Liotta, L.A.; Steeg, P.A.; Stetler-Stevenson, W.G. Cancer metastasis and angiogenesis: an imbalance of positive and negative regulation. *Cell* **1991**, *64*, 327.

(2) Testa, J.E.; Quigley, J.P. The role of urokinase-type plasminogen activator in aggressive tumor cell behavior. *Cancer Metastasis Rev.* **1990**, *9*, 353.

(3) Hamdy, F.C.; Fadlon, E.J.; Cottam, D.; Lawry, J.; Thurroll, W.; Silcocks, P.B.; Anderson, J.B.; Williams, J.L.; Rees, R.C. Matrix Metalloproteinase-9 Expression in Primary Human Prostatic Adenocarcinoma and Benign Protstatic Hyperplasia. *Br. J. Cancer* **1994**, *69*, 177.

(4) Boag, A.H.; Young, I.D. Increased Expression of the 72-Kd Type-IV Collagenase in Prostatic Adenocarcinoma. Demonstration by Immunohistochemistry and In-Situ Hybridization. *Am. J. Pathol.* **1994**, *144*, 585.

(5) Basset, P.; Bellocq, J.P.; Wolf, C.; Stoll, I.; Hutin, P.; Limacher, J.M.; Podhajcer, O.L.; Chenard, M.P.; Rio, M.C.; Chambon, P. A novel metalloproteinase gene specifically expressed in stromal cells of breast carcinomas. *Nature* **1990**, *348*, 699.

(6) Poulsom, R.; Hanby, A.M.; Pignatelli, M.; Jeffrey, R.E.; Longcroft, J.M.; Rogers, L.; Stamp, G.W. Expression of Gelatinase A and TIMP-2 mRNAs in Desmoplastic Fibroblasts in Both Mammary Carcinomas and Basal Cell Carcinomas. *J. Clin. Pathol.* **1993**, *46*, 429.

(7) Monteagudo, C.; Merino, M.J.; San-Juan, J.; Liotta, L.A.; Stetler-Stevenson, W.G. Immunohistochemical distribution of type IV collagenase (Gelatinase) in normal, benign and malignant breast tissue. *Amer. J. of Path.* **1990**, *136*, 585.

(8) D'Errico, A.; Garbisa, S.; Liotta, L.A.; Castranovo, V.; Stetler-Stevenson, W.G.; Grigioni, W.F. Augmentation of type IV collagenase (Gelatinase), laminin receptor and Ki62

proliferation antigen associated with human colon, gastric and breast carcinoma progression. *Modern Path.* **1991**, *4*, 239.

(9) Brown, P.D.; Bloxidge, R.E.; Anderson, E.; Howell, A. Expression of activated gelatinase in human invasive breast carcinoma. *Clin. Exp. Metastasis* **1993**, *11*, 183.

(10) Wang, X.; Fu, X.; Brown, P.D.; Crimmin, M.J.; Hoffman, R.M. Matrix Metalloproteinase Inhibitor BB-94 (Batimastat) Inhibits Human Colon-Tumor Growth and Spread in a Patient-Like Orthotopic Model in Nude-Mice. *Cancer Res.* **1994**, *54*, 4726.

(11) Davies, B.; Brown, P.D.; East, N.; Crimmin, M.J.; Balkwill, F.R. A Synthetic Matrix Metalloproteinase Inhibitor Decreases Tumor Burden and Prolongs Survival of Mice Bearing Human Ovarian Carcinoma Xenografts. *Cancer Res.* **1993**, *53*, 2087.

(12) Zhang, D.; Botos, I.; Gomis-Ruth, F.X.; Doll, R.; Blood, C.; Fox, J.W.; Bode, W.; Njoroge, F.G.; Meyer, E. Structural Interaction of Natural and Synthetic Inhibitors with the Venom Metalloproteinase, Atrolysin-C (Form- D). *Proc. Natl. Acad. Sci. USA* **1994**, *91*, 8447.

(13) Massova, I. ; Fridman, R.; Mobashery, S. Structural Insights into the Catalytic Domains of Human Matrix Metalloprotease-2 and Human Matrix Metalloprotease-9: Implications for Substrate Specificities, *J. Mol. Mod.* **1997**, *3*, 17.

(14) Massova, I.; Kotra, L. P.; Fridman, R.; Mobashery, S. Matrix Metalloproteases: Structures, Evolution and Diversification, *FASEB J.* **1998**, *12*, 1075.

(15) Massova, I.; Kotra, L. P.; Mobashery, S. Structural Insight into the Binding Motifs for Calcium Ion and the Non-Catalytic Zinc in Matrix Metalloproteases, *Bioorganic Med. Chem. Lett.* **1998**, *8*, 853.

(16) Olson, M. W.; Gervasi, D. C.; Mobashery, S.; Fridman, R. Kinetic Analysis for the Binding of the Latent and Active Forms of the Human Matrix metalloprotease-2 and -9 to TIMP-1 and TIMP-2, *J. Biol. Chem.* **1997**, *272*, 29975.

(17) Mobashery, S.; Ghosh, S.; Tamura, S. Y.; Kaiser, E. T. Design of an Effective Mechanism-Based Inactivator for a Zinc Protease, *Proc. Natl. Acad. Sci. U. S. A.* **1990**, *87*, 578.

(18) Ghosh, S. S.; Wu, Y. Q.; Mobashery, S. Peptidic Mechanism-Based Inactivators for Carboxypeptidase A. *J. Biol. Chem.* **1991**, **266**, 8759.

(19) Wu, Y. Q.; Mobashery, S. Targeting Renal Dipeptidase (Dehydropeptidase I) for Inactivation by Mechanism-Based Inactivators. *J. Med. Chem.* **1991**, *34*, 1914.

(20) Ghosh, S. S.; Said-Nejad, O.; Roestamadji, J.; Mobashery, S. The First Mechanism-Based Inactivator for Angiotensin-Converting Enzyme. *J. Med. Chem.* **1992**, *35*, 4175.

(21) Levy, O. E.; Taibi, P.; Mobashery, S.; Ghosh, S. S. A Mechanism-Based Inactivation Study of Neutral Endopeptidase 24.11. *J. Med. Chem.* **1993**, *36*, 2408.

(22) Tanaka,Y.; Grapsas, I.; Dakoji, S.; Cho, Y.J.; Mobashery, S. Conscripting the Active-Site Zinc Ion in Carboxypeptidase A in Inactivation Chemistry by a New Type of Irreversible Enzyme Inactivator. *J. Am. Chem. Soc.* **1994**, *116*, 7475.

(23) Brown, S.; Bernardo, M.; Li, Z. H., Kotra, L. P.; Tanaka, Y.; Fridman, R.; Mobashery, S. Potent and Selective Mechanism-Based Inhibition of Gelatinases, *J. Am. Chem. Soc.* **2000** *122*, 6799-6800.

(24) Toth, M.; Bernardo, M. M.; Soloway, P. D.; Gervasi, D. C.; Soloway, P. D.; Wang, Z.; Bigg, H. F.; Overall, C. M.; DeClerk, Y. A.; Tschesche, H.; Cher, M. L.; Brown, S.; Mobashery, S.; Fridman, R. TIMP-2 Acts Synergistically with Synthetic MMP Inhibitors but not with TIMP-4 to Enhance the MT1-MMP-dependent Activation of Pro-MMP-2, *J. Biol. Chem.*, **2000** (submitted).

APPENDICES

J. Mol. Model. **1997**, *3*, 17 – 30

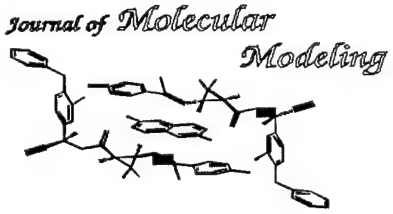

Structural Insights into the Catalytic Domains of Human Matrix Metalloprotease-2 and Human Matrix Metalloprotease-9: Implications for Substrate Specificities

Irina Massova, Rafael Fridman,§ and Shahriar Mobashery*

Department of Chemistry and the Barabara Ann Karmanos Cancer Institute, Wayne State University, Detroit, Michigan 48202, USA; Phone: 313-577-3924; Fax: 313-577-8822 (som@mobashery.chem.wayne.edu)

§ Department of Pathology

Received: 8 October 1996 / Accepted: 24 December 1996 / Published: 20 January 1997

Abstract

Structural information for the gelatinases A (MMP-2) and B (MMP-9), two members of the matrix metalloprotease (MMP) family of enzymes, has been elusive. For the first time, computational structures for the catalytic domains of MMP-2 and MMP-9 are reported herein using the program COMPOSER and the reported three-dimensional structures of the fibroblast collagenase (MMP-1), neutrophil collagenase (MMP-8) and stromelysin-1 (MMP-3). The details of the structures of the catalytic domains of gelatinases and interactions with the protein substrate are discussed. The first analysis of the extent of hydrophobicity of surfaces in the active sites of six MMPs (including the two gelatinases reported herein) is presented to provide distinction for substrate specificity among these metalloproteases. The information from the extent of hydrophobicity/hydrophilicity analysis and general topology for these MMPs was utilized in the proposal of a method for categorization of MMPs of known three-dimensional fold. These efforts provide the first information useful to experimentalists working on the biochemical properties of these important members of the MMP family of enzymes, and provide for an opportunity to compare and contrast structures of gelatinases, collagenases and stromelysins.

Keywords: Matrix metalloprotease, gelatinase A, gelatinase B, catalytic domain structure, substrate specificity

Introduction

Members of the family of matrix metalloproteases (MMPs) play central roles in the remodeling and turnover of extracellular matrix (ECM) in normal and pathological processes, including wound healing, angiogenesis, arthritis and cancer. This family of enzymes includes collagenases, stromelysins, gelatinases [1 ,2], and membrane-type MMPs [3, 4, 5]. All members of the MMP family share certain common features, which include an N-terminal propeptide which maintains latency in the zymogenic forms, a zinc-containing catalytic domain, and a C-terminal fragment referred to as the hemopexin/vitronectin-like domain [1, 2]. The gelatinases contain an additional fibronectin-like region intercalated within the catalytic domain [6, 7]. The membrane-type MMPs

* *To whom correspondence should be addressed*

contain an additional transmembrane domain which plays a role in anchoring the enzyme on the plasma membrane.

Structural information for the catalytic domains of two collagenases (MMP-1 [8] and MMP-8 [9]), and stromelysin-1 (MMP-3 [10]) are now available [11]. The general folding patterns of the catalytic domains in these proteins is well conserved, and each contains two zinc- and at least one calcium-binding sites. To date, any such structural information is lacking for gelatinases. However, from amino-acid sequence alignments for MMP-2 and MMP-9, the disjointed (*vide infra*) active-site domains of these enzymes are known to contain approximately 160-168 amino-acid residues.

The catalytic domains of gelatinases, which includes the catalytic zinc-binding site, are homologous with high degree of amino acid sequence identity to those of the fibroblast collagenase (MMP-1), neutrophil collagenase (MMP-8) and stromelysin-1 (MMP-3) [1]. Gelatinases cleave gelatin, collagens type IV, V, VII, XI, fibronectin, elastin, laminin, entactin, ß-amyloid, galectin-3 and proteoglycans [1, 2, 6, 7, 12 – 16], but gelatinases have never been shown to have any activity against connective tissue collagens. It was widely believed that while MMP-1 could degrade native fibrillar collagen type I, gelatinases were only active against denatured collagen. However, Aimes and Quigley [17] have shown recently that MMP-2 can cleave collagen fibrils and native type I collagen at a Gly-Ile/Leu peptide bond, displaying a specificity and maximal rate similar to that of MMP-1. These findings indicate that gelatinases share both sequence homology and active-site topology with collagenases.

Information on the structures of gelatinases has not been available in part due to the fact that these enzymes have not been crystallized. Furthermore, since the catalytic domains of gelatinases is larger due to the insertion of a 174-175 amino acid fibronectin-like domain in the vicinity of the active site in each case, the analysis of the structure by NMR has not been attempted. We describe herein the nature of our computational models for the catalytic domains of MMP-2 and MMP-9, which should prove useful in the study of the mechanism of the catalytic function of these important enzymes. Furthermore, these structures would provide an opportunity for structure-based efforts in design of inhibitors and study of substrate preference for this family of enzymes.

Materials and Methods

The amino-acid sequences of human MMP-2 (accession no. P08253) and MMP-9 (accession no. P14780) were obtained from the GenBank. The coordinates for homologous proteins with reported structures were taken from the Brookhaven Protein Database (1cgl, MMP-1; 1mnc, MMP-8; 2str, MMP-3). The amino-acid numbering system for the MMP-1 [8], the MMP-8 [9] and MMP-3 [10] have been described previously.

The folded structures for MMP-2 and MMP-9 were determined by the use of the software COMPOSER [18] implemented in SYBYL, version 6.22 [19]. COMPOSER aligns protein amino-acid sequence for a protein of unknown structure with those of homologous proteins of known structure based on topological similarities of their secondary structure elements and amino-acid sequence identities. This protocol is used to construct the three-dimensional framework of the structure. The use of COMPOSER is recommended for proteins that have amino-acid sequence identities which exceed 30% [20]. The amino-acid identity for MMPs within the catalytic domain (which includes the active-site zinc binding fold) ranges between 56-64%. Chothia and Lesk [21] indicate that reliability of the predicted structure exceeds 90% when amino-acid sequence identities are >50%. So, the reliability of the models reported here is very high. We added 116 water molecules to the gelatinase models which occupy the average positions in the homologous proteins of known structures and the energy of the entire complex was minimized by the AMBER force field [22]. Additional force-field parameters were developed for the zinc ion[23], based on our survey of all zinc-containing metalloproteases available from the Brookhaven Protein Data Bank. The reliability of these force-field parameters for zinc were verified by energy minimization of the collagenase structure (1cge) using these parameters. For these efforts, the structure of the MMP-1 was energy-minimized by AMBER using the additional parameters for the zinc ion developed by us and the resultant structure was compared with the crystallographic coordinates. The rms deviation for the Cα for the energy-minimized and crystallographic structures was 0.51 Å, and for active-site residues, as well as residues coordinating the catalytic zinc ion was 0.33 Å. For a crystal structure with resolution of 1.9 Å, as is the case for 1cge, the reliability of the positions of atoms after refinement is ±0.2 to ±0.3 Å [24], which fall approximately in the range of the rms deviation that we see for the protein after energy minimization, using our force-field parameters.

Gelatinases have a fibronectin-like domain of 174-175 amino-acid residues, which is inserted in the primary structure of the catalytic domain. This domain is replaced by a short loop of four amino acids in collagenases and stromelysin-1. In our model building for the gelatinases, we left out the sequence for the fibronectin-like domain, hence the models are comprised of two continuous sequences of polypeptides. This omission of the fibronectin-like domain, in our opinion, would not introduce structural variation into the conformation of the active site in light of the fact that the beginning of the domain is 16-19 Å away from the catalytic zinc ion, such that it would exist laterally to the catalytic domain. This omission of the fibronectin-like domain created a gap in the primary structure; however, in light of the stability of the structure of the folded proteins, it is significant that energy-minimization of the complexes of the sequences of the two polypeptides did not move apart during the energy-minimization procedure.

The autocatalytic cleavage site of MMP-2 (...DVANYNFF...) was fitted as a substrate into the active

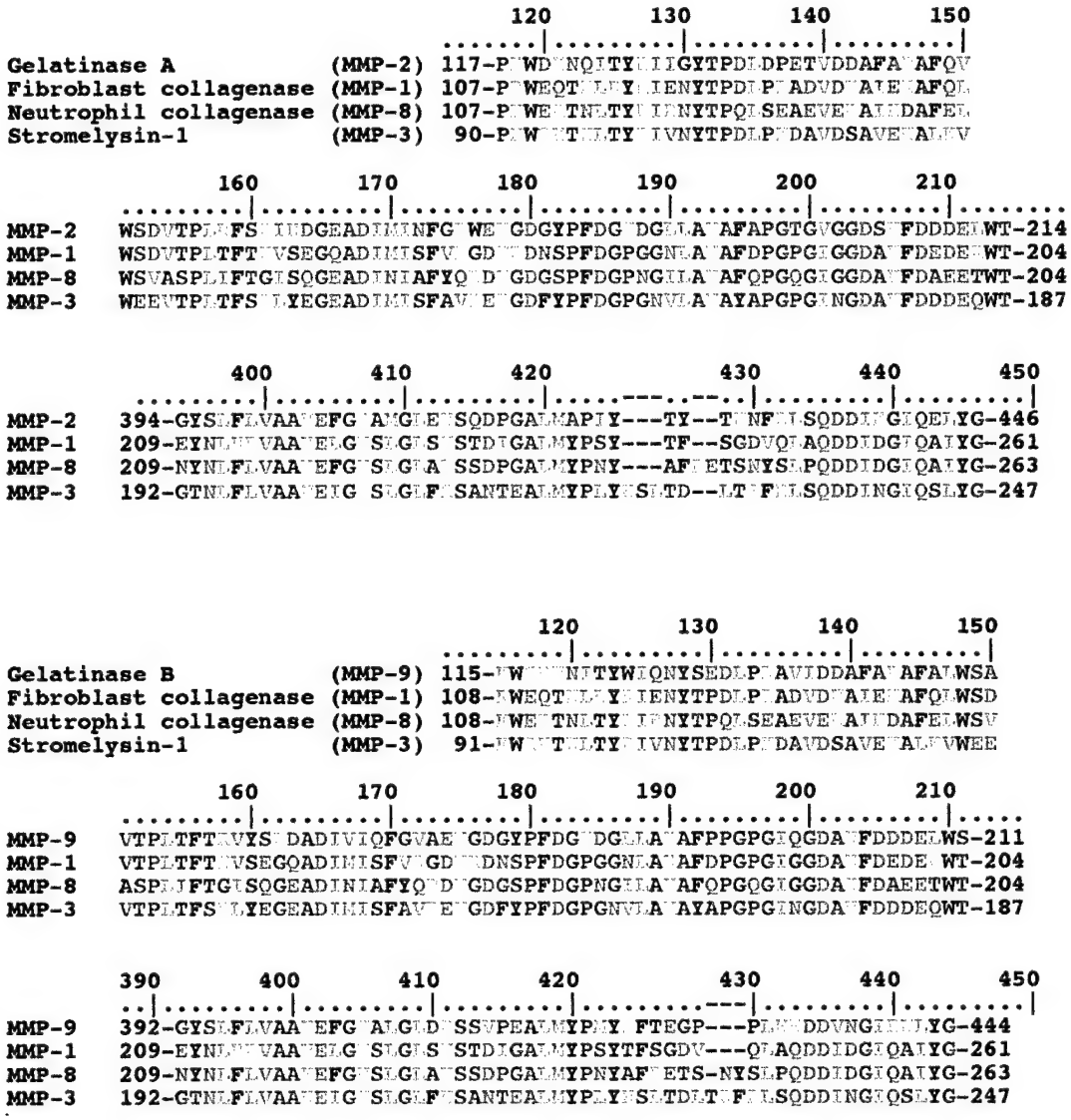

Figure 1. *Multiple amino-acid sequence alignment for the catalytic domains of human gelatinases A (MMP-2) and B (MMP-9) with human fibroblast collagenase (MMP-1), human neutrophil collagenase (MMP-8), and human stromelysin-1 (MMP-3) according to both sequence homology and topological similarity carried out by the program COMPOSER. Amino acids are colored according to their physico-chemical properties as the following: Pro, Gly, Ala, Ser, and Thr are in red; His, Arg, and Lys are in cyan; Tyr, Phe, and Trp are in blue; Asn, Asp, Gln, and Glu are in gray; Ile, Leu, Val, and Met are in green.*

site of the catalytic domain of MMP-2. The scissile carbonyl group was presented as a hydrated amide to mimic the transition state for the hydrolytic reaction. Water molecules were added to cover the substrate within the active site and the energy of the entire non-covalent enzyme-substrate complex was minimized by the AMBER force field, supplemented with our zinc parameters. The energy minimization was continued until one of these conditions was observed: (1) 50000 cycles of energy minimization were completed, (2) norm of the gradient of the energy became less than 0.001 kcal/(mol·Å), or (3) the difference in energy values for successive iterations in energy minimization cycles was within 0.001 kcal/mol.

Table 1. *The extent of sequence identity and similarity scores for MMP-2 and MMP-9 compared to MMPs with known structures.*

	MMP-2 (Pro117-Thr214...Gly394-Gly446)			MMP-9 (Lys115-Ser211...Gly392-Gly444)		
Enzyme	Homology Regions	% Sequence Identity	Similarity Score	Homology Regions	% Sequence Identity	Similarity Score
MMP-1	Pro107-Thr204 Glu209-Gly261	58	30	Arg108-Thr204 Glu209-Gly261	56	36
MMP-3	Pro90-Thr187 Gly192-Gly247	64	45	Lys91-Thr187 Gly192-Gly247	59	28
MMP-8	Pro107-Thr204 Gln209-Gly263	60	22	Lys108-Thr204 Gln209-Gly263	57	27

Results and Discussion

The catalytic domains of MMP-2 and MMP-9 both share considerable sequence similarity to MMP-1, MMP-3 and MMP-8. Figure 1 shows the multiple sequence alignment of both gelatinases with the three MMPs for which structures are known, carried out by the program COMPOSER. Table 1 summarizes the extent of amino-acid sequence identities and the similarity scores among the gelatinases and the three MMPs. The similarity score is an important factor for analysis by the COMPOSER program. It is the mean difference between the amino-acid sequence identity and the identity measured after the amino-acid sequences of the two proteins that are being compared to each other have been randomized 25 times. In order for two proteins to be considered homologous, the similarity score should be higher than 3 for most cases. The higher this number, the more significant is the percent of homology for the two proteins which are being compared. For our case, this similarity score is at the minimum 22, indicating the high homology of our proteins of interest to those for which structural information is available. Percent of amino-acid sequence identity among these proteins ranges from 56% to 64%, which gives a reliability for the computed coordinates of our models within the topologically identical regions in excess of 90% [21].

We decided to carry out an additional control experiment to investigate the reliability of the COMPOSER protocol for our application. We attempted to predict the folded structure for the MMP-1 based on the known structures of the MMP-3 and MMP-8, and amino-acid sequences of the proteins. Of the several crystal structures of the MMP-1 which are already available [8, 25], we used the structure 1cge for comparison with its predicted structure. The extent of sequence identity of the human MMP-1 with the MMP-3 and MMP-8 are 60% and 64%, and the similarity scores are 28 and 30, respectively. Figure 2 shows the outcome of the COMPOSER analysis for this protein and compares the predicted structure with that reported for the crystal structure. With the sole exception of the loop comprised of residues 241-247 (at 5 o'clock in Figure 2), the remainder of the backbone elements of the predicted structure superimposed nearly perfectly on the crystal structure. The similarity of the two structures is remarkable since no energy-minimization was carried out in this case. Indeed, the position of the loop may improve if minimization of the energy was carried out. If the loop is left out of the analysis, the rms deviation for the Cα from residues 112-261 for the predicted and X-ray structures is 0.46 Å; that for residues Arg-214, Val-215, Glu-219, His-218, His-222, and His-228, the histidines are the ligands to the active-site zinc ion and the other three are important active-site residues, for this protein for the two structures was 0.24 Å. The same analysis was carried out in predicting the structure of the MMP-8, and the predicted structure was similar to the crystal structure in this case as well (data not shown).

These control computations demonstrated the utility of the COMPOSER software in accurately predicting the structure of the catalytic domains of MMPs. Therefore, this program was used for the generation of the structures of the catalytic domains for MMP-2 and MMP-9. The predicted structures for the backbones of the structurally conserved regions for the two gelatinases superimposed well with those for the three known structures for MMPs (data not shown). Therefore, the general fold is extremely well-conserved and the differences in the structures of the catalytic domains of the two gelatinases and other MMPs rest with the variations on the individual amino-acid substitutions within the sequences of the proteins (*vide infra*). Figure 3 shows the energy-minimized catalytic domain for MMP-2 (that for MMP-9 is highly similar). Table 2 shows the major secondary elements of the structures of these two gelatinases.

The two catalytic domains for MMP-2 and MMP-9 are not only homologous to other MMPs of known structure, but

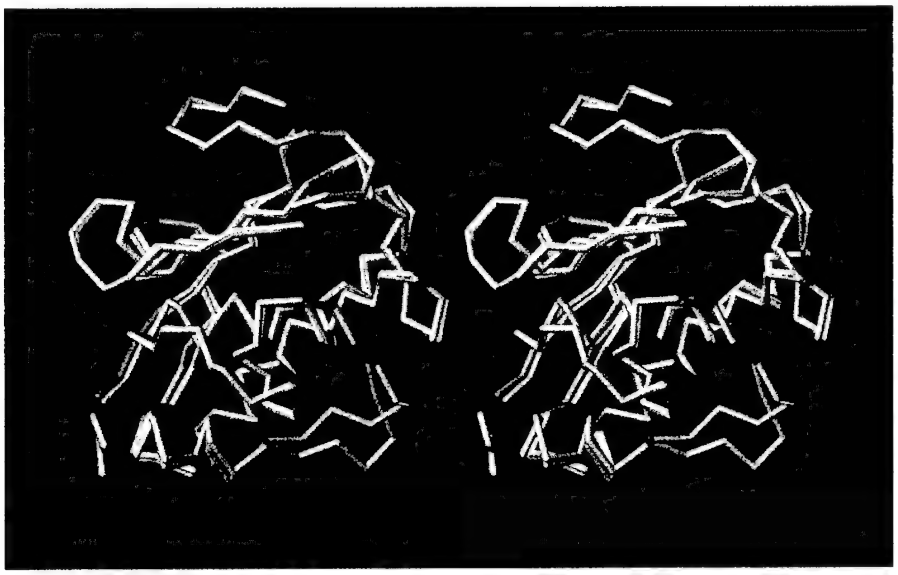

Figure 2. *Superimposition of the backbone of the predicted structure (in white) and the crystal structure (in cyan) for the MMP-1.*

they are highly homologous to one another. The percent of identity for the entire sequences of MMP-2 and MMP-9 is 48%, and when this comparison is made for the catalytic domains, the numbers are even higher. One sees from Lys-118 to Thr-214 and from Gly-394 to Gly-446 for MMP-2, and from Lys-115 to Ser-211 and from Gly-392 to Gly-444 for MMP-9 an identity of 65% [26]. Interestingly, the highly conserved regions include the zinc- and calcium-binding loops, an α-helix (B) and a β-strand (IV) within the active site, and the S_1'-binding pocket [27]. It is noteworthy that all amino-acid residues which are within the binding region of the substrate are strictly conserved, and only few residues pointing to the outside of the binding site are variable. The only variable residues within the active site are Glu-412, Ala-422, Ile-424 for MMP-2 and Asp-410, Tyr-420, Met-422 for MMP-9, respectively. It is important to point out that for two α-helices (A and C), the amino-acid residues which are located on the surface of the protein core are not conserved, however, those which point inward are highly conserved. Furthermore, the amino-acid residues sequestered on turns and loops tend to be more variable.

Figure 3. *The stereoview of the energy-minimized structure for the catalytic domain of MMP-2. The α-helices are in blue, the β-strands are in green, and other secondary structures are shown in yellow. The smaller orange sphere (at 1 o'clock) is the calcium ion, and the two larger spheres are zinc ions.*

Table 2. *Summary of the secondary structure elements of MMP-2 and MMP-9.*

MMP-2		MMP-9	
Segment [a]	**Structure [b]**	**Segment [a]**	**Structure [b]**
Gln123-Ile128	β-Strand I	Asn120-Ile125	β-Strand I
Pro137-Val154	α-Helix A	Arg134-Val151	α-Helix A
Pro156-His163	β-Strand II	Pro153-Tyr160	β-Strand II
Ile169-Arg175	β-Strand III	Ile166-Val172	β-Strand III
Ala192-Phe195	β-Strand IV	Ala189-Phe192	β-Strand IV
Gly203-Asp208	β-Strand V	Gly200-Asp205	β-Strand V
Leu397-Met409	α-Helix B	Leu395-Leu407	α-Helix B
Gln435-Tyr445	α-Helix C	Lys433-Tyr443	α-Helix C

[a] Numbering of the amino acids in the proteins is according to the GenBank.

[b] The terminology for the secondary structural elements is according to Lovejoy, B.; Cleasby, A.; Hassell, A. M.; Longley, K.; Luther, M. A.; Weigl, D.; McGeehan, G.; McElroy, A. B.; Drewry, D.; Lambert, M. H.; Jordan, S. R. *Science* **1994**, *263*, 375.

The substrate specificity of the gelatinases remains elusive, in part due to the fact that not many cleavage sites in protein substrates for gelatinases are known. Table 3 summarizes the known non-collagenic cleavage sites for protein substrates for gelatinases. An inspection of the amino acids around the cleavage sites indicated the preponderance of hydrophobic residues, although hydrophilic amino-acid residues are also found distributed throughout the sequences. To gain insight into substrate binding in the active site of the catalytic domain, we have modeled one sequence for the autocatalytic cleavage site of proMMP-2 into the active site of MMP-2 (Figure 4). The scissile carbonyl is shown hydrated in Figure 4 to mimic the transition-state species for the substrate hydrolysis. Figure 5 shows the schematic arrangement of interactions of the substrate in the active site. Since the active sites of the gelatinases are very similar in topology, only the active site of MMP-2 will be discussed. The active site of MMP-2 is an extended cleft region with an α-helix (B) and a β-strand (IV) forming two of the walls of the cleft. It would appear that the β-strand facilitates the orientation of the substrate for proper active-site binding by formation of an antiparallel β-sheet with the substrate. The same observation was recently made with regards to the binding of the substrate in the active site of MMP-8 [28], except that the binding of the substrate to the active site of MMP-2 appears to be somewhat more extended (discussed in more detail below).

As shown in Figure 4, many of the amino acids that line up the active-site cavity are conserved in all MMPs. However, the few exceptions are amino-acid residues 182, 188, 189, 190, 196, 395, 399, 400, 412, and 424 [26]. It is plausible that in conjunction with potential interactions of substrates with other enzyme domains, the variations of these amino acids would define the substrate specificity for each individual MMP. Furthermore, the loop comprised of residues 424-432 should be important for substrate specificity. Only residue Tyr-425 within this loop is invariant among all MMPs. This loop forms a wall of the S_1' pocket, known to be important in interactions of the substrates with the active site. The deep S_1' pocket of MMP-2 is of the same dimensions as that for the MMP-8. However, we hasten to add that the backbone of the MMP-1, in somewhat of a contrast to that for the MMP-8, traces that for MMP-2 more closely (Table 4). The principal structural difference is, however, the position of the side chain at residue Leu-399. In MMP-1 it is an arginine, which makes the S_1' cavity more shallow. Both gelatinases and MMP-8 have a leucine residue at this position that makes the cavity a deeper and more hydrophobic one.

Three hydrophobic amino-acid residues, Tyr-425, Tyr-395, and Leu-191 cluster in MMP-2 to form a hydrophobic core that constitutes the S_3' binding site. Hence, existence of a hydrophobic functionality at P_3' should be expected in preferred substrates, consistent with the results tabulated in Table 3. Of these three amino acids, that at position 395 is variable among MMPs, with substitutions of Thr, Asn, and Ile seen besides Tyr. The side chains of the substrate at positions P_2' and P_4' would point to the medium. These sites are bordered by the variable residues Leu-190, Gly-189, Asp-188, and Ile-424, which we suggest may play a role in defining substrate specificity. A tyrosine is found at position 182 of gelatinases. The orientation of this amino acid is such that it would force the substrate to bind the active site of MMP-2 as an extended β-strand. In contrast, a serine is found at this position in the MMP-1 and MMP-8. Grams et al. [28] have

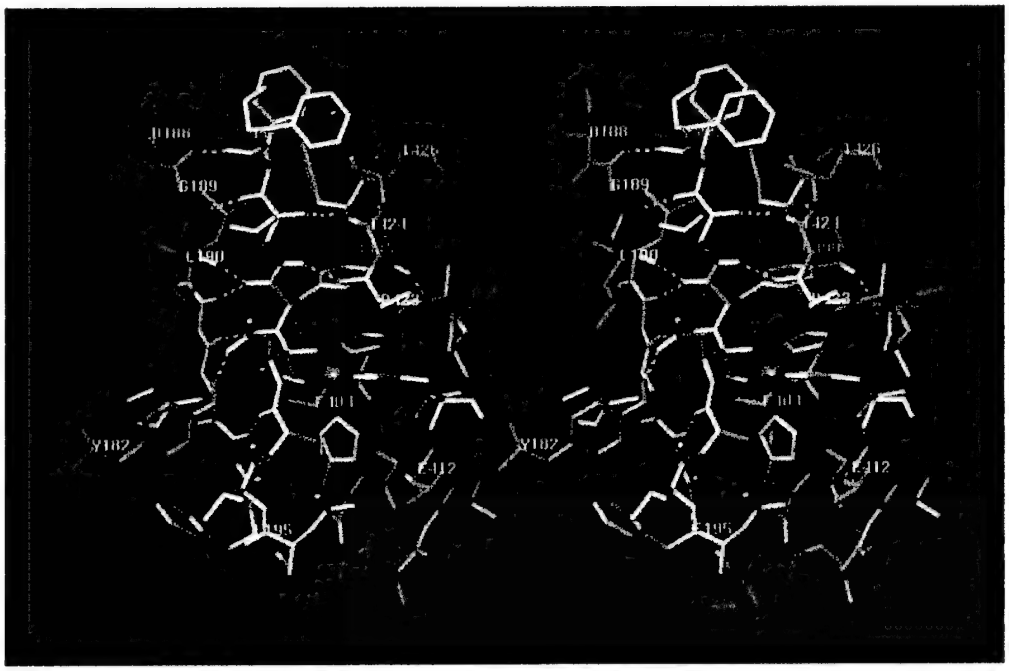

Figure 4. *Stereoview of the energy-minimized model for the complex of a peptide substrate based on an autocatalytic cleavage site of proMMP-2 in the active site of MMP-2. The peptide substrate (shown in white) is hydrated at the scissile carbonyl to mimic the transition state for the hydrolytic reaction, the oxygens of which are shown coordinated to the catalytic active-site zinc ion (orange sphere). The residues which are conserved for all MMPs are depicted in yellow, and the variable residues are in green. Only non-hydrogen atoms are shown, except when a hydrogen bond is involved between the substrate and the active site, where hydrogens are retained. Hydrogen bonds are shown in broken blue lines.*

suggested recently in their model for the binding of a substrate to the active site of the MMP-8 that the shorter side chain of this amino acid would permit a bend in the substrate conformation near this residue. Hence, according to this model, the substrate binding to MMP-8 takes place with a less extensive β-sheet formation than does for gelatinases.

The additional fibronectin-like domain of the gelatinases, which was left out from our models of the catalytic domains, has been suggested to facilitate binding of the enzyme to native and denatured collagen type I [29], but it is not directly involved in the catalytic activity [29, 30, 31,32]. A deletion mutant of the latent MMP-2 lacking this domain maintained self-activation in the presence of 4-aminophenyl

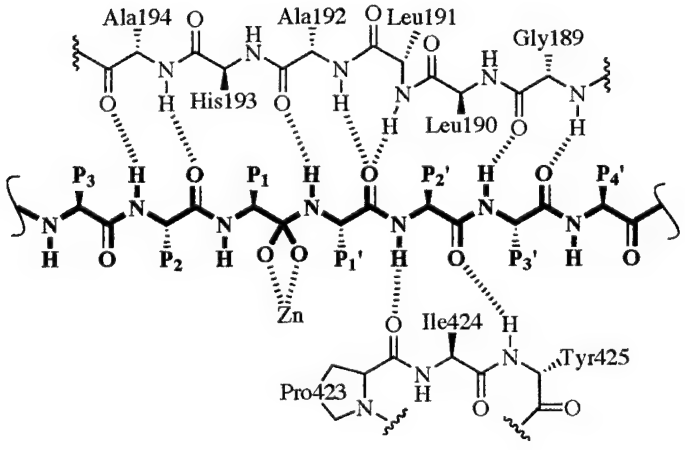

Figure 5. *Schematic representation of interactions of the autocatalytic cleavage site of proMMP-2 in the active site of MMP-2. The substrate is shown in bold-faced drawing.*

Table 3. *Some amino-acid sequences for non-collagenic protein substrates for gelatinases and the sites of enzymatic hydrolysis (indicated by ~).*

Substrate	Amino Acid Sequence	Enzyme
β-amyloid [a]	SNKGAIIGLM~VGGVVIATVI	MMP-2
β-amyloid [a]	GSNKGAIIGL~MVGGVVIATV	MMP-2
β-amyloid [a]	DSGYEVHHQK~LVFFAEDVGS	MMP-2
galectin-3 [b]	AYPGQAPPGA~YHGAPGAYPG	MMP-2 and MMP-9
aggrecan [c]	GEDFVDIPEN~FFGVGGEEDI	MMP-2 and MMP-9
FGFR-1 [d]	LEALEERPAV~MTSPLYLEII	MMP-2
MMP-2 (gelA) [e]	PRCGNPDVAN~YNFFPRKPKW	MMP-2
MMP-9 (gelB) [f]	PRCGVPDLGR~FQTFEGDLKW	MMP-2
MMP-9 (gelB) [f,g]	YRYGYTRVAE~MRGESKSLGP	MMP-2 and MMP-9
MMP-9 (gelB) [g]	GELDSATLKA~MRTPRCGVPD	MMP-9
MMP-9 (gelB) [g]	QSTLVLFPGD~LRTNLTDRQL	MMP-9
MMP-9 (gelB) [g]	ESKSLGPALL~LLQKQLSLPE	MMP-9
human cartrilage link protein [h]	YTLDHDRAIH~IQAENGPHLL	MMP-2 and MMP-9
human cartrilage link protein [h]	HIQAENGPHL~LVEAEQAKVF	MMP-2

[a] Roher, A. E.; Kasunic, T. C.; Woods, A. S.; Cotter, R. J.; Ball, M. J.; Fridman, R. *Biophys. Res. Comm.* **1994**, *205*, 1755.

[b] Ochieng, J.; Fridman, R.; Nangia-Makker, P.; Liotta, L. A.; Stetler-Stevenson, W. G.; Raz, A. *Biochemistry* **1994**, *33*, 14109.

[c] Fosang, A. J.; Neame, P. J.; Last, K.; Hardingham, T. E.; Murphy, G.; Hamilton, J. A. *J. Biol. Chem.* **1992**, *267*, 19470.

[d] Levi, E.; Fridman, R.; Miao, H.-Q.; Ma, Y.-C.; Yayon, A.; Vlodavsky, I. *Proc. Natl. Acad. Sci. U.S.A.* **1996** (in press).

[e] Stetler-Stevenson, W. G.; Krutzsch, H. C.; Wacher, M. P.; Margulies, I. M. K.; Liotta, L. A. *J. Biol. Chem.* **1989**, *264*, 1353; a number of autocatalytic sites for MMP-2 have also been reported (Bergmann, U.; Tuuttila, A.; Stetler-Stevenson, W. G.; Tryggvason, K. *Biochemistry* **1994**, *34*, 2819).

[f] Fridman, R.; Toth, M.; Peña, D.; Mobashery, S. *Cancer Res.* **1995**, *55*, 2548.

[g] Sang, Q. X; Birkedal-Hansen, H.; Van Wart, H. E. *Biochimica et Biophysica Acta-Protein Structure and Molecular Enzymology*. **1995**, *1251*, 99.

[h] Nguyen, Q.; Murphy, G.; Hughes, C. E.; Mort, J. S.; Roughley, P. J. *Biochem. J.* **1993**, *295*, 595.

mercuric acetate, and demonstrated similar activity as the full length enzyme with a peptide substrate, but showed somewhat reduced activity with gelatin as substrate [31, 33]. In a recent publication, Bányai et al. [34] suggested that the three homologous modules of the fibronectin domain form an extension to the active-site cleft of MMP-2, and therefore may be necessary for full activity of MMP-2. However, the findings of Ye et al. [33] are in conflict with the conclusion of Bányai et al. Ye et al. [33] showed that a truncated 19-kDa catalytic domain of MMP-2 lacking the fibronectin gelatin-binding domain displayed activity close to the full length enzyme, along with similar specificity toward various substrates, including gelatin. Ye et al. [33] concluded that the fibronectin domain was located remote from the catalytic domain of MMP-2, and that the removal of the fibronectin domain had no appreciable effect on either the structure or the catalytic ability of the catalytic domain. Our results reported herein support the conclusions of Ye et al.

Unlike gelatinases, the substrate specificity for other MMPs appears to be determined by the hemopexin-like domain [35,36]. A recent study reported the crystal structure of the porcine synovial collagenase, which includes the catalytic and hemopexin-like domains [37]. This structure shows that the hemopexin-like domain is freely hinged to the catalytic domain by a 17-residue linker, and that the hemopexin-like domain makes little contact with the catalytic domain [36, 37]. Furthermore, the crystallized full-length porcine synovial collagenase displays no structural difference when missing the hemopexin-like domain [37]. Removal of the C-terminal domain of the interstitial collagenase and

Table 4. *Categorization of matrix metalloproteases, and some features of the active sites.*

Enzyme	Group	S_1 [a]	S_1' [b]			No. of Residues for the Loop in the S_1' Pocket [c]
MMP-1	2B	N	R	L	V	7
MMP-2	1A	L	L	L	F	7
MMP-3	1A	V	L	L	F	10
MMP-7	2A	T	Y	V	F	9
MMP-8	2B	I	L	L	Y	9
MMP-9	1A	L	L	L	P	7

[a] Residues matched to the position corresponding to residue 182 in MMP-2.

[b] Residues matched to the position corresponding to residues 399, 400 and 431 in MMP-2.

[c] Number of residues between Tyr-425 and Leu-433 (numbering according to MMP-2), which constitute a portion of the wall of the S_1' pocket. All six enzymes have Tyr and Leu at these positions, respectively.

stromelysin-1 had no effect on the activity against casein, gelatin and a peptide substrate, but affected activity against native collagen [35]. Thus, similarly to the fibronectin-like domain of the gelatinases, the hemopexin-like domain of collagenase and stromelysin may play a role in substrate specificity.

The hemopexin/vitronectin-like domain of the gelatinases share high degree of amino-acid sequence identity to the same domain of the collagenases, and recent crystal structure reported by two different groups [38, 39] indicated similarity of the structures. Domain analysis revealed an important role for the C-terminal domain of the progelatinases in regulation of activity and inhibition by TIMPs. These studies showed that the C-terminal domain is (i) the major binding region for TIMPs in the proenzyme forms [40, 41, 42], (ii) it is not required for catalytic activity [40, 43], and (iii) it is required for the plasma membrane-dependent activation of proMMP-2 [43]. All these observations permit us to suggest that the missing fibronectin and hemopexin-like domains of the gelatinases should have no effect on the geometry of our models for the catalytic domains.

Finally, the zinc- and calcium-binding sites in the catalytic domains of gelatinases appear nearly identical to those in the MMPs of known structure. Figure 6 shows a schematic representation of the metal-binding sites.

Figure 7 shows the Connolly water-accessible surfaces for the active sites for six matrix metalloproteases, shown from the same perspective. At first glance, the overall size and topology of the six active sites are similar, hence one would anticipate some overlap in substrate profiles. This

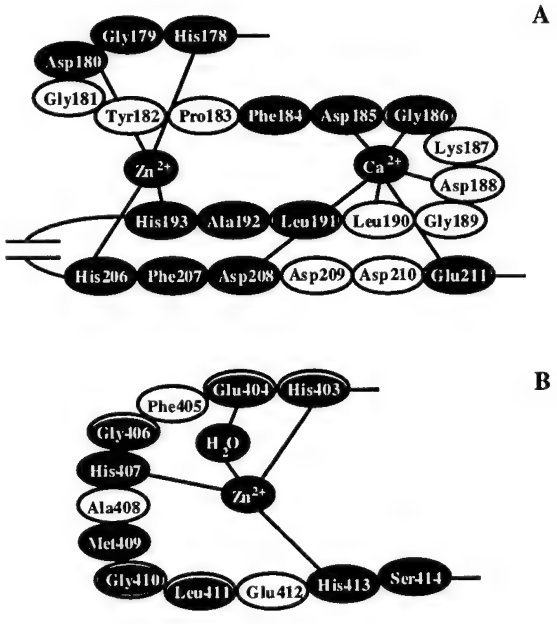

Figure 6. *Schematic of metal-binding sites in MMP-2 for (A) the structural metal-binding sites and (B) the catalytic metal-binding site. The hydrolytic water (shown in part B) is coordinated to the zinc ion, and in turn, it makes a hydrogen bond to the side chain of the active-site general base, Glu-404. Conserved residues in all MMPs are shown in black (exceptions are Asp-178 for MMP-11, Arg-179 for MMP-1, Met-411 for MMP-7, and Thr-414 for MMP-11; all other MMP have Leu-409), and residues shown in white are variable.*

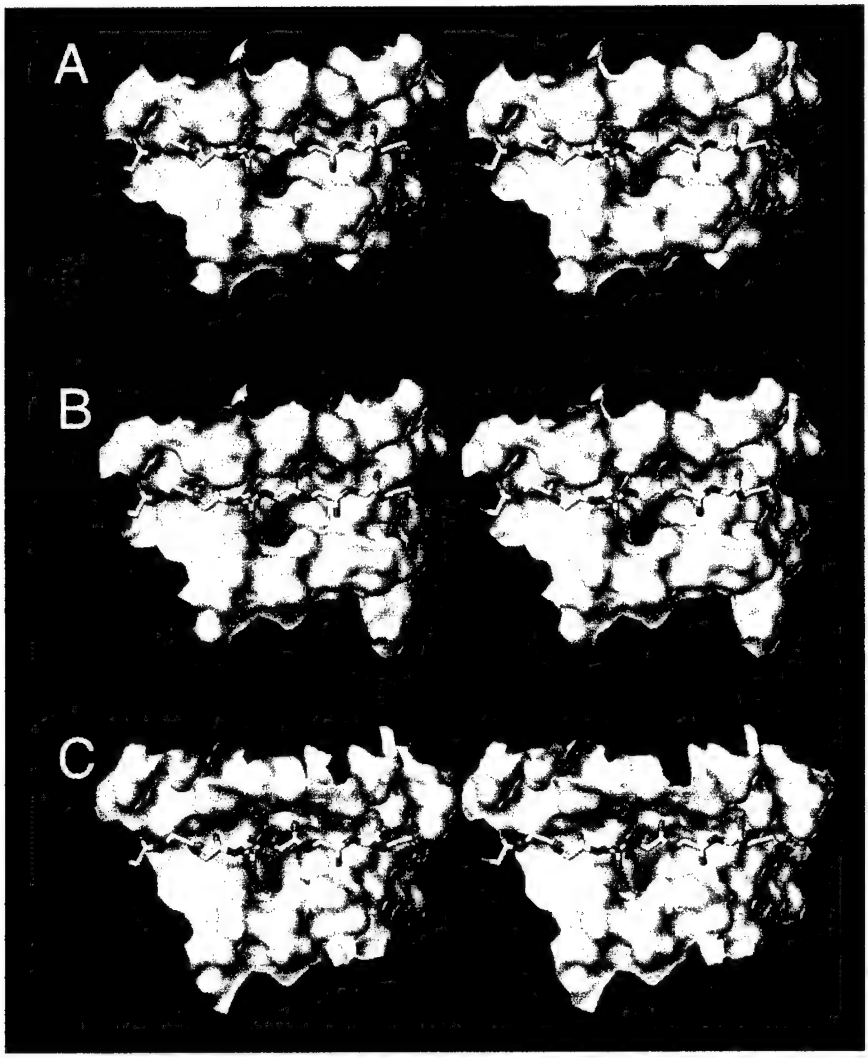

Figure 7 (continuous next page). *The stereoviews for the water-accessible Connolly surfaces for the active sites of MMPs are colored according to the following criteria: hydrophobic surfaces are shown in green, hydrophilic surfaces are in yellow, except that contributed by the zinc ion, which is depicted in orange. The water-accessible surfaces are comprised of both side-chain and main-chain functions, of which the latter is primarily involved in hydrogen bonding with substrate backbone amide functions. Only the backbone of a hypothetical substrate is shown bound in the active site, the atoms of which are colored according to atom types: white for carbon, red for oxygen, and blue for nitrogen; hydrogens are not shown. The substrate scissile carbonyl is depicted as hydrated, to mimic the structure of the transition-state species, which the enzyme stabilizes. The perspectives for figures in parts A-F are identical. The cavity in the middle of each structure is the S_1' pocket. The subsites to the right of the zinc ion are the primed sites, and those to the left are unprimed sites. (A) MMP-2 (reported in this manuscript), (B) MMP-9 (also reported in this manuscript), (C) MMP-1, (D) MMP-8, (E) MMP-3, and (F) MMP-7.*

notion finds support in recent publication of Aimes and Quigley [17], showing that MMP-2 can cleave fibrillar and native collagen type I at the same position as MMP-1, with a comparable rate. However, K_m for MMP-2 is approximately eight-fold higher than that for MMP-1, which may be due to the small differences in the two active sites. Insofar as K_m may approximate K_s, this difference may account for approximately 1 kcal/mol of binding energy difference, which is relatively small and may be the consequence of differential effects between the two active sites in hydrophobicity, steric hindrance, or even weak electrostatic interactions.

Based on the extent of surface hydrophobicity, we can divide these enzymes (shown in Figure 7) into two groups, 1

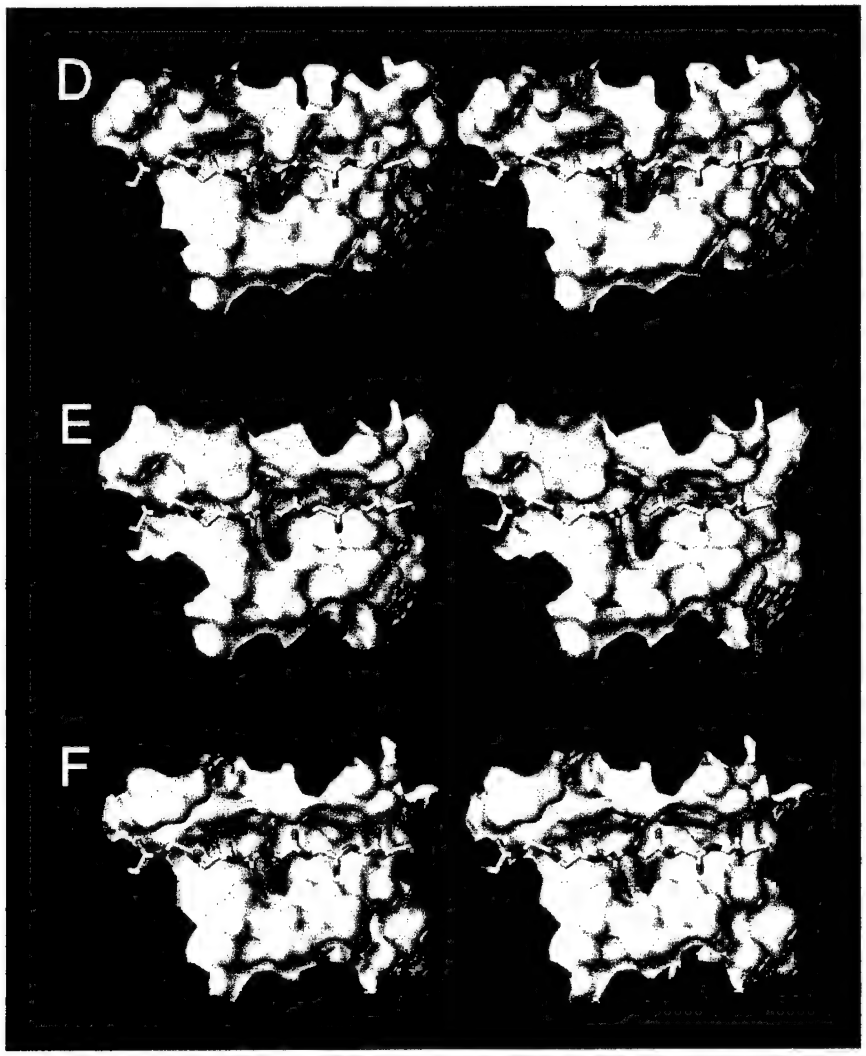

Figure 7 (continued).

and 2. Group 1 includes MMP-2, MMP-3 and MMP-9 (Figures 7A, E, and B), and group 2 includes MMP-1, MMP-7 and MMP-8 (Figures 7C, F, and D). In assessing the extent of hydrophobicity for each of these enzymes, we have analyzed the 32 amino acids that create each active site. Group 1 enzymes (MMP-2, MMP-3 and MMP-9) had 65–67% of their active sites as hydrophobic surface, in contrast to 54-57% for group 2 enzymes (MMP-1, MMP-7 and MMP-8). A portion of the hydrophilic surface in the active site is involved in electrostatic anchoring of the backbone of the substrate by hydrogen bonding, which is similarly present in all these enzymes. The remainder of the surface should play a role in defining the specificity for substrate by each of these enzymes. In our opinion the difference of 10% in the hydrophobic surfaces of the group 1 and group 2 enzymes is quite significant for the substrate specificity issue.

A second issue germane to the enzyme specificity is the degree of openness of the active site, particularly on the unprimed [27] portions. These six related enzymes can be divided into groups A and B based on this property. Group A includes MMP-2, MMP-3, MMP-7, and MMP-9, all of which have a tyrosine in the left upper quadrant of the active site (Figure 7), whereas MMP-1 and MMP-8 (belonging to group B) have the less bulky and less hydrophobic serine at this position. The bulk of Tyr-182, as well as that for a Leu-190 near the S_1 site, is the structural factor that influence the decrease of gelatinase activity with synthetic peptide substrates possessing residues larger than glycine or alanine at position P_1 [44, 45]. The classifications of MMPs of known structures by our system of groups 1 and 2, and groups A and B are given in Table 4.

Table 5. *Percentages for preferences for hydrophobic residues near the cleavage sites for known non-collagenic substrates (references are given in Table 3) for MMP-2.*

	P_5	P_4	P_3	P_2	P_1	P_1'	P_2'	P_3'	P_4'	P_5'
Autocleavage sites of MMP-2 in 2 min of incubation [a]	43	57	86	29	57	100	71	57	86	71
Other autocleavage sites of MMP-2 during 8 min to 15 h of incubation [b]	71	59	82	59	53	76	71	76	65	47
All sites [c]	58	58	88	58	55	88	67	73	73	58

[a] Total of seven. [b] Total of 17. [c] Total of 33.

The issue of the hydrophobic S_1' pocket (shown as the cavity in the center of the surfaces shown in Figure 7) has been addressed in many publications [9, 28, 46], and we will not elaborate much on this matter here. However, we note that along with the nature of the residues that line up this pocket, the length of the loop which forms the larger portion of the wall of this cavity should be important for flexibility of the enzyme to accommodate the side chain of the residue at position P_1' of the substrate. Among the six enzymes shown in Figure 7, MMP-7 has the smallest S_1' pocket, lined up with bulky residues such as valine and tyrosine (Table 4), in good agreement with the kinetics findings of Netzel-Arnett et al. [44] that MMP-7 is the least tolerant of these metalloproteases for the bulk of the residue that fits in the pocket. On the other hand, for the two collagenases, the loop is the larger for MMP-8 (9 residues; Table 4), compared to a shorter loop (7 residue) for the MMP-1. Our observation here is consistent with the kinetic measurements of Netzel-Arnett et al. [47], which indicated that a five-fold increase in k_{cat}/K_m activity for the MMP-8 when the P_1' residue in the substrate was changed from isoleucine to the bulkier tyrosine, whereas the same structural change in substrate resulted in a two fold decrease in k_{cat}/K_m for the MMP-1. The issue of the size of the S_1' pocket for gelatinases was discussed earlier in the manuscript.

Our structure-based categorization of these enzymes based on the hydrophobic/hydrophilic properties of the surfaces of the active sites, and the general topology (given in Table 4), agree closely with the classification offered for these enzymes based on specificity toward natural substrates [1]. Our groups 1A, 2B, and 2A correspond to groups I, II, and III of Woessner, respectively. The only exception is MMP-3 which falls into group 1A according to our structure-based scheme, and into group III according to Woessner. A more precise categorization of this family of enzymes should await further structural information for other related enzymes, both for the catalytic domains and entire enzymes.

From our discussion of the issue of the extent of hydrophobicity/hydrophilicity of the surfaces of the active sites for gelatinases would follow that substrate preference is not an all-or-none issue, rather the specificity preference represents a continuum. Bergmann et al. [48] observed that all autolytic sites, of which there are in excess of 20, within the primary structure of the latent form of MMP-2 are located in the N-terminal propeptide and catalytic domains, and none was found in the fibronectin or hemopexin domains. We analyzed the cleavage sites of autodegradation for MMP-2 [48] using our model for the catalytic domain of MMP-2 and the crystal structure for the N-terminal propeptide of MMP-3 [49]. Since the coordinates for two small stretches of amino acids within the propeptide of MMP-3 did not refine [49], we obtained structural information for 19 of the 23 cleavage sites. Analysis revealed that among these 19 sites, six were parts of β-strands, seven were within turns, loops or random coils, and six were located in α-helices.

The lack of this all-or-none effect in substrate preference for gelatinases may actually be an evolutionary adaptation by these enzymes. A statistical analysis of the preponderance of hydrophobicity for amino-acid residues in substrates for MMP-2, including the autolytic sites, tabulated in Table 5 reveals the clear preference of MMP-2 for hydrophobic substrates [50]. The stictest requirement seen in protein substrates is for the P_1' position, but also unexpectedly, for the P_3 position, for each of which an 88% preference for hydrophobic amino acids is observed. The preference for hydrophobicity at the P_3 position is consistent with our model of substrate binding in the active site as an extended β-strand in the unprimed direction, which forces the P_3 amino acid to occupy the hydrophobic space near the Tyr-182 residue. This portion of the active site is primarily composed of hydrophobic functionalities (upper left quadrant of Figure 7A). Because of the aforementioned "continuum" in substrate preference by gelatinases, these enzymes can accommodate a fairly diverse range of peptide substrates [44, 45]. However, the results of the statistical analysis in Table 5 reveal that the preference for substrate structure within the first couple minutes of the enzymic reaction (i.e., kinetic control), as opposed to lengthier incubation times (i.e., thermodynamic control), are quite distinct for P_5, P_2, P_3', and P_5'. In the first two minutes of the autoactivation of MMP-2 preference is seen for hydrophilic residues at P_2 (in more than two-thirds

of the cases) and virtually no discrimination for the nature of hydrophobicity/hydrophilicity at positions P_5, P_4, P_1 and P_3' (Table 5). Overall, MMP-2 prefers more hydrophobic residues at primed sites of substrate than at unprimed positions, which is consistent with the description of the active site surface depicted in Figure 7A.

Our analysis of the computational models for MMP-2 and MMP-9 provides for the first time an indepth insight into the structural parameters for the catalytic domains of gelatinases, and discusses the implication for substrate specificity. The information disclosed in this manuscript should stimulate further work on structures for these enzymes and should prove helpful in design of inhibitors and analysis of the mechanisms of the biological function in the future.

Acknowledgments. IM is a recipient of the Rumble and Heller Predoctoral Fellowships. The research in the Chemistry Department was supported in part by grants from the Karmanos Cancer Institute and the U.S. Army. The work in the Pathology Department was supported by the NIH grant CA 61986 (to RF).

References

1. Woessner, J. F., Jr. *FASEB J.* **1991**, *5*, 2146.
2. Matrisian, L. M. *Trends Genet.* **1990**, *6*, 121.
3. Sato, H.; Takino, T.; Okada, Y.; Cao, J.; Shinagawa, A.; Yamamoto, E.; Seiki, M. *Nature* **1994**, *370*, 61.
4. Takino, T.; Sato, H.; Shinagawa, A.; Seiki, M. *J. Biol. Chem.* **1995**, *270*, 23013.
5. Will, H.; Hinzmann, B. *Eur. J. Biochem.* **1995**, *231*, 602.
6. Collier, I. E.; Wilhelm, S. M.; Eisen, A. Z.; Marmer, B. L.; Grant, G. A.; Seltzer, J. L.; Kronberger, A.; He, C.; Bauer, E. A.; Goldberg, G. I. *J. Biol. Chem.* **1988**, *263*, 6579.
7. Wilhelm, S. M.; Collier, I. E.; Marmer, B. L.; Eisen, A. Z.; Grant, G. A.; Goldberg, G. I. *J. Biol. Chem.* **1989**, *264*, 17213.
8. Lovejoy, B.; Cleasby, A.; Hassell, A. M.; Longley, K.; Luther, M. A.; Weigl, D.; McGeehan, G.; McElroy, A. B.; Drewry, D.; Lambert, M. H.; Jordan, S. R. *Science* **1994**, *263*, 375.
9. Stams, T.; Spurlino, J. C.; Smith, D. L.; Wahl, R. C.; Ho, T. F.; Qoronfleh, M. W.; Banks, T. M.; Rubin, B. *Nature Struct. Biol.* **1994**, *1*, 119.
10. Gooley, P. R.; O'Connell, F.; Marcy, A. I.; Cuca, G. C.; Salowe, S. P.; Bush, B. L.; Hermes, J. D.; Esser, C. K.; Hagmann, W. K.; Springer, J. P.; Johnson, B. A. *Nature Struct. Biol.* **1994**, *1*, 111.
11. During preparation of this manuscript the crystal structure for matrilysin (MMP-7) also became available [Browner, M. F.; Smith, W. W.; Castelhano, A. L. *Biochemistry* **1995**, *34*, 6602].
12. Nguyen, Q.; Murphy, G.; Hughes, C. E.; Mort, J. S.; Roughley, P. J. *Biochem. J.* **1993**, *295*, 595.
13. Sires, U. I.; Griffin, G. L.; Broekelman, T. J.; Mecham, R. P.; Murphy, G.; Chung, A. E.; Welgus, H. G.; Senior, R. M. *J. Biol. Chem.* **1993**, *268*, 2069.
14. Fosang, A. J.; Neame, P. J.; Last, K.; Hardingham, T. E.; Murphy, G.; Hamilton, J. A. *J. Biol. Chem.* **1992**, *267*, 19470.
15. Ochieng, J.; Fridman, R.; Nangia-Makker, P.; Liotta, L. A.; Stetler-Stevenson, W. G.; Raz, A. *Biochemistry.* **1994**, *33*, 14109.
16. Roher, A. E.; Kasunic, T. C.; Woods, A. S.; Cotter, R. J.; Ball, M. J.; Fridman, R. *Biophys. Res. Comm.* **1994**, *205*, 1755.
17. Aimes, R. T.; Quigley, J. P. *J. Biol. Chem.* **1995**, *270*, 5872.
18. Blundell, T. L.; Carney, D. P.; Gardner, S.; Hayes, F. R. F.; Howlin, B.; Hubbard, T. J. P.; Overington, J. P.; Singh, D. A.; Sibanda, B. L.; Sutcliffe, M. J. *Eur. J. Biochem.* **1988**, *172*, 513.
19. Tripos Associates, 1699 S. Hanley Road, Suite 303, St Louis, MO 63144.
20. Srinivasan, N.; Blundell, T. L. *Protein Eng.* **1993**, *6*, 501.
21. Chothia, C.; Lesk, A. M. *EMBO J.* **1986**, *5*, 823.
22. Weiner, S. J.; Kollman, P. A.; Case, D. A.; Singh, U. C.; Ghio, C.; Alagona, G.; Profeta, S.; Weiner, P. *J. Am. Chem. Soc.* **1984**, *106*, 765.
23. Bonded model for the zinc ion was used with the following constants: force constant for bonds is 400 kcal/mol·Å; force constant for the angle X-Y-Zn is 55 kcal/mol·rad^2, where X is hydrogen, 70 kcal/mol·rad^2, where Y is nitrogen, and 100 kcal/mol·rad^2 in all other cases, including the X-Zn-Y angles. Parameters for van der Waals interactions are 1.85 Å and 0.06 kcal/mol. Equilibrium bonds and angles were averaged from the available crystallographic data from other metalloproteases.
24. Fersht, A. *Enzyme Structure and Mechanism*, 2nd Ed., **1985**, pp 5-7, W.H. Freeman and Co., New York.
25. Lovejoy, B.; Hassell, A. M.; Luther, M. A.; Weigl, D.; Jordan, S. R. *Biochemisty* **1994**, *33*, 8207.
26. Amino-acid numbering is according to the numbering for the sequences of MMP-2 and MMP-9 available from GenBank.
27. The terminology for specificity of subsites in the active site and the complementary features for the substrate are after the recommendations of Berger and Schechter [Berger, A.; Schechter, I. *Phil. Trans. R. Soc. London B* **1970**, *257*, 249].
28. Grams, F.; Reinemer, P.; Powers, J. C.; Kleine, T.; Pieper, M.; Tschesche, H.; Huber, R.; Bode, W. *Eur. J. Biochem.* **1995**, *228*, 830.
29. Steffensen, B.; Wallon, U. M.; Overall, M. *J. Biol. Chem.* **1995**, *270*, 11555.

30. Strongin, A. Y.; Collier, I. A.; Krasnov, P. A.; Genrich, L. T.; Marmer, B. L.; Goldberg, G. I. *Kidney International* **1993**, *43*, 158.
31. Murphy, G.; Nguyen, Q.; Cockett, M. I.; Atkinson, S. J.; Allan, J. A.; Knight, C. G.; Willenbrock, F.; Docherty, A. J. *J. Biol. Chem.* **1994**, *269*, 6632.
32. Allan, A. J.; Docherty, A. J. P.; Barker, P. J.; Huskissonm, N. S.; Reynolds, J. J.; Murphy, G. *Biochem. J.* **1995**, *309*, 299.
33. Ye, Q.-Z.; Johnson, L. L.; Yu, A. E.; Hupe, D. *Biochemistry* **1995**, *34*, 4702.
34. Bányai, L.; Tordai, H.; Patthy, L. *J. Biol. Chem.* **1996**, *267*, 12003.
35. Murphy, G.; Allan, J. A.; Willenbrock, F.; Cockett, M. I.; O'Connell, J. P.; Docherty, A. J. *J. Biol. Chem.* **1992**, *267*, 9612.
36. Bode, W. *Structure* **1995**, *3*, 527.
37. Li, J.; Brick, P.; O'Hare, M. C.; Skarzynski, T.; Lloyd, L. F.; Curry, V. A.; Clark, I. M.; Bigg, H. F.; Hazleman, B. L.; Cawston, T. E.; Blow, D. M. *Structure.* **1995**, *3*, 541.
38. Libson, A. M.; Gittis, A. G.; Collier, I. E.; Marmer, B. L.; Goldberg, G. I.; Lattman, E. E. *Nature Struct. Biol.* **1995**, *2*, 938.
39. Gohlke, U.; Gomis-Rüth, F.-X.; Crabbe, T.; Murphy, G.; Docherty, A. J. P.; Bode, W. *FEBS Lett.* **1996**, *378*, 126.
40. Fridman, R.; Fuerst, T.; Bird, R. E.; Hoyhtya, M.; Oelkuct, M.; Kraus, S.; Komarek, D.; Liotta, L.; Merman, M.; Stetler-Slevenson, G. *J. Biol. Chem.* **1992**, *267*, 15398.
41. Howard, E. W.; Banda, M. J. *J. Biol. Chem.* **1991**, *266*, 17972.
42. Goldberg, G. I.; Strongin, A. Y.; Collier, I. E.; Genrich, L. T.; Marmer, B. L. *J. Biol. Chem.* **1992**, *267*, 4583.
43. Murphy, G.; Willenbrock, F.; Ward, R. V.; Cockett, M. I.; Eaton, D.; Docherty, A. J. P. *Biochem. J.* **1992**, *283*, 637.
44. Netzel-Arnett, S.; Sang, Q.-X.; Moor, W. G. I.; Navre, M.; Birkedal-Hansen, H.; Van Wart, H. E. *Biochemistry* **1993**, *32*, 6427.
45. McGeehan, G. M.; Bickett, D. M.; Green, M.; Kassel, D.; Wiseman, J. S.; Berman, J. *J. Biol. Chem.* **1994**, *269*, 32814.
46. Bode, W.; Reinemer, P.; Huber, R.; Kleine, T.; Schnierer, S.; Tschesche, H. *EMBO J.* **1994**, *13*, 1263.
47. Netzel-Arnett, S.; Fields, G.; Birkedal-Hansen, H.; Van Wart, H. E. *J. Biol. Chem.* **1991**, *266*, 6747.
48. Bergmann, U.; Tuuttila, A.; Stetler-Stevenson, W. G.; Tryggvason, K. *Biochemistry* **1995**, *34*, 2819.
49. Becker, J. W.; Marcy, A. I.; Rokosz, L. L.; Axel, M. G.; Burbaum, J. J.; Fitzgerald, P. M. D.; Cameron, P. M.; Esser, C. K.; Hagmann, W. K.; Hermes, J. D.; Springer, J. P. *Protein Sci.* **1995**, *4*, 1966.
50. Since only seven cleavage sites are known for MMP-9, we could not carry out the statistical analysis for this enzyme as well. However, since both the structures for the active sites of the two gelatinases are nearly identical (Figs. 7A and 7B), and that the two enzymes have similar substrate profiles, we believe that our discussion of the statistical analysis for MMP-2 is also valid for MMP-9.

THE JOURNAL OF BIOLOGICAL CHEMISTRY Appendix II Vol. 272, No. 47, Issue of November 21, pp. 29975–29983, 1997

Printed in U.S.A.

Kinetic Analysis of the Binding of Human Matrix Metalloproteinase-2 and -9 to Tissue Inhibitor of Metalloproteinase (TIMP)-1 and TIMP-2*

(Received for publication, June 6, 1997, and in revised form, September 2, 1997)

Matthew W. Olson‡§, David C. Gervasi‡§, Shahriar Mobashery¶, and Rafael Fridman‡§‖

From the ‡Department of Pathology and the §Karmanos Cancer Institute and ¶Department of Chemistry, Wayne State University, Detroit, Michigan 48201

The dissociation constants (K_d) of tissue inhibitor of metalloproteinase (TIMP)-1 and TIMP-2 for the active and latent forms of matrix metalloproteinase (MMP)-2 and MMP-9 were evaluated using surface plasmon resonance (SPR) and enzyme inhibition studies. SPR analysis shows biphasic kinetics with high (nM) and low (μM) affinity binding sites of TIMP-2 and TIMP-1 for MMP-2 (72- and 62-kDa species) and MMP-9 (92- and 82-kDa species), respectively. In contrast, binding data of TIMP-2 to an MMP-2 45-kDa active form lacking the C-terminal domain and to an MMP-2 C-terminal domain (CTD) fragment displays monophasic kinetics with K_d values of 315 and 60 nM, respectively. This suggests that the CTD contains the high affinity binding site, whereas the catalytic domain contains the low affinity site. Also, binding of TIMP-2 to pro-MMP-2 is stronger at both the high and low affinity sites than the corresponding binding of TIMP-2 to the MMP-2 62-kDa form demonstrating the importance of the N-terminal prodomain. In addition, the K_d value of TIMP-1 for the MMP-2 62-kDa species is 28.6 nM at the high affinity site, yet neither the MMP-2 45-kDa species nor the CTD interacts with TIMP-1. Enzyme inhibition studies demonstrate that TIMPs are slow binding inhibitors with monophasic inhibition kinetics. This suggests that a single binding event results in enzyme inhibition. The kinetic parameters for the onset of inhibition are fast ($k_{on} \sim 10^5$ M^{-1} s^{-1}) with slow off rates ($k_{off} \sim 10^{-3}$ s^{-1}). The inhibition constants (K_i) are in the 10^{-7}–10^{-9} M range and correlate with the values determined by SPR.

The gelatinases MMP-2 (gelatinase A) and MMP-9 (gelatinase B) are two members of the MMP[1] family, a group of zinc-dependent endopeptidases known to hydrolyze many components of the extracellular matrix (1). Like other MMPs, the gelatinases are produced in a latent form (pro-MMP) requiring activation and are inhibited by TIMPs (1–3). A unique characteristic of the gelatinases is the ability of their zymogens to form tight non-covalent and stable complexes with TIMPs. It has been shown that pro-MMP-2 binds TIMP-2 (4), whereas pro-MMP-9 binds TIMP-1 (5). Although the physiological significance of the proenzyme-inhibitor complex is not completely understood, the complex may play a role in zymogen stabilization and activation (6–8). The interactions of TIMP-2 with pro-MMP-2 and of TIMP-1 with pro-MMP-9 were previously examined by analysis of enzyme activity using truncated enzymes and inhibitors (9–11). These studies demonstrated that the CTD of gelatinases increases the rate of association of the TIMPs for the active enzymes. Studies with activated and C-terminally truncated enzymes demonstrated that the catalytic domain is also involved in TIMP binding (9, 11). However, to date, no quantitative binding analyses of TIMP-1 or TIMP-2 for the latent forms of MMP-2 and MMP-9 have been described. We report herein the first such quantitative binding analysis by surface plasmon resonance (SPR) using highly purified recombinant enzymes and inhibitors (for reviews of SPR see Refs. 12–14). In addition, we report a quantitative analysis of the affinities of TIMP-1 and TIMP-2 for the active forms of either MMP-2 or MMP-9 both in the presence and absence of a substrate. These studies quantitatively define the nature of the unique interactions of MMP-2 and MMP-9 forms with TIMP-1 and TIMP-2.

EXPERIMENTAL PROCEDURES

Buffers—Buffer B (10 mM sodium acetate (pH 4.5)), buffer W (7.8 mM NaH_2PO_4, 8 mM Na_2HPO_4 (pH 7.2), 137 mM NaCl, 0.1 mM $CaCl_2$, 3 mM KCl, 1.5 mM KH_2PO_4, and 0.02% Tween 20), buffer C (50 mM Tris (pH 7.5), 150 mM NaCl, 5 mM $CaCl_2$, 0.02% Brij-35), buffer HA (25 mM Tris (pH 7.5), 25 mM NaCl, and 0.02% Brij-35), buffer R (50 mM Tris (pH 7.5), 5 mM $CaCl_2$, 0.01% Brij-35), and phosphate-buffered saline (10 mM $NaPO_4$ (pH 7.2), 150 mM NaCl) were used.

Proteins and Enzymes—Molecular weight marker proteins for SDS-PAGE were purchased from Bio-Rad. Human recombinant stromelysin 1 was the generous gift of Dr. Paul Cannon (Center for Bone and Joint Research, Palo Alto, CA). A recombinant C-terminal fragment of human MMP-2, comprising amino acids 440–660 (15), was the generous gift of Dr. G. I. Goldberg (Washington University, St. Louis, MO).

Chromatographic Supports—Gelatin-agarose (4% cross-linked), heparin-agarose, Reactive Red 120-agarose, and lectin lentil-Sepharose 4B were purchased from Sigma. A Resource S column and Sephadex-G50 (fine) were purchased from Pharmacia Biotech Inc.

Expression and Purification of Gelatinases and TIMPs—Human pro-MMP-2, pro-MMP-9, and their inhibitors TIMP-1 and TIMP-2 were expressed in a recombinant vaccinia virus mammalian cell expression system, as described earlier (16). Pro-MMP-2 and pro-MMP-9 were purified to homogeneity from the media of infected HeLa cells by gelatin-agarose chromatography, as described previously (16). The protein concentrations of pro-MMP-2 and pro-MMP-9 were determined using their molar extinction coefficients of 122,800 and 114,360 M^{-1} cm^{-1}, respectively (2). The MMP-2 45-kDa active form was isolated as described (17). The MMP-2 62-kDa species was freshly prepared by incubating pro-MMP-2 with 1 mM *p*-aminophenylmercuric acetate (dissolved in 200 mM Tris) for 30 min at 37 °C. Under these conditions, only the MMP-2 62-kDa species was detected by gelatin zymography. To isolate the MMP-9 82-kDa species, 1 mg of pro-MMP-9 was incubated

* This work was supported by National Institutes of Health Grant CA-61986 (to R. F.), a Wayne State University postdoctoral fellowship (to M. W. O.), and U. S. Army Grant DAMD17-97-1-7174 (to S. M.). The costs of publication of this article were defrayed in part by the payment of page charges. This article must therefore be hereby marked "*advertisement*" in accordance with 18 U.S.C. Section 1734 solely to indicate this fact.

‖ To whom correspondence should be addressed: Dept. of Pathology, Wayne State University, 540 E. Canfield Ave., Detroit, MI 48201. Tel.: 313-577-1218; Fax: 313-577-8180; E-mail: rfridman@med.wayne.edu.

[1] The abbreviations used are: MMP, matrix metalloproteinase; TIMP, tissue inhibitor of metalloproteinase; PAGE, polyacrylamide gel electrophoresis; Me_2SO, dimethyl sulfoxide; CTD, C-terminal domain; SPR, surface plasmon resonance; MT1-MMP, membrane type 1-MMP.

with 20 μg of a recombinant catalytic domain of stromelysin 1 for 2 h at 37 °C. The sample was subjected to gelatin-agarose column chromatography to remove the stromelysin 1, and the fractions containing the 82-kDa activated MMP-9 were detected by gelatin zymography. The protein concentrations of the active species of MMP-2 (45 kDa) and MMP-9 (82 kDa) were determined by amino acid analysis or from their molar extinction coefficients (18). The MMP-2 (45 kDa) and MMP-9 (82 kDa) species were distributed in aliquots, flash frozen in liquid nitrogen, and stored at −80 °C. Both enzymes were stable for at least 12 months at −80 °C, as determined by gelatin zymography.

Recombinant human TIMP-2 was purified from media of infected HeLa cells as described (16), with the exception that instead of the CM-Sepharose matrix, the medium containing TIMP-2 was chromatographed on a Resource S column. TIMP-1 was purified by lectin lentil-Sepharose chromatography, as described (17). The TIMP-1-containing fractions were pooled, dialyzed against buffer HA to an ionic equivalent of less than 50 mM NaCl, and loaded onto a heparin-agarose column (5 ml) equilibrated with the same buffer. After the column was washed with HA buffer supplemented with 100 mM NaCl, TIMP-1 was eluted with a linear gradient of NaCl (200–400 mM) in HA buffer. The TIMP-1-containing fractions were pooled and dialyzed against phosphate-buffered saline. The protein concentrations of the recombinant TIMP-1 and TIMP-2 were determined using their molar extinction coefficients of 26,500 and 39,600 M^{-1} cm^{-1}, respectively (3). Purified TIMP-1 and TIMP-2 were distributed in aliquots, flash frozen in liquid nitrogen, and stored at −80 °C.

SDS-Polyacrylamide Gel Electrophoresis and Zymography—SDS-polyacrylamide gel electrophoresis (SDS-PAGE) was performed according to Laemmli (19). The proteins were visualized by staining overnight with a 0.25% solution of Coomassie Brilliant Blue R-250 in 45% methanol and 10% acetic acid and destaining in a solution of 20% methanol and 10% acetic acid. Zymography in a 10% SDS-PAGE containing 0.1% gelatin was performed as described (20).

Radioiodination of TIMPs—TIMP-1 and TIMP-2 were iodinated with carrier-free $Na^{125}I$ (100 mCi/ml, Amersham Corp.) using IODO-GEN (Pierce). Briefly, glass vials were coated with 2 μg of IODO-GEN dissolved in 100% chloroform and dried with a stream of dry nitrogen. Twenty micrograms of either TIMP-1 or TIMP-2 were placed in an IODO-GEN-coated vial and allowed to incubate for 1 min at 25 °C. $Na^{125}I$ (200 μCi) was added to each vial, and the iodination reaction was allowed to continue for 2 min at 25 °C. The reaction was stopped by the addition of bovine serum albumin (fraction V, Sigma) and NaI (Sigma) to final concentrations of 1 mg/ml and 1 mM, respectively. Unincorporated $Na^{125}I$ was removed immediately using a 1-ml Sephadex-G50 (fine) spin column equilibrated in buffer C. The specific activity was determined by trichloroacetic acid-precipitable counts (>90% in the pellet), and the protein was quantitated by SDS-PAGE, Coomassie Blue staining of the gels, and densitometric scanning immediately after destaining. Densitometric analysis was performed using an AMBIS Image Analysis and Acquisition™ system (San Diego, CA) connected to a Dell 486/33 microcomputer equipped with the AMBIS Quant Probe™ software, version 4.01. The amount of ^{125}I-TIMPs was determined using known quantities of unlabeled purified TIMPs as standards electrophoresed in parallel. The specific activities of ^{125}I-TIMP-1 and ^{125}I-TIMP-2 were calculated to be 1.12 and 1.41 μCi/μg, respectively.

Determination of Kinetic and Equilibrium Constants by SPR—TIMP-gelatinase interaction studies were performed using a Fison Iasys™ instrument. CM5™ research grade cells (Fison Iasys™) were used for all experiments. The carboxymethyl dextran matrix of the sensor cell was activated for 6 min using 0.2 ml of a mixture of 0.2 M 1-ethyl-3-[(3-dimethylamino)propyl]-carbodiimide and 0.05 M *N*-hydroxysuccinimide. After activation, the sensor cell was washed rapidly four times with 200 μl of buffer W followed by immediate immobilization of TIMP-1 and TIMP-2. Immobilization conditions were as follows: TIMP-1 (2 μg) or TIMP-2 (1 μg) was covalently coupled to the activated matrix in buffer B at a stirring rate of 50 for 9 min at 25 °C, followed by a single 200-μl wash with buffer B. The unreacted *N*-hydroxysuccinimide esters were quenched by a 200-μl injection of 0.1 M ethanolamine-HCl (pH 8.0). Finally, the sensor cell was washed with four 200-μl injections of buffer W. Under these conditions, 300 arc seconds of TIMP-1 and 400 arc seconds of TIMP-2 were immobilized. TIMP-gelatinase binding reactions were carried out in buffer W at a stirring speed of 50 at 25 °C. The cell was regenerated after gelatinase binding with a single 15-s pulse of 200 μl of 20 mM HCl. These regeneration conditions allowed for the retention of greater than 95% of the original TIMP binding capacity. The equilibrium constants (K_d) were calculated from the rate constants for association (k_a) and dissociation (k_d) from the equation $K_d = k_d/k_a$. For biphasic binding $K_d = k_d(2)/k_a(1)$ and $k^d(1)/k_a(2)$ for the low and high affinity binding sites, respectively. The binding constants for each analyte protein were determined in duplicate using at least five different concentrations of analyte (8.7–624 nM), in a final volume of 200 μl, where the response increased as a function of analyte concentration. For TIMP-1 pro-MMP-9 and MMP-9 (82 kDa) were both titrated from 10 to 200 nM; pro-MMP-2 and MMP-2 (62 kDa) were titrated from 20 to 250 and from 20 to 200 nM, respectively; MMP-2 (45 kDa) and the MMP-2 CTD were titrated from 55 to 440 and from 80 to 1250 nM, respectively. For TIMP-2 pro-MMP-9 and MMP-9 (82 kDa) were titrated from 100 to 420 and from 20 to 220 nM, respectively; pro-MMP-2 and MMP-2 (62 kDa) were titrated from 8.5 to 70 and from 10 to 120 nM, respectively; MMP-2 (45 kDa) and the MMP-2 CTD were titrated from 50 to 500 and from 15 to 330 nM, respectively. Furthermore, each analyte protein (200 nM) was subjected to analysis using a derivatized sensor cell to determine the amount of nonspecific binding to the carboxymethyl dextran matrix. In each case, less than a 7-arc second increase was observed. The binding curves were analyzed using the nonlinear data fitting program "Iasys Fasffit™" using both monophasic and biphasic models to obtain the first-order association rate constant and the dissociation rate constant.

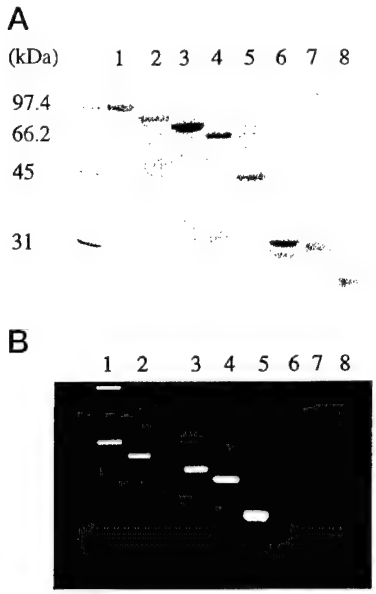

FIG. 1. **SDS-PAGE and zymographic analysis of purified gelatinases and TIMPs.** *A*, MMP-2 (latent and active species), MMP-9 (latent and active species), MMP-2 CTD, TIMP-1, and TIMP-2 were incubated for 120 min at 25 °C and subjected to 10% SDS-PAGE under reducing conditions. Proteins were detected by Coomassie Blue staining. *Lane 1,* pro-MMP-9 (2.5 μg). *Lane 2,* MMP-9 (82 kDa) (2 μg). *Lane 3,* pro-MMP-2 (2.5 μg). *Lane 4,* MMP-2 (62 kDa) (2.2 μg). *Lane 5,* MMP-2 (45 kDa) (2 μg). *Lane 6,* MMP-2 CTD (2 μg). *Lane 7,* TIMP-1 (3.5 μg). *Lane 8,* TIMP-2 (2 μg). *B*, MMP-2 and MMP-9 (latent and active species), MMP-2 CTD, TIMP-1, and TIMP-2 were incubated for 120 min at 25 °C and subjected to gelatin zymography. *Lane 1,* pro-MMP-9 (0.5 ng). *Lane 2,* MMP-9 (82 kDa) (0.15 ng). *Lane 3,* pro-MMP-2 (0.8 ng). *Lane 4,* MMP-2 (62 kDa) (0.2 ng). *Lane 5,* MMP-2 (45 kDa) (0.1 ng). *Lane 6,* MMP-2 CTD (100 ng). *Lane 7,* TIMP-1 (100 ng). *Lane 8,* TIMP-2 (115 ng).

Binding of TIMPs to Gelatinases in Solution—^{125}I-TIMP-1 or ^{125}I-TIMP-2 were incubated at 1:1 or 3:1 molar ratios with the latent and active forms of MMP-2 and MMP-9 for 30 min at 25 °C in buffer C. Binding reactions were carried out in 500 μl (final volume) where the concentration of the gelatinases was 25 nM or in 40 μl (final volume) where the concentration of enzymes was 450 nM. After binding, a 50-μl aliquot of gelatin-agarose matrix (a 50:50 slurry in buffer C) was added to each sample followed by incubation for 30 min at 25 °C. Each sample was centrifuged, washed three times with 400 μl of buffer C, and the resulting supernatant discarded. The radioactivity in the pellets was measured in a Packard 5650 gamma counter for 3 min. The amount of bound TIMP (pmol) was determined from the specific activity.

Gelatin-Agarose Chromatography of TIMP-Gelatinase Complexes—Pro-MMP-9 and pro-MMP-2 (200 pmol) were combined with TIMP-1 and TIMP-2 (600 pmol), respectively, in buffer C (final volume of 0.1 ml) and incubated for 40 min at 25 °C. These mixtures were then applied to a gelatin-agarose column (0.1 ml) and equilibrated with buffer C, and

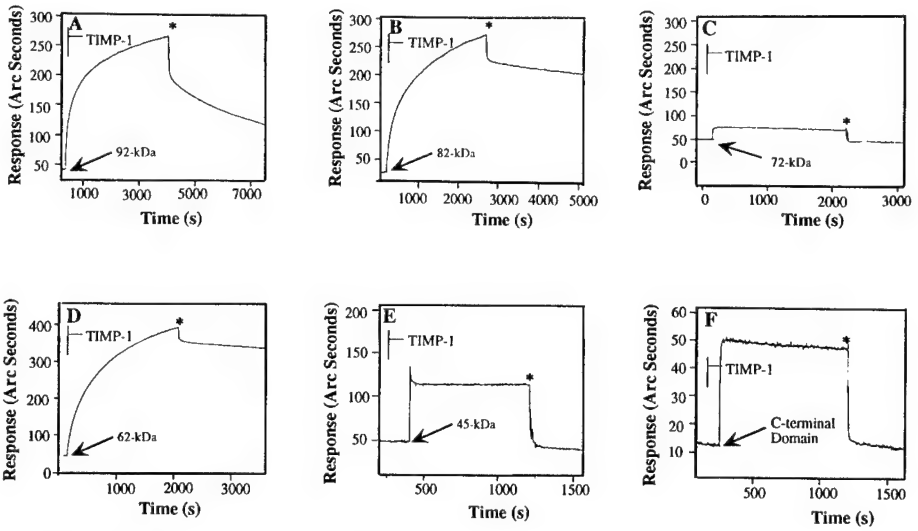

FIG. 2. **Sensorgrams of MMP-2 and MMP-9 binding to immobilized TIMP-1.** Latent and active MMP-2 and MMP-9 species were allowed to bind to TIMP-1 and examined by SPR as described under "Experimental Procedures." *A*, pro-MMP-9 (92 kDa), 40 nM. *B*, MMP-9 (82 kDa), 40 nM. *C*, pro-MMP-2 (72 kDa), 250 nM. *D*, MMP-2 (62 kDa), 65 nM. *E*, MMP-2 (45 kDa), 440 nM. *F*, MMP-2 CTD, 625 nM. The *asterisk* indicates the end of the association phase.

the flow-through fraction was collected. The column was washed with 0.4 ml of buffer C, and 0.1-ml fractions were collected. The protein complexes were eluted with buffer C supplemented with 10% dimethyl sulfoxide (Me_2SO), and 0.1-ml fractions were collected. Twenty-five microliters of each fraction were analyzed by SDS-PAGE. Quantitation of the TIMPs and gelatinases in the complexes was determined by densitometric scanning of Coomassie Blue-stained gels, as described above, using known amounts of standard proteins.

Fluorometric Activity Assay for MMP-2 and MMP-9—The active forms of MMP-2 and MMP-9 were assayed for activity using the fluorescence quenching substrate $MOAcPLGLA_2pr(Dnp)$-AR-NH_2 (Peptide Institute, Inc., Japan, and first described by Knight *et al.* (21)). The peptide substrate was dissolved in 100% Me_2SO. Each assay was carried out at 25 °C in 2 ml (final volume) of 50 mM HEPES (pH 7.5), 150 mM NaCl, 5 mM $CaCl_2$, 0.01% Brij-35, and Me_2SO (1% v/v), containing substrate and enzyme and/or inhibitor at the indicated concentrations. Substrate hydrolysis was monitored using a Spex Fluorolog 1681 (Spex Industries Inc.) fluorescence spectrophotometer with excitation and emission wavelengths set at 328 and 393 nm, respectively and controlled by an IBM-compatible computer using the dm3000 software provided by SPEX™. The slit widths were maintained at 1 mm and the band pass was 3 nm. Fluorescent measurements were taken every 20 s with a 3-s integration time.

For the determination of the K_m and k_{cat} values of the MMP-2 and MMP-9 active species, the fluorescent substrate was used in the concentration range of 0.05 to 6.5 μM with 0.4 pmol (0.2 nM) of enzyme. The reaction was allowed to proceed for 6 min, and the initial velocity of each reaction was determined using the data collected up to 4 min. Three reaction rate determinations were made for each substrate concentration. The K_m and V_{max} values were determined by double-reciprocal analysis by linear regression using LINEST (Microsoft Excel™ version 5.0).

To determine the association constants (k_{on}), the first-order binding constants were determined under the following conditions. The substrate concentration for each assay was 7 μM, a substrate concentration 2–4-fold greater than the experimentally determined K_m. TIMP-1 and TIMP-2 were added to the reaction, and the assay was initiated by addition of a 1 μM stock of enzyme to give a final concentration of 1 nM. The reaction was allowed to proceed for 10 min, and the rate of substrate cleavage was measured in triplicate for each TIMP concentration examined. For the MMP-2 45-kDa species, the concentrations of TIMP-1 and TIMP-2 were varied from 0 to 200 and from 0 to 100 nM, respectively. For the MMP-2 62-kDa species, both TIMP-1 and TIMP-2 were used in the concentration range of 0 to 30 nM. For the MMP-9 82-kDa species, TIMP-1 was used in the concentration range of 0 to 30 nM, and TIMP-2 was used in the concentration range of 0 to 60 nM. The first-order rate constant, k, was determined from the intersection point of the tangent to the curve at $I = \times$ to the curve at $I = 0$ where $k = 1/t$, as described by Morrison and Walsh (22), where the data points gave equal increments of product formation as a function of time in the absence of inhibitor. The first-order rate constant, k, for each TIMP concentration was plotted as a function of TIMP concentration. The slope and error of the slope of this line gives the on-rate, k_{on}, and was determined by linear regression using LINEST (Microsoft Excel™ v5.0).

The dissociation constants (k_{off}) were determined in triplicate as follows. The MMP-2 45-kDa species was combined with TIMP-1 or TIMP-2 at a final concentration of 2 μM enzyme and 2.4 μM of either TIMP-1 or TIMP-2. The enzyme and inhibitor were allowed to incubate for 1 h at 25 °C. The k_{off} value of TIMP-1 and TIMP-2 for the MMP-2 (62 kDa) and MMP-9 (82 kDa) species were determined similarly, except that the enzyme and inhibitor were incubated at concentrations of 300 and 360 nM, respectively, for 1 h at 25 °C. The sample was added to the cuvette (final volume of 2 ml) containing 12 μM peptide substrate and a final concentration of 1 nM enzyme. The recovery of enzyme activity was followed for up to 40 min. The data were analyzed by the method of Glick *et al.* (23). The error of the slope of this line was determined by linear regression using LINEST (Microsoft Excel™ version 5.0). The inhibition constants (K_i) were calculated by $K_i = k_{off}/k_{on}$.

RESULTS

Analysis of Purified Gelatinases and TIMPs—Determination of the binding constants for gelatinase-TIMP complexes requires pure enzymes and inhibitors. To this end, human recombinant latent and active MMP-2 and MMP-9 and TIMP-1 and TIMP-2 were purified to homogeneity. To address the role of the MMP-2 CTD and the catalytic site of MMP-2, we purified a C-terminally truncated MMP-2 45-kDa form (17) and obtained a purified recombinant CTD fragment (15). Fig. 1, *A* and *B*, demonstrates the purity and lack of any contaminating proteins in the samples used for kinetic analyses. Furthermore, active enzymes were not detected in the latent enzymes and vice versa (Fig. 1, *A* and *B*). Incubation of the enzymes for 120 min at 25 °C prior to electrophoresis confirmed their stability, an essential requirement for the SPR analysis.

SPR Analysis of Gelatinase-TIMP Interactions—The kinetic and equilibrium constants for gelatinase-TIMP interactions were determined by SPR (12–14) using a Fison Iasys™ instrument. Since both TIMP-1 and TIMP-2 are acid stable (3), the inhibitors were chemically linked to the carboxymethyl dextran matrix on a sensor cell as described under "Experimental Procedures." Dilute solutions of latent or active MMP-2 or MMP-9 species (analytes) were allowed to bind to the immobilized TIMPs as a function of time. The results of typical binding assays are shown in the sensorgrams of Figs. 2 and 3. Only pro-MMP-9, active MMP-9 (82 kDa), and active MMP-2 (62 kDa) bound to TIMP-1 (Fig. 2, *A*, *B*, and *D*). In contrast, MMP-2 (latent and active forms), its CTD, and active MMP-9 bound to TIMP-2 (Fig. 3, *B–F*). The arc second "responses" observed with pro-MMP-2, the 45-kDa species, and the CTD to immobilized TIMP-1 (Fig. 2, *C*, *E*, and *F*) or with pro-MMP-9 to immobilized TIMP-2 (Fig. 3*A*), even at concentrations approaching 650 nM analyte, represent merely a change in the refractive index and not specific binding. The same refractive index change was

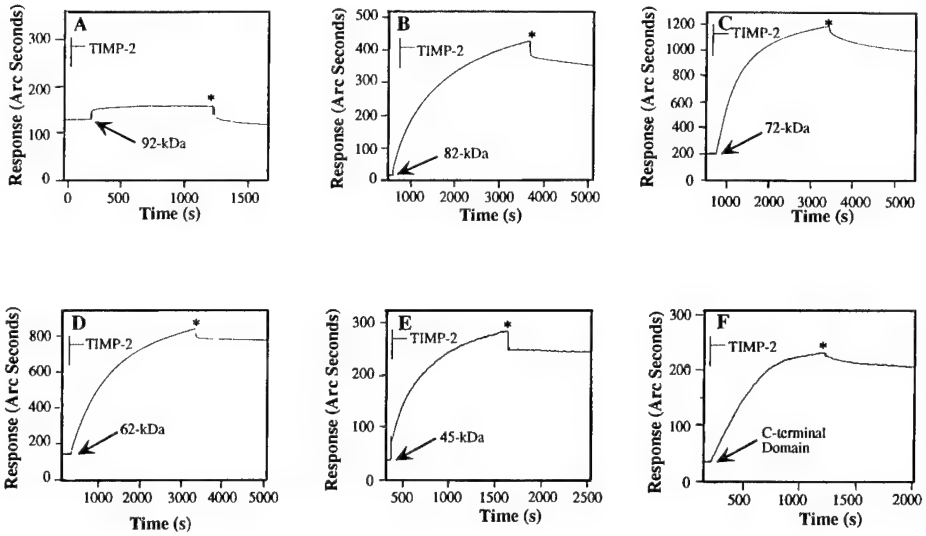

FIG. 3. **Sensorgrams of MMP-2 and MMP-9 binding to immobilized TIMP-2.** Latent and active MMP-2 and MMP-9 species were allowed to bind to TIMP-2 and examined by SPR as described under "Experimental Procedures." *A*, pro-MMP-9 (92 kDa), 205 nM. *B*, MMP-9 (82 kDa), 40 nM. *C*, pro-MMP-2 (72 kDa), 20 nM. *D*, MMP-2 (62 kDa), 20 nM. *E*, MMP-2 (45 kDa), 440 nM. *F*, MMP-2 CTD, 42 nM. The *asterisk* indicates the end of the association phase.

observed when the enzymes or domains thereof were allowed to bind to a sensor cell derivatized in the absence of TIMPs (data not shown).

SPR Analysis of Gelatinase-TIMP Interactions Reveal Low and High Affinity Sites—The association rate constant (k_a), dissociation rate constant (k_d), and equilibrium constant (K_d) of MMP-2 and MMP-9 forms for TIMP-1 and TIMP-2 were calculated from the data obtained from the Fison Iasys™ analyses (Table I and Table II). To determine if the data fit the monophasic or biphasic models for nonlinear curve fitting, the following criteria were followed. First, random residuals for the nonlinear curve fitting of both the association and dissociation phases were required. Second, replotting of the ln of the association phase *versus* time and of the ln of the dissociation phase *versus* time was required to fit the theoretical plot provided by the software program Iasys Fasffit™. Third, the root mean square deviation following nonlinear curve fitting for each model was required to be less than 1%. For the monophasic model, the root mean square deviation was consistently greater than 5% for the association and dissociation rate constant determinations. However, analysis of the data fit the biphasic model since it showed that the root mean square deviation value ranged between 0.001 and 0.38% for the first-order association rate constant and dissociation rate constant values. As shown in Tables I and II, these analyses indicated the existence of high and low affinity binding sites. The K_d values of TIMP-1 for the MMP-9 latent and active species were 35 and 23.9 nM for the high affinity site and 7.4 and 3.1 μM for the low affinity site, respectively. Interestingly, the k_a and k_d values of TIMP-1 for the latent and active MMP-9 forms and the MMP-2 (62 kDa) active species were similar for both the high and low affinity sites (Table I). With TIMP-2, the K_d values for the latent and active MMP-2 species and the active MMP-9 were 5.2, 23.1, and 57.9 nM for the high affinity site and 0.19, 2.7, 12.7 μM for the low affinity site, respectively (Table II). Binding of the active MMP-2 (45 kDa) species and the CTD to TIMP-2 only fit the monophasic model, where the root mean square deviation value was consistently less than 0.092% for the first-order association rate constant and dissociation rate constant values. This indicates a single binding site with K_d values of 315 and 61.6 nM, respectively (Table II). The lower K_d value for the TIMP-2·MMP-2 CTD complex suggests that the high affinity binding site resides within this domain.

Analysis of Gelatinase-TIMP Interactions in Solution—Previous studies suggested a 1:1 stoichiometry of gelatinase-TIMP complexes (9, 10, 24). Due to the nature of the SPR analysis that requires immobilization of TIMPs, we examined the binding of gelatinases to the inhibitors in solution. To this end, unlabeled or radioiodinated TIMPs were allowed to bind to gelatinases, and the resultant complexes were analyzed by gelatin-agarose precipitation and gelatin-agarose chromatography. Binding of TIMP-1 and TIMP-2 to the latent and active forms of MMP-2 and MMP-9 was examined at concentrations at or near the K_d values for the high affinity site as determined by SPR using equimolar concentrations of enzymes and inhibitors. To account for the presence of the low affinity site, we also carried out similar experiments using a 3-fold molar excess inhibitor. Complex formation of the gelatinases and TIMPs at or near the K_d value for the high affinity site would be expected to reflect TIMP:gelatinase ratios of 0.5:1 and 1:1, whereas binding in the presence of excess TIMP would be expected to show a stoichiometry greater than 1:1 due to the low affinity site. Binding of equimolar and 3-fold molar excess of either ^{125}I-TIMP-1 (Fig. 4*A*) or ^{125}I-TIMP-2 (Fig. 4*B*) to pro-MMP-9, MMP-9 (82 kDa), pro-MMP-2, and MMP-2 (62 kDa) demonstrated a stoichiometry of 0.65–0.84:1 (equimolar) and 0.9–0.94:1 (3-fold molar excess), indicating a 1:1 stoichiometry. Under the same conditions, the active MMP-2 (45 kDa) species showed no detectable binding to either TIMP-1 or TIMP-2 in agreement with the K_d value determined by SPR (Table II). Since the SPR data indicated the existence of a low affinity site with K_d values in the micromolar range (Tables I and II), we asked whether the stoichiometry of the enzyme-inhibitor complex could be forced to a ratio approaching 1:2 in solution. To this end, binding was carried out at concentrations of enzyme and inhibitor 20-fold greater than the K_d for the high affinity site and at either equimolar ratios or 3-fold molar excess inhibitor. Fig. 4, *C* and *D*, shows that at 1:1 molar ratios, the stoichiometry is 1:1, as expected from the K_d values determined by SPR. Under conditions of 3-fold molar excess inhibitor, gelatin-agarose precipitation experiments showed an increase in ^{125} I-TIMP binding to the enzymes with enzyme:inhibitor ratios of 1:1.4 to 1:1.8. In addition, coprecipitation of ^{125}I-TIMP-2 was observed with the active MMP-2 (45 kDa) species, consistent with a ~1:1 stoichiometry (Fig. 4*D*). In contrast, ^{125}I-TIMP-1 failed to coprecipitate with the 45-kDa species, regardless of the enzyme and TIMP concentrations used (Fig. 4, *A* and *C*).

Analysis of the stoichiometry of pro-MMP-2·TIMP-2 and pro-MMP-9·TIMP-1 complexes was also performed by densitometric analysis of SDS-polyacrylamide gels of enzyme-inhibitor complexes subjected to gelatin-agarose chromatography, as de-

TABLE I

Kinetic and equilibrium constants of gelatinase forms with TIMP-1 determined by SPR analysis

The errors for the k_a and k_d rate constants are expressed as the standard deviation of the slope and the standard deviation of five analyte concentrations, respectively, from two separate experiments. The errors for the K_d values represent the sum of the errors from the k_a and k_d values.

Analyte protein	$k_{a\,(1)}$	$k_{a\,(2)}$	$k_{d\,(1)}$	$k_{d\,(2)}$	K_d	K_d
	$M^{-1}\,s^{-1} \times 10^{-3}$		$s^{-1} \times 10^{3}$		μM	nM
MMP-9 species						
92 kDa	34.2 ± 0.2	4.0 ± 0.3	29.7 ± 3.9	1.2 ± 0.2	7.4 ± 0.9	35.0 ± 5.8
82 kDa	51.8 ± 0.1	7.4 ± 0.3	23.0 ± 3.2	1.2 ± 0.2	3.1 ± 0.4	23.9 ± 3.8
MMP-2 species						
72 kDa	NB[a]	NB	NB	NB		
62 kDa	44.0 ± 0.3	4.0 ± 0.7	33.9 ± 2.9	1.3 ± 0.2	8.5 ± 0.7	28.6 ± 4.5
45 kDa	NB	NB	NB	NB		
CTD	NB	NB	NB	NB		

[a] NB, no binding.

TABLE II

Kinetic and equilibrium constants of gelatinase forms with TIMP-2 determined by SPR analysis

The errors for the k_a and k_d rate constants are expressed as the standard deviation of the slope and the standard deviation of five analyte concentrations, respectively, from two separate experiments. The errors for the K_d values represent the sum of the errors from the k_a and k_d values.

Analyte protein	$k_{a\,(1)}$	$k_{a\,(2)}$	$k_{d\,(1)}$	$k_{d\,(2)}$	K_d	K_d
	$M^{-1}\,s^{-1} \times 10^{-3}$		$s^{-1} \times 10^{3}$		μM	nM
MMP-9 species						
92 kDa	NB[a]	NB	NB	NB		
82 kDa	22.8 ± 0.2	2.6 ± 0.2	33.1 ± 3.5	1.3 ± 0.2	12.7 ± 1.3	57.9 ± 7
MMP-2 species						
72 kDa	140.6 ± 0.6	24.7 ± 1.9	4.7 ± 0.4	0.7 ± 0.1	0.19 ± 0.02	5.2 ± 0.4
62 kDa	32.6 ± 0.3	4.8 ± 0.8	12.7 ± 0.6	0.8 ± 0.1	2.7 ± 0.1	23.1 ± 4.1
45 kDa	3.2 ± 0.2		1.0 ± 0.1			315 ± 34
CTD	92.1 ± 3.9		5.7 ± 0.9			61.6 ± 11

[a] NB, no binding.

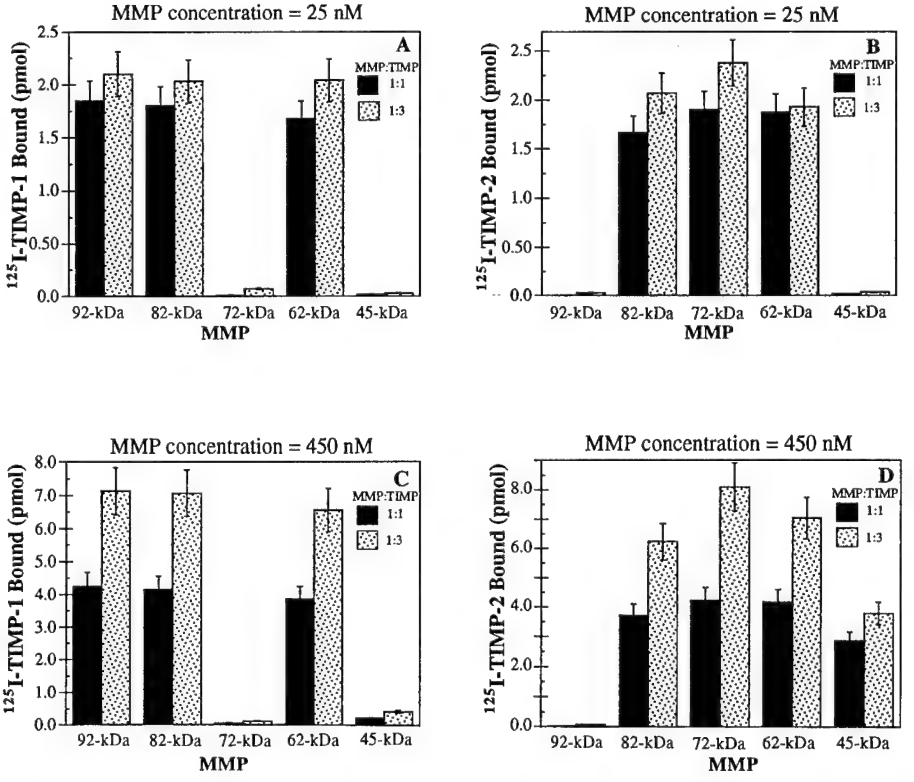

FIG. 4. **Coprecipitation of gelatinase-TIMP complexes.** ^{125}I-TIMP-1 and ^{125}I-TIMP-2 were allowed to bind to MMP-9 (latent and active species) and to MMP-2 (latent and active species) for 30 min at 25 °C, and the resulting complexes were subjected to precipitation with gelatin-agarose as described under "Experimental Procedures." *A*, gelatinases (25 nM) incubated with 25 nM (*solid bars*) or 75 nM (*dotted bars*) ^{125}I-TIMP-1. *B*, gelatinases (25 nM) incubated with 25 nM (*solid bars*) or 75 nM (*dotted bars*) ^{125}I-TIMP-2. *C*, gelatinases (450 nM) incubated with 450 nM (*solid bars*) or 1.4 μM (*dotted bars*) ^{125}I-TIMP-1. *D*, gelatinases (450 nM) incubated with 450 nM (*solid bars*) or 1.4 μM (*dotted bars*) ^{125}I-TIMP-2. The *error bars* represent the standard deviation from three independent determinations.

scribed under "Experimental Procedures." Densitometric analysis of the gels depicted in Fig. 5, *A* and *B*, revealed a stoichiometry ranging from 1.4:1 to 1.5:1 for the TIMP-1·pro-MMP-9 complex and from 1.5:1 to 1.6:1 for the TIMP-2·pro-MMP-2 complex (data not shown). Thus, at micromolar concentrations of enzyme and an excess of inhibitor, a second TIMP molecule can bind to the proenzyme form, in agreement with the data obtained by the coprecipitation experiments.

Catalytic Competence of Active Gelatinases—Previous studies reported "apparent" K_i values of TIMP-1 and TIMP-2 for

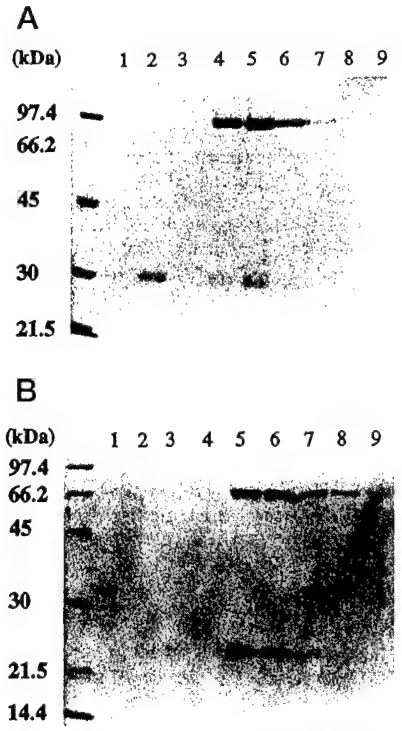

FIG. 5. **Gelatin-agarose chromatography of gelatinase-TIMP complexes.** *A*, TIMP-1 (600 pmol) and pro-MMP-9 (200 pmol) were allowed to complex for 40 min at 25 °C and subjected to gelatin-agarose column chromatography followed by 10% SDS-PAGE under reducing conditions as described under "Experimental Procedures." Proteins were detected by Coomassie Blue staining: *lane 1* wash fraction number 1; *lane 2*, wash fraction number 2; *lane 3*, wash fraction number 3; *lane 4*, elution fraction 1; *lane 5*, elution fraction 2; *lane 6*, elution fraction 3; *lane 7*, elution fraction 4; *lane 8*, elution fraction 5; *lane 9*, elution fraction 6. *B*, same as in *A* except that TIMP-2 (600 pmol) and pro-MMP-2 (200 pmol) were subjected to 12% SDS-PAGE. *Lane 1* wash fraction number 1; *lane 2*, wash fraction number 2; *lane 3*, wash fraction number 3; *lane 4*, wash fraction 4; *lane 5*, elution fraction 1; *lane 6*, elution fraction 2; *lane 7*, elution fraction 3; *lane 8*, elution fraction 4; *lane 9*, elution fraction 5.

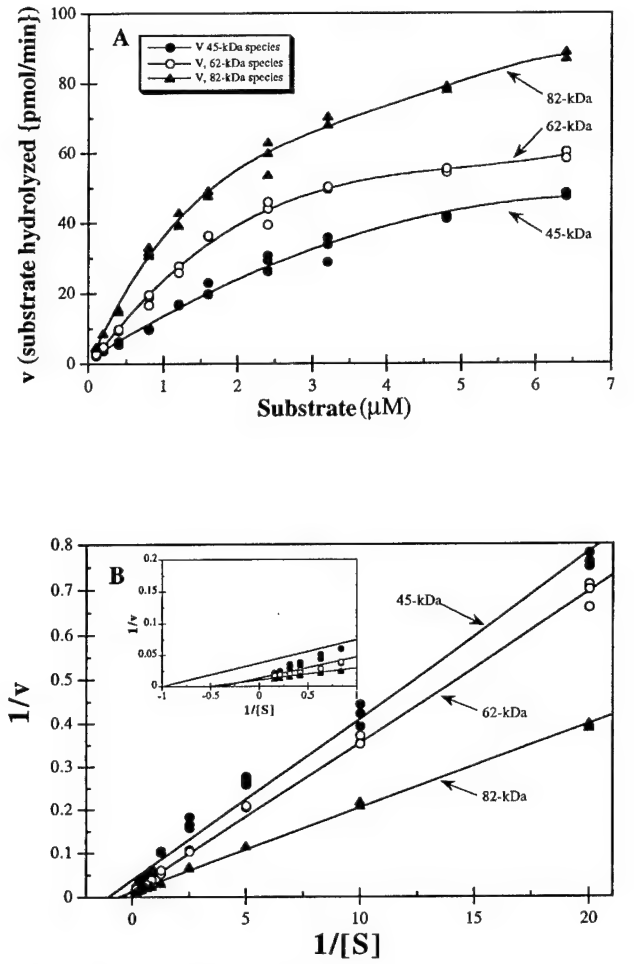

FIG. 6. **Initial velocity and double-reciprocal analysis for MMP-2 and MMP-9 active forms for MOAcPLGLA$_2$pr(Dnp)-AR-NH$_2$ hydrolysis.** *A*, initial rates were determined by the fluorescence peptide assay. Each assay was performed in triplicate, contained 0.4 pmol (0.2 nM) of enzyme, and was allowed to proceed for 6 min as described under "Experimental Procedures." *B*, Lineweaver-Burk Plot of the data from *A*. The *inset* in *B* represents a magnification of the substrate concentrations between 1.25 and 6.5 μM. *Open circles*, MMP-2 62-kDa species; *closed circles*, MMP-2 45-kDa species; *closed triangles*, MMP-9 82-kDa species.

MMP-2 and MMP-9 in the picomolar range (9, 10, 25). Since K_d is equal to K_i, when inhibition is studied, the data derived from SPR analysis indicated K_i values in the nanomolar range. Therefore, binding and affinity of the TIMPs for the gelatinases were evaluated using enzymatic activity assays with the peptide substrate MOAcPLGLA$_2$pr(Dnp)-AR-NH$_2$ (21). As shown in Fig. 6*A*, the enzymes show saturation kinetics in hydrolysis of the peptide substrate. Double-reciprocal analysis of the data (Fig. 6*B*) allowed for determination of the K_m, k_{cat}, and k_{cat}/K_m values (Table III). Insofar as K_m may approximate K_s, and as such give an expression of affinity, these enzymes show essentially the same affinity for the substrate with K_m values in the range of 1.5 to 3 μM. In addition, the correlation coefficient (r^2) values for the fitted lines are ~0.99 (Fig. 6*B*). Thus, the results indicate that all these enzymes are equally competent as catalysts in hydrolysis of the synthetic substrate with k_{cat}/K_m values equivalent to or greater than values obtained previously (10, 11).

Enzymatic Determination of the Inhibition Constant of TIMP-1 and TIMP-2 for the Gelatinases—We examined the binding of TIMP-1 and TIMP-2 to the active forms of MMP-2 and MMP-9 by enzyme inhibition assays as described under "Experimental Procedures." As shown in Fig. 7, TIMP-1 and TIMP-2 inhibit each enzyme. However, TIMP-1 failed to inhibit the active MMP-2 (45 kDa) species even at concentrations of 200 nM (Fig. 7*A*). The pattern of inhibition was consistent with a slow binding process (22). This type of behavior is characterized by the formation of curves that display a time-dependent onset of inhibition within the period that substrate turnover is linear in the absence of inhibitor. For slow binding inhibition, the first-order rate constant (k) is equal to the rate of product formation that is derived from the asymptote, where the k value is determined from the intersection point of the tangent to the curve at $t = 0$, as given by the expression $P = v_0 t$. The asymptote of the curve is given by the equation $P = v_S t + (v_0 - v_S)/k$. At this point, $k = 1/t$ (22). The association rate constant (k) for the formation of enzyme-inhibitor complexes is determined from these progress curves of substrate hydrolysis. The second-order rate constant (k_{on}) is provided by linear regres-

TABLE III
Enzymatic parameters for the hydrolysis of MOACPLG-A$_2$pr(DNP)-AR-NH$_2$ by gelatinases

The error is expressed as the standard deviation of the intercepts from three data sets.

Enzyme	K_m	k_{cat}	k_{cat}/K_m
	μM	s^{-1}	$M^{-1}\ s^{-1}$
MMP-9, 82 kDa	2.46 ± 0.34	4.41 ± 0.55	(17.9 ± 0.2) × 10^5
MMP-2, 62 kDa	3.06 ± 0.74	3.18 ± 0.46	(10.4 ± 0.2) × 10^5
MMP-2, 45 kDa	1.52 ± 0.29	1.30 ± 0.21	(8.6 ± 1.6) × 10^5

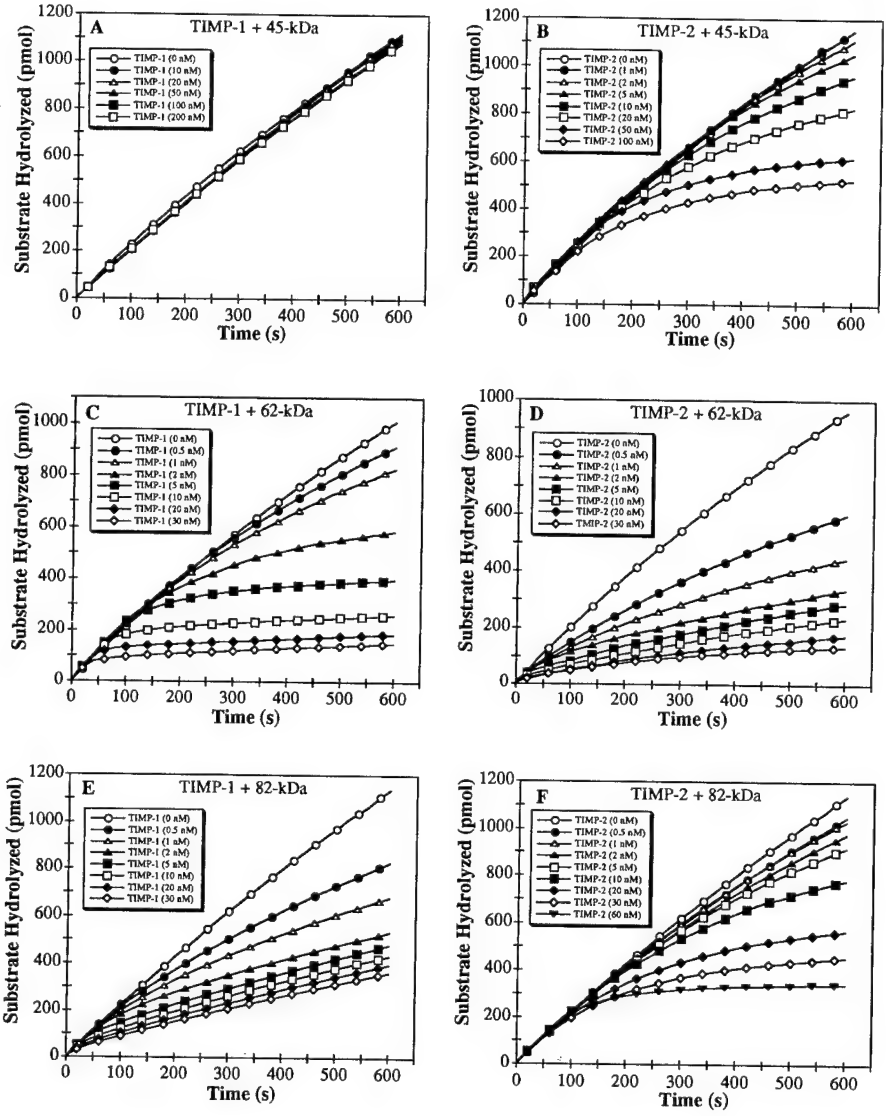

FIG. 7. **Slow binding inhibition of gelatinases by TIMP-1 and TIMP-2.** The active species of MMP-2 and MMP-9 (1 nM) were assayed with increasing concentrations of TIMP-1 and TIMP-2 as described under "Experimental Procedures." *A*, *C*, and *E*, TIMP-1 with MMP-2 (45 kDa), MMP-2 (62 kDa), and MMP-9 (82 kDa), respectively. *B*, *D*, and *F*, TIMP-2 with MMP-2 (45 kDa), MMP-2 (62 kDa), and MMP-9 (82 kDa), respectively.

sion of k as a function of inhibitor concentration. The off-rate (k_{off}) was determined by the recovery of enzyme activity (Fig. 8).

Tables IV and V show the k_{on} and k_{off} values using the analysis described above. TIMP-1 inhibits both MMP-9 (82 kDa) and MMP-2 (62 kDa) enzymes with comparable rate constants for inhibition onset (k_{on}) and recovery of activity (k_{off}), and by consequence result in similar K_i values (8.5 and 9.7 nM, respectively). The k_{on} is fast ($>10^5$ M^{-1} s^{-1}) and k_{off} is slow ($\sim 10^{-3}$ s^{-1}), resulting in effective inhibition. The same trend is true for TIMP-2 with MMP-9 (82 kDa) and MMP-2 (62 kDa) enzymes (K_i values of 43.4 and 7.2 nM, respectively). For the active MMP-2 (45 kDa) species, the k_{on} (1.4×10^4 M^{-1} s^{-1}) was considerably slower resulting in a K_i value of 275 nM, indicative of a relatively poor affinity of the inhibitor for the truncated enzyme. The k_{on} values (Tables IV and V) of TIMP-1 for MMP-2 (62 kDa) and MMP-9 (82 kDa) and of TIMP-2 for MMP-2 (62 and 45 kDa) and MMP-9 (82 kDa) species were consistently greater (2.5 to 7-fold) than those determined by SPR (Tables I and II). Likewise, the k_{off} values (Tables IV and V) were 1.5 to 3-fold higher than those determined by SPR (Tables I and II). The calculated K_i values of TIMP-1 and TIMP-2 for the MMP-2 (62 and 45 kDa) and MMP-9 (82 kDa) (Tables IV and V) species were in the nanomolar range and within 3-fold of the K_d values determined by SPR (Tables I and II).

DISCUSSION

We have carried out a comprehensive study to determine the kinetic parameters for the binding of TIMP-1 and TIMP-2 to the latent and active forms of MMP-2 and MMP-9. The results of the SPR analyses were consistent with previous studies (4, 5, 9–11) demonstrating binding of TIMP-1 to the latent and active MMP-9 and MMP-2 (62 kDa) species, and binding of TIMP-2 to the latent and active MMP-2 species, and the active form of MMP-9 (82 kDa). In addition, TIMP-1 and TIMP-2 failed to interact with pro-MMP-2 and pro-MMP-9, respectively (for reviews see Refs. 2 and 3), as expected. We have also shown that TIMP-1, in contrast to TIMP-2, did not bind to the CTD of MMP-2 or to the MMP-2 45-kDa species. SPR methodology for analysis of TIMP-MMP interactions was used in a previous study by Bodden *et al.* (26) which demonstrated k_a, k_d, and K_d values of 8.9×10^4 M^{-1} s^{-1}, 3.6×10^{-4} s^{-1}, and 4.1 nM, respectively, for the complex of TIMP-1 with active MMP-1. The K_d values of the MMP-1/TIMP-1 interaction (determined by SPR) are 7- and 14-fold lower than those for TIMP-1 with the active MMP-9 (82 kDa) and MMP-2 (62 kDa) species, respectively, as reported here. This suggests that TIMP-1 may be a more efficient inhibitor of MMP-1 than of MMP-9 and MMP-2.

Previous studies demonstrated that binding of TIMP-1 and

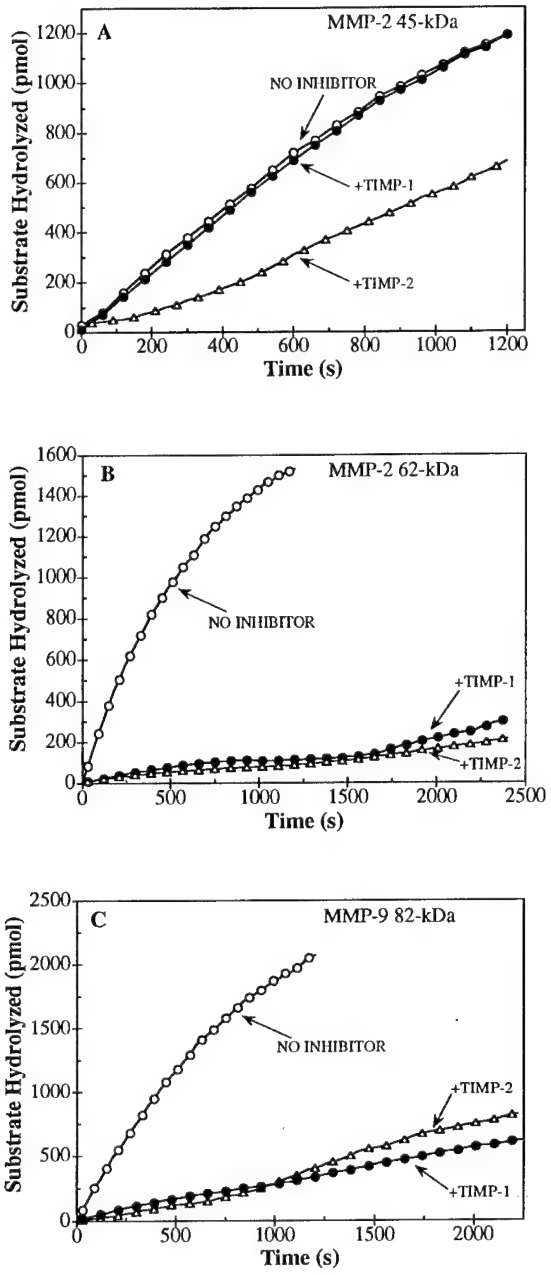

FIG. 8. **Dissociation of the MMP-2 and MMP-9 active species from TIMP-1 and TIMP-2.** The active species of MMP-2 and MMP-9 were preincubated with TIMP-1 and TIMP-2, and then the recovery of activity was monitored as described under "Experimental Procedures." *Open circles*, enzymes without TIMPs; *closed circles*, enzymes with TIMP-1; and *open triangles*, enzymes with TIMP-2. *A*, substrate hydrolysis by active MMP-2 (45 kDa). *B*, substrate hydrolysis by active MMP-2 (62 kDa). *C*, substrate hydrolysis by active MMP-9 (82 kDa).

TIMP-2 to MMP-9 and MMP-2 is mediated by two distinct domains of the inhibitor molecules and two domains of the enzymes (3, 9–11, 25, 27). The N-terminal domains of TIMPs were shown to bind to the enzymes within the active site domain, and the C-terminal regions of TIMPs were shown to bind to the C-terminal domain of the enzyme. Consistent with this model, we have found biphasic binding kinetics of TIMP-1 for MMP-9 (the latent and active forms) and MMP-2 (62 kDa) active form and of TIMP-2 for active MMP-9 (82 kDa) and MMP-2 (72- and 62-kDa species) that were indicative of the existence of high and low affinity binding sites. This was further supported by the results with the CTD of MMP-2 and the MMP-2 (45 kDa) species that, in contrast to pro-MMP-2 and

TABLE IV
Association, dissociation and inhibition constants for gelatinase/TIMP-1 interactions

The errors for the k_{on} and k_{off} values are expressed as the deviation of the slopes. The error for K_i value is the sum of the error from the k_{on} and k_{off} values.

Enzyme	k_{on}	k_{off}	K_i
	$M^{-1}\ s^{-1} \times 10^{-5}$	$s^{-1} \times 10^{3}$	nM
MMP-9, 82 kDa	2.48 ± 0.47	2.1 ± 1.1	8.5 ± 2.9
MMP-2, 62 kDa	2.46 ± 0.17	2.4 ± 0.7	9.7 ± 1.7
MMP-2, 45 kDa	NB[a]	NB	NB

[a] NB, no binding.

TABLE V
Association, dissociation and inhibition constants for gelatinase/TIMP-2 interactions

The errors for the k_{on} and k_{off} values are expressed as the deviation of the slopes. The error for K_i value is the sum of the error from the k_{on} and k_{off} values.

Enzyme	k_{on}	k_{off}	K_i
	$M^{-1}\ s^{-1} \times 10^{-5}$	$s^{-1} \times 10^{3}$	nM
MMP-9, 82 kDa	0.57 ± 0.03	2.5 ± 0.6	43.4 ± 7.4
MMP-2, 62 kDa	2.23 ± 0.64	1.6 ± 0.6	7.2 ± 2.5
MMP-2, 45 kDa	0.14 ± .01	3.8 ± 0.5	275 ± 31.1

active MMP-2 (62 kDa), showed monophasic binding kinetics with TIMP-2. Thus, the data obtained with the 45-kDa species and the CTD suggest that the latter contains the high affinity site, whereas the lower affinity binding site resides within the catalytic domain. SPR analysis of the 45-kDa species also suggested the contribution of the CTD for the binding of TIMP-2 to the low affinity site. Indeed, the K_d value describing the affinity of TIMP-2 for the 45-kDa species (315 nM) was 8.5-fold lower than that for the low affinity site of TIMP-2 for the MMP-2 62-kDa form (2.7 μM), which presumably resides within the catalytic domain. Thus, removal of the CTD appears to increase the affinity of TIMP-2 for the catalytic domain. Alternatively, the low affinity site in the MMP-2 62-kDa enzyme may be different from that in the 45-kDa species, and its accessibility is only possible after removal of the CTD. The lack of any measurable binding of TIMP-1 to both the 45-kDa active species and the CTD were unexpected since the 62-kDa form bound TIMP-1 with high affinity. Since the binding of the 62-kDa species to TIMP-1 also showed biphasic binding, it is possible that the CTD of MMP-2 may work synergistically with the active site in promoting TIMP-1 binding.

The contribution of the N-terminal prodomain of the gelatinases for the binding of TIMPs was also made apparent by the SPR analysis, particularly with MMP-2. Here, removal of the N-terminal prodomain resulted in a decreased affinity of TIMP-2 for the active (62 kDa) form, at both the low (14-fold reduction) and high affinity (5-fold reduction) sites. In contrast, this effect was less apparent with MMP-9 and TIMP-1. The affinity of TIMP-1 to both the low and high affinity sites for pro-MMP-9 and active MMP-9 varied by approximately 2-fold. Nevertheless, it was interesting to observe biphasic binding of TIMP-1 to pro-MMP-9 since the N-terminal prodomain has been suggested to preclude pro-MMP-9/TIMP-1 interaction at sites other than the CTD (3, 10). Thus, the SPR data suggest that TIMP-1 may also bind to a site different than the CTD of pro-MMP-9.

The biphasic binding observed by SPR agreed with data obtained in the solution binding experiments and were consistent with a 1:1 stoichiometry. These studies also showed that latent and active gelatinase forms, except for the 45-kDa MMP-2 species, can bind a second TIMP molecule under conditions of excess inhibitor and at micromolar concentrations.

We have also observed that binding of gelatinases to the TIMPs, at concentrations near or below the K_d values, for the high affinity sites showed sub-stoichiometric enzyme-inhibitor complexes consistent with K_d values in the nanomolar range. Likewise, binding at concentrations greater than the K_d values for the high affinity sites resulted in the generation of near-stoichiometric complexes. Taken together, these data suggest that the two sites of interaction are unique and can bind inhibitor independently. It is difficult to envision the evolutionary reason for conservation of the second TIMP binding site, if it were irrelevant *in vivo*. The existence of the second site awaits resolution of the crystal structures of the gelatinase-TIMP complexes. Furthermore, regarding pro-MMP-2, the interaction of this enzyme with TIMP-2 will have to be addressed in the context of a current model describing the association of pro-MMP-2 with a MT1-MMP·TIMP-2 complex (7).

We determined the k_{on}, k_{off}, and K_i values by enzyme inhibition analysis and demonstrated that both TIMP-1 and TIMP-2 behave as slow binding inhibitors. Using kinetic treatment for slow binding inhibition (22), the results indicated that the association of TIMPs and gelatinases is rapid ($k_{on} \sim 10^5\ M^{-1}\ s^{-1}$). Furthermore, the dissociation of the enzyme-inhibitor complexes was slow ($k_{off} \sim 10^{-3}\ s^{-1}$), resulting in a very effective inhibition of activity. The k_{off} values were determined from recovery of enzyme activity as a function of time, which allowed for the determination of the K_i value. This value was calculated to be in the nanomolar range, similar to the results obtained by the SPR analysis. Also, in agreement with the SPR results, the enzyme-inhibition studies demonstrated that the 45-kDa species of MMP-2 exhibited a 35-fold reduction in affinity (275 nM) for TIMP-2 when compared with the 62-kDa enzyme. Similar to these results, Taylor *et al.* (28) showed a 10–20-fold decrease in the affinity (247 nM) of TIMP-1 for a C-terminally truncated MMP-1 as opposed to the full-length active enzyme. Collectively, these findings support the importance of the C-terminal domain for the effective inhibition by TIMPs among distinct members of the MMP family.

Previous studies determined that the K_i values of TIMP-1 and TIMP-2 for MMP-2 and MMP-9 are in the $\leq 10^{-9}$ M range (9, 10, 25). However, these K_i values were reported as apparent in nature (9, 10). Nevertheless, these values are 3–4 orders of magnitude lower that the K_d and K_i values reported herein using SPR and enzyme-inhibition studies, respectively. This discrepancy may be due to differences in the following: (i) substrate (0.5 μM, Ref. 9, *versus* 7 μM); (ii) enzyme (0.05 nM, Ref. 9, *versus* 1 nM); and (iii) inhibitor (0.1 nM, Ref. 9, *versus* 0.5–30 nM) concentrations for association rate determinations; and (iv) differences in enzyme and inhibitor concentrations used in the determination of the dissociation rate constants (0.002 nM, Ref. 9, *versus* 1 nM). Furthermore, regarding the MMP-9·TIMP-1 complex, k_{off} values were not determined; thus, K_i values could not be obtained (10). Our data, however, are in close agreement with the SPR analysis and the enzyme inhibition studies performed by others. Yu *et al.*[2] recently reported that pro-MMP-2 binds to immobilized TIMP-2 with biphasic kinetics and with a K_d value of ~4 nM. Also, Bodden *et al.* (26) reported K_d values of 4.1 nM by SPR analysis for a complex of active MMP-1 with TIMP-1, and Taylor *et al.* (28) reported K_d values of ~20 and 8 nM for MMP-1 with TIMP-1 by enzyme inhibition studies.

[2] Yu, A. E., Fisher, R. J., Kleiner, D. E., and Stetler-Stevenson, W. G. (1996) Abstract from the Inhibitors of Metalloproteinases in Development and Disease TIMPs, September 25–29, 1996, Banff, Alberta, Canada.

It is significant that the SPR analysis, which evaluates protein-protein interactions without regard for inhibition of enzymatic activity, indicated biphasic behavior and provided K_d values for the high affinity site similar to the K_i values determined from enzyme inhibition assays. The fact that the kinetics of inhibition are monophasic clearly indicates that one binding event accounts for the onset of enzymatic inhibition. However, the presence of a second gelatinase-TIMP interaction site in the latent and active forms was clearly evident in the SPR experiments with the 45-kDa species of MMP-2 and the CTD fragment. The role of the second site in manifestation of enzyme inhibition is unclear. We wish to underscore that the kinetic parameters for enzyme inhibition corresponded closely (within 3-fold) to those for the high affinity phase of the protein-protein interaction determined by SPR analysis. Thus, two entirely distinct analyses provided essentially similar results. The ultimate structural information should await elucidation of the crystal structures for the gelatinases and gelatinase-inhibitor complexes.

Acknowledgments—We are indebted to Drs. Steven Ledbetter and Roger Poorman (Pharmacia-Upjohn) for their assistance with the use of the Fison Iasys™ instrument, to Dr. G. I. Goldberg (Washington University, St. Louis, MO) for providing the CTD of MMP-2, and to Dr. Paul Cannon (Center for Bone and Joint Research, Palo Alto, CA) for the human stromelysin 1.

REFERENCES

1. Matrisian, L. (1990) *Trends Genet.* **6,** 121–125
2. Murphy, G., and Crabbe, T. (1995) *Methods Enzymol.* **248,** 470–484
3. Murphy, G., and Willenbrock, F. (1995) *Methods Enzymol.* **248,** 496–510
4. Goldberg, G. I., Marrmer, B. L., Grant, G. A., Eisen, A. Z., Wilhelm, S., and He, C. (1989) *Proc. Natl. Acad. Sci. U. S. A.* **86,** 8207–8211
5. Wilhelm, S. M., Collier, I. E., Marmer, B. L., Eisen, A. Z., Grant, G. A., and Goldberg, G. I. (1989) *J. Biol. Chem.* **264,** 17213–17221
6. Will, H., Atkinson, S. J., Butler, G. S., Smith, B., and Murphy, G. (1996) *J. Biol. Chem.* **271,** 17119–17123
7. Strongin, A. Y., Collier, I., Bannikov, G., Marmer, B. L., Grant, G. A., and Goldberg, G. I. (1995) *J. Biol. Chem.* **270,** 5331–5338
8. Pei, D., and Weiss, S. J. (1996) *J. Biol. Chem.* **271,** 9135–9140
9. Willenbrock, F. Crabbe, T., Slocombe, P. M., Sutton, C. W., Docherty, A. J. P., Cockett, M. I., O'Shea, M., Brocklehurst, K., Phillips, I. R., and Murphy, G. (1993) *Biochemistry* **32,** 4330–4337
10. O'Connell, J. P., Willenbrock, F., Docherty, A. J. P., Eaton, D., and Murphy, G. (1994) *J. Biol. Chem.* **269,** 14967–14973
11. Nguyen, Q., Willenbrock, F., Cockett, M. I., O'Shea, M., Docherty, A. J. P., and Murphy, G. (1994) *Biochemistry* **33,** 2089–2095
12. O'Shannessy, D. J., Brigham-Burke, K., Soneson, K., Hensley, P., and Brooks, I. (1994) *Methods Enzymol.* **240,** 323–349
13. Karlsson, R., Michealsson, A., and Mattsson, L. (1991) *J. Immunol. Methods* **145,** 229–240
14. Malmqvist, M. (1993) *Nature* **361,** 186–187
15. Lisbon, A. M., Gittis, A. G., Collier, I. E., Marmer, B. L., Goldberg, G. I., and Lattman, E. E. (1995) *Nat. Struct. Biol.* **11,** 938–942
16. Fridman, R., Fuerst, T. R., Bird, R. E., Hoyhtya, M., Oelkuct, T. M., Kraus, S., Komarek, D., Liotta, L. A., Berman, M. L., and Stetler-Stevenson, W. G. (1992) *J. Biol. Chem.* **267,** 15398–15405
17. Fridman, R., Toth, M., Peña, D., and Mobashery, S. (1995) *Cancer Res.* **55,** 2548–2555
18. Gill, S. C., and von Hippel, P. H. (1989) *Anal. Biochem.* **182,** 319–326
19. Laemmli, U. K. (1970) *Nature* **227,** 680–685
20. Brown, P. T., Levey, A. T., Margulies, I. M. K., Liotta, L. A., and Stetler-Stevenson, W. G. (1990) *Cancer Res.* **50,** 6184–6191
21. Knight, C. G., Willenbrock, F., and Murphy, G. (1992) *FEBS Lett.* **296,** 263–266
22. Morrsion, J. F., and Walsh, C. T. (1988) *Adv. Enzymol. Relat. Areas Mol. Biol.* **61,** 201–301
23. Glick, B. R., Brubacher, L. J., and Leggett, D. J. (1978) *Can. J. Biochem.* **56,** 1055–1057
24. Stetler-Stevenson, W. G., Krutzsch, H. C., and Liotta L. A. (1989) *J. Biol. Chem.* **264,** 17374–17378
25. Murphy, G. Willenbrock, F., Ward, R. V., Cockett, M. I., Eaton, D., and Docherty, A. J. P. (1992) *Biochem. J.* **283,** 637–641
26. Bodden, M. K., Harber, G. J., Birkedal-Hansen, B., Windsor, L. J., Caterina, N. C. M., Engler, J. A., and Birkedal-Hansen, H. (1994) *J. Biol. Chem.* **269,** 18943–18952
27. Murphy, G., Houbrechts, A., Cockett, M. I., Williamson, R. A., O'Shea, M., and Docherty, A. J. P. (1991) *Biochemistry* **30,** 8097–8102
28. Taylor, K. B., Windsor, J., Caterina, N. C. M., Bodden, M. K., and Engler, J. A. (1996) *J. Biol. Chem.* **271,** 23938–23945

Appendix III

Pergamon

Bioorganic & Medicinal Chemistry Letters 8 (1998) 853–858

BIOORGANIC & MEDICINAL CHEMISTRY LETTERS

STRUCTURAL INSIGHT INTO THE BINDING MOTIFS FOR THE CALCIUM ION AND THE NON-CATALYTIC ZINC IN MATRIX METALLOPROTEASES

Irina Massova, Lakshmi P. Kotra, and Shahriar Mobashery*

Department of Chemistry, Wayne State University, Detroit, MI 48202-3489, U.S.A.

Received 19 January 1998; accepted 23 February 1998

Abstract: The binding motifs for the structural zinc and calcium ions in matrix metalloproteases (MMPs) were investigated by analyzing the three-dimensional structural models of 23 representative MMPs.

Matrix metalloproteinases (MMPs) constitute a major group of proteases that carry out a myriad of physiological and pathological functions. These functions include embryogenesis, angiogenesis, wound healing, inflammation, arthritis, and cancer metastasis.[1,2] These enzymes are zinc-dependent endopeptidases known for their ability to cleave extra-cellular matrix constituents, as well as non-matrix proteins. MMPs have developed into a unique group of zinc-dependent proteinases characterized by the incorporation of various protein domains in their structures, which mediate interactions with substrates and inhibitors.[3] The implication of MMPs in cancer metastasis and angiogenesis has raised considerable interest in the MMP family since they represent attractive targets for development of novel anticancer drugs. Therefore, understanding of the structure and function of these key enzymes would have significant implications toward these efforts.

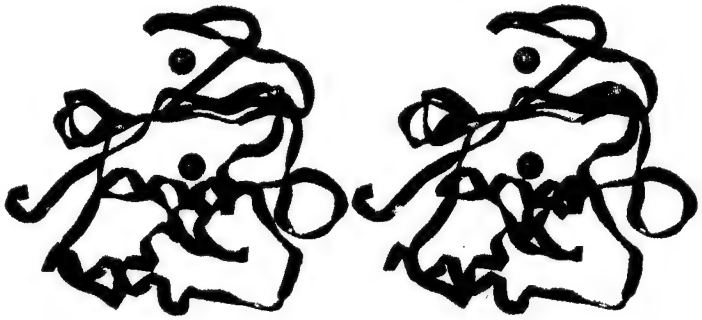

Figure 1. Stereo view of the ribbon drawing of the backbone of the catalytic domain of MMP-19. The red sphere represents the catalytic zinc ion, the green sphere represents the structural zinc ion and the orange sphere represents the calcium ion.

A total of 64 MMPs have been sequenced to date, of which 15 are from human. These human enzymes have counterparts in other vertebrates. Furthermore, MMPs have even been identified in invertebrates[4-6] and three have recently been sequenced from plant sources.[7] MMPs, in general, possess a propeptide domain (N-terminal), a catalytic domain and a hemopexin-like domain (C-terminal; except for MMP-7 which lacks it).[8] MMP-2 and -9 further possess a fibronectin-like domain and membrane-type MMPs (MT-MMPs) have acquired a transmembrane domain. In the catalytic domain, there are two zinc ions and at least one calcium ion coordinated to various residues (Figure 1). One of the two zinc ions is present in the active site, and is intimately involved in

0960-894X/98/$19.00
PII: S0960-894X(98)00128-0

binding to this structural zinc ion. For the majority of MMPs (except for MMP-11, MMP-17, CMMP and XMMP), this site consists of the side chains of an aspartic acid and three histidine residues; which are consistent with the existing crystal structures. Two of the coordinating histidine imidazoles are bound as His_δ and one as His_ε (Figure 2; the three-dimensional structure of this site is shown in Figure 3A). The signature for this site in the 60 MMPs is the sequence(s) ***H*$_\delta$-[GN]-*D*-X(2)-[PAS]-F-*D*-[GA]-X(4)-[LIRV]-[AG]-*H*$_\delta$-[AV]-[FYS]-P-X(5,7,9)-*H*$_\varepsilon$-[FL]-*D*-X(2)-*E*-X-W**, where residues that provide side chains for coordination to zinc and calcium are shown in bold italics, X (5,7,9) indicates 5, 7, or 9 variable residues in between the flanking sites (H_δ is a histidine protonated at $N_{\delta 1}$ and H_ε is a histidine protonated at $N_{\varepsilon 2}$). The first phenylalanine and the second phenylalanine/tyrosine (i.e., the FYS sequence) in this pattern are brought close to the coordinated histidines by the enzyme fold. This creates an increased hydrophobic environment, which presumably would enhance the binding affinity for the metal ions. The human MMP-11 has an aspartic acid instead of one of the His_δ. This is in contrast to the MMP-11 from rabbit and mouse, which still have a histidine at this position (data not shown). Therefore, we conclude that MMP-11 (compared to those from human, rabbit and mouse) does not have a unique motif for binding of the structural zinc.

```
MMP-1 human        DIMISFVRGDHRDNSP-FDG PGGNLAHAFQPGPGIGGD-AHFDEDERWTNN---------
MMP-2 human        DIMINFGRWEHGDGYP-FDG KDGLLAHAFAPGTGVGGD-SHFDDDELWTLGEGQVVRVKY
MMP-3 human        DIMISFAVREHGDFYP-FDG PGNVLAHAYAPGPGINGD-AHFDDDEQWTKD---------
MMP-7 human        DIMIGFARGAHGDSYP-FDG PGNTLAHAFAPGTGLGGD-AHFDEDERWTDG---------
MMP-8 human        DINIAFYQRDHGDNSP-FDG PNGILAHAFQPGQGIGGD-AHFDAEETWTNT---------
MMP-9 human        DIVIQFGVAEHGDGYP-FDG KDGLLAHAFPPGPGIQGD-AHFDDDELWSLGKGVVVPTRF
MMP-10 human       DIMISFAVKEHGDFYS-FDG PGHSLAHAYPPGPGLYGD-IHFDDDEKWTED---------
MMP-11 human       DIMIDFARYWDGDDLP-FDG PGGILAHAFFPKTHREGD-VHFDYDETWTIGDDQ------
MMP-12 human       DILVVFARGAHGDFHA-FDG KGGILAHAFGPGSGIGGD-AHFDEDEFWTTH---------
MMP-13 human       DIMISFGIKEHGDFYP-FDG PSGLLAHAFPPGPNYGGD-AHFDDDETWTSS---------
MT1-MMP human      DIMIFFAEGFHGDSTP-FDG EGGFLAHAYFPGPNIGGD-THFDSAEPWTVRNEDL-----
MT2-MMP human      DIMVLFASGFHGDSSP-FDG TGGFLAHAYFPGPGLGGD-THFDADEPWTFSSTDL-----
MT3-MMP human      DIPIIFASGFHGDSSP-FDG EGGFLAHAYFPGPGIGGD-THFDSDEPWTLGNPNH-----
MT4-MMP human      DIQIDFSKADHNDGYP-FDA -RRHRAHAFFPGHHHTAGYTHFNDDEAWTFRSSDA-----
MMP19 human        DIRLSFHGRQSSYCSNTFDG PGRVLAHADIPELG----SVHFDEDEFWTEGTY-------
Collagenase-4 frog DIEISFTAGDHKDNSP-FDG SGGILAHAFQPGNGIGGD-AHFDEDETWTKT---------
MMP newt           DIQISFGAREHGDFNP-FDG PYGTLAHAFAPGTGIGGD-AHFDEDEKWSKV---------
CMMP chicken       DIMVAFGTKAHGHCPRYFDG PLGVLAHAFPPGSGFGGD-VHFDEDEDWTMG---------
Enamelysin pig     DIMISFETGDHGDSYP-FDG PRGTLAHAFAPGEGLGGD-THFDNAEKWTMG---------
Envelysin          DIRIKFGSYDHGDGIS-FDG RGGVLAHAFLPRNG----DAHFDDSETWTEGTR-------
MMP nematode       DIYIAFEKGEHSDGFP-FDG QDGVVAHAFYPRDG----RLHFDAEEQWSLNSV-------
XMMP frog          DIKLGFGRGRHLGCSRAFDG SGQEFAHAWFLGD------IHFDDDEHFTAPS--------
MMP cress          DITIGFYTGDHGDGEP-FDG VLGTLAHAFSPPSG----KFHLDADENWVVSGDL------
```

Figure 2. Multiple-sequence alignment of the structural zinc and calcium binding regions in the catalytic domains of 23 representative MMPs. The structural zinc binding residues in majority of MMPs are given in blue - three histidines and one aspartic acid; the structural zinc binding domain in MMP-19, CMMP, and XMMP are in green. The residues that coordinate to the calcium ion are in pink; "underlined" amino acids chelate to the calcium ion via their backbone carbonyl moiety; the variation which was observed in the calcium binding site of MMP-17 (MT4-MMP) is given in cyan.

The remaining MMPs, those of chicken CMMP, the frog XMMP, and the human MMP-19 (Figure 2), each possess unique motifs for binding to the structural zinc ion. The chicken CMMP has a histidine where the

majority of MMPs have an aspartic acid coordinated to the second zinc ion. Consequently, the structural zinc ion in this enzyme is coordinated by four histidine residues (His-171, His-173, His-187 and His-200; Figure 3B). Such coordination would force the cysteine adjacent to the fourth coordinated histidine (Cys-174) to point to the outside milieu. This cysteine may provide a site for protein dimerization, as it is entirely exposed and available. Such active dimer formation has been reported for MMP-9, for example.[19] We also investigated the possibility for the existence of another binding mode for the second zinc ion, where the three original histidines and the cysteine are coordinated to the zinc ion (Figure 3C). Such structural alternative is a distinct possibility, and it would still be a novel motif for coordination to the structural zinc. The frog XMMP has a cysteine residue at the same position as in the sequence of CMMP. However, it is missing the aspartic acid at the usual location typical for most MMPs for coordination to the second zinc ion. This enzyme has a glycine in the place of aspartic acid, which obviously cannot provide metal coordination (Figure 2). Therefore, for XMMP the only possibility is to have three histidines (His-270, His-286 and His-294) and the cysteine (Cys-273) side chains to coordinate to the second zinc ion (Figure 3D).

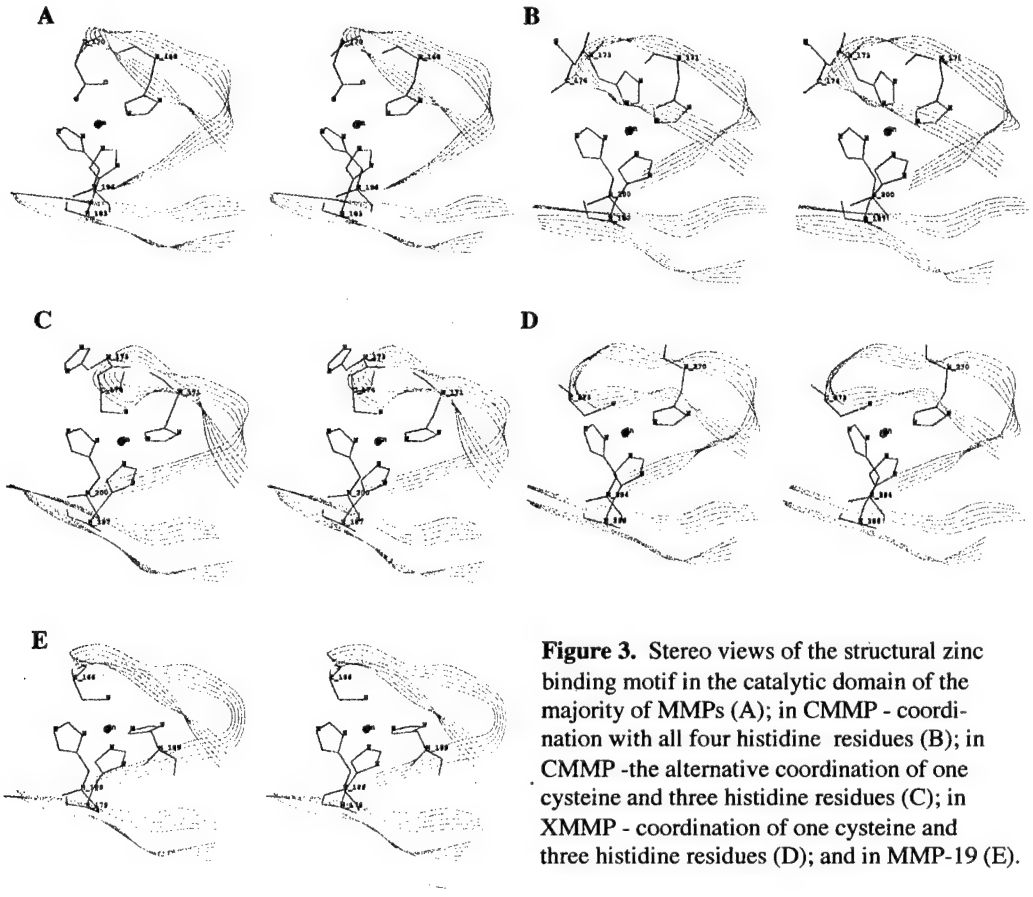

Figure 3. Stereo views of the structural zinc binding motif in the catalytic domain of the majority of MMPs (A); in CMMP - coordination with all four histidine residues (B); in CMMP -the alternative coordination of one cysteine and three histidine residues (C); in XMMP - coordination of one cysteine and three histidine residues (D); and in MMP-19 (E).

Analysis of the structure for MMP-19 showed that this enzyme has two histidines for metal coordination at the usual places and one cysteine at the corresponding position already discussed in the sequences for CMMP and XMMP. However, MMP-19 possesses a non-coordinating serine (Ser-163) at the position where the majority of MMPs have the third histidine. Interestingly, the third coordinating histidine (His-159, Figure 3E) in this enzyme is provided at an entirely distinct position, four residues to the N-terminus. Whereas the position of the amino acid is different and indeed on a different β-strand, it provided the side chain for the fourth coordination site in a perfectly acceptable orientation in space (for example, compare the positions of His-159 and His-270 in Figures 3E and 3D, respectively).

Binding of the calcium ion brings six specific elements of MMP catalytic domain for coordination in an octahedral fashion. Three of these elements are the side chains of two aspartic acids and one glutamic acid, which are conserved in all 23 MMPs except in MT4-MMP (*vide infra*, Figure 2). The remaining three calcium ligands are provided by the backbone carbonyl oxygens of three residues within a turn made up of five amino acids (Figure 2). A typical calcium-binding motif is shown in Figure 4A. The only exception to this general picture would appear to be MT4-MMP (MMP-17), which has undergone one amino acid deletion in this turn (i.e., it has a four-amino acid turn). In human MMP-17 (MT4-MMP), an asparagine residue is observed instead of the second aspartic acid (Figure 2). The coordination to the calcium ion for MT4-MMP (MMP-17) is shown in Figure 4B.

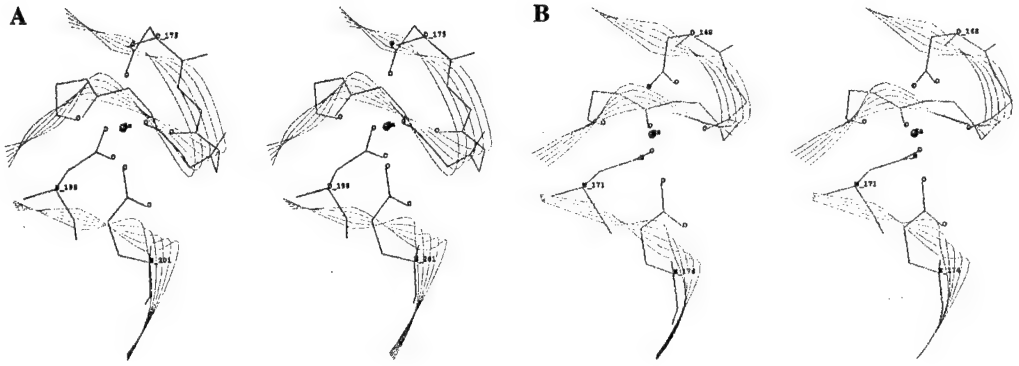

Figure 4. Stereo views of the calcium binding motif in majority of MMPs, except for MMP-17 (A); that for MMP-17 (B).

In conclusion, there are at least four different motifs for the binding to the structural zinc ion that are discernible from the three-dimensional structure analysis. However, the calcium binding motif is more strictly conserved. These variations in the metal-binding motifs preserve the topology of the structural zinc-binding site, as well as the calcium-binding site, and hence the general fold for the catalytic domain is highly preserved. The second zinc binding site is present in all MMPs and is important for the activity of these enzymes. Hence, the structural variations that are noted here in the coordination to the structural zinc ion may be indicative of the different outcomes for selection of novel enzymic activities. Furthermore, dendrogram analysis of the catalytic

domain sequence alignment for MMPs indicates that these variations in the zinc-binding motif came about as a consequence of independent evolutionary processes, unrelated to one another.[20] Since these motifs are absent in other members of the metzincin family of enzymes, we venture to say that the existence of these metal-binding sites in MMPs must have arisen in response to specific needs unique to MMPs with reference to their substrate specificities. The information provided herein is intended to stimulate interest in exploring the role of these motifs in MMPs geared toward understanding the substrate specificities for these enzymes, which are not understood to any appreciable degree at the present. Our understanding of the actual functions of the MMPs is at a rudimentary stage at the present and as more sequences of MMPs become available, the analysis presented here should be updated and correlated with the new structural information to shed light on the various properties of these important enzymes.

Acknowledgments. This work was supported by a grant from the US Army (DAMD17-97-1-7174). IM was a recipient of the Rumble and Heller predoctoral fellowships. We acknowledge Markku Kurkinen for providing us with the amino-acid sequence for CMMP.

References.

1. Chen, W. -T. *Curr. Opinion Cell Biol.* **1992**, *4*, 802.
2. Hagmann, W. K.; Lark, M. W.; Becker, J. W. In *Ann. Rev. Med. Chem.*; Bristol, J. A., Ed.; Academic Press, 1996; Vol. 31, pp 231-240.
3. Baramova, E.; Foidart, J. -M. *Cell Biol. Int.* **1995**, *19*, 239.
4. Lepage, T.; Gache, C. *EMBO J.* **1990**, *9*, 3003.
5. Namura, K.; Shimuzu, T.; Kinoh, H.; Sendai, Y.; Inomata, M.; Suzuki, N. *Biochemistry* **1997**, *36*, 7225.
6. Wilson, R.; Ainscough, R.; Anderson, K.; Baynes, C.; Berks, M.; Bonfield, J.; Burton, J.; Connell, M.; Copsey, T.; Cooper, J.; Coulson, A.; Craxton, M.; Dear, S.; Du, Z.; Durbin, R.; Favello, A.; Fraser, A.; Fulton, L.; Gardner, A.; Green, P.; Hawkins, T.; Hiller, L.; Jier, M.; Johnston, L.; Jones, M.; Kershaw, J.; Kirsten, J.; Laisster, N.; Latreille, P.; Lightning, J.; Lloyd, C.; Mortimore, B.; O'Callaghan, M.; Parsons, J.; Percy, C.; Rifken, L.; Roopra, A.; Saunders, D.; Shownkeen, R.; Sims, M.; Smaldon, N.; Smith, A.; Smith, M.; Sonnhammer, E.; Staden, R.; Sulston, J.; Thierry-Mieg, J.; Thomas, K.; Vaudin, M.; Vaughan, K.; Waterston, R.; Watson, A.; Weinstock, L.; Wilkinson-Sproat, J.; Wohldman, P. *Nature* **1994**, *368*, 32.
7. McGeehan, G.; Burkhart, W.; Anderegg, R.; Becherer, D.; Gillikin, J. W.; Graham, J. S. *Plant Physiol.* **1992**, *99*, 1179.
8. Murphy, G.; Knäuper, V. *Matrix Biol.* **1997**, *15*, 511.
9. Bode, W.; Reinemer, P.; Huber, R.; Kleine, T.; Schnierer, S.; Tschesche, H. *EMBO J.* **1994**, *13*, 1263.
10. Salowe, S. P.; Marcy, A. I.; Cuca, G. C.; Smith, C. K.; Kopka, I. E.; Hagman, W. K.; Hermes, J. D. *Biochemistry* **1993**, *31*, 4535.
11. Willenbrock, F.; Murphy, G.; Phillips, I. R.; Brocklehurst, K. *FEBS Lett.* **1995**, *358*, 189.
12. Lovejoy, B.; Cleasby, A.; Hassell, A. M.; Longley, K.; Luther, M. A.; Weigl, D.; McGeehan, G.; McElroy, A. B.; Drewry, D.; Lambert, M. H.; Jordan, S. R. *Science* **1994**, *263*, 375.
13. Wetmore, D. R.; Hardman, K. D. *Biochemistry* **1996**, *35*, 6549.
14. Browner, M. F.; Smith, W. W.; Castelhano, A. L. *Biochemistry* **1995**, *34*, 6602.
15. Gooley, P. R.; O'Connell, F.; Marcy, A. I.; Cuca, G. C.; Salowe, S. P.; Bush, B. L.; Hermes, J. D.; Esser, C. K.; Hagmann, W. K.; Springer, J. P.; Johnson, B. A. *Nature Struct. Biol.* **1994**, *1*, 111.
16. Stams, T.; Spurlino, J. C.; Smith, D. L.; Wahl, R. C.; Ho, T. F.; Qoronfleh, M. W.; Banks, T. M.; Rubin, B. *Nature Struct. Biol.* **1994**, *1*, 119.
17. Coordinates for the three-dimensional structures of the 17 MMPs that were modeled will be made available from our group web site, http://sun2.chem.wayne.edu/~somgroup upon acceptance of this manuscript.
18. Massova, I.; Fridman, R.; Mobashery, S. *J. Mol. Model.* **1997**, *3*, 17.
19. Clegg, P. D.; Burke, R. M.; Coughlan, A. R.; Riggs, C. M.; Carter, S. D. *Equine Vet. J.* **1997**, *29*, 343.
20. Massova, I.; Kotra, L. P.; Fridman, R.; Mobashery, S. *FASEB J.* submitted.

Matrix metalloproteinases: structures, evolution, and diversification

IRINA MASSOVA,*[,1] LAKSHMI P. KOTRA,* RAFAEL FRIDMAN,[†]
AND SHAHRIAR MOBASHERY*[,2]

*Department of Chemistry, and [†]Department of Pathology and Karmanos Cancer Institute, Wayne State University, Detroit, Michigan 48202–3489, USA

ABSTRACT **A comprehensive sequence alignment of 64 members of the family of matrix metalloproteinases (MMPs) for the entire sequences, and subsequently the catalytic and the hemopexin-like domains, have been performed. The 64 MMPs were selected from plants, invertebrates, and vertebrates. The analyses disclosed that as many as 23 distinct subfamilies of these proteins are known to exist. Information from the sequence alignments was correlated with structures, both crystallographic as well as computational, of the catalytic domains for the 23 representative members of the MMP family. A survey of the metal binding sites and two loops containing variable sequences of amino acids, which are important for substrate interactions, are discussed. The collective data support the proposal that the assembly of the domains into multidomain enzymes was likely to be an early evolutionary event. This was followed by diversification, perhaps in parallel among the MMPs, in a subsequent evolutionary time scale. Analysis indicates that a retrograde structure simplification may have accounted for the evolution of MMPs with simple domain constituents, such as matrilysin, from the larger and more elaborate enzymes.—Massova, I., Kotra, L. P., Fridman, R., Mobashery, S. Matrix metalloproteinases: structures, evolution, and diversification. *FASEB J.* 12, 1075–1095 (1998)**

Key Words: extracellular matrix · MMP · hemopexin · tissue inhibitor of matrix metalloproteinase

BACKGROUND

The interactions of cells with the extracellular matrix (ECM)[3] are critical for the normal development and function of the organism. Modulation of cell–matrix interactions occurs through the action of unique proteolytic systems responsible for hydrolysis of a variety of ECM components. By regulating the integrity and composition of the ECM structure, these enzyme systems play a pivotal role in the control of signals elicited by matrix molecules, which regulate cell proliferation, differentiation, and cell death. The turnover and remodeling of ECM must be highly regulated since uncontrolled proteolysis contributes to abnormal development and to the generation of many pathological conditions characterized by either excessive degradation or a lack of degradation of ECM components. Matrix metalloproteinases (MMPs) are a major group of enzymes that regulate cell–matrix composition. The MMPs are zinc-dependent endopeptidases known for their ability to cleave one or several ECM constituents, as well as nonmatrix proteins. They comprise a large family of proteases that share common structural and functional elements and are products of different genes. Ample evidence exists on the role of MMPs in normal and pathological processes, including embryogenesis, wound healing, inflammation, arthritis, and cancer. The association of MMPs with cancer metastasis has raised considerable interest because they represent an attractive target for development of novel antimetastatic drugs aimed at inhibiting MMP activity. Therefore, understanding the structure and function of these key enzymes has significant implications for cancer therapy (1–5).

Most members of the MMP family are organized into three basic, distinctive, and well-conserved domains based on structural considerations: an amino-terminal propeptide; a catalytic domain; and a hemopexin-like domain at the carboxy-terminal (**Fig. 1**). The propeptide consists of approximately 80–90 amino acids containing a cysteine residue, which interacts with the catalytic zinc atom via its side chain thiol group. A highly conserved sequence (. . .PRCGXPD. . .) is present in the propeptide. Removal of the propeptide by proteolysis results in zymogen activation, as all members of the MMP family are produced in a latent form. The catalytic domain contains two zinc ions and at least one calcium

[1] Current address: University of California at San Francisco, 513, Parnassus, S926, San Francisco, CA 94143–0446, USA.

[2] Correspondence: Shahriar Mobashery, Department of Chemistry, Wayne State University, Detroit, MI 48202–3489, USA. E-mail: som@mobashery.chem.wayne.edu

[3] Abbreviations: ECM, extracellular matrix; MMPs, matrix metalloproteinases; TIMPs, tissue inhibitors of metalloproteinases; MT-MMPs, membrane-type MMPs.

0892-6638/98/0012-1075/$02.25 © FASEB

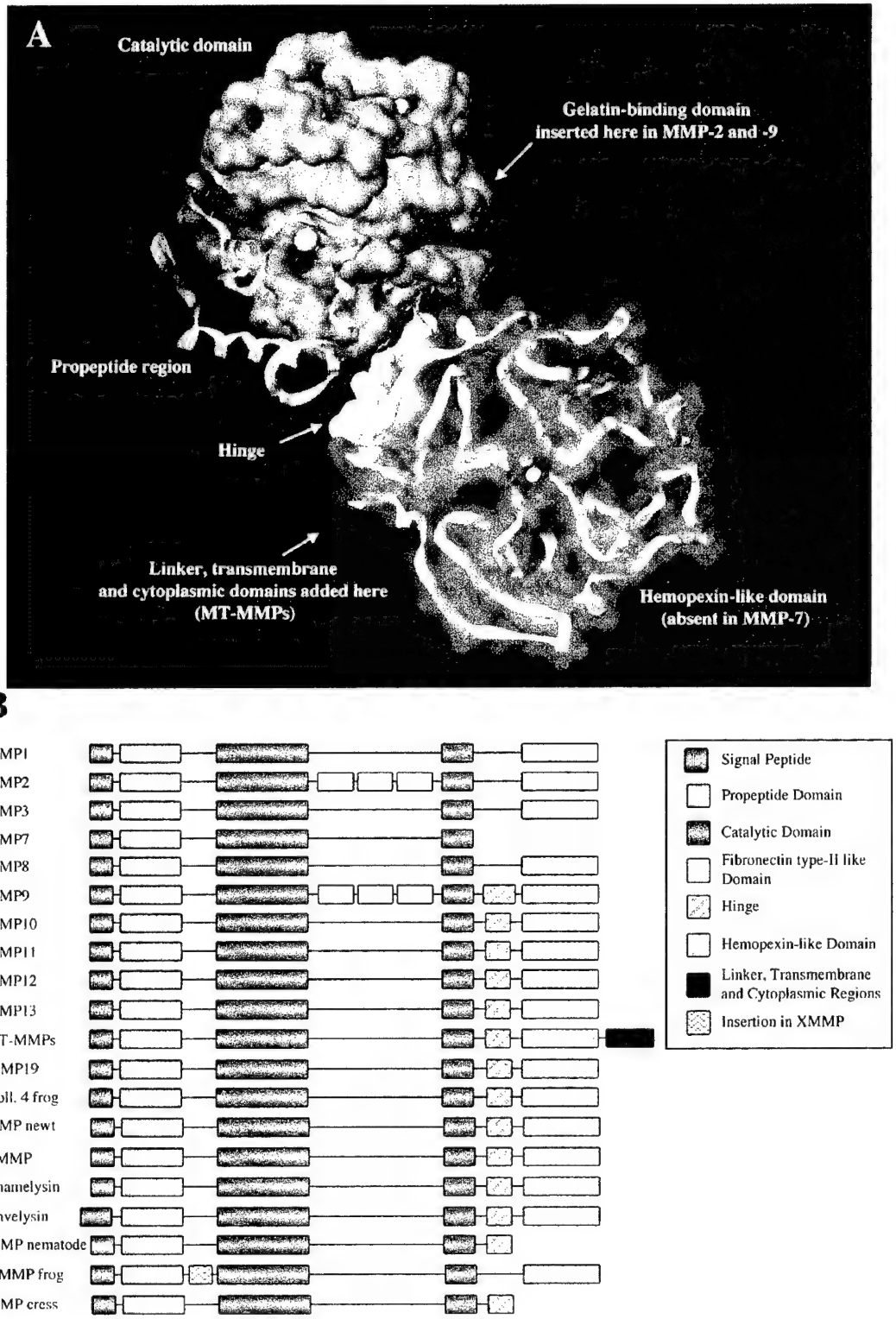

Figure 1. *A)* Basic domain structures of MMPs. The images for the propeptide region and the catalytic and homopexin-like domains shown here are from crystallographic sources. The propeptide region is taken from the X-ray structure for stomelysin (PDB code: 1slm) and the remaining portions of the structure are taken from the X-ray structure of the full-length collagenase (PDB code: 1fbl). Catalytic zinc is shown as an orange sphere; calcium ions in the catalytic domain and the hemopexin-like domain are shown in cyan. The propeptide region is shown by the green ribbon, catalytic domain as a surface in pink, hinge region as a surface in white, and the hemopexin-like domain is represented by the ribbon drawing in yellow. *B)* Schematics of the domain structures of the 23 representative MMPs. Catalytic domain (represented by green) has an insertion of gelatin binding domain in MMP-2 and MMP-9. In all other MMPs, the catalytic domain is a continuous entity.

ion coordinated to various residues. One of the two zinc ions is present in the active site and is involved in the catalytic processes of the MMPs. The second zinc ion (also known as structural zinc) and the calcium ion are present in the catalytic domain approximately 12 Å away from the catalytic zinc. The catalytic zinc ion is essential for the proteolytic activity of MMPs; the three histidine residues that coordinate with the catalytic zinc are conserved among all the MMPs. Little is known about the roles of the second zinc ion and the calcium ion within the catalytic domain, but the MMPs are shown to possess high affinities for structural zinc and calcium ions (6, 7). The hemopexin-like domain of MMPs is highly conserved and shows sequence similarity to the plasma protein, hemopexin. The hemopexin-like domain has been shown to play a functional role in substrate binding and/or in interactions with the tissue inhibitors of metalloproteinases (TIMPs), a family of specific MMP protein inhibitors (8, 9). In addition to these basic domains, the family of MMPs evolved into different subgroups by incorporating and/or deleting structural and functional domains. For example, MMP-2 and MMP-9, also known as gelatinases, incorporated the three repeats homologous to the type-II module of fibronectin into the catalytic domain that has been shown to be involved in binding to denatured collagen or gelatin (10). This domain, known as the gelatin binding domain or fibronectin type-II-like domain, is unique to the gelatinases, and so these enzymes are regarded as a separate subgroup among members of the MMP family. Incorporation of a hydrophobic stretch of approximately 25 amino acids, representing a putative transmembrane domain at the carboxy terminus and recognition motif (RXKR) for furin-like convertases at the end of the propeptide domain, is a characteristic of the membrane-type MMPs (MT-MMPs) (11, 12) except MT4-MMP (vide infra). MMP-11 also contains this furin recognition motif and, similar to the MT-MMPs, it is processed into the active form intracellularly (13). Additional insertion to the three basic MMP domains also includes a proline-rich 54 amino acid insertion in MMP-9 with sequence similarity to the α_2 chain of collagen V (14). Finally, MMP-7 lacks the hemopexin-like domain and represents the smallest member of the MMP family.

The catalytic activity of the MMPs is regulated at multiple levels including transcription, secretion, activation, and inhibition. The last is accomplished by members of the TIMP family, which presently includes four proteins: TIMP-1, TIMP-2, TIMP-3, and TIMP-4 (8, 15). Binding of the TIMPs to the catalytic domain results in efficient inhibition of enzymatic activity of MMPs. In the case of gelatinases, the TIMPs have been shown to bind to the zymogen forms of the enzymes. This interaction has been suggested to provide an extra level of regulation by potentially preventing activation (15, 16). However, it has recently been shown that TIMP-2 forms a trimolecular complex on the surface of the cell with MT1-MMP and proMMP-2, and regulates the formation and levels of concentration of mature MMP-2 (17). The crystal structure of the catalytic domain of MMP-3 in complex with TIMP-1 has been solved and shows that Cys^1 of the inhibitor interacts with the catalytic zinc ion of the MMP through the α-amino and its carbonyl group, whereas the Thr^2 side chain extends into the S_1' specificity pocket of the enzyme (9). A critical step in the control of MMP activity is regulated by the generation of active enzyme species with proteolytic activity. The process of activation involves sequential cleavage of the propeptide, which disrupts coordination between the cysteine thiol in the propeptide region with the zinc atom in the catalytic domain. This process is proteolytic and may involve other MMPs acting in a cascade of zymogen activation.

MMPs belong to the superfamily of zinc-peptidases, and the evolutionary relationship of this superfamily has been reviewed (18, 19). Sang and Douglas (20) analyzed 30 MMP sequences from various sources by multiple-sequence alignment, but their study was limited to analysis of the primary sequences. A total of 66 MMPs have been sequenced to date, of which 17 are from humans, including the recently discovered human enamelysin (MMP-20) and a functional enzyme encoded by the mmp20 gene (GenBank accession number AJ003147, maps to chromosome 16) in the familial Mediterranean fever gene in humans (21, 22). These human enzymes have counterparts in other vertebrates. MMPs have even been identified in invertebrates (23–25) and three have recently been sequenced from plant sources (mouse ear cress MMPs, **Table 1**). MMPs are probably more ancient than is currently realized. Their origin might actually be traceable back to bacteria in that a certain amino acid sequence for *Bacteroides fragilis* metalloproteinase toxin-2 (GenBank accession number U90931) has 59% sequence identity to the continuous 27 amino acid stretch in human MMP-1, which includes the catalytic zinc binding domain and the 'methionine turn' (this is a strictly conserved region with a methionine in the catalytic domain of MMPs responsible for the structural integrity of the zinc binding site). A salient question is why such multiplicity of these enzymes is seen in nature. We wish to add to this question an additional inquiry: What makes them different, and how does the difference in amino acid sequences give rise to structural elements that, in turn, would render a given MMP a distinct enzyme? We have compared amino acid sequences from 64 MMPs from various organisms, vertebrates, invertebrates, and plants to address these questions. Using the available crystal structures for four MMPs (26–29), we have modeled the 3-dimensional structures of several representative members of the remaining MMPs to gain insight into

TABLE 1. *Sources of various MMPs used in multiple-sequence alignment*

Gene, organism	Common name	Accession #	Database
MMP-2 (gelatinase A)			
Mmp2, Mus musculus	Mouse	P33434	Swiss-Prot
Mmp2, Rattus norvegicus	Rat	P33436	Swiss-Prot
MMP2, Homo sapiens	Human	P08253	Swiss-Prot
Mmp2, Oryctolagus cuniculus	Rabbit	P50757	Swiss-Prot
Mmp2, Gallus gallus	Chicken	Q90611	Swiss-Prot
MMP-9 (gelatinase B)			
Mmp9 or Clg4b, Mus musculus	Mouse	P41245	Swiss-Prot
Mmp9, Rattus norvegicus	Rat	P50282	Swiss-Prot
MMP9, Homo sapiens	Human	P14780	Swiss-Prot
Mmp9, Oryctolagus cuniculus	Rabbit	P41246	Swiss-Prot
Mmp9, Bos taurus	Bovin	P52176	Swiss-Prot
Mmp9, Synops pyrrhogaster	Newt	Q98856	TREMBL
MMP-12 (macrophage metalloelastase)			
Rattus norvegicus	Rat	X98517	GenBank
Oryctolagus cuniculus	Rabbit	U88652	GenBank
MMP12 or *HME, Homo sapiens*	Human	P39900	Swiss-Prot
Mmp12 or *Mme, Mus musculus*	Mouse	P34960	Swiss-Prot
MMP-13 (collagenase-3)			
Mmp13, Mus musculus	Mouse	P33435	Swiss-Prot
Mmp13, Rattus norvegicus	Rat	P23097	Swiss-Prot
MMP13, Homo sapiens	Human	P45452	Swiss-Prot
gene A, Xenopus laevis	Frog	U41824	GenBank
Mmp13, Xenopus laevis	Frog	Q10835	Swiss-Prot
Cynops pyrrhogaster	Newt	D82055	GenBank
Collagenase-4			
Xenopus laevis	Frog	L76275	GenBank
MMP-3 (stromelysin-1)			
Mmp3, Mus musculus	Mouse	P28862	Swiss-Prot
Mmp3, Rattus norvegicus	Rat	P03957	Swiss-Prot
MMP3 or *STMY1, Homo sapiens*	Human	P08254	Swiss-Prot
Mmp3, Oryctolagus cuniculus	Rabbit	P28863	Swiss-Prot
Equus caballus	Horse	U62529	GenBank
MMP-10 (stromelysin-2)			
MMP10 or *STMY2, Homo sapiens*	Human	P09238	Swiss-Prot
Mmp10, Rattus norvegicus	Rat	P07152	Swiss-Prot
MMP-1 (interstitial collagenase)			
Mmp1 or *Clg, Bos taurus*	Bovin	P28053	Swiss-Prot
Mmp1, Sus scrofa	Pig	P21692	Swiss-Prot
MMP1 or *CLG, Homo sapiens*	Human	P03956	Swiss-Prot
Mmp1, Oryctolagus cuniculus	Rabbit	P13943	Swiss-Prot
Rana catesbeiana	Bull frog	Q11133	Swiss-Prot
MMP-8 (neutrophil collagenase)			
MMP8 or *CLG1, Homo sapiens*	Human	P22894	Swiss-Prot
CMMP			
Gallus gallus	Chicken		
Enamelysin			
Bos taurus	Bovin	AF009922	GenBank
Sus scrofa	Pig	U54825	GenBank
MMP-7 (matrilysin)			
Mmp7, Mus musculus	Mouse	Q10738	Swiss-Prot
Mmp7, Rattus norvegicus	Rat	P50280	Swiss-Prot
Mmp7, Felis silvestris	Cat	P55032	Swiss-Prot
MMP7, Homo sapiens	Human	P09237	Swiss-Prot
MMP-11 (stromelysin-3)			
MMP11 or *STMY3, Homo sapiens*	Human	P24347	Swiss-Prot
Mmp11, Mus musculus	Mouse	Q02853	Swiss-Prot
Xenopus laevis	Frog	Q11005	Swiss-Prot
Rattus norvegicus	Rat	P97576	TREMBL
MMP-16 (MT3-MMP)			
MMP16 or *MMPX2, Homo sapiens*	Human	P51512	Swiss-Prot
MT3-MMP, Gallus gallus	Chicken	U66463	GenBank

(*continued on next page*)

TABLE 1. (*continued*)

Gene, organism	Common name	Accession #	Database
MMP-14 (MT1-MMP)			
MMP14 or *MMP-X1, Homo sapiens*	Human	P50281	Swiss-Prot
Mmp14 or *MT-MMP, Rattus norvegicus*	Rat	Q10739	Swiss-Prot
Mmp14 or *MT-MMP, Mus musculus*	Mouse	P53690	Swiss-Prot
Mmp14, Oryctolagus cuniculus	Rabbit	Q95220	Swiss-Prot
MMP-15 (MT2-MMP)			
MMP15, Homo sapiens	Human	P51511	Swiss-Prot
MMP-17 (MT4-MMP)			
MMP17, Homo sapiens	Human	X89576	GenBank
MMP-19			
MMP19, Homo sapiens	Human	X92521	GenBank
Plant metalloproteases			
Glycine max	soybean	U63725	GenBank
Arabidopsis thaliana	Mouse ear cress	O04529	TREMBL
Arabidopsis thaliana	Mouse ear cress	E327511	GenBank
Envelysin			
Hemicentrotus pulcherrimus	Sea urchin	AB000719	GenBank
Paracentrotus lividus	Sea urchin	P22757	Swiss-Prot
Zinc protease			
T21D11.1, Caenorhabditis elegans	Nematode	U00038	GenBank
XMMP			
Xenopus laevis	Frog		
Others			
Cynops pyrrhogaster	Newt	D82053	GenBank
Cynops pyrrhogaster	Newt	D82054	GenBank

their similarities and differences (30, 31). We have analyzed the entire sequences, the catalytic domains, and hemopexin-like domains of the 64 members of the MMP family in terms of structures, evolution, and interactions with substrates and inhibitors. We also provide an analysis of the structural zinc binding site and the calcium binding site. These are the first comprehensive analyses of this important family of enzymes, and provide fundamental information on evolution and properties of MMPs.

EXPERIMENTAL PROCEDURES

Amino acid sequences of MMPs were obtained from the GenBank, TREMBL, and Swiss-Prot data banks. The sources for all sequences are given in Table 1. A total of 64 different MMPs were used for this analysis [human enamelysin and the mmp20 gene product with GenBank accession # AJ003147 were not included because they were reported after the completion of our analysis. However, we conducted a separate multiple-sequence analysis with the 64 sequences and the two new MMP sequences after preparing this review. This analysis showed that the clustering pattern was identical to that reported in this article. Human enamelysin grouped with other enamelysins, and the mmp20 gene product showed the closest homology to MT4-MMP]. The multiple-sequence alignments were performed using the program PileUp from the Wisconsin package version 9. Four human MMPs [fibroblast (MMP-1, 1cgl) (26) and neutrophil (MMP-8, 1mnc) (27) collagenases, matrilysin (MMP-7, 1mmq) (28), and stromelysin-1 (MMP-3, 1slm) (29)] have recently been crystallized and their coordinates are available. We used structural information to predict the 3-dimensional structures for the homologous metalloproteinases using the program COMPOSER (Tripos Associates, Inc., St. Louis, Mo.).

We recently reported the computational 3-dimensional models for the catalytic domains of MMP-2 and MMP-9 (30) and also predicted the folding of an additional 17 representative MMP enzymes for which such information has been lacking (31). These 17 proteins are human MMP-10, MMP-11, MMP-12, MMP-13, MT1-MMP (MMP-14), MT2-MMP (MMP-15), MT3-MMP (MMP-16), MT4-MMP (MMP-17), MMP-19 (also referred to as MMP-18), pig enamelysin, sea urchin envelysin, stromelysin-like MMP from newt, collagenase-4 from frog, nematode MMP, chicken CMMP, frog XMMP, and MMP from mouse ear cress.

RESULTS AND DISCUSSION

Multiple-sequence analysis for the 64 MMPs was conducted on three different sets of data. In the first set,

the complete sequences, including the signal and propeptide regions, were used (**Fig. 2*A***). A simplified schematic presentation of Fig. 2*A* is shown as Fig. 2*B*. The entire sequences were used to understand the overall evolutionary pathways for diversification. Evolution occurs via separate events of sequence modification of the entire gene such as point mutations, insertions, deletions, gene splitting, and fusions. Mu-

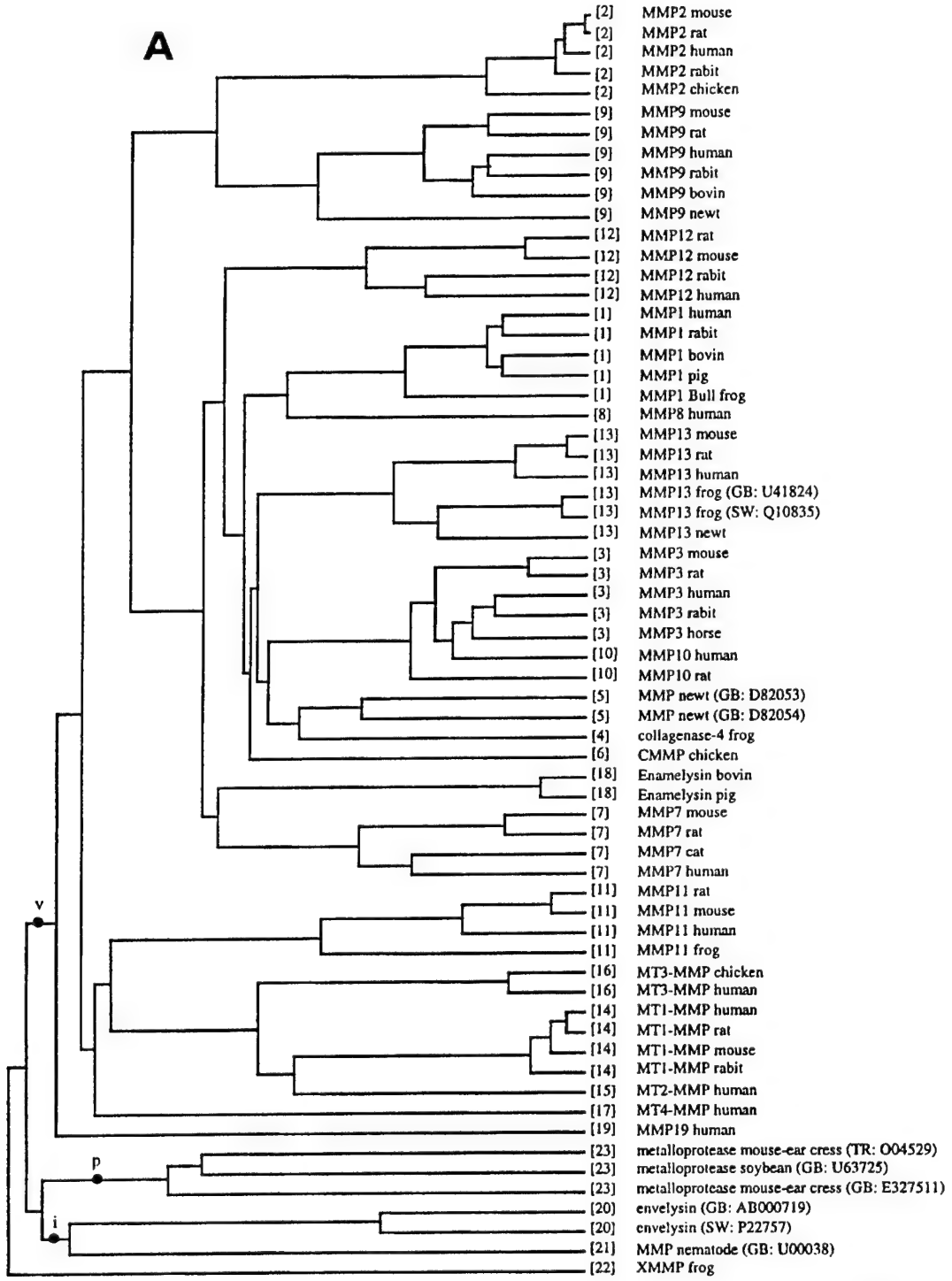

(*continued on next page*)

Figure 2. *A)* Dendrogram for the multiple-sequence analysis of the complete amino acid sequences for 64 MMPs. Numbers in brackets represent the classes. The letter 'v' indicates the branch for vertebrate MMPs, 'i' indicates invertebrate MMPs, and 'p' indicates the plant MMPs. *B)* Simplified schematic of the dendrogram shown in panel *A*. The numbers within circles represent chromosomal origin for human MMPs, when available.

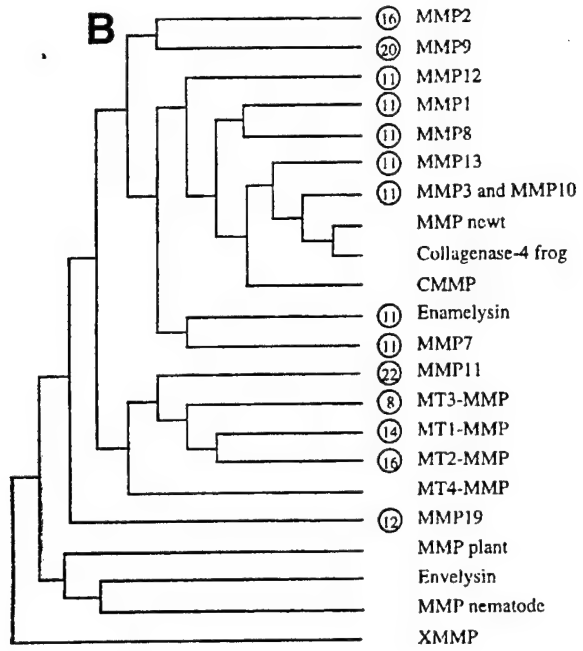

Figure 2. (*continued*)

tations occur at random regardless of the function of the region of the gene or the domain in order to increase diversity throughout the genes in question, which is why this sequence analysis on the entire protein is informative. The second and third sets for multiple-sequence analyses were carried out on sequence stretches corresponding to the catalytic and hemopexin-like domains of the MMPs (**Fig. 3** and **Fig. 4**, respectively). These two sets were chosen to study the different evolutionary pressures on these specific domains en route to diversification. Mutations that impair catalytic ability would not be selected. In contrast, substrate specificities for the majority of the MMPs are believed to have been determined by the interactions of protein substrates and TIMPs with either the hemopexin-like domain or the gelatin binding domain (in the case of gelatinases) (32, 33). Hence, evolution of these domains may reflect evolution of substrate specificities and interactions with TIMPs. Therefore, comparison of the data for analyses of the catalytic domain and hemopexin-like domain with those of the complete sequences would provide information on whether the assembly of the genes encoding these domains occurred at a later time than the differentiation of MMPs into separate subfamilies.

Analysis of the entire sequences and the separate analyses of the catalytic and hemopexin-like domains are quite revealing. Analysis of the entire sequences and of the catalytic domains gave rise to 22 distinct subfamilies of MMPs. The number for each cluster is given in brackets and is arbitrary. We tried to correlate the number for the clusters with those for the given MMP when possible. For example, cluster 1 is given to MMP-1. Each analysis produced clusters of enzymes that were individually comprised of MMPs of a given type. The only exceptions were MMP-3 and MMP-10 (stromelysins-1 and -2, respectively), which clustered into one subfamily (Figs. 2 and 3). However, these stromelysins formed two independent groups in the alignment of the hemopexin-like domains, giving rise to a total of 23 distinct subfamilies of MMPs for this analysis. **Figure 5** provides the alignment for the amino acid sequences of the 23 representative enzymes using the PileUp program. This alignment was made consistent with the alignments found by the program COMPOSER, which takes into account the predicted folded structures of the proteins. COMPOSER assigns different contributions for the 'structurally conserved regions', such as elements of well-defined secondary structure, for example, β-strands and α-helices, as opposed to loops, which are considered to be variable areas. In contrast, PileUp does not differentiate between secondary structure elements as does COMPOSER, but rather performs the alignment based solely on sequence homology of amino acids. Therefore, sequence alignments found by COMPOSER and PileUp are based on different principles, yet they have the potential to complement each other. We have edited the result of the PileUp alignment from the insight gained by the COMPOSER analysis, since the 3-dimensional structural information would enhance reliability of this type of analysis considerably. Major protein structural blocks, β-strands and α-helices, have a greater tendency to be conserved during the evolutionary process than do mere sequences of amino acids.

Multiple-sequence analysis of the complete sequences of MMPs

The 22 major subfamilies of MMPs, as discerned from the multiple-sequence analysis and the dendrogram for the 64 MMPs, are shown in Fig. 2*A*, with a simplified version depicted in Fig. 2*B*. The chromosome locations for human MMPs are shown (in circles) in Fig. 2*B* when available. Members of each subfamily generally display similar substrate profiles in different organisms. MMP-3 and MMP-10 clustered in one group, and show almost identical properties and substrate profiles (8). Genes of the more closely clustered human MMPs all seem to have originated from the same chromosome 11, reflecting the evolutionary process suggested in Fig. 2*B*.

It has been proposed that the origin of MMPs could be traced to before the emergence of vertebrates from invertebrates (34, 35). Recent sequencing of three plant MMPs found these enzymes to be homologous to MMPs from vertebrate and invertebrate origins, indicating that this evolutionary process is even more ancient than previously appreciated

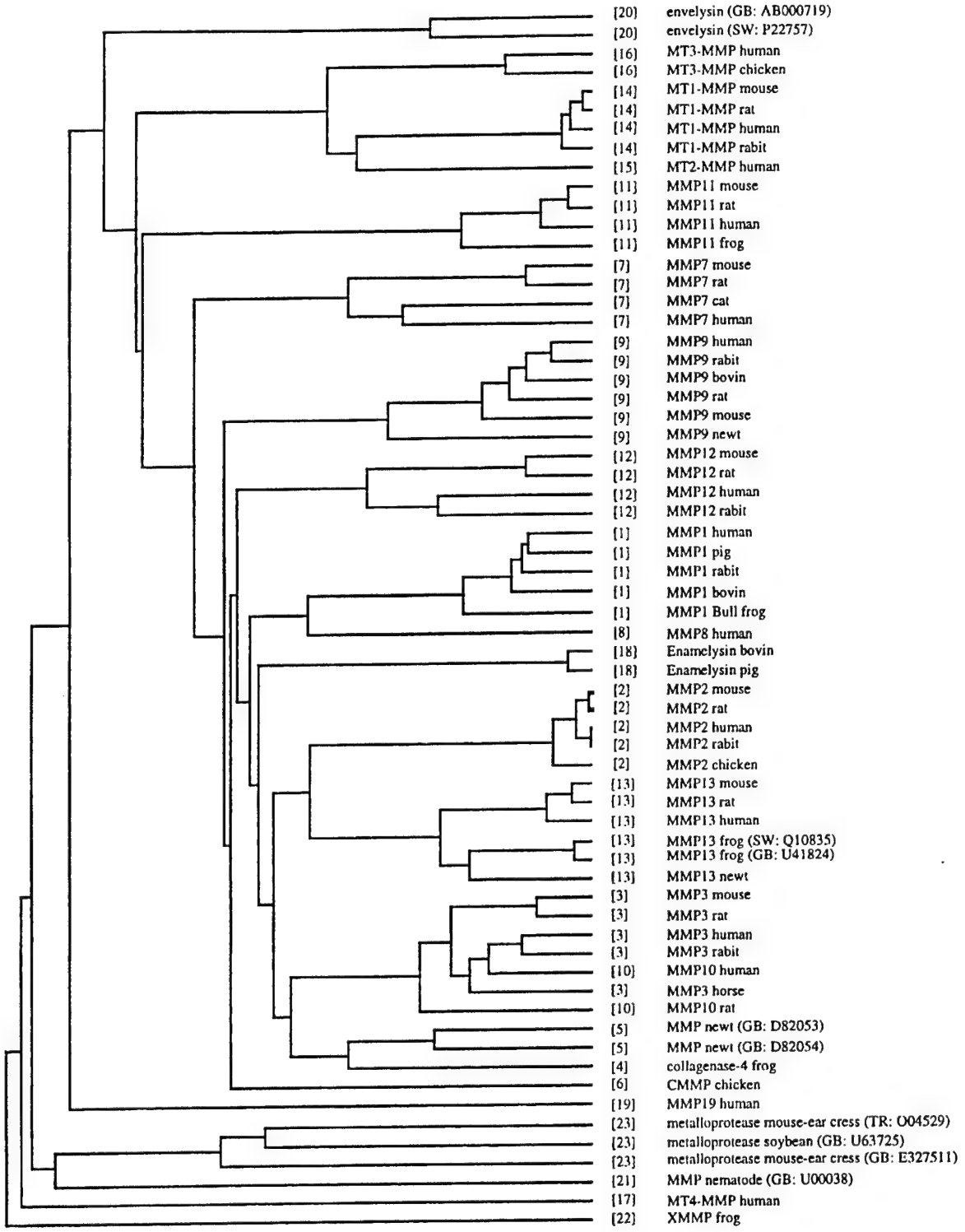

Figure 3. Dendrogram for the multiple-sequence analysis for the sequence of amino acids in the catalytic domains for 64 MMPs. The numbers in brackets represent the classes.

(Table 1) (36). Furthermore, the discovery of a peptide sequence for a metal-containing enzyme from *B. fragilis* suggests that MMPs may be more ancient yet (37), given that bacteria have been around for longer than 3.5 billion years. The three main branches of the dendrogram in Fig. 2*A* give rise to the lines that lead to enzymes from the vertebrate (depicted as the 'v' branch), invertebrate (depicted as the 'i' branch), and plant (depicted as the 'p' branch) MMPs, respectively. The only exception is the XMMP from

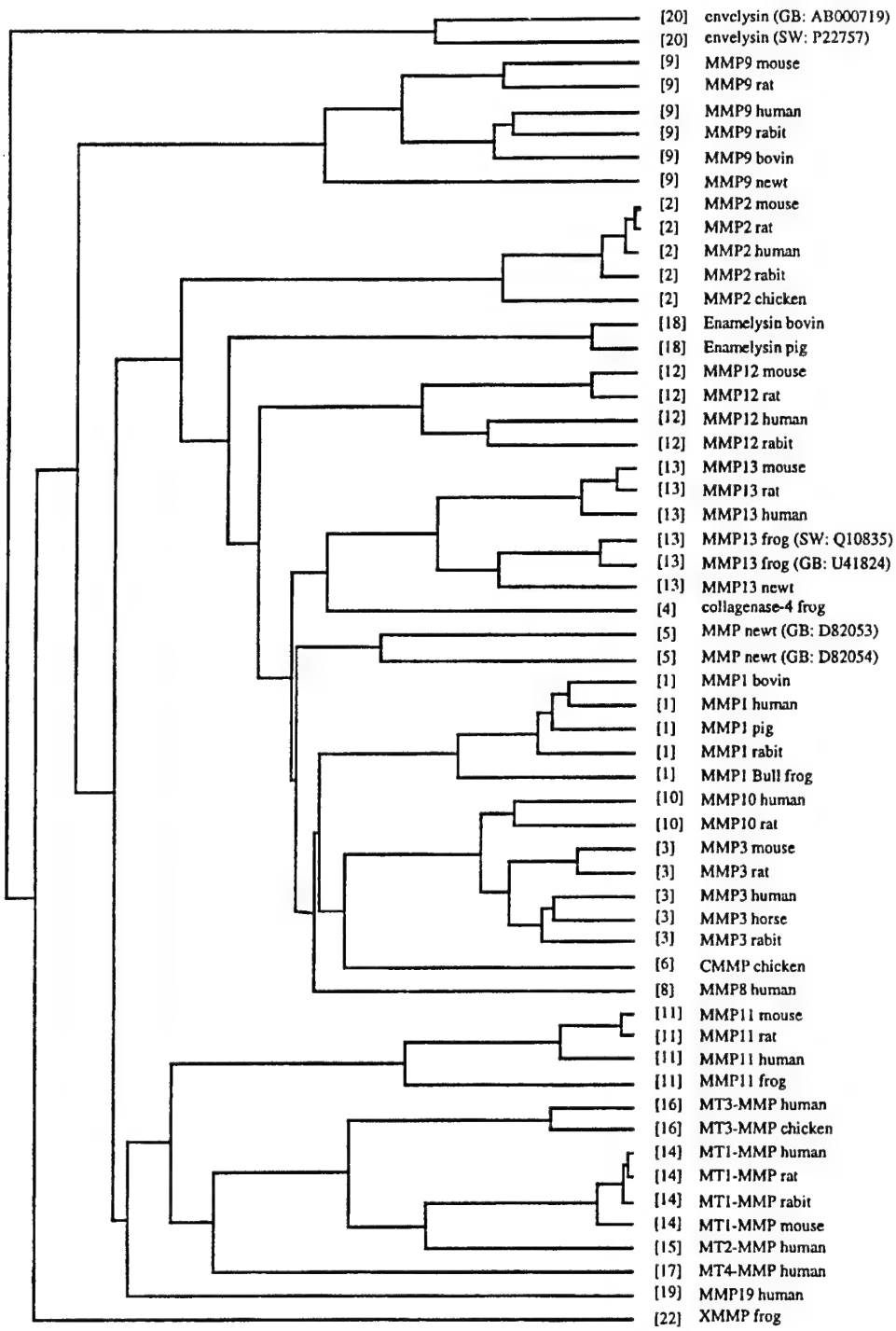

Figure 4. Dendrogram for the multiple-sequence analysis of the hemopexin-like domain sequences for 64 MMPs. Numbers in parentheses represent the class.

Xenopus (38). Plant and invertebrate MMPs show a stronger relationship among themselves than to the vertebrate MMPs (Fig. 2*A*). Thus, the vertebrate enzymes are more remotely related to plant and invertebrate MMPs. Although one would expect that the plant MMPs are the most ancient, and therefore the enzymes least related to all other MMPs, our analysis shows that the frog XMMP is the enzyme least related to all other MMPs, itself forming a separate group. This indicates that XMMP either represents a separate yet unidentified group of MMPs or is the last extant member of a primordial MMP. The first possibility seems to be more likely in our view, because XMMP possesses a hemopexin-like domain that is absent in plant MMPs and the nematode enzyme. Indeed, the plant and nematode MMPs have the sim-

plest domain structures. It may be suggested that at some point during evolution, the genes encoding the primordial MMP and hemopexin-like domain joined together, and XMMP probably originated after this event. Based on our analysis of Fig. 2*A*, we see that the sequence of MMP-7 fits well into the alignment of the entire sequences. This is also true for the sequence of the catalytic domains (vide infra), indicating that this enzyme has not existed as an evolutionary exception, or oddity, by not having the hemopexin-like domain. In light of what appears to be an independent, and perhaps parallel, evolution for MMP-7, the lack of hemopexin-like domain in matrilysin represents a deletion of this domain during evolution (Fig. 1*A*).

One can see four major subgroups within the vertebrate branch (Fig. 2*A*). One is formed by MMP-19 itself (some refer to this as MMP-18), which is least related to other vertebrate MMPs, besides XMMP. The next branch is that of MMP-11 (stromelysin-3) clustered together with the MT-MMPs. MT4-MMP (MMP-17) shares less similarity to other members of this branch of membrane-type enzymes, and the rest of this subgroup is more closely related to MMP-11 than to MT4-MMP. Both MMP-11 and the MT-MMPs possess the furin recognition site and can be activated by furin-like convertases (11, 39). The third branch is comprised exclusively of gelatinases, whereas the last branch is made up of all remaining vertebrate MMPs.

Figures 2–4 reveal 22–23 distinct MMPs subfamilies, sequence similarities of which were preserved among various organisms during evolution. It is likely that one would find counterparts to each MMP in various vertebrate organisms. The entire amino acid sequence alignment of the 23 representative members of these subfamilies is shown in Fig. 5. Human enzymes have been selected in all cases when available. The simplified domain structures of these 23 MMPs are shown in the schematic of Fig. 1*B*. Consistent with earlier knowledge, the analysis depicted in Fig. 5 and the alignment produced by the PileUp program revealed that all MMPs, except that from nematode, have signal sequences, followed by the propeptide region containing the characteristic motif called the 'cysteine switch' (40). The common pattern for this cysteine switch is [**PSL**]-[**RT**]-**C**-[**GS**]-[**VNL**]-[**PASYE**]-**D**, where boldface letters designate the most commonly found amino acids. In addition, MMP-11 and the MT-MMPs (except MT4-MMP) contain a RXKR motif in the propeptide that has been postulated to represent a cleavage site for furin-like enzymes (11, 13, 39). This cleavage pattern also appears in nematode MMP (two repeats) and in XMMP, as seen in the sequence alignment. MT4-MMP and the mmp20 gene product have a variation of the furin-like recognition sequence as RRRR (instead of RXKR) at this position.

The sequence of the nematode MMP seems to be considerably shorter at the amino terminus (24), which either reflects that the amino-terminal portion of the enzyme was not sequenced entirely or that this enzyme has a totally different mechanism for activation. The amino-terminal portion of the nematode MMP that precedes the catalytic domain has only 48 amino acids, compared to 100–200 amino acids in other MMPs. The propeptide sequence forms a cap over the active site of this MMP, with the critical cysteine residue providing the fourth coordination to the catalytic zinc ion, as seen in the crystal structure of stromelysin-1 (41). We also see a conserved signature for the catalytic zinc ion binding site of MMPs, with the consensus pattern containing a so-called methionine turn (40, 42), [**VAIT**]-[**AG**]-[**ATV**]-***H***-**E**-[**FLIV**]-**G**-***H***-[**ALMSV**]-[**LIM**]-**G**-[**LM**]-X-***H***-[**SITV**]-X(5)-[**LAFIV**]-***M***, where X denotes any residue and X(5) means there are five residues between the flanking sites. The three histidines shown in italics chelate the catalytic zinc ion, and the methionine (also depicted in italics) is located underneath the cavity formed by these histidines, providing increased hydrophobicity in this area to enhance zinc binding ability of histidines (42).

Multiple-sequence analysis of regions encoding the catalytic domain of MMPs

Figure 3 shows the multiple-sequence analysis carried out for the regions encoding exclusively the catalytic domains. Again one sees 22 distinct clusters, with MMP-3 and MMP-10 in one group. We no longer see three clearly delineated (separate) large groups for invertebrate, vertebrate, and plant MMPs, although there appears to be some tendency for MMPs from these sources to group together. The catalytic domains of the MT-MMPs do not usually appear to be closely related to one another (for example, position of MT4-MMP in Fig. 3). An unexpected finding was

Figure 5. Amino acid sequence alignment for the 23 representative MMPs. The pound sign '#' marks the residues important for binding of the zinc ion in the active site of MMPs. The symbol '@' denotes the residues coordinated to the structural zinc ion, '%' marks residues that coordinate to the calcium ion by their side chain functions, and the letter 'B' labels residues that contribute their main-chain carbonyl moieties for coordination to the calcium ion. The letters 'X', 'Y', and 'Z' denote the structurally variable loops important for substrate binding to the catalytic domain. The residues marked by 'J' provide elements of their backbone to anchor the substrate. *continued on next page*

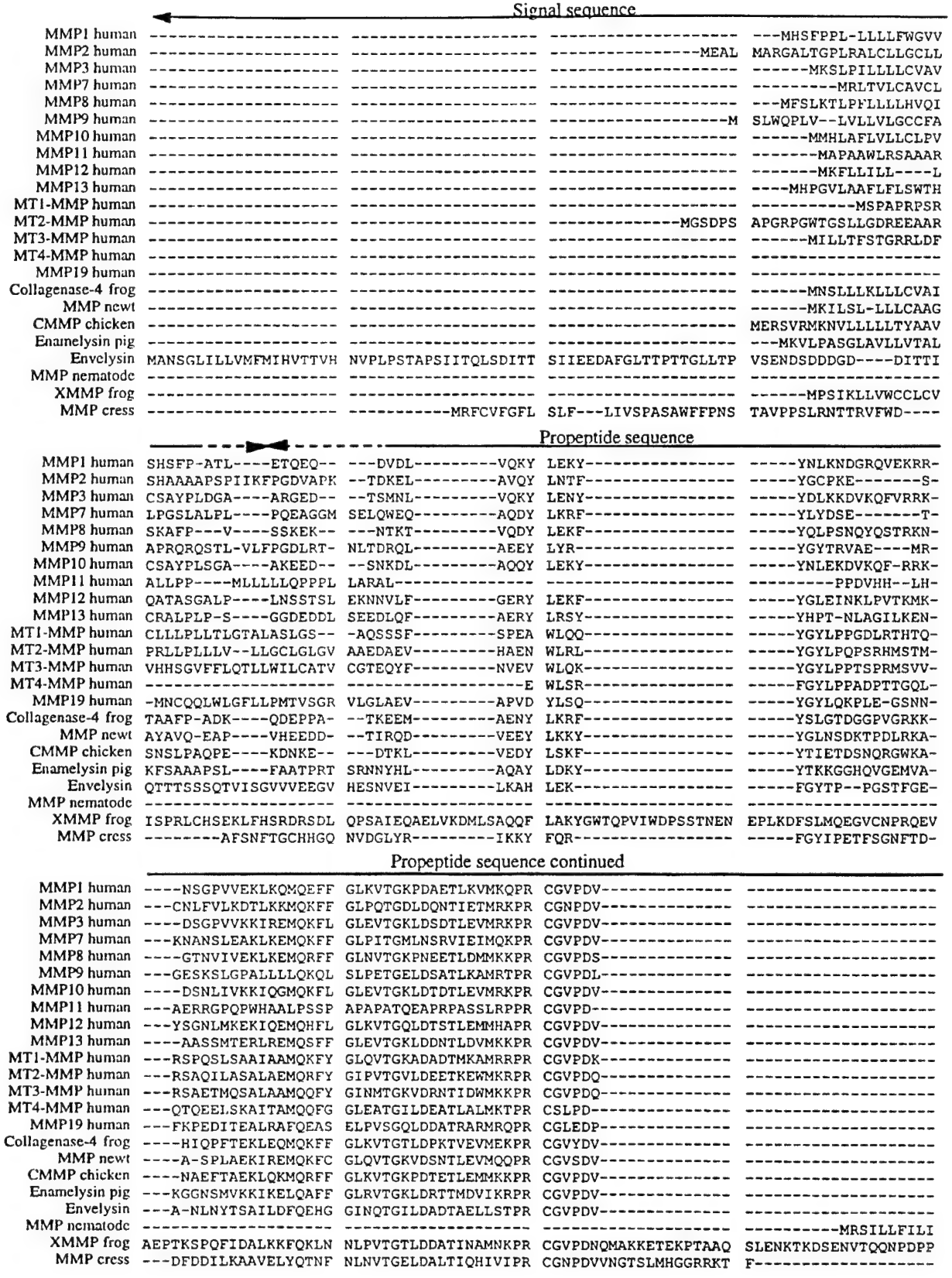

MMP1 human	----------	----------	----------	---MHSFPPL-LLLLFWGVV
MMP2 human	----------	----------	----------MEAL	MARGALTGPLRALCLLGCLL
MMP3 human	----------	----------	----------	------MKSLPILLLLCVAV
MMP7 human	----------	----------	----------	---------MRLTVLCAVCL
MMP8 human	----------	----------	----------	---MFSLKTLPFLLLLHVQI
MMP9 human	----------	----------	----------M	SLWQPLV--LVLLVLGCCFA
MMP10 human	----------	----------	----------	------MMHLAFLVLLCLPV
MMP11 human	----------	----------	----------	-------MAPAAWLRSAAAR
MMP12 human	----------	----------	----------	-------MKFLLILL----L
MMP13 human	----------	----------	----------	----MHPGVLAAFLFLSWTH
MT1-MMP human	----------	----------	----------	----------MSPAPRPSR
MT2-MMP human	----------	----------	----------MGSDPS	APGRPGWTGSLLGDREEAAR
MT3-MMP human	----------	----------	----------	------MILLTFSTGRRLDF
MT4-MMP human	----------	----------	----------	----------
MMP19 human	----------	----------	----------	----------
Collagenase-4 frog	----------	----------	----------	------MNSLLLKLLLCVAI
MMP newt	----------	----------	----------	------MKILSL-LLLCAAG
CMMP chicken	----------	----------	----------	MERSVRMKNVLLLLLTYAAV
Enamelysin pig	----------	----------	----------	---MKVLPASGLAVLLVTAL
Envelysin	MANSGLILLVMFMIHVTTVH	NVPLPSTAPSIITQLSDITT	SIIEEDAFGLTTPTTGLLTP	VSENDSDDDGD----DITTI
MMP nematode	----------	----------	----------	----------
XMMP frog	----------	----------	----------	------MPSIKLLVWCCLCV
MMP cress	----------	----------MRFCVFGFL	SLF---LIVSPASAWFFPNS	TAVPPSLRNTTRVFWD----
MMP1 human	SHSFP-ATL----ETQEQ--	---DVDL---------VQKY	LEKY----------	-----YNLKNDGRQVEKRR-
MMP2 human	SHAAAAPSPIIKFPGDVAPK	--TDKEL---------AVQY	LNTF----------	-----YGCPKE-------S-
MMP3 human	CSAYPLDGA----ARGED--	--TSMNL---------VQKY	LENY----------	-----YDLKKDVKQFVRRK-
MMP7 human	LPGSLALPL----PQEAGGM	SELQWEQ---------AQDY	LKRF----------	-----YLYDSE-------T-
MMP8 human	SKAFP---V----SSKEK--	---NTKT---------VQDY	LEKF----------	-----YQLPSNQYQSTRKN-
MMP9 human	APRQRQSTL-VLFPGDLRT-	NLTDRQL---------AEEY	LYR----------	-----YGYTRVAE----MR-
MMP10 human	CSAYPLSGA----AKEED--	--SNKDL---------AQQY	LEKY----------	-----YNLEKDVKQF-RRK-
MMP11 human	ALLPP----MLLLLLQPPPL	LARAL----------	----------	---------PPDVHH--LH-
MMP12 human	QATASGALP----LNSSTSL	EKNNVLF---------GERY	LEKF----------	-----YGLEINKLPVTKMK-
MMP13 human	CRALPLP-S----GGDEDDL	SEEDLQF---------AERY	LRSY----------	-----YHPT-NLAGILKEN-
MT1-MMP human	CLLLPLLTLGTALASLGS--	-AQSSSF---------SPEA	WLQQ----------	-----YGYLPPGDLRTHTQ-
MT2-MMP human	PRLLPLLLV--LLGCLGLGV	AAEDAEV---------HAEN	WLRL----------	-----YGYLPQPSRHMSTM-
MT3-MMP human	VHHSGVFFLQTLLWILCATV	CGTEQYF---------NVEV	WLQK----------	-----YGYLPPTSPRMSVV-
MT4-MMP human	----------	----------E	WLSR----------	-----FGYLPPADPTTGQL-
MMP19 human	-MNCQQLWLGFLLPMTVSGR	VLGLAEV---------APVD	YLSQ----------	-----YGYLQKPLE-GSNN-
Collagenase-4 frog	TAAFP-ADK----QDEPPA-	--TKEEM---------AENY	LKRF----------	-----YSLGTDGGPVGRKK-
MMP newt	AYAVQ-EAP----VHEEDD-	--TIRQD---------VEEY	LKKY----------	-----YGLNSDKTPDLRKA-
CMMP chicken	SNSLPAQPE----KDNKE--	---DTKL---------VEDY	LSKF----------	-----YTIETDSNQRGWKA-
Enamelysin pig	KFSAAAPSL----FAATPRT	SRNNYHL---------AQAY	LDKY----------	-----YTKKGGHQVGEMVA-
Envelysin	QTTTSSSQTVISGVVVEEGV	HESNVEI---------LKAH	LEK----------	-----FGYTP--PGSTFGE-
MMP nematode	----------	----------	----------	----------
XMMP frog	ISPRLCHSEKLFHSRDRSDL	QPSAIEQAELVKDMLSAQQF	LAKYGWTQPVIWDPSSTNEN	EPLKDFSLMQEGVCNPRQEV
MMP cress	--------AFSNFTGCHHGQ	NVDGLYR---------IKKY	FQR----------	-----FGYIPETFSGNFTD-
MMP1 human	----NSGPVVEKLKQMQEFF	GLKVTGKPDAETLKVMKQPR	CGVPDV----------	----------
MMP2 human	---CNLFVLKDTLKKMQKFF	GLPQTGDLDQNTIETMRKPR	CGNPDV----------	----------
MMP3 human	----DSGPVVKKIREMQKFL	GLEVTGKLDSDTLEVMRKPR	CGVPDV----------	----------
MMP7 human	---KNANSLEAKLKEMQKFF	GLPITGMLNSRVIEIMQKPR	CGVPDV----------	----------
MMP8 human	----GTNVIVEKLKEMQRFF	GLNVTGKPNEETLDMMKKPR	CGVPDS----------	----------
MMP9 human	---GESKSLGPALLLLQKQL	SLPETGELDSATLKAMRTPR	CGVPDL----------	----------
MMP10 human	----DSNLIVKKIQGMQKFL	GLEVTGKLDTDTLEVMRKPR	CGVPDV----------	----------
MMP11 human	---AERRGPQPWHAALPSSP	APAPATQEAPRPASSLRPPR	CGVPD----------	----------
MMP12 human	---YSGNLMKEKIQEMQHFL	GLKVTGQLDTSTLEMMHAPR	CGVPDV----------	----------
MMP13 human	----AASSMTERLREMQSFF	GLEVTGKLDDNTLDVMKKPR	CGVPDV----------	----------
MT1-MMP human	---RSPQSLSAAIAAMQKFY	GLQVTGKADADTMKAMRRPR	CGVPDK----------	----------
MT2-MMP human	---RSAQILASALAEMQRFY	GIPVTGVLDEETKEWMKRPR	CGVPDQ----------	----------
MT3-MMP human	---RSAETMQSALAAMQQFY	GINMTGKVDRNTIDWMKKPR	CGVPDQ----------	----------
MT4-MMP human	---QTQEELSKAITAMQQFG	GLEATGILDEATLALMKTPR	CSLPD----------	----------
MMP19 human	---FKPEDITEALRAFQEAS	ELPVSGQLDDATRARMRQPR	CGLEDP----------	----------
Collagenase-4 frog	----HIQPFTEKLEQMQKFF	GLKVTGTLDPKTVEVMEKPR	CGVYDV----------	----------
MMP newt	----A-SPLAEKIREMQKFC	GLQVTGKVDSNTLEVMQQPR	CGVSDV----------	----------
CMMP chicken	----NAEFTAEKLQKMQRFF	GLKVTGKPDTETLEMMKKPR	CGVPDV----------	----------
Enamelysin pig	---KGGNSMVKKIKELQAFF	GLRVTGKLDRTTMDVIKRPR	CGVPDV----------	----------
Envelysin	---A-NLNYTSAILDFQEHG	GINQTGILDADTAELLSTPR	CGVPDV----------	----------
MMP nematode	----------	----------	----------	----------MRSILLFILI
XMMP frog	AEPTKSPQFIDALKKFQKLN	NLPVTGTLDDATINAMNKPR	CGVPDNQMAKKETEKPTAAQ	SLENKTKDSENVTQQNPDPP
MMP cress	---DFDDILKAAVELYQTNF	NLNVTGELDALTIQHIVIPR	CGNPDVVNGTSLMHGGRRKT	F----------

(*continued on next page*)

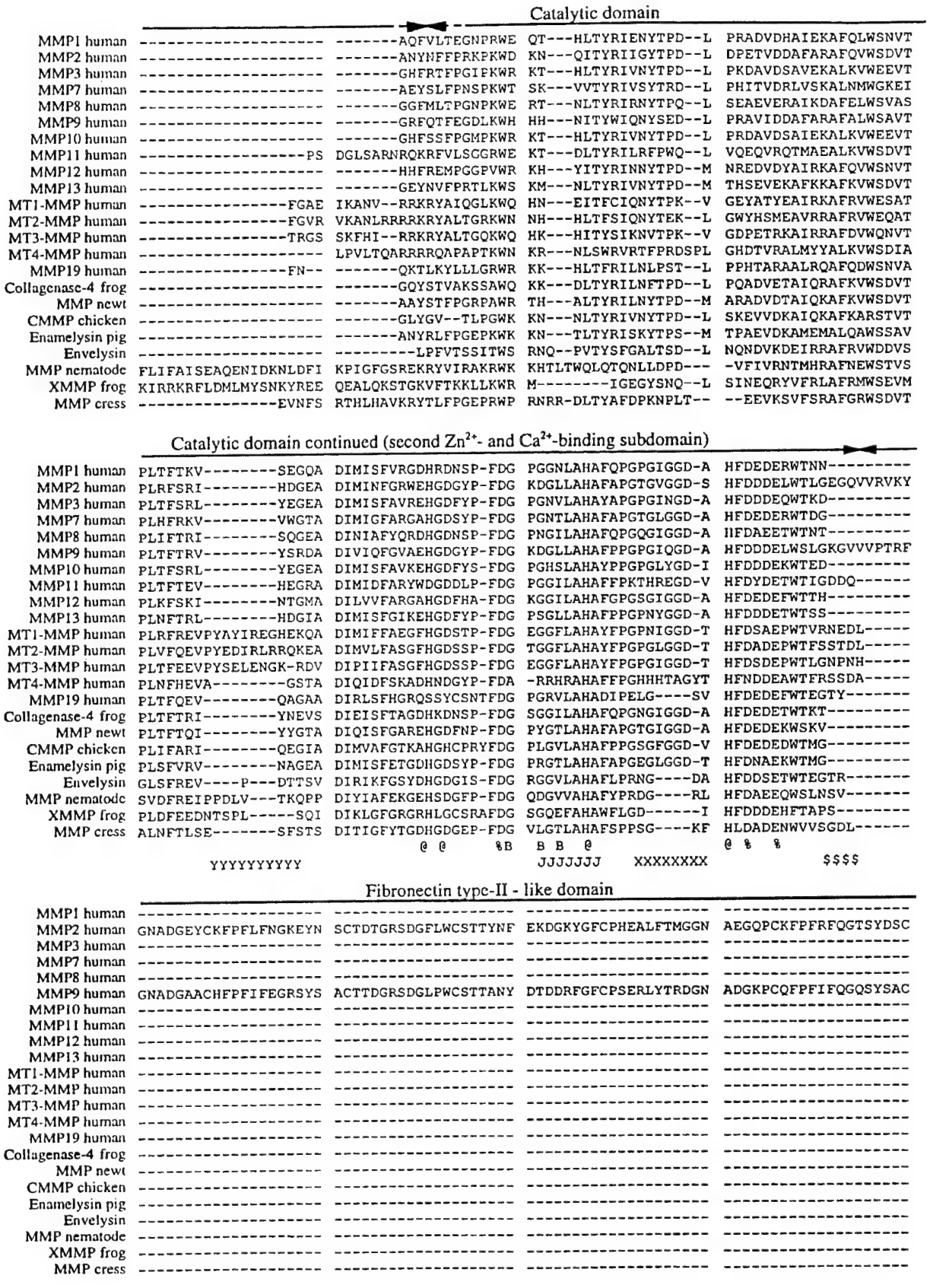

Figure 5. (*continued*)

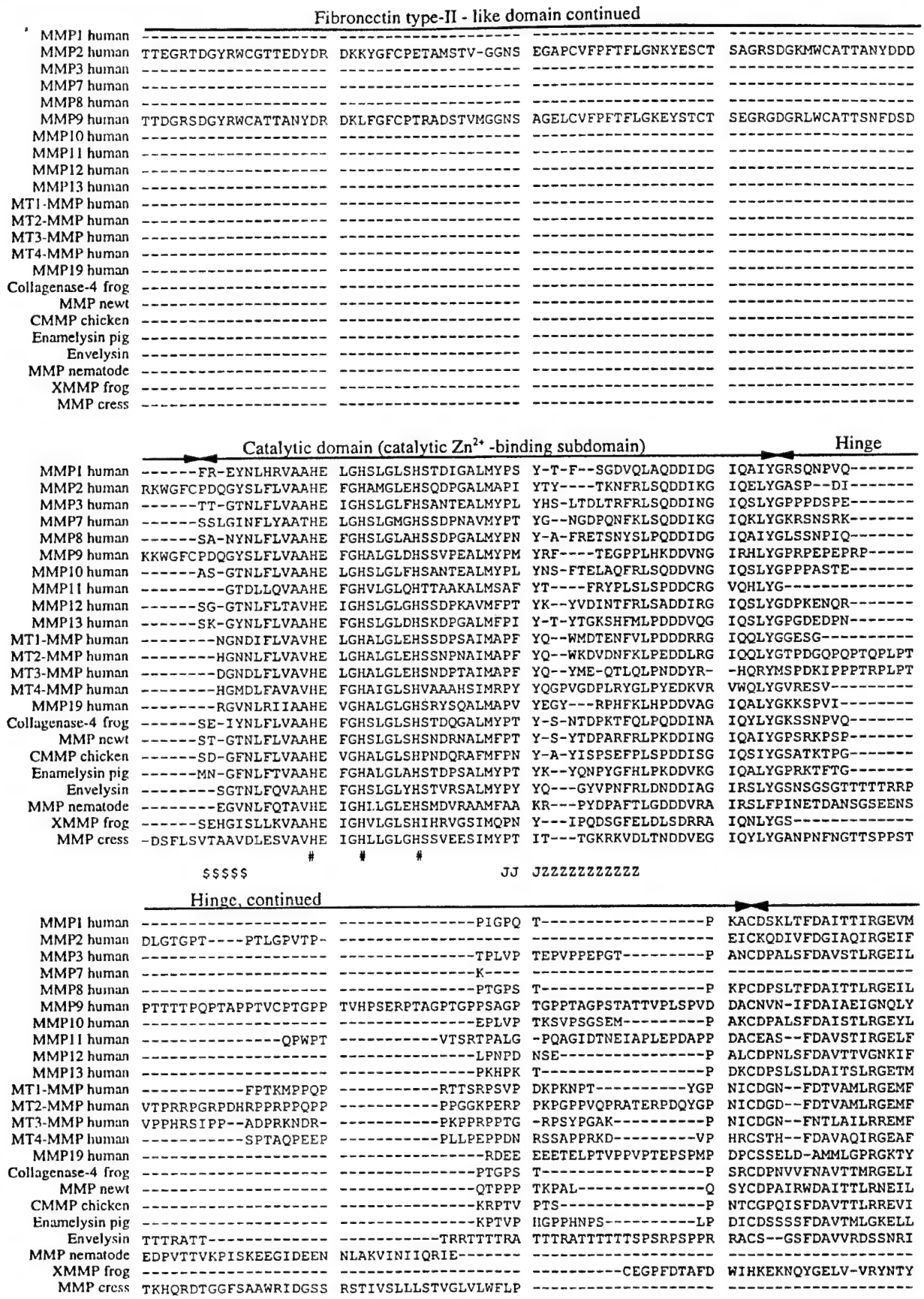

Figure 5. (*continued*)

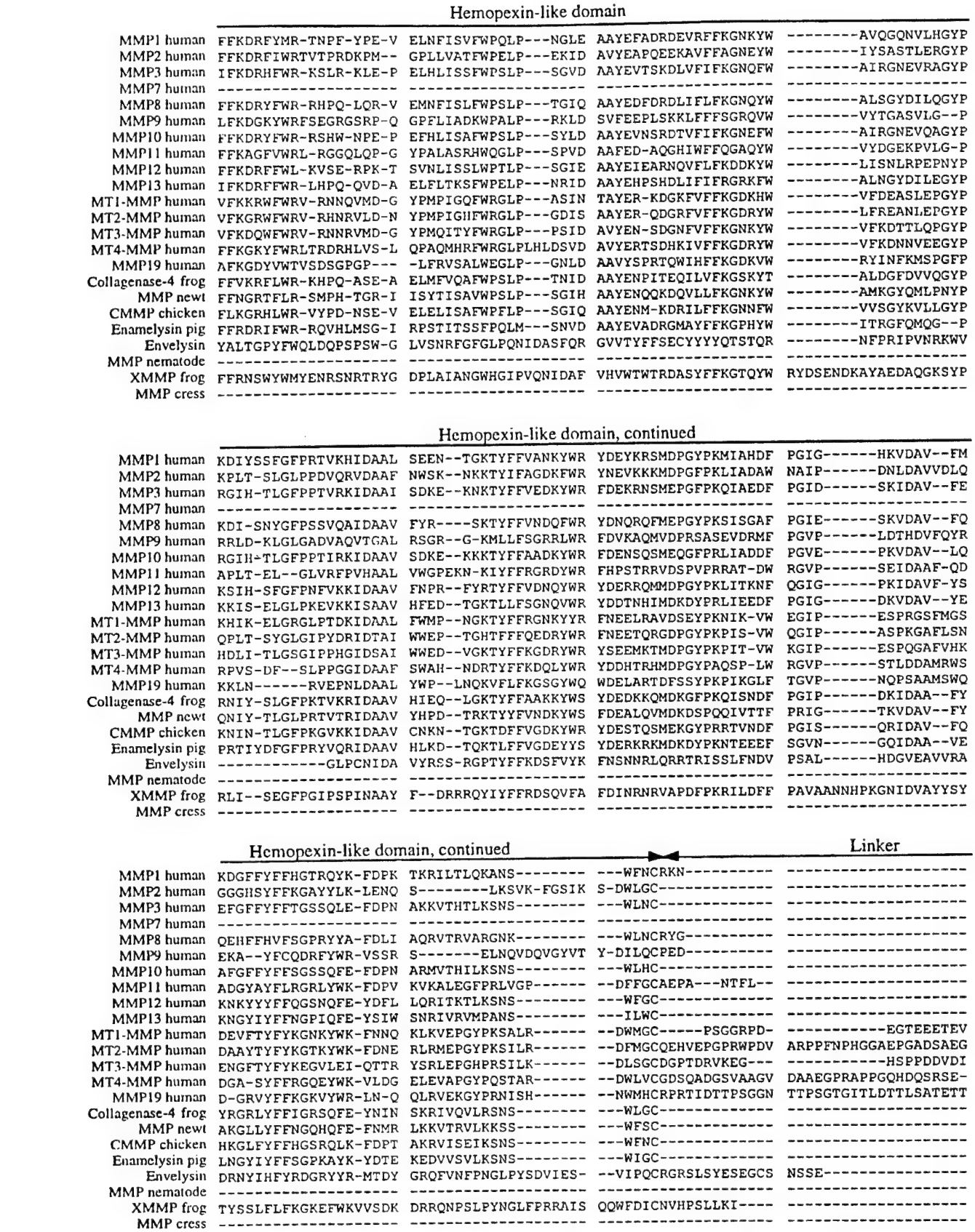

Figure 5. (*continued*)

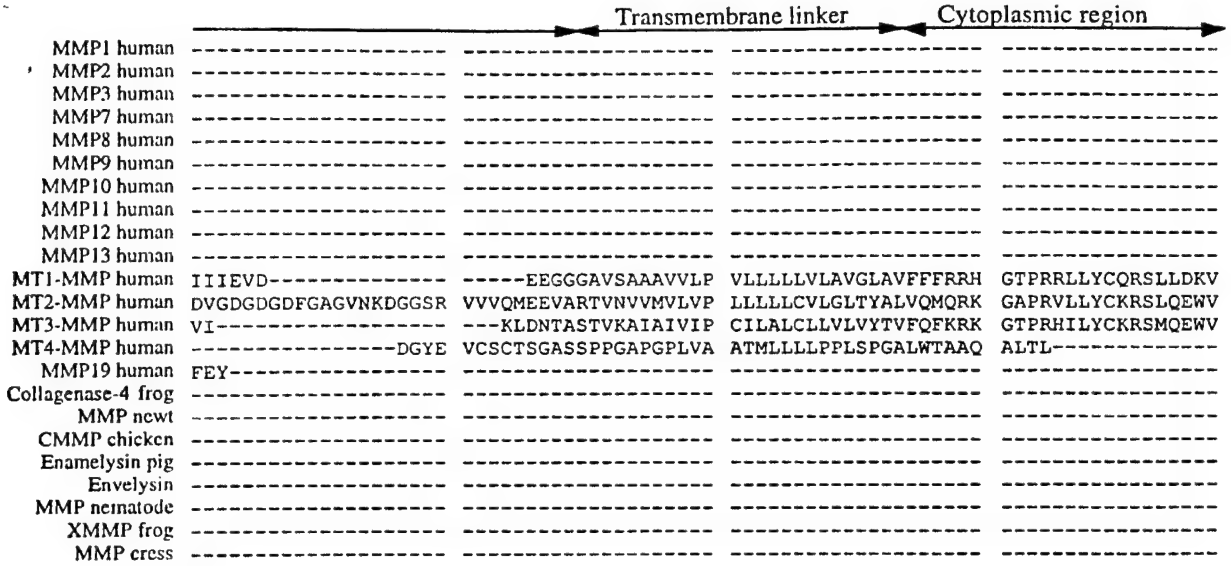

Figure 5. (*continued*)

that the catalytic domains of MMP-2 and MMP-9 (gelatinases) are not clustered together. Also, unlike sequence analysis for the entire enzymes, sequences for the catalytic domains did not sequester according to the location of the respective genes within the given chromosome. These observations collectively argue for the fact that the catalytic domains of these MMPs likely evolved in parallel, indicating that the selection pressure for the catalytic domain was distinct in the course of the diversification of this family of enzymes.

Three-dimensional structures of the catalytic domains of the 23 representative MMPs

The unique features of 3-dimensional structures of these enzymes were studied by developing computational models for the 23 catalytic domains. The crystal structures of the catalytic domains of four MMPs (MMP-1, MMP-3, MMP-7, and MMP-8) have been elucidated (26–29). We modeled the catalytic domain structures of the remaining 19 representative enzymes on the basis of the similar fold of the proteins that have been crystallized (30, 31; coordinates for the structures of the modeled MMP catalytic domains can be obtained from our group web page: http://sun2.science.wayne.edu/~somgroup). Closer examination of the structures of the catalytic domains revealed that a conserved aspartic acid is found in the vicinity of the methionine turn, the side chain of which is buried inside the core of the domain. The only variation to this pattern is seen in the rabbit MT1-MMP, which has a glutamic acid in this position. The two side chain oxygens of the aspartic acid form two critical structural hydrogen bonds to the backbone amides, one with the methionine of the methionine turn and another with the residue preceding the methionine. The conservation of this pattern/motif in all 64 known MMPs argues that these three histidines are absolutely required structural elements for the precise positioning of the catalytic zinc ion for effective catalysis. These three amino acids are marked with the pound sign (#) in Fig. 5.

We investigated the nature of two additional zinc and calcium binding sites formed by β-strands and turns in the proximity of the catalytic zinc in all the MMPs (31). The 64 MMPs developed at least four different ways to bind to this structural zinc ion. For the majority of MMPs (60 enzymes representing 20 subfamilies of the total of 23 identified by us), this site is provided by the side chains of an aspartic acid and three histidines (marked as an in Fig. 5). The signature for the binding site of the structural zinc and the calcium ion in the 60 MMPs is ***H***$_{\delta}$-[**GN**]-***D***-X(2)-[**PAS**]-**F**-***D***-[**GA**]-X(4)-[**LIRV**]-[**AG**]-***H***$_{\delta}$-[**AV**]-[**FYS**]-P-X(5,7,9)-***H***$_{\varepsilon}$-[**FL**]-***D***-X(2)-**E**-X-**W**. The letters in bold italics represent residues that provide side chains for coordination to the structural zinc and calcium; X(5, 7, 9) indicates five, seven, or nine variable residues in between the flanking sites. The . . .FYS. . . region in this pattern is close to the coordinated histidines, a result of the enzyme fold. The presence of these hydrophobic residues creates an increased hydrophobic environment and enhances the binding affinity for the metal ions. The human MMP-11 has an aspartic acid instead of one of His$_{\delta}$, which is different from the MMP-11 from rabbit and mouse, which still have a histidine at this position, suggesting that MMP-11 (comparing those from human, rabbit, and mouse) does not possess a unique motif for binding of the structural zinc. The chicken CMMP, the frog XMMP, and the human MMP-19 form a separate subfamily in the multiple-sequence

dendrograms and each has a unique motif for coordination to the structural zinc ion (31). The chicken CMMP has a histidine present where the majority of MMPs have an aspartic acid coordinated to the second zinc ion. A cysteine residue (Cys^{174}) adjacent to the fourth coordinated histidine implicates two possibilities for the binding mode of the structural zinc in CMMP. This cysteine may either provide a site for protein dimerization or another binding mode for the second zinc ion in CMMP (three original histidines and the cysteine coordinated to the zinc ion). This cysteine residue is also present in the sequence of the frog XMMP at the same position. The structural zinc coordination in MMP-19 is seen with two histidines at usual positions and one cysteine at the corresponding position as discussed for CMMP and XMMP, and the third histidine four residues toward the amino terminus. It has a noncoordination serine at the position where most MMPs have the third histidine (Fig. 5). The position of the third histidine is on a different β-strand, and the orientation of the side chain for the fourth coordination site is perfectly acceptable. Hence, the variations noted in the coordination to structural zinc ion may be indicative of the different outcomes for selection of novel enzymic activities. Furthermore, the dendrogram shown in Fig. 3 indicates that these variations in the zinc binding motif came about as a consequence of independent, unrelated evolutionary processes.

Calcium ion coordinates with six elements in the 3-dimensional structures of catalytic domains of MMPs, which come into close proximity for coordination as an octahedron. In all 64 MMPs, three of these elements, which are the side chains of amino acid residues, are conserved. These are two aspartic acids and one glutamic acid (marked by '%' in Fig. 5). A minor variation is seen only for the human MT4-MMP, which has an asparagine residue instead of the second aspartic acid. The other three calcium ligands are provided by the backbone carbonyl oxygens of three residues within a turn. Positions are marked by the letter 'B' in Fig. 5. The spatial location of the catalytic zinc ion, structural zinc ion, and the calcium ion are shown in **Fig. 6**.

Multiple-sequence analysis of regions encoding the hemopexin-like domain of MMPs

Figure 4 shows the results of multiple-sequence alignment for the hemopexin-like domains by themselves. This domain is absent in MMP-7 (matrilysin), in all known plant MMPs, and in the nematode MMP. The sequences of the hemopexin-like domains of invertebrate MMPs are the least related to all other MMPs, which indicates their ancient origin. In some MMPs, the hemopexin-like domains have been shown to facilitate binding and denaturation of the macromolecular substrates; it would be interesting to correlate clustering schemes for the hemopexin-like domains of MMPs to their substrate specificities. Because of the multiplicity of the known substrates for some of these enzymes and, in contrast, the paucity of any information on substrates for other MMPs, it is extremely difficult to draw any substantial conclusions on this issue. On the other hand, one cannot help but notice the diversification of the hemopexin-like domains seen in these proteins; insofar as this domain is clearly linked to the issue of substrate specificity, the diversity in this domain for the various MMPs indicates different evolutionary tangents pursued by these functionally distinct enzymes.

Murphy and Knäuper (32) recently reviewed the role of the hemopexin-like domains in relation to the substrate specificities and activities of various MMPs. It was suggested that the hemopexin-like domains mediate binding of MMP-1, MMP-8, MMP-13, and MMP-3 to collagen and that the complex participates in the cleavage of triple helical collagen. In the case of MMP-2 and MMP-9, the hemopexin-like domain is important for interactions with TIMPs, although the high degree of sequence similarity and the likely structures of the hemopexin-like domains of the gelatinases suggest there is a high degree of specificity in the binding of TIMPs to the latent forms of these enzymes. For example, TIMP-1 binds exclusively to latent MMP-9 (K_i ~35 nM), whereas TIMP-2 binds to latent MMP-2 (K_i ~5 nM) (43). We have recently shown a biphasic binding of TIMP-1 and TIMP-2 to the latent forms of MMP-9 and MMP-2, respectively, with the hemopexin-like domain representing the high-affinity binding site (43). Removal of the hemopexin-like domain of MMP-2 decreases the affinity of TIMP-2 for the active site without significantly affecting enzymatic activity. TIMP-1, which efficiently inhibits the active form of MMP-2, does not bind to a carboxy-terminally truncated MMP-2 form, demonstrating the importance of the hemopexin-like domain in interactions of TIMP-1 with active MMP-2 (43). The hemopexin-like domain of MMP-2 has also been shown to play a role in zymogen activation by MT1-MMP (44, 45). It has also been suggested that the hemopexin-like domain of MMP-2 plays a role in the binding of the enzyme to integrin $\alpha_v\beta_3$ (46, 47), a process that may facilitate localization of MMP-2 on the cell surface. The alignment of the hemopexin-like domains shows that MMP-2 and MMP-9 fall into two different clusters. The hemopexin-like domain of MMP-9 diverges at a higher hierarchial level, implicating that it is somewhat different from that of MMP-2 even though both are involved in TIMP binding. In contrast to gelatinases, there is not enough biochemical data on the various roles of hemopexin-like domains for all known MMPs, which may be different in each case. The interesting diversification of this domain and its effect on the functions of various MMPs can also be seen in the dendrogram of Fig. 4.

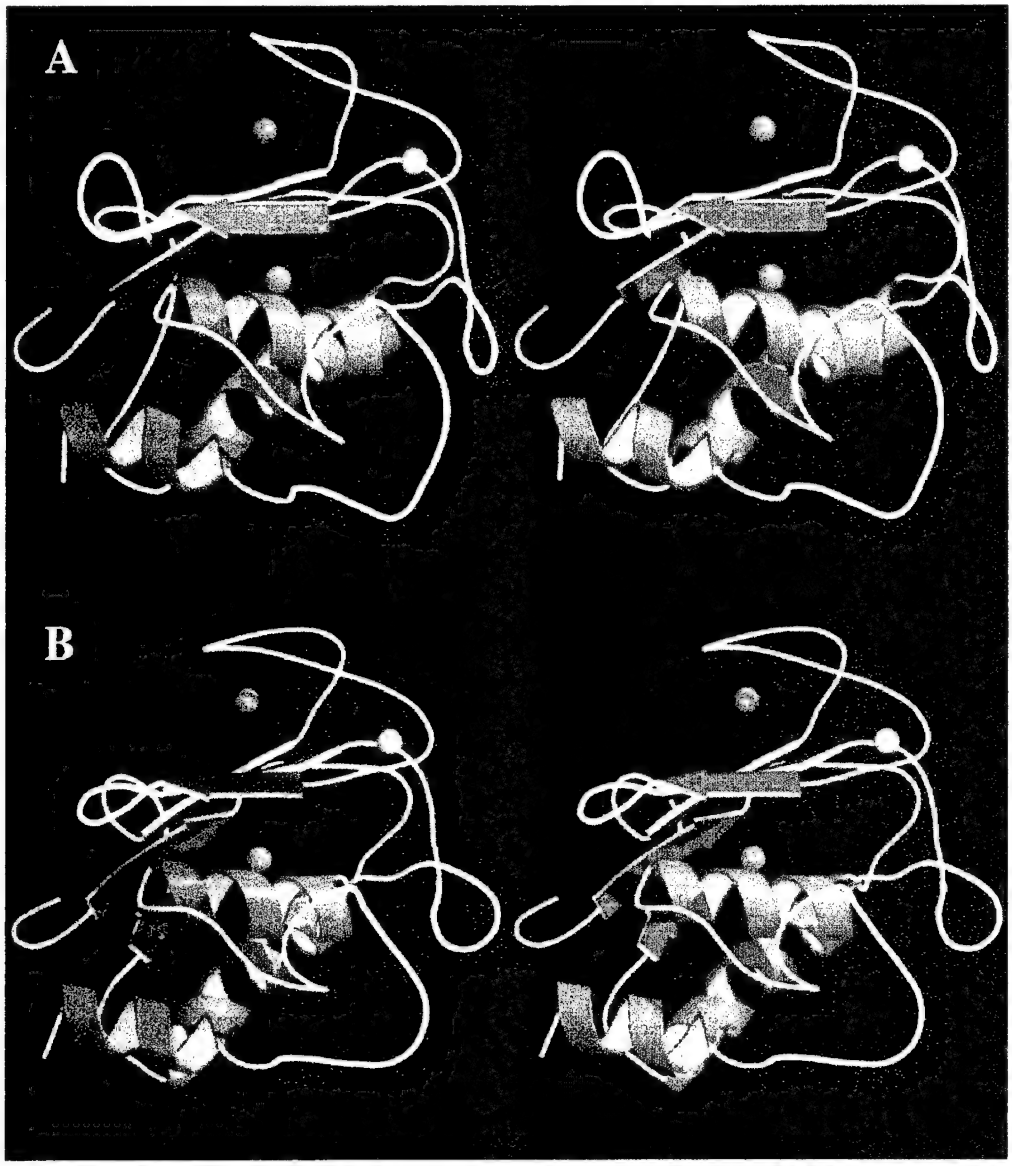

Figure 6. Ribbon drawing of the modeled 3-dimensional structures for the catalytic domains of MMP-12 (*A*) and MMP-19 (*B*). Red spheres represent the zinc ions and the green sphere represents the calcium ion. Catalytic zinc ion is located at the center of the catalytic domain and structural zinc is at the 12 o'clock position. The variable loops at 10, 5, and 3 o'clock (designated by 'X', 'Z', and '$' in Fig. 5, respectively) are shown in white. The two models are similar structurally, except for the variable regions (shown in white). Figures were prepared using MOLSCRIPT and Raster3D rendering programs (57, 58).

With the exception of envelysin and XMMP, all other hemopexin-like domains fall under one cluster. The hemopexin-like domain of MMP-9 formed a cluster by itself (vide infra), whereas those of MMP-11, MMP-19, and the MT-MMPs formed a separate cluster; all remaining MMPs constitute an additional cluster.

The hemopexin-like domain of envelysin forms a separate cluster from those of the other MMPs. Envelysin degrades the protective fertilization envelope, a complex of glycoproteins, releasing the embryos of sea urchin, although the individual glycoproteins have not yet been identified. Envelysin is also known to hydrolyze small peptides like substance P, oxidized insulin B, and collagenase substrate-like small peptide (48). In a recent study, it was also shown that the hemopexin-like domain of envelysin determines substrate specificity for this enzyme (24). The substrate specificity of envelysin is believed to be similar to that of stromelysin-1, which also degrades the fertilization envelope proteins of greater than 100 kDa. From the position of envelysin in the dendrogram as well as from the available functional data on this enzyme, it would appear that the hemopexin-like domain of this MMP is distinct from the rest and diverged early from those of the other MMPs.

Enamelysin is detected during the development of the enamel matrix and is expressed specifically in the enamel tissue. According to this report as well as one by other investigators (49), enamelysin forms a separate subfamily of MMPs. It is difficult to correlate its substrate specificity to the hemopexin-like domain alignment from the limited biochemical data available. However, its position suggests that it may be quite different from other collagenases. Recently, MMP-20 has been sequenced and its gene has been mapped to chromosome 11 (21). Our analysis of the complete sequences of MMPs (without human enamelysin) showed that pig enamelysin and other MMPs that are mapped together to chromosome 11 cluster together (Fig. 2*B*). In GenBank, another human metalloproteinase that is a product of the gene mmp20 has recently been reported (accession number AJ003144); this enzyme is mapped to chromosome 16. Only 183 amino acids are reported in its sequence; it probably is not sequenced completely and is not included in our current analysis (22).

The hemopexin-like domain of MMP-12 shows clustering by itself into a separate subfamily in close relation to enamelysin. Thus, the hemopexin-like domain of MMP-12 appears to have diverged into a separate subfamily (i.e., specialized) earlier than the hemopexin-like domains of the stromelysins and collagenases (MMP-1, MMP-3, MMP-8, MMP-10, and MMP-13, the exception being MMP-11), underscoring the role of MMP-12 as an 'elastase'. Despite the lack of a hemopexin-like domain, MMP-7 possesses a substrate preference similar to that of MMP-12, suggesting that the influence of the hemopexin-like domain on substrate interactions is limited, and other sites may play a role in determining substrate specificity. Indeed, comparison of the entire sequences of MMP-7 and MMP-12 (Fig. 2) shows that the clusters of these enzymes are equally remote from other MMPs, which, to put it another way, are equally distinct from other collagenases, gelatinases, stromelysins, and MT-MMPs.

MMP-13 possesses a substrate specificity that is broader than that of the other collagenases such as MMP-1 and MMP-8. The hemopexin-like domain of MMP-13 distinguishes itself by clustering into a separate subfamily, diverged at a higher level of hierarchy than MMP-1 and MMP-8. The frog collagenase-4 cleaves collagen type I, similar to MMP-1, and also possesses a weak gelatinolytic activity. This enzyme has been classified as a different type of collagenase due to its characteristic cleavage pattern of gelatin (50). This is supported by analysis of the sequences of hemopexin-like domains presented here, where the hemopexin-like domain of collagenase-4 clusters differently than those of other collagenases.

The newt MMPs have not been studied extensively to define their substrate specificities. However, in a sequence comparison study, these were classified as 'stromelysin type' (51). In our analysis, the newt MMPs also fell into a subfamily comprised of collagenases and stromelysins (MMP-13, MMP-1, MMP-10, CMMP, and MMP-8). MMP-1, MMP-10, MMP-3, MMP-8, and CMMP form closely akin, independent clusters, indicating that they are related, yet possess differentiated substrate specificities.

The hemopexin-like domain of MMP-11 (stromelysin-3), along with that of MMP-19 and MT-MMPs, diverged and formed a separate subfamily. MMP-11 is the first MMP reported to be activated intracellularly by means of a furin-like convertase and has been shown to be unable to cleave any of the major extracellular matrix components like other collagenases and stromelysins (52). The hemopexin-like domain of MMP-11 clustered separately in our analysis, suggesting distinct functional properties. Analysis of the role of the hemopexin-like domains and their relation to substrate specificities, if any, for the MT-MMP subfamily is more complex due to the presence of the transmembrane domain (vide infra). The hemopexin-like domains of all four known MT-MMPs form a subfamily of their own. Though there is not enough biochemical data on MT-MMPs, from the alignment of the hemopexin-like domains one can say that these domains have diverged to a significant extent from those of the other MMPs (except MMP-11), suggesting that their functional roles are different from the rest. XMMP has not been studied extensively for natural substrates. However, the results of the alignment of the complete sequence and the hemopexin-like domain of XMMP suggest that the substrate profile of XMMP may also be different from those of the other MMPs.

General folding of the catalytic domains of MMPs

In a previous study of the structural aspects of MMP-2 and MMP-9 (30), we investigated the binding modes of peptide substrates in the active sites of six MMPs (four crystallized and two modeled). Residues marked by the letter 'J' in Fig. 5 provide the anchoring interaction to the backbone elements of a potential substrate. The general structural comparison of the 23 representative MMPs revealed four areas of topological variability in the catalytic domains of the 64 MMPs. These areas are formed by four loops, three of which are located in the vicinity of the substrate binding region. These regions are marked by the letters 'X', 'Y', 'Z', and '$' (Fig. 5). Figure 6 shows the ribbon representation for two typical folds found for MMPs: one is for the human MMP-12 and another is MMP-19 (Fig. 6*A*, *B*, respectively). The three variable loops (at 10, 5, and 3 o'clock positions designated (in Fig. 5) as X, Z, and $, respectively) that could have contact with the bound substrates (vide infra) are shown in white in Fig. 6. The Y loop is located far from the substrate binding area on the

catalytic domain and is not especially highlighted in Fig. 6 (at 10 o'clock). The region designated by the letter X (at 10 o'clock in Fig. 6) is formed by the turn between the two antiparallel β-strands. These β-strands provide some of the binding ligands for the structural zinc and calcium binding sites. Our previous models for substrate binding in the active site of MMPs revealed that substrate can acquire an extended conformation (30). In such a binding mode, the unprimed portions [for convention on identification of substrates in protein–substrate complexes and their binding sites in proteases, consult Berger and Schechter (53)] of substrates would have contacts to the X loop. This loop is shorter in the human MMP-19 (Fig. 6*B*), frog XMMP, envelysins, plant MMPs, and nematode MMP than in all other MMPs. The shorter X loop makes the unprimed areas of the active site more open in these enzymes. The $ loop has contacts with the primed portion of the substrate (P_3' position) and is located at 3 o'clock in Fig. 6. The Z region (at 5 o'clock in Fig. 6) is an "Ω" loop, which forms the S_1' binding pocket; in the crystallized full-length porcine MMP-1, this loop has contacts through side chains and bridging water molecules to the hemopexin-like domain of the enzyme (54, 55). The length of this loop will control the size of the residue at P_1' position of the substrate. The composition of the loop will have an effect on substrate specificity (30). Furthermore, binding of protein substrates by some MMPs is influenced by interactions with the hemopexin-like domain (32). Nonetheless, the specificity of small synthetic substrates is triggered by their interactions solely with the active site in the catalytic domain and its surroundings. This is probably true even for gelatinases, since the catalytic domain of MMP-2 with excised gelatin binding domain is still active in hydrolysis of synthetic peptides (10, 56). Substrates interact with the loops designated X, $, and Z at unprimed and primed portions, and structural variability of these loops provide the diversity of such interactions.

CONCLUSION

The foregoing examined sequence similarities, sequence alignments, and structural aspects in arriving at an understanding of the important functions for the family of matrix metalloproteinases. Our analysis of the structures of MMPs in view of their evolutionary relationship follow the limitations of the primary sequence alignment and the prediction of the 3-dimensional structures, but present a distinctive way of looking at the multidomain structures like those of MMPs. The fact that alignment of the entire sequences and those for the catalytic domains and the hemopexin-like domains produced essentially the same numbers for the clusters (22–23 clusters) and that the composition for the clusters appear to be the same in each case is not coincidental. What this reveals to us is the likely scenario that domain assemblies occurred in an early stage of the diversification of these enzymes and that they progressed through the evolutionary process independent of one another, and perhaps in parallel to each other. This fact does not divorce itself from the obvious premise that at some primordial point in the evolution of these enzymes they must have existed as simple single-domain proteins that underwent gene fusions to generate the more complicated multidomain enzymes. This point is perhaps best underscored by the examples of the three plant MMPs and the sole enzyme from nematode. These clearly are modern variants of enzymes that did not undergo major structural elaboration in their development. However, our analysis also demonstrates that there are examples where evolution progressed in the reverse direction: a more complicated multidomain enzyme underwent truncation in its gene sequence to give rise to a less elaborated protein of fewer domains. An example of this type of retrograde process is matrilysin (MMP-7), which contains only the signal peptide, the propeptide, and the catalytic domain.

It is not clear how many more MMPs exist in nature, and our understanding of the actual functions of these enzymes is now at a rudimentary stage. As more sequences of MMPs become available, the analysis presented here should be updated and correlated with the new structural information that will be determined for these important enzymes. Nonetheless, the exercise presented here is the first step toward appreciation of the evolutionary processes that led to the diversification of these enzymes, with the attendant myriad of activities of central importance to both the physiology and pathology of living organisms. FJ

This work was supported by grants from the U.S. Army (to S.M.) and the Karmanos Cancer Institute (to S.M. and R.F.). R.F. is also supported by National Institutes of Health grant CA-61986. I.M. was a recipient of the Rumble and Heller predoctoral fellowships. We acknowledge Markku Kurkinen for providing us with the amino acid sequences for CMMP.

REFERENCES

1. Woodhouse, E. C., Chuaqui, R. F., and Liotta, L. A. (1997) General mechanisms of metastasis. *Cancer* **80 (Suppl. 8)**, 1529–1537
2. Chambers, A. F., and Matrisian, L. M. (1997) Changing views of the role of matrix metalloproteinases in metastasis. *J. Natl. Cancer Inst.* **89**, 1260–1270
3. Coussens, L. M., and Werb, Z. (1996) Matrix metalloproteinases and the development of cancer. *Chem. Biol.* **3**, 895–904
4. Yu, A. E., Hewitt, R. E., Connor, E. W., and Stetler-Stevenson, W. G. (1997) Matrix metalloproteinases. Novel targets for directed cancer therapy. *Drugs Aging* **11**, 229–244
5. Kohn, E. C., and Liotta, L. A. (1995) Molecular insights into cancer invasion: strategies for prevention and intervention. *Cancer Res.* **55**, 1856–1862

6. Bode, W., Reinemer, P., Huber, R., Kleine, T., Schnierer, S., and Tschesche, H. (1994) The X-ray crystal structure of the catalytic domain of human neutrophil collagenase inhibited by a substrate analogue reveals the essentials for catalysis and specificity. *EMBO J.* **13**, 1263–1269
7. Salowe, S. P., Marcy, A. I., Cuca, G. C., Smith, C. K., Kopka, I. E., Hagman, W. K., and Hermes, J. D. (1992) Characterization of zinc-binding sites in human stromelysin-1: stoichiometry of the catalytic domain and identification of a cysteine ligand in the proenzyme. *Biochemistry* **31**, 4535–4540
8. Borden, P., and Heller, R. A. (1997) Transcriptional control of matrix metalloproteinases and the tissue inhibitors of matrix metalloproteinases. *Crit. Rev. Eukaryot. Gen. Expression* **7**, 159–178
9. Gomis-Rüth, F.-X., Maskos, K., Betz, M., Bergner, A., Huber, R., Suzuki, K., Yoshida, N., Nagase, H., Brew, K., Bourenkov, G. P., Bartunik, H., and Bode, W. (1997) Mechanism of inhibition of the human matrix metalloproteinase stromelysin-1 by TIMP-1. *Nature (London)* **389**, 77–81
10. Murphy, G., Nguyen, Q., Cockett, M. I., Atkinson, S. J., Allan, J. A., Knight, C. G., Willenbrock, F., and Docherty, A. J. P. (1994) Assessment of the role of the fibronectin-like domain of gelatinase A by analysis of a deletion mutant. *J. Biol. Chem.* **269**, 6632–6636
11. Sato, H., Kinoshita, T., Takino, T., Nakayama, K., and Seiki, M. (1996) Activation of a recombinant membrane type 1-matrix metalloproteinase (MT1-MMP) by furin and its interaction with tissue inhibitor of metalloproteinases (TIMP)-2. *FEBS Lett.* **393**, 101–104
12. Puente, X. S., Pendás, A. M., Llano, E., Velasco, G., and López-Otín, C. (1996) Molecular cloning of a novel membrane-type matrix metalloproteinase from a human breast carcinoma. *Cancer Res.* **56**, 944–949
13. Santavicca, M., Noel, A., Angliker, H., Stoll, I., Segain, J. P., Anglard, P., Chretien, M., Seidah, N., and Basset, P. (1996) Characterization of structural determinants and molecular mechanisms involved in pro-stromelysin-3 activation by 4-aminophenylmercuric acetate and furin-type convertases. *Biochem. J.* **315**, 953–958
14. Wilhelm, S. M., Collier, I. E., Marmer, B. L., Eisen, A. Z., Grant, G. A., and Goldberg, G. I. (1989) SV40-transformed human lung fibroblasts secrete a 92-kDa type IV collagenase which is identical to that secreted by normal human macrophages. *J. Biol. Chem.* **264**, 17213–17221
15. Fridman, R., Bird, R. E., Hoyhtya, M., Oelkuct, M., Komarek, D., Liang, C.-M., Berman, M. L., Liotta, L. A., Stetler-Stevenson, W. G., and Fuerst, T. R. (1993) Expression of human recombinant 72 kDa gelatinase and tissue inhibitor of metalloproteinase-2 (TIMP-2): characterization of complex and free enzyme. *Biochem. J.* **289**, 411–416
16. Goldberg, G. I., Strongin, A., Collier, I. E., Genrich, L. T., and Marmer, B. L. (1992) Interaction of 92-kDa type IV collagenase with tissue inhibitor of metalloproteinases prevents dimerization, complex formation with interstitial collagenase, and activation of the proenzyme with stromelysin. *J. Biol. Chem.* **267**, 4583–4591
17. Butler, G. S., Butler, M. J., Atkinson, S. J., Will, H., Tamura, T., van Westrum, S. S., Crabbe, T., Clements, J., d'Ortho, M.-P., and Murphy, G. (1998) The TIMP2 membrane type 1 metalloproteinase 'receptor' regulates the concentration and efficient activation of progelatinase A. *J. Biol. Chem.* **273**, 871–880
18. Stöcker, W., Grams, F., Baumann, U., Reinemer, P., Gomis-Rüth, F.-X., McKay, D. B., and Bode, W. (1995) The metzincins—topological and sequential relations between the astacins, adamalysins, serralysins, and matrixins (collagenases) define a superfamily of zinc-peptidases. *Protein Sci.* **4**, 823–840
19. Rawlings, N. D., and Barrett, A. J. (1995) Evolutionary families of metallopeptidases. *Methods Enzymol.* **248**, 183–228
20. Sang, Q. A., and Douglas, D. A. (1996) Computational sequence analysis of matrix metalloproteinases. *J. Protein Chem.* **15**, 137–160
21. Llano, E., Pendás, A. M., Knäuper, V., Sorsa, T., Salo, T., Salido, E., Murphy, G., Simmer, J. P., Bartlett, J. D., and López-Otín, C. (1997) Identification and structural and functional characterization of human enamelysin (MMP-20). *Biochemistry* **36**, 15101–15108
22. Bernot, A., Clepet, C., Dasilva, C., Devaud, C., Petit, J.-L., Caloustian, C., Cruaud, C., Samson, D., Pulcini, F, Weissenbach, J., Heilig, R., Notanicola, C., Domingo, C., Rozenbaum, M., Benchetrit, E., Tpaloglu, R., Dewalle, M., Dross, C., Hadjari, P., Dupont, M., Demaille, J., Touitou, I., Smaoui, N., Nedelec, B., Méry, J.-P., Chaabouni, H., Delpech, M., and Grateau, G. (1997) A candidate gene for familial Mediterranean fever. *Nature Genet.* **17**, 25–31
23. Lepage, T., and Gache, C. (1990) Early expression of a collagenase-like hatching enzyme gene in the sea urchin embryo. *EMBO J.* **9**, 3003–3012
24. Namura, K., Shimuzu, T., Kinoh, H., Sendai, Y., Inomata, M., and Suzuki, N. (1997) Sea urchin hatching enzyme (Envelysin): cDNA cloning and deprivation of protein substrate specificity by autocatalytic degradation. *Biochemistry* **36**, 7225–7238
25. Wilson, R., Ainscough, R., Anderson, K., Baynes, C., Berks, M., Bonfield, J., Burton, J., Connell, M., Copsey, T., Cooper, J., Coulson, A., Craxton, M., Dear, S., Du, Z., Durbin, R., Favello, A., Fraser, A., Fulton, L., Gardner, A., Green, P., Hawkins, T., Hiller, L., Jier, M., Johnston, L., Jones, M., Kershaw, J., Kirsten, J., Laisster, N., Latreille, P., Lightning, J., Lloyd, C., Mortimore, B., O'Callaghan, M., Parsons, J., Percy, C., Rifken, L., Roopra, A., Saunders, D., Shownkeen, R., Sims, M., Smaldon, N., Smith, A., Smith, M., Sonnhammer, E., Staden, R., Sulston, J., Thierry-Mieg, J., Thomas, K., Vaudin, M., Vaughan, K., Waterston, R., Watson, A., Weinstock, L., Wilkinson-Sproat, J., and Wohldman, P. (1994) 2.2 Mb of contiguous nucleotide sequence from chromosome III of *C. elegans*. *Nature (London)* **368**, 32–38
26. Lovejoy, B., Cleasby, A., Hassell, A. M., Longley, K., Luther, M. A., Weigl, D., McGeehan, G., McElroy, A. B., Drewry, D., Lambert, M. H., and Jordan, S. R. (1994) Structure of the catalytic domain of fibroblast collagenase complexed with an inhibitor. *Science* **263**, 375–377
27. Stams, T., Spurlino, J. C., Smith, D. L., Wahl, R. C., Ho, T. F., Qoronfleh, M. W., Banks, T. M., and Rubin, B. (1994) Structure of human neutrophil collagenase reveals large S_1' specificity pocket. *Nature Struct. Biol.* **1**, 119–123
28. Gooley, P. R., O'Connell, F., Marcy, A. I., Cuca, G. C., Salowe, S. P., Bush, B. L., Hermes, J. D., Esser, C. K., Hagmann, W. K., Springer, J. P., and Johnson, B. A. (1994) The NMR structure of the inhibited catalytic domain of human stromelysin-1. *Nature Struct. Biol.* **1**, 111–118
29. Browner, M. F., Smith, W. W., and Castelhano, A. L. (1995) Matrilysin-inhibitor complexes: common themes among metalloproteases. *Biochemistry* **34**, 6602–6610
30. Massova, I., Fridman, R., and Mobashery, S. (1997) Structural insight into the catalytic domains of human matrix metalloprotease-2 and human matrix metalloprotease-9: implications for substrate specificities. *J. Mol. Mod.* **3**, 17–30
31. Massova, I., Kotra, L. P., and Mobashery, S. (1998) Structural insight into the binding motifs for the calcium ion and the noncatalytic zinc in matrix metalloproteases. *Bioorg. Med. Chem. Lett.* **8**, 853–858
32. Murphy, G., and Knäuper, V. (1997) Relating matrix metalloproteinase structure to function: why the 'hemopexin' domain? *Matrix Biol.* **15**, 511–518
33. Murphy, G., Allan, J. A., Willenbrock, F., Crockett, M. I., O'Connell, J. P., and Docherty, J. P. (1992) The role of the C-terminal domain in collagenase and stromelysin specificity. *J. Biol. Chem.* **267**, 9616–9618
34. Murphy, G. J., Murphy, G., and Reynolds, J. J. (1991) The origin of matrix metalloproteinases and their familial relationships. *FEBS Lett.* **289**, 4–7
35. De Souza, S. J., and Brentani, R. (1993) Sequence homology between a bacterial metalloproteinase and eukaryotic matrix metalloproteinases. *J. Mol. Evol.* **36**, 596–598
36. McGeehan, G., Burkhart, W., Anderegg, R., Becherer, D., Gillikin, J. W., and Graham, J. S. (1992) Sequencing and characterization of the soybean leaf metalloproteinase. *Plant Physiol.* **99**, 1179–1183
37. Franco, A. A., Mundy, L. M., Trucksis, M., Wu, S., Kaper, J. B., and Sears, C. L. (1997) Cloning and characterization of the *Bacteroides fragilis* metalloprotease toxin gene. *Infect. Immunol.* **65**, 1007–1013
38. Yang, M., Murray, M. T., and Kurkinen, M. (1997) A novel metalloproteinase gene (XMMP) encoding vitronectin-like motifs is transiently expressed in *Xenopus laevis* early embryo development. *J. Biol. Chem.* **272**, 13527–13533

39. Pei, D., and Weiss, S. J. (1995) Furin-dependent intracellular activation of the human stromelysin-3 zymogen. *Nature (London)* **375**, 244–247
40. Van Wart, H. E., and Birkedal-Hansen, H. (1990) The cysteine switch: a principle of regulation of metalloproteinase activity with potential applicability to the entire matrix metalloproteinase gene family. *Proc. Natl. Acad. Sci. USA* **87**, 5578–5582
41. Becker, J. W., Marcy, A. I., Rokosz, L. L., Axel, M. G., Burbaum, J. J., Fitzgerald, P. M. D., Cameron, P. M., Esser, C. K., Hagmann, W. K., Hermes, J. D., and Springer, J. P. (1995) Stromelysin-1: three-dimensional structure of the inhibited catalytic domain and of the C-truncated proenzyme. *Protein Sci.* **4**, 1966–1976
42. Bode, W., Grams, F., Reinemer, P., Gomis-Rüth, F. X., Baumann, U., McKay, D. B., and Stocker, W. (1996) The metzincin-superfamily of zinc-peptidases. *Adv. Exp. Med. Biol.* **389**, 1–11
43. Olson, M. W., Gervasi, D. C., Mobashery, S., and Fridman, R. (1997) Kinetic analysis of the binding of human matrix metalloproteinase-2 and -9 to tissue inhibitor of metalloproteinase (TIMP)-1 and TIMP-2. *J. Biol. Chem.* **272**, 29975–29983
44. Strongin, A. Y., Collier, I. E., Bannikov, G., Marmer, B. L., Grant, G. A., and Goldberg, G. I. (1995) Mechanism of cell surface activation of 72-kDa type IV collagenase. *J. Biol. Chem.* **270**, 5331–5338
45. Gohlke, U., Gomis-Rüth, F. X., Crabbe, T., Murphy, G., Docherty, A. J., and Bode, W. (1996) The C-terminal (hemopexin-like) domain structure of human gelatinase A (MMP-2): structural implications for its function. *FEBS Lett.* **378**, 126–130
46. Brooks, P. C., Stromblad, S., Sanders, L. C., von Schalscha, T. L., Aimes, R. T., Stetler-Stevenson, W. G., Quigley, J. P., and Cheresh, D. A. (1996) Localization of matrix metalloproteinase-2 to the surface of invasive cells by interaction with integrin $\alpha_v\beta_3$. *Cell* **85**, 683–693
47. Brooks, P. C., Silletti, S., von Schalscha, T. L., Friedlander, M., and Cheresh, D. A. (1998) Disruption of angiogenesis by PEX, a noncatalytic metalloproteinase fragment with integrin binding activity. *Cell* **92**, 391–400
48. Namura, K., Tanaka, H., Kikkawa, Y., Yamaguchi, M., and Suzuki, N. (1991) The specificity of sea urchin hatching enzyme (envelysin) places it in the mammalian matrix metalloproteinases. *Biochemistry* **30**, 6115–6123
49. Bartlett, J. D., Simmer, J. P., Xue, J., Margolis, H. C., and Moreno, E. C. (1996) Molecular cloning and mRNA tissue distribution of a novel matrix metalloproteinase isolated from porcine enamel organ. *Gene* **183**, 123–128
50. Stolow, M. A., Bauzon, D. D., Li, J., Sedgwick, T., Liang, V. C.-T., Sang, Q. A., and Shi, Y.-B. (1996) Identification and characterization of a novel collagenase in *Xenopus laevis*: possible roles during frog development. Mol. Biol. Cell. **7**, 1471–1483
51. Miyazaki, K., Uchiyama, K., Imokawa, Y., and Yoshizato, K. (1996) Cloning and characterization of cDNAs for matrix metalloproteinases of regenerating newt limbs. *Proc. Natl. Acad. Sci. USA* **93**, 6819–6824
52. Noel, A., Santavicca, M., Stoll, I., L'Hoir, C., Staub, A., Murphy, G., Rio, M. C., and Basset, P. (1995) Identification of structural determinants controlling human and mouse stromelysin-3 proteolytic activities. *J. Biol. Chem.* **270**, 22866–22872
53. Berger, A., and Schechter, I. (1970) Mapping the active site of papain with the aid of peptide substrates and inhibitors. *Phil. Trans. R. Soc. London B Biol. Sci.* **257**, 249–264
54. Li, J., Brick, P., O'Hare, M. C., Skarzynski, T., Lloyd, L. F., Curry, V. A., Clark, I. M., Bigg, H. F., Hazelman, B. L., Cawston, T. E., and Blow, D. M. (1995) Structure of full-length porcine synovial collagenase reveals a C-terminal domain containing a calcium-linked, four-bladed β-propeller. *Structure* **3**, 541–548
55. Bode, W. (1995) A helping hand for collagenases: the hemopexin-like domain. *Structure* **3**, 527–530
56. Ye, Q. Z., Johnson, L. L., Yu, A. E., and Hupe, D. (1995) Reconstructed 19 kDa catalytic domain of gelatinase A is an active proteinase. *Biochemistry* **34**, 4702–4708
57. Kräulis, P. J. (1991) MOLSCRIPT: a program to produce both detailed and schematic plots of protein structures. *J. Appl. Cryst.* **24**, 946–950
58. Merritt, E. A., and Bacon, D. J. (1997) Raster3D photorealistic molecular graphics. *Methods Enzymol.* **277**, 505–524

THE JOURNAL OF BIOLOGICAL CHEMISTRY
Vol. 275, No. 4, Issue of January 28, pp. 2661–2668, 2000
Printed in U.S.A.

Characterization of the Monomeric and Dimeric Forms of Latent and Active Matrix Metalloproteinase-9

DIFFERENTIAL RATES FOR ACTIVATION BY STROMELYSIN 1*

(Received for publication, May 21, 1999, and in revised form, October 6, 1999)

Matthew W. Olson‡§, M. Margarida Bernardo‡, Martin Pietila‡, David C. Gervasi‡, Marta Toth‡, Lakshmi P. Kotra¶, Irina Massova¶, Shahriar Mobashery¶, and Rafael Fridman‡‖

From the ‡Department of Pathology and Karmanos Cancer Institute and the ¶Department of Chemistry, Wayne State University, Detroit, Michigan 48201

Matrix metalloproteinase-9 (MMP-9) is a member of the MMP family that has been associated with degradation of the extracellular matrix in normal and pathological conditions. A unique characteristic of MMP-9 is its ability to exist in a monomeric and a disulfide-bonded dimeric form. However, there exists a paucity of information on the properties of the latent (pro-MMP-9) and active MMP-9 dimer. Here we report the purification to homogeneity of the monomer and dimer forms of pro-MMP-9 and the characterization of their biochemical properties and interactions with tissue inhibitor of metalloproteinase (TIMP)-1 and TIMP-2. Gel filtration and surface plasmon resonance analyses demonstrated that the pro-MMP-9 monomeric and dimeric forms bind TIMP-1 with similar affinities. In contrast, TIMP-2 binds only to the active forms. After activation, the two enzyme forms exhibited equal catalytic competence in the turnover of a synthetic peptide substrate with comparable kinetic parameters for the onset of inhibition with TIMPs and for dissociation of the inhibited complexes. Kinetic analyses of the activation of monomeric and dimeric pro-MMP-9 by stromelysin 1 revealed K_m values in the nanomolar range and relative low k_{cat} values (1.9×10^{-3} and 4.1×10^{-4} s^{-1}, for the monomer and dimer, respectively) consistent with a faster rate (1 order of magnitude) of activation of the monomeric form by stromelysin 1. This suggests that the rate-limiting event in the activation of pro-MMP-9 may be a requisite slow unfolding of pro-MMP-9 near the site of the hydrolytic cleavage by stromelysin 1.

Matrix metalloproteinase-9 (MMP-9),[1] also known as gelatinase B, is a member of the MMP family of zinc-dependent endopeptidases known for their ability to degrade many extracellular matrix (ECM) components (1, 2). MMP-9 is secreted in a latent form (pro-MMP-9) by a variety of normal and transformed cells and has been implicated in the pathogenesis of several human diseases including arthritis (3), cardiovascular disease (4, 5), and cancer metastasis (6, 7). MMP-9 has also been suggested to play a role in the degradation of ECM during inflammation (8), wound healing (9, 10), trophoblast implantation (11), and angiogenesis (12). Structurally, pro-MMP-9 is closely related to pro-MMP-2 (gelatinase A) with both enzymes containing a fibronectin-like type II module (gelatin-binding domain) inserted into the catalytic domain that is thought to facilitate interaction of the enzymes with collagen molecules (13, 14). The zymogenic forms of both enzymes interact, via their C-terminal domain (hemopexin-like domain), with tissue inhibitors of metalloproteinases (TIMPs), a family of specific endogenous MMP inhibitors (15, 16). Pro-MMP-9 binds to TIMP-1 (1), whereas pro-MMP-2 binds to TIMP-2 (17) and to TIMP-4 (18). After activation, any TIMP molecule efficiently inhibits the enzymatic activity by binding to the catalytic domain of the MMP (16).

Despite the similarities that exist between pro-MMP-9 and pro-MMP-2, the former is unique in several aspects including its gene regulation, structure, and function (2, 14). Pro-MMP-9 is glycosylated and contains an additional 54-amino acid proline-rich insertion of unknown function between the catalytic and the hemopexin-like domains (1). In addition, pro-MMP-9, in contrast to pro-MMP-2, exists in two major forms: a monomeric (~92 kDa) and a disulfide-bonded homodimeric (~220 kDa) form (1). Both the monomeric and dimeric forms of pro-MMP-9 forms have been identified in a variety of pro-MMP-9-producing cells including normal (19–21) and tumor cells (1, 22) and in various biological fluids (23, 24) and tissues (25, 26), indicating that they are physiological forms of the enzyme. In addition, a 125–130-kDa form of pro-MMP-9 present in neutrophil granules has been reported to be a complex of the enzyme with lipocalin (NGAL) (19, 20).

Studies examining the activation, catalytic activity, and interactions with TIMPs of pro-MMP-9 and MMP-9 have focused mainly on the monomeric form of the enzyme. Thus, little is known about the biochemical properties of the homodimeric form. A previous study examined the structural requirements for the formation of the pro-MMP-9 homodimer and its interaction with TIMP-1 (27). However, the kinetics of activation, the catalytic efficiencies, and the inhibition by TIMPs of the monomeric and dimeric forms remained unknown. Here, we report the first comprehensive study aimed at characterizing the biochemical properties of both the latent and active pure monomeric and dimeric forms.

* This work was supported by National Institutes of Health Grant CA-61986 (to R. F.) and United States Army Grant DAMD17-97-1--174 (to S. M.). The costs of publication of this article were defrayed in part by the payment of page charges. This article must therefore be hereby marked "*advertisement*" in accordance with 18 U.S.C. Section 1734 solely to indicate this fact.

§ Current address: Biochemistry/Molecular Biology, Infectious Disease Research, Wyeth-Ayerst Research, Pearl River, NY 10965.

‖ To whom correspondence should be addressed: Dept. of Pathology, Wayne State University, 540 E. Canfield Ave., Detroit, MI 48201. Tel.: 313-577-1218; Fax: 313-577-8180; E-mail: rfridman@med.wayne.edu.

[1] The abbreviations used are: MMP, matrix metalloproteinase; TIMP, tissue inhibitor of metalloproteinase; ECM, extracellular matrix; PAGE, polyacrylamide gel electrophoresis; SPR, surface plasmon resonance; PBS, phosphate-buffered saline; pro-MMP-9_M, pro-MMP-9 monomer; pro-MMP-9_D, pro-MMP-9 dimer; mAb, monoclonal antibody; pAb, polyclonal antibody.

EXPERIMENTAL PROCEDURES

Buffers—Buffer C (50 mM HEPES (pH 7.5), 150 mM NaCl, 5 mM $CaCl_2$, and 0.02% Brij-35); buffer B (10 mM sodium acetate (pH 4.5)); buffer W (7.8 mM NaH_2PO_4, 8 mM Na_2HPO_4 (pH 7.2), 137 mM NaCl, 0.1 mM $CaCl_2$, 3 mM KCl, 1.5 mM KH_2PO_4, and 0.02% Tween 20); buffer R (50 mM HEPES (pH 7.5), 150 mM NaCl, 5 mM $CaCl_2$, 0.01% Brij-35, and 1% (v/v) Me_2SO); buffer D (50 mM Tris (pH 7.4), 150 mM NaCl, 5 mM $CaCl_2$, and 0.02% Brij-35) and lysis buffer (25 mM Tris-HCl (pH 7.5), 1% Nonidet P-40, 100 mM NaCl, 5 mM EDTA, 20 mM *N*-ethylmaleimide, 10 μg/ml aprotinin, 1 μg/ml pepstatin A, 1 μg/ml leupeptin, 2 mM benzamidine, and 1 mM phenylmethylsulfonyl fluoride).

Expression and Purification of Pro-MMP-9 and TIMPs—Human recombinant pro-MMP-9, TIMP-1, and TIMP-2 were produced in mammalian cells using a recombinant vaccinia virus mammalian cell expression system, as described previously (28). Pro-MMP-9 was purified to homogeneity from the media of infected HeLa cells by gelatin-agarose chromatography, as described previously (29). The concentration of pro-MMP-9 was determined using the molar extinction coefficient of 114,360 M^{-1} cm^{-1} (14). Recombinant TIMP-1 and TIMP-2 were purified as described previously (30). Protein concentrations of TIMP-1 and TIMP-2 were determined using their molar extinction coefficients of 26,500 and 39,600 M^{-1} cm^{-1}, respectively (16).

Purification of the Monomeric and Dimeric Forms of Pro-MMP-9—A sample (7600 pmol) of purified pro-MMP-9 diluted in buffer C was layered onto four polyallomer tubes containing a preformed 20–35% glycerol gradient prepared in buffer C. The tubes were then centrifuged (63 h, 4 °C) in a SW41 rotor at 37,000 rpm, after which nine fractions (~200 μl each) were collected and assayed for the presence of monomeric or dimeric forms by gelatin-zymography. Fractions containing homogeneous monomeric (pro-MMP-9_M) or dimeric (pro-MMP-9_D) forms were pooled, and their protein concentrations were determined from the molar extinction coefficients: for pro-MMP-9_M, 103,645 M^{-1} cm^{-1}; and for pro-MMP-9_D, 198,609 M^{-1} cm^{-1} (31).

Radioiodination of TIMPs—TIMP-1 and TIMP-2 were iodinated with carrier free $Na^{125}I$ (100 mCi/ml, Amersham Pharmacia Biotech) using IODOGEN (Pierce) as described previously (30). The specific activities of ^{125}I-TIMP-1 and ^{125}I-TIMP-2 were calculated to be 0.035 and 0.045 μCi/pmol, respectively.

Size-exclusion Chromatography—Ten pmol of purified pro-MMP-9_M or pro-MMP-9_D were each incubated (1 h, 22 °C) with either ^{125}I-TIMP-1 or ^{125}I-TIMP-2 (20 pmol with pro-MMP-9_M and 30 pmol with pro-MMP-9_D) in a final volume of 0.25 ml. The mixtures were then subjected to gel filtration using a Superose-12 column pre-equilibrated with buffer C. As control, ^{125}I-TIMP-1 or ^{125}I-TIMP-2 (30 pmol) were chromatographed alone under the same conditions. Fractions (350 μl) were collected and analyzed for radioactivity in a γ counter (Packard model 5650). The amount (picomoles) of ^{125}I TIMP-1 or ^{125}I-TIMP-2 bound to the pro-MMP-9 forms was determined from the specific activity.

SDS-PAGE and Gelatin Zymography—SDS-PAGE was performed according to Laemmli (32). Proteins were visualized by staining overnight with a 0.25% solution of Coomassie Brilliant Blue R-250 in 45% methanol and 10% acetic acid, and destained in a solution of 20% methanol and 10% acetic acid. Gelatin zymography was performed as described (33).

Preparation of Breast Tumor Extract—A fresh tissue biopsy (~50 mg) (kindly provided by Dr. D. Visscher, Department of Pathology, Harper Hospital, Detroit, MI) of a breast carcinoma was minced into small pieces and resuspended in 500 μl of cold lysis buffer. The pieces were homogenized on ice with a pestle (Kontes, Vineland, NJ) in a microcentrifuge tube, followed by a centrifugation (14,000 rpm) of the homogenate for 10 min at 4 °C. The supernatant was collected, and the protein concentration was determined by the BCA protein assay (Pierce). The protein concentration was adjusted to 1 μg/μl of 1× sample buffer, and the sample was then subjected to gelatin zymography as described above and to immunoblot analysis, as described (21), using an anti-MMP-9 rabbit polyclonal antibody (pAb 109) raised against a synthetic peptide (APRQRQSTLVLTPGDLRT) from the prodomain of human pro-MMP-9 (a generous gift from Dr. Stetler-Stevenson, NCI, National Institutes of Health, Bethesda, MD).

Pulse-Chase Analysis of Pro-MMP-9 Biosynthesis—Monkey kidney BS-C-1 cells (80% confluent) in 60-mm dishes were co-infected with 3 plaque-forming units/cell of vTF7–3 vaccinia virus encoding for T7 RNA polymerase and with 3 plaque-forming units/cell of a recombinant vaccinia virus containing the full-length cDNA of human pro-MMP-9 (vT7-GELB) as described (28). Four hours after infection, the medium was aspirated and the cell monolayer was gently washed with warm PBS. The cells were incubated (30 min) with 1.5 ml/dish starving medium (Dulbecco's modified Eagle's medium without methionine supplemented with 25 mM Hepes and 0.5% fetal bovine serum). The cells were then pulsed with 500 μCi/ml [^{35}S]methionine in starvation medium (1.5 ml/dish) for 15 min at 37 °C. After the pulse, the dishes were placed on ice, the medium was aspirated and the cells were washed twice with PBS before the addition of 1 ml/dish chase medium (Dulbecco's modified Eagle's medium with 10% fetal bovine serum and 4.8 mM methionine). At the end of the chase periods (0–240 min at 37 °C), the medium was collected; the cells were washed with cold PBS and lysed with 1 ml/dish lysis buffer. The lysates were clarified by a brief centrifugation and were pre-absorbed on protein G-Sepharose beads. The lysates and the media were subjected to immunoprecipitation with either a mAb to pro-MMP-9 (CA-209) or mouse IgG and protein G-Sepharose beads, as described (21). The immunoprecipitates were mixed with Laemmli sample buffer, with or without β-mercaptoethanol, and resolved by 8–16% SDS-PAGE followed by autoradiography.

Fluorometric Activity Assay for MMP-9_M and MMP-9_D—To obtain the active monomer and dimer, purified pro-MMP-9_M (100 pmol) or pro-MMP-9_D (60 pmol) in buffer C were incubated (2 h at 37 °C) with 25 pmol of heat-activated recombinant human stromelysin 1 (MMP-3, a generous gift from Dr. Paul Cannon, Center for Bone and Joint Research, Palo Alto, CA). The activated monomer (MMP-9_M) and dimer (MMP-9_D) were then subjected to gelatin-agarose chromatography to remove stromelysin 1, as described (30). Fractions containing MMP-9_M or MMP-9_D were detected by gelatin zymography and pooled. Enzyme concentrations were determined by titration with TIMP-1 and from their native molar extinction coefficients of 99,817 and 191,349 M^{-1} cm^{-1}, respectively, as determined by the method of Gill and von Hippel (31). The activities of the purified MMP-9_M and MMP-9_D were assayed using the fluorescence quenched substrate MOCAcPLGLA$_2$pr(Dnp)-AR-NH_2 (Peptide Institute, Inc. Japan), as described (30, 34). Each assay was carried out at 25 °C in 2 ml (final volume) of buffer R containing enzyme and and/or inhibitor at the indicated concentrations. The substrate concentration was varied from 0.05 to 8.0 μM. The enzyme concentrations were 0.2 and 0.1 nM for MMP-9_M and MMP-9_D, respectively. Substrate hydrolysis was monitored using a Photon Technology International (PTI) fluorescence spectrophotometer with excitation and emission wavelengths set at 328 and 393 nm, respectively, controlled by a Pentium™ computer using the RatioMaster™ hardware and FeliX™ software provided by PTI. The excitation and emission band passes were 1 and 3 nm, respectively. Fluorescent measurements were taken with a 4-s integration time. Three initial rate determinations were made for each substrate concentration. The K_m and V_{max} values were determined by non-linear regression analyses using GraphPad Prism™ and examined by double-reciprocal analysis by linear regression using LINEST (Microsoft Excel™ version 5.0).

Degradation of Gelatin by MMP-9_M and MMP-9_D—Increasing concentrations (0.07–0.3 nM) of active site-titrated (with TIMP-1) MMP-9_M and MMP-9_D were incubated with 1 μM fluorescein-labeled DQ™ gelatin (Molecular Probes, Eugene, OR) in buffer D, in a total volume of 2 ml. Substrate hydrolysis was monitored over a 1-h period at 25 °C using a PTI spectrofluorometer at excitation and emission wavelengths of 495 and 515 nm, respectively. Excitation and emission band passes were 1 and 3 nm, respectively. Background fluorescence due to DQ™ gelatin was measured with substrate in the absence of enzymes and was subtracted from each trace. A fluorescein (Molecular Probes) standard curve was used to correlate the fluorescence increase with the amount of released fluorescein.

Kinetic Analysis of the Activation of Pro-MMP-9_M and Pro-MMP-9_D by Stromelysin 1—Human recombinant pro-stromelysin 1 was heat activated at 55 °C for 1 h. The amount of catalytically competent stromelysin 1 was determined by active-site titration with human recombinant TIMP-1. Stromelysin 1 activity was measured with 5 μM fluorogenic peptide substrate MOCAcRPKPVE-Nva-WRK(Dnp)-NH_2 (35) (Peptides International, Louisville, KY) in buffer R, at excitation and emission wavelengths of 325 and 393 nm, respectively. Activation of pro-MMP-9_M or pro-MMP-9_D was monitored in reaction mixtures containing 2–120 nM of either substrate and 0.5 nM stromelysin 1 in 70 μl of buffer D at 37 °C. At varying times, aliquots (20 μl) of the reaction mixture were added to acrylic cuvettes containing 2 ml of 7 μM MOCAcPLGLA$_2$pr(Dnp)-AR-NH_2 in buffer R at 25 °C. Less than 10% of hydrolysis of the fluorogenic substrate was monitored, as described by Knight (36). Hydrolysis of this peptide by stromelysin 1 at the concentrations used (0.5–9 nM) was insignificant when compared with the hydrolysis by MMP-9. The MMP-9 (monomer or dimer) concentrations were calculated using the Michaelis-Menten equation and the k_{cat} and K_m values for the reaction of the enzyme (monomer and dimer) with the

fluorogenic substrate, as described above. Initial velocities of pro-MMP-9_M or pro-MMP-9_D activation were determined from the linear increase in MMP-9 concentration as a function of time. The kinetic parameters k_{cat} and K_m were obtained by non-linear least squares fitting of the initial rate dependence on the total pro-MMP-9 concentration to the Michaelis-Menten equation using SCIENTIST (Micro-Math Scientific Software, Salt Lake City, UT). The values for $t_{1/2}$ were calculated from the following general relationship for first-order reactions: $k_{cat} \times t_{1/2} = 0.693$.

Determination of Kinetic and Equilibrium Constants by SPR—Interactions of latent and active monomer and dimer pro-MMP-9/MMP-9 with TIMP-1 and TIMP-2 were studied using a Fison Iasys^{TS} instrument. TIMP-1 (69 pmol) and TIMP-2 (42 pmol) were immobilized onto activated CM5 sensor cells (Fison), as described (30). Under these conditions, 320–380 arc s of TIMP-2 and 310–360 arc s of TIMP-1 were covalently coupled. Binding reactions were carried out essentially as described previously (30). The equilibrium constants (K_d) were calculated from the rate constants for association (k_a) and dissociation (k_d) from the equation $K_d = k_d/k_a$. For biphasic binding $K_d = k_{d(2)}/k_{a(1)}$ and $k_{d(1)}/k_{a(2)}$ for the low and high affinity binding sites, respectively. The binding constants for each analyte protein were determined in duplicate using at least six different concentrations of analyte (2–400 nM), in a final volume of 200 μl, where the response increased as a function of analyte concentration. For TIMP-1 and TIMP-2, pro-MMP-9_M and active MMP-9_M were titrated from 10 to 125 nM and proMMP-9_D and active MMP-9_D were titrated from 5 to 75 nM. Furthermore, each analyte protein (100 nM) was subjected to analysis using a derivatized sensor cell to determine the amount of nonspecific binding to the carboxymethyl dextran matrix. No binding of the analyte protein to the underivatized matrix was observed. The binding curves were analyzed using the nonlinear data-fitting program Iasys Fastfit™, using both monophasic and biphasic models to obtain the rate constants. Analysis of the data fit the biphasic model, as we have previously described in detail (30).

Enzyme Inhibition Studies—To determine the inhibition constant (K_i) of TIMP-1 and TIMP-2 for the active monomer and dimer, the rate constants (k_{on} and k_{off}) were determined under the following conditions, and from these the K_i was calculated (*i.e.* k_{off}/k_{on}). The fluorogenic peptide substrate concentration for each assay was 7 μM, a concentration ~5-fold greater than the experimentally determined K_m for the reaction of the substrate with MMP-9_M and MMP-9_D. TIMP-1 (0–30 nM) or TIMP-2 (0–60 nM) were added to the fluorogenic substrate solution, and the assay was initiated by addition of enzyme to give a final concentration of 1 nM for MMP-9_M and 0.5 nM for MMP-9_D. The reaction was allowed to proceed for 6 min, and the rate of substrate cleavage was measured in triplicate for each inhibitor concentration examined. The first-order rate constant, k, was determined from the intersection point of the tangent to the curve at $I = x$ to the curve at $I = 0$ where $k = 1/t$, as described (37), where the data points gave equal increments of product formation as a function of time in the absence of inhibitor. The first-order rate constant, k, for each TIMP concentration was plotted as a function of TIMP concentration. The slope and error of the slope of this line gives the on-rate, k_{on}, as determined by linear regression using LINEST (Microsoft Excel™ version 5.0). The dissociation rate constants (k_{off}) were determined in triplicate as follows. MMP-9_M or MMP-9_D (300 nM) and inhibitors (330 nM) were incubated for 1 h at 25 °C. These reaction mixtures were added to a cuvette containing 2 ml of a 12 μM peptide substrate solution. The final enzyme concentration was 0.5 nM. The recovery of enzyme activity was followed for up to 40 min, and the data were analyzed as described (38). The error of the slope of this line was determined by linear regression using LINEST (Microsoft Excel™ version 5.0). The inhibition constants (K_i) were calculated from $K_i = k_{off}/k_{on}$.

Computer Modeling—The primary sequence of pro-MMP-9 was obtained from the Swiss-Prot data bank (code COG9_HUMAN, total 707 amino acids). A complete model of pro-MMP-9 was constructed as described below. The signal peptide was removed from the complete sequence, and the remaining sequence was divided into prodomain, catalytic, gelatin-binding, and hemopexin-like domains. Homology models were constructed using the COMPOSER module in Sybyl version 6.4; the modeling of the three-dimensional structure of the catalytic domain of MMP-9 has been published previously (13). The hemopexin-like domain of pro-MMP-9 was modeled using the structures of the hemopexin-like domains of pro-MMP-2 (Protein Data Bank codes 1gen and 1rtg), fibroblast collagenase (code 1fbl), and collagenase-3 (code 1pex), following similar procedures that were used for the modeling of the catalytic domain (13, 39–41). The gelatin-binding domain was modeled using the NMR structure of the fibronectin type-II model (code 1fn2) (42). The prodomain of pro-MMP-9 was modeled based on the x-ray structure of homologous prodomain of stromelysin-1 (code 1slm) (43). In modeling the prodomain, residues upstream of 44 were considered in the homology model building because no homologous sequences were found from residues 21–43. Individual domains of human pro-MMP-9 were thus constructed using homology modeling and three-dimensional structure alignment, and the two contiguous domains were organized and linked appropriately in space. The collagen V-like hinge region of pro-MMP-9 was not modeled due to the lack of any homologous protein that could serve as a three-dimensional template. The complete structure of pro-MMP-9 was energy-minimized using AMBER 5.0 software package on a Silicon Graphics Octane workstation with dual processors, for 20,000 cycles (13). However, we have disclosed in this report only the arrangements of the contiguous regions of the prodomain and catalytic domains, since they are pertinent to the discussion. The graphical analysis of the resulting structure was performed using Sybyl software version 6.4.

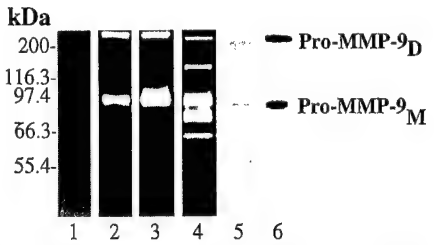

FIG. 1. **Expression of pro-MMP-9_M from pro-MMP-9_D.** Samples of recombinant pro-MMP-9 (*lanes 2* and *6*, 10 ng/lane), serum-free conditioned media of tumor necrosis factor-α-treated MCF10A cells (*lane 3*, 20 μl) and of a homogenate of a breast carcinoma biopsy (*lanes 4* and *5*, 30 μg/lane) were subjected to gelatin zymography (*lanes 2–4*) and immunoblot analysis (*lanes 4* and *5*) using a polyclonal antibody (pAb 109) to pro-MMP-9 recognizing the latent form. *Lane 1* shows the molecular weight standards under non reducing conditions.

RESULTS

Expression of Pro-MMP-9_M and Pro-MMP-9_D—As shown in the zymogram of Fig. 1, pro-MMP-9 in monomeric (~92 kDa) and dimeric (~210 kDa) forms can be found in preparations of purified recombinant enzyme (Fig. 1, *lane 2*), in serum-free conditioned media of tumor necrosis factor-α-treated non-malignant MCF10A breast epithelial cells (Fig. 1, *lane 3*) and in a tissue homogenate derived from a human breast carcinoma biopsy (Fig. 1, *lane 4*). The tumor sample contains several gelatinolytic bands migrating at ~72, 85, 92, 130, and 225 kDa. To confirm the nature of the MMP-9 forms detected in the tumor homogenate, we carried out an immunoblot analysis using a polyclonal antibody to the prodomain of pro-MMP-9. The tumor homogenate contained two immunoreactive forms of ~92 and 225 kDa (Fig. 1, *lane 5*) consistent with these forms being the monomeric and dimeric forms of pro-MMP-9.

Biosynthesis of Pro-MMP-9_M and Pro-MMP-9_D—The biosynthesis of pro-MMP-9_M and pro-MMP-9_D was examined by pulse-chase analysis in BSC-1 cells infected with a recombinant vaccinia virus expressing human pro-MMP-9. After the chase period, the resulting media and cell lysates were immunoprecipitated with a mAb against pro-MMP-9 and subjected to SDS-PAGE analysis under non-reducing and reducing conditions followed by autoradiography. As shown in Fig. 2, the pro-MMP-9_M precursor form (~85 kDa) was rapidly synthesized and gradually converted to the fully glycosylated mature form (~92 kDa), which was then secreted into the extracellular space (Fig. 2, *extracellular*). Precursor pro-MMP-9_D (~190 kDa) was clearly noticeable in the lysates as early as 5 min after the pulse, consistent with the dimer being composed of two precursor monomers. Thus, under these conditions, dimerization occurs intracellularly and appears to be independent of glycosylation. After 30 min, a dimer of ~210 kDa was detected in the lysates, possibly representing dimerization of mature monomer forms or, alternatively, complete glycosylation of the

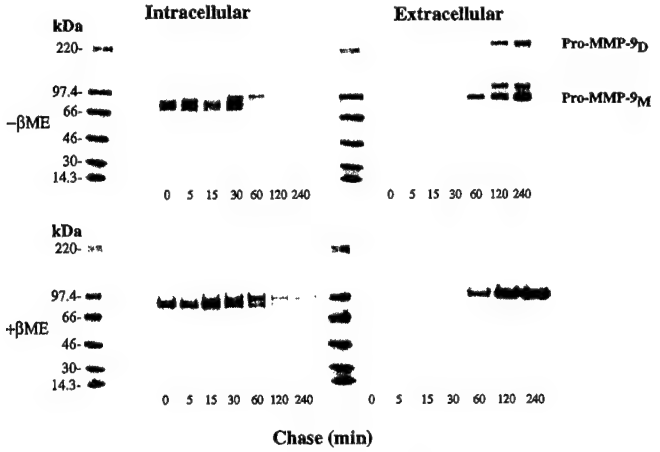

FIG. 2. **Pulse-chase analysis of pro-MMP-9 biosynthesis.** Infected BSC-1 cells were subjected to pulse-chase analysis, as described under "Experimental Procedures." At the end of the chase periods (0–240 min), the cells (intracellular) and the media (extracellular) were subjected to immunoprecipitation with an anti-MMP-9 mAb (CA-209). The immunoprecipitates were subjected to 8–16% SDS-PAGE analysis under non-reducing (*−β-ME*) or reducing (*+β-ME*) conditions followed by autoradiography. ^{14}C-Labeled molecular weight standards, electrophoresed under reducing conditions, were used as reference.

immature dimer (Fig. 2). After 60 min into the chase period, the mature pro-MMP-9 monomer and dimer were detected in the media (Fig. 2, *extracellular*). In the presence of a reducing agent (Fig. 2, *+β-mercaptoethanol*), only pro-MMP-9_M was detected (21) consistent with dimerization involving the formation of a disulfide bond (27). Pulse-chase samples prepared in the presence or absence of 20 nM *N*-ethylmaleimide showed similar results demonstrating that dimerization was not a consequence of *in vitro* oxidation during cell lysis (data not shown).

A ~120-kDa protein of unknown origin was also immunoprecipitated from the media and was only observed under non-reducing conditions (Fig. 2, *extracellular*). The 120-kDa protein is not likely to be a complex of the monomeric form with TIMP-1 (31 kDa), as reported by Moll *et al.* (22), since it did not co-immunoprecipitate with a polyclonal antibody to TIMP-1 (data not shown), known to co-precipitate the enzyme/inhibitor complex (21). Consistently, a radiolabeled 31-kDa protein was not detected under reducing conditions in the pulse-chase experiment. Indeed, vaccinia-infected cells do not express endogenous TIMPs (28). Furthermore, a 25-kDa protein, consistent with the molecular mass of lipocalin (19, 20), which is known to form a complex with neutrophil pro-MMP-9, could not be detected under reducing conditions (Fig. 2, *+β-mercaptoethanol*). Interestingly, the 120-kDa protein was not detected in purified preparations of recombinant pro-MMP-9 (Fig. 3), suggesting that it is a minor component.

Purification of Pro-MMP-9_M and Pro-MMP-9_D—To characterize the biochemical properties of the pure monomeric and dimeric forms, these forms were isolated from each other using glycerol-gradient sedimentation. Since pro-MMP-9_D sediments faster than pro-MMP-9_M, near base-line separations were achieved as shown in the zymogram of Fig. 3*A*. Gradient fractions containing pro-MMP-9_M or pro-MMP-9_D were pooled, activated or not with stromelysin 1, and examined by non-reducing SDS-PAGE followed by Coomassie Blue staining (Fig. 3*B*) and by gelatin zymography (Fig. 3*C*). These analyses revealed that the purified pro-MMP-9_M (Fig. 3, *B* and *C*, *lane 3*) or pro-MMP-9_D (Fig. 3*B*, *lane 5*, and *C*, *lane 4*) were homogeneous. Incubation of pro-MMP-9_M and pro-MMP-9_D with stromelysin 1 resulted in the processing of these two forms to low molecular mass species of ~82 kDa (Fig. 3*B*, *lane 4*, and *B*, *lane 5*) and ~200 kDa (Fig. 3, *B* and *C*, *lane 6*).

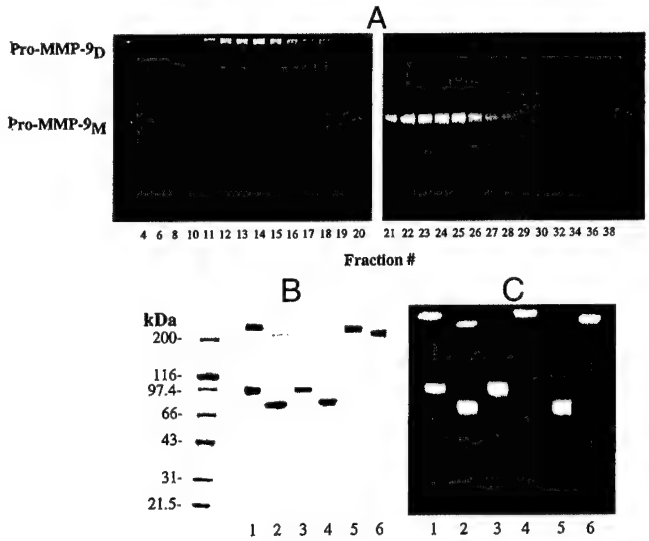

FIG. 3. **Purification of pro-MMP-9_M from pro-MMP-9_D by glycerol-gradient sedimentation.** Recombinant pro-MMP-9 was subjected to glycerol-gradient sedimentation, as described under "Experimental Procedures." *A*, the gradient fractions (1 μl) were analyzed by gelatin-zymography. *B* and *C*, purified pro-MMP-9_M and pro-MMP-9_D forms were incubated (2 h, 37 °C) with (*2B*, *2C*, *4B*, *5C*, *6B*, and *6C*) or without (*1B*, *1C*, *3B*, *3C*, *4C*, and *5B*) stromelysin 1. The latent and active forms were analyzed by 8–16% by SDS-PAGE and Coomassie Blue staining under non-reducing conditions (*B*) or by gelatin-zymography (*C*). *Lane 1*, pro-MMP-9; *lane 2*, MMP-9; *lane 3*, purified pro-MMP-9_M; *lanes 4B* and *5C* purified MMP-9_M; *lanes 5B* and *4C* purified pro-MMP-9_D; *lane 6*, purified MMP-9_D.

Catalytic Competence of MMP-9_M and MMP-9_D—We determined the K_m and k_{cat} values for the hydrolysis of the fluorogenic peptide substrate MOCAcPLGLA_2pr(Dnp)-AR-NH_2 by MMP-9_M and MMP-9_D. The data showed saturation kinetics by the two purified enzyme forms similar to that reported for MMP-9, a mixture of monomeric and dimeric forms (30). Nonlinear least-squares fits of the data to the Michaelis-Menten equation allowed for determination of the K_m, k_{cat}, and k_{cat}/K_m values. The enzymes showed essentially the same affinity for the substrate with K_m values of 1.28 ± 0.08 and 1.32 ± 0.06 μM for the monomeric and dimeric species, respectively. The k_{cat} and k_{cat}/K_m values for the hydrolysis of the peptide substrate by MMP-9_M and MMP-9_D were also essentially similar with k_{cat} values of 2.72 ± 0.13 and 8.67 ± 0.24 s^{-1} and k_{cat}/K_m values of (2.13 ± 0.14) × 10^6 and (6.56 ± 0.22) × 10^6 M^{-1} s^{-1}, for the monomer and dimer, respectively.

The ability of MMP-9_M and MMP-9_D to degrade a natural substrate was examined using fluorescein-labeled gelatin. These data showed that MMP-9_M and MMP-9_D cleaved the gelatin substrate with similar catalytic efficiency, as indicated by the identical linear dependence of the initial rates of gelatin cleavage as a function of enzyme concentration (0–0.3 nM) (data not shown). Determination of the kinetic parameters (k_{cat} and K_m) of this reaction was not possible due to the collisional quenching of the fluorescein-labeled fragments released at the concentrations of gelatin used (25 nM to 1 μM).

Differential Kinetics of Activation of Pro-MMP-9_M and Pro-MMP-9_D by Stromelysin 1—Stromelysin 1 is an efficient activator of pro-MMP-9 (44, 45). Therefore, we wished to compare the kinetics of activation of isolated pro-MMP-9_M and pro-MMP-9_D by stromelysin 1. After exposure of pro-MMP-9_M or pro-MMP-9_D to stromelysin 1, the enzymatic activities of the generated active species were measured using the fluorogenic peptide substrate. Nonlinear least-squares analysis of the data according to the Michaelis-Menten equation provided the kinetic parameters listed in Table I. Thus, pro-MMP-9_D is acti-

TABLE I
Kinetic parameters for pro-MMP-9 monomer and dimer activation by stromelysin-1

Increasing concentrations of pro-MMP-9_M and pro-MMP-9_D (2–120 nM) were incubated with 0.5 nM stromelysin 1 in a total volume of 70 μl of buffer D, at 37 °C. MMP-9_M and MMP-9_D were assayed with the fluorogenic substrate (7 μM) in buffer R at 25 °C. Analogous results were obtained from three independent experiments. The kinetic parameters were evaluated from nonlinear regression analysis, as described under "Experimental Procedures."

Substrate	K_m	k_{cat}	k_{cat}/K_m
	nM	s^{-1}	$M^{-1}\,s^{-1}$
Pro-MMP-9_M	13 ± 3	$(1.9 \pm 0.1) \times 10^{-3}$	$(1.5 \pm 0.4) \times 10^{5}$
Pro-MMP-9_D	25 ± 7	$(4.1 \pm 0.4) \times 10^{-4}$	$(1.6 \pm 0.4) \times 10^{4}$

vated with a catalytic efficiency 10-fold lower than that of pro-MMP-9_M due to a difference in the values of k_{cat} since the K_m values are within the experimental error. At subsaturating substrate concentrations, the initial rates of activation of pro-MMP-9_M and pro-MMP-9_D varied linearly with stromelysin 1 concentration and the slopes of the lines correlated with the determined kinetic parameters.

Pro-MMP-9_M and Pro-MMP-9_D Bind TIMP-1—Previous experiments in our laboratory, in which pro-MMP-9 and TIMP-1 were co-expressed in the vaccinia expression system, demonstrated that both the monomeric and dimeric forms of the enzyme co-precipitated with TIMP-1 using either anti-TIMP-1 or anti-MMP-9 antibodies.[2] These studies suggested that both pro-MMP-9 forms bind the inhibitor. Here we investigated the ability of purified pro-MMP-9_M and pro-MMP-9_D to form a stable complex with TIMP-1 using size-exclusion chromatography. Prior to gel filtration, purified pro-MMP-9_M or pro-MMP-9_D was incubated with molar excess concentrations of ^{125}I-TIMP-1 and the mixtures were then chromatographed on a Superose-12 column. Fig. 4 shows the column profiles of ^{125}I-TIMP-1 alone and of mixtures of ^{125}I-TIMP-1 with either pro-MMP-9_M or pro-MMP-9_D. These column profiles (Fig. 4) and analysis of the eluted fractions by immunoblot and autoradiography (data not shown) demonstrated that a fraction of the ^{125}I-TIMP-1 co-chromatographed with the monomeric and dimeric forms of proMMP-9 consistent with formation of stable complexes. The sum of the radioactivity present in peak 1 (enzyme/inhibitor complex) and in peak 2 (^{125}I-TIMP-1 alone) of the column profiles revealed an enzyme: inhibitor ratio of 1:1.26 for the pro-MMP-9_M/TIMP-1 complex and of 1:1.84 for the pro-MMP-9_D/TIMP-1 complex consistent with a stoichiometry of 1:1 and 1:2, respectively. As controls, mixtures of either pro-MMP-9_M or pro-MMP-9_D with ^{125}I-TIMP-2 chromatographed under the same conditions failed to demonstrate complex formation (data not shown). These experiments demonstrate that both the monomeric and dimeric forms of pro-MMP-9 bind TIMP-1.

SPR Analyses of Latent and Active Monomer and Dimer with TIMP-1 and TIMP-2—Previously, we reported the binding affinities of pro-MMP-9 and MMP-9 with TIMP-1 and TIMP-2 using SPR (30). Here we used SPR to examine the binding kinetics of purified pro-MMP-9_M and pro-MMP-9_D and their active species with TIMP-1 and TIMP-2. As expected, pro-MMP-9_M and pro-MMP-9_D did not bind to TIMP-2. However, the active MMP-9 species demonstrated distinct association and dissociation phases of binding to TIMP-2. The calculated association rate constant (k_a), dissociation rate constant (k_d), and equilibrium constant (K_d) values from the SPR analyses are summarized in Table II. These analyses indicated the existence of high and low affinity binding sites, as reported previously for the binding of TIMP-1 to pro-MMP-9 and MMP-9 (30), known to be a mixture of both monomeric and dimeric forms. The data also indicated a somewhat greater affinity (1.4–1.7-fold) of the dimeric form (latent and active) for TIMP-1 at the high affinity site (Table II). Both MMP-9_M and MMP-9_D bound to TIMP-2 with biphasic binding kinetics. However, the affinity of TIMP-2, at the high affinity site, for the active MMP-9 forms was ~2-fold lower than that exhibited by TIMP-1 (Table II).

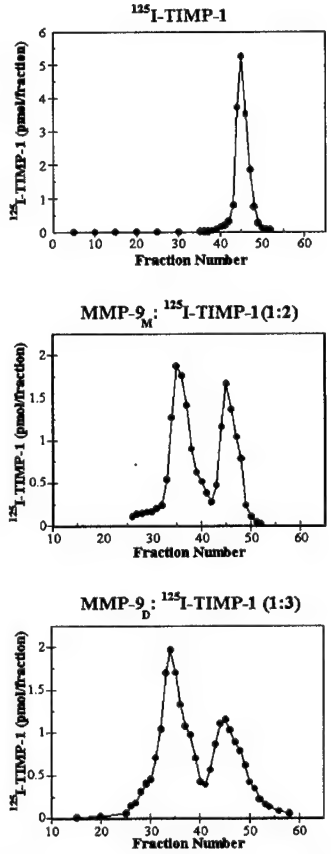

FIG. 4. **Gel filtration of pro-MMP-9_M and pro-MMP-9_D with ^{125}I-TIMP-1.** Purified pro-MMP-9_M and pro-MMP-9_D (10 pmol) were incubated (1 h, 22 °C) with 20 or 30 pmol of ^{125}I-TIMP-1, respectively. The mixtures were then subjected to gel filtration using a Superose-12 column, as described under "Experimental Procedures." The radioactivity in the eluted fractions (350 μl) was measured in a γ counter, and the amount (picomoles) of TIMP-1 was determined from the specific activity.

K_i Determination of TIMP-1 and TIMP-2 for MMP-9_M and MMP-9_D—To further examine the binding of TIMP-1 and TIMP-2 to the purified MMP-9 forms, we carried out enzyme inhibition studies. As we have previously reported with MMP-2 and MMP-9 (30), TIMP-1 and TIMP-2 inhibited the active monomeric and dimeric species in a process consistent with slow binding inhibition (data not shown). Table III shows the k_{on}, k_{off}, and calculated K_i values determined as described under "Experimental Procedures." TIMP-1 inhibits MMP-9_M and MMP-9_D with comparable rate constants for the inhibition onset (k_{on}) and recovery of activity (k_{off}), and therefore results in similar K_i values. The k_{on} is fast ($>3 \times 10^5\ M^{-1}\ s^{-1}$) and k_{off} is slow ($\sim 2.5 \times 10^{-3}\ s^{-1}$), resulting in effective inhibition. The same trend is true for TIMP-2. The 3–5-fold difference between the K_i values of TIMP-1 and TIMP-2 for the MMP-9 species is attributed to the k_{on}, which is 3–5-fold greater for TIMP-1 than for TIMP-2. The k_{off} values of TIMP-1 and TIMP-2 for each MMP-9 species are essentially similar. The k_{on} and k_{off} values of TIMP-1 and TIMP-2 for MMP-9_M and MMP-9_D determined

[2] M. Pietila and R. Fridman, unpublished data.

TABLE II

Interactions of TIMPs with the latent and active monomeric and dimeric species of MMP-9, as evaluated by SPR

TIMP-1 (69 pmol) and TIMP-2 (42 pmol) were immobilized onto activated CM5 sensor cells. The binding constants for each analyte protein were determined in duplicate using at least six different concentrations (2–400 nM) in a final volume of 200 μl of buffer W. The parameters k_a, k_d, and K_d are defined under "Experimental Procedures."

Analyte protein	$k_{a(1)}$[a]	$k_{a(2)}$	$k_{d(1)}$	$k_{d(2)}$	K_d	K_d
	$M^{-1}\,s^{-1} \times 10^{-4}$	$M^{-1}\,s^{-1} \times 10^{-4}$	$s^{-1} \times 10^{2}$	$s^{-1} \times 10^{3}$	μM	nM
TIMP-1						
Pro-MMP-9_M	7.97 ± 0.47	1.01 ± 0.07	3.17 ± 0.09	3.65 ± 0.47	3.15 ± 0.51	45.8 ± 4.3
Pro-MMP-9_D	14.3 ± 1.56	2.9 ± 0.29	4.66 ± 1.22	3.90 ± 1.13	2.26 ± 0.41	27.2 ± 5.4
MMP-9_M	8.62 ± 0.65	0.93 ± 0.08	2.68 ± 0.53	3.67 ± 1.12	3.67 ± 0.31	42.5 ± 8.1
MMP-9_D	14.5 ± 1.40	1.68 ± 0.21	4.29 ± 1.54	4.17 ± 1.35	2.56 ± 0.62	28.6 ± 7.4
TIMP-2						
MMP-9_M	4.11 ± 0.33	1.36 ± 0.14	7.14 ± 1.73	4.02 ± 0.71	5.24 ± 0.90	98.0 ± 12.5
MMP-9_D	8.80 ± 1.19	1.66 ± 0.31	8.93 ± 2.15	5.86 ± 2.25	5.37 ± 1.14	65.7 ± 17.1

[a] (1) and (2) refer to the first and the second phase of kinetics.

TABLE III

Association, dissociation, and inhibition constants for MMP-9 monomer and dimer interactions with TIMPs

To determine k_{on} MMP-9_M and MMP-9_D were added to a 7 μM fluorogenic substrate solution in buffer R containing increasing TIMP-1 (0–30 nM) or TIMP-2 (0–60 nM) resulting in final enzyme concentrations of 1 and 0.5 nM, respectively. The dissociation rate constants were determined by diluting a preincubated (for 1 h at 25 °C) reaction mixture containing enzymes (300 nM) and inhibitors (330 nM) into 2 ml of a 12 μM fluorogenic substrate solution in buffer R, resulting in a final enzyme concentrations of 0.5 nM. All assays were carried out in triplicate. The k_{on}, k_{off}, and K_i values were calculated as described under "Experimental Procedures."

Enzyme	k_{on}	k_{off}	K_i
	$M^{-1}\,s^{-1}$	s^{-1}	nM
TIMP-1			
MMP-9_M	$(3.12 \pm 0.60) \times 10^5$	$(2.55 \pm 0.43) \times 10^{-3}$	8.17 ± 1.11
MMP-9_D	$(4.04 \pm 0.28) \times 10^5$	$(2.88 \pm 0.11) \times 10^{-3}$	7.13 ± 0.26
TIMP-2			
MMP-9_M	$(9.89 \pm 0.98) \times 10^4$	$(2.57 \pm 0.23) \times 10^{-3}$	25.9 ± 2.4
MMP-9_D	$(8.44 \pm 0.43) \times 10^4$	$(3.05 \pm 0.22) \times 10^{-3}$	36.1 ± 2.2

from the inhibition experiments are in agreement with the values determined by SPR analyses (Table II). Hence, the calculated K_i values of TIMP-1 and TIMP-2 were in the nanomolar range and within 2-5-fold of the K_d values determined by SPR.

DISCUSSION

Pro-MMP-9 is unique among the members of the MMP family in that it forms dimers consisting of covalently tethered monomers via a disulfide bond that can also be found in tissues. However, the biochemical properties of the monomeric and dimeric forms remained unknown. We have shown that the process of dimerization occurs intracellularly and concomitantly with glycosylation. Accordingly, both the precursor and mature forms of the pro-MMP-9_D can be detected in the cellular compartment during pro-MMP-9 biosynthesis. However, only mature pro-MMP-9_M and pro-MMP-9_D are secreted. Under reducing conditions, only monomeric pro-MMP-9 was detected, consistent with disulfide-bond formation during intracellular dimerization. The identity of the cysteine residue(s) that predisposes pro-MMP-9 to dimerization is unknown. Based on the crystal structure of the homologue C-terminal domain of pro-MMP-2 (36), the conserved Cys^{516} and Cys^{704} in the hemopexin-like domain of pro-MMP-9 are likely to be disulfide-bonded precluding a role for these cysteine residues in dimer formation. Site directed mutagenesis studies also excluded Cys^{674} in this process (27, 46). Consistently, a computational model of the three-dimensional structure of the hemopexin like-domain of pro-MMP-9,[3] based on the crystal structure of the same domain of pro-MMP-2 (39), suggests that Cys^{674}, although unique to pro-MMP-9, is unlikely to be involved in dimerization, since it is solvent-inaccessible. Pro-MMP-9 contains an additional Cys at position 468 located in the collagen V-like hinge region that may be responsible for the dimerization. However, its role in dimer formation remains to be established.

Expression of pro-MMP-9 in the vaccinia system allowed us to obtain sufficient amount of recombinant enzyme for isolation and purification of the monomeric species from the dimeric form. Several procedures were tested to purify the monomer from the dimer including gelatin-affinity chromatography (27), ion-exchange chromatography, gel filtration, and glycerol gradient sedimentation. However, the latter proved to be the most efficient and consistent method to obtain homogeneous preparations of monomer and dimer. Purified pro-MMP-9_M and pro-MMP-9_D were examined for their interactions with TIMP-1 and TIMP-2 using gel filtration and SPR analyses. These studies showed that both pro-MMP-9 species could form stable complexes with TIMP-1 but not with TIMP-2. These data are in disagreement with a previous study showing a lack of complex formation between TIMP-1 and pro-MMP-9_D (27). This discrepancy may be related to the method of purification of the monomeric from the dimeric form (gelatin-affinity chromatography (Ref. 27) *versus* glycerol-gradient sedimentation) and/or the use of recombinant TIMP-1 expressed in bacteria (27) *versus* mammalian cell-expressed TIMP-1 (this study). We have found that the binding of TIMP-1 to pro-MMP-9_M or pro-MMP-9_D was consistent with a stoichiometry of 1:1 and 2:1 molar ratio, respectively, suggesting that two high affinity binding sites for TIMP-1 are available in the dimeric form. These sites are likely to be located in the hemopexin-like domain, which is the major TIMP-1 binding site of pro-MMP-9 (44). The gel filtration data were supported by SPR analyses demonstrating binding of TIMP-1 to the monomer and dimer (latent and active) with biphasic kinetics. Thus, dimerization has no apparent effect on the binding kinetics of TIMP-1 and the affinity values are in agreement with our previous data with pro-MMP-9 and MMP-9, monomer and dimer mixtures (30). Although the nature of the second TIMP-1 binding site is unknown, the results presented here suggest that it is structurally different from the site required for dimerization since the dimer also binds TIMP-1. These results are in agreement with the study of Goldberg *et al.* (27) showing that mutations disrupting TIMP-1 binding had no effect on dimerization. Consistent with our previous SPR data with pro-MMP-9 (30) and the gel filtration experiments, TIMP-2 showed no binding to pro-MMP-9_M or pro-MMP-9_D. However, both MMP-9_M and MMP-9_D exhibited biphasic TIMP-2 binding kinetics with an affinity that was ~2-fold lower than that exhibited by TIMP-1, at the high affinity site. Consistently, enzyme inhibition studies showed that both MMP-9_M and MMP-9_D were equally inhibited by

[3] I. Massova, L. Kotra, and S. Mobashery, unpublished data.

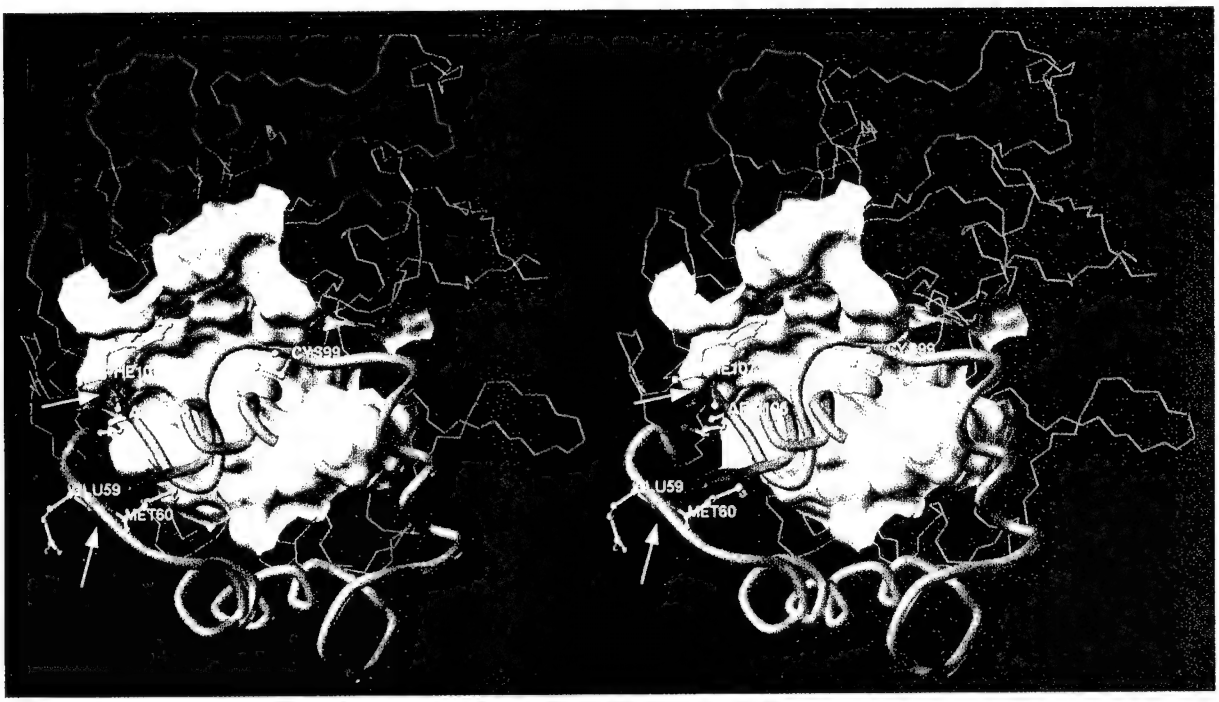

FIG. 5. **Stereo view of the energy-minimized computational model for the prodomain and the catalytic domain of pro-MMP-9.** The catalytic domain is shown in *green* with the active site depicted as a *green* surface. The catalytic zinc ion is depicted as an *orange sphere*. The backbone of the prodomain is represented as a *tube*. The backbone of the prodomain in *magenta* is released after the first hydrolytic step by stromelysin 1 at the Glu^{59}-Met^{60} peptide bond (indicated by the *arrow* at 7 o'clock). The remainder of the prodomain, given in *orange*, is released after the second hydrolytic step at the Arg^{106}-Phe^{107} peptide bond (indicated by the *arrow* at 9 o'clock). The side chains of residues Glu^{59}, Met^{60}, Arg^{106}, and Phe^{107} are shown in the ball-and-stick representation. Cys^{99}, whose side chain thiol coordinates with the catalytic zinc ion, is shown in *yellow*.

TIMP-1 (K_i = 7–8 nM) and TIMP-2 (K_i = 26–36 nM) with kinetics consistent with slow binding inhibition, as previously reported (30). It should be noted that the K_d values obtained by SPR analysis were concordant with the K_i values obtained by enzyme inhibition studies.

Kinetic studies with MMP-9_M and MMP-9_D indicate no significant differences in the hydrolytic capacity of the MMP-9 forms against a fluorogenic peptide substrate and gelatin, a natural substrate of the enzyme (14). Furthermore, no evidence of cooperative interaction between the two active sites in terms of substrate hydrolysis and TIMP inhibition was observed, as determined by the enzyme kinetic studies with the peptide substrate. However, we have found a significant difference in the catalytic efficiency of pro-MMP-9_M and pro-MMP-9_D activation by stromelysin 1 with pro-MMP-9_D being activated with a lower efficiency (10-fold), as indicated by k_{cat}/K_m values for the activation reaction. The K_m values are in the nanomolar range for both pro-MMP-9 forms, consistent with the fact that stromelysin 1 is readily saturated by pro-MMP-9 (44, 45). The K_m values in the nanomolar range have also been observed for a number of proteolytic enzymes of the blood coagulation cascade with their substrates (47). Since catalysis is very slow, K_m equals K_s. This indicates that the affinity (K_s) of stromelysin 1 for proMMP-9 is high. For the same reason, $k_{cat} = k_2$. The microscopic rate constant k_2 is that for the peptide hydrolysis (hydrolytic) step, beyond the Michaelis-Menten complex. It is of interest that k_{cat} values for turnover of the two forms of pro-MMP-9 are exceedingly small (in the range of 10^{-3} to 10^{-4} s^{-1}; Table 1). A low K_m is consistent with a low value for k_{cat}, since the ratio k_{cat}/K_m has a limit set by the rate of diffusion. However, the resultant k_{cat}/K_m values are in the respectable range of 10^4 to 10^5 M^{-1} s^{-1}. These values further suggest that stromelysin 1 is an efficient physiological activator of pro-MMP-9 (48).

The low k_{cat} values for activation of the two pro-MMP-9 forms by stromelysin 1 are worthy of comment. Highly catalytically competent enzymes, which often operate at the diffusion limit, may have k_{cat} values in the range of 10^3 s^{-1}. Clearly, stromelysin 1 does not merit this distinction. This raises the question: why is the k_{cat} value for the activation of pro-MMP-9 so low? The crystal structure of the catalytic domain of stromelysin 1 indicates that the active site is an extended cleft (43, 49, 50). Proteases generally prefer unstructured peptides as substrates. This appears to be the case for stromelysin 1, based on the topology of its active site. The high affinity of stromelysin 1 for pro-MMP-9 indicates that the complex between the two enzymes forms readily, even in the nanomolar range for the pro-MMP-9 concentration. Despite this, turnover is slow ($t_{1/2}$ of 6.1 ± 0.3 and 28 ± 2 min computed from the k_{cat} values for the monomeric and dimeric forms, respectively). Ogata *et al.* (45) first reported that the activation of pro-MMP-9 by stromelysin 1 is a sequential process involving two cleavage sites, first in the Glu^{59}-Met^{60} bond followed by the cleavage of the Arg^{106}-Phe^{107} peptide bond. The first cleavage generates an inactive 85-kDa intermediate form within seconds (44), whereas the second cleavage site generates the fully active 82-kDa MMP-9 species (29, 45). Fig. 5 shows a view of the energy-minimized computational model that we have generated for the catalytic domain of pro-MMP-9 and its requisite prodomain. As seen in this image, the Glu^{59}-Met^{60} bond is fully exposed near the surface of the protein, and hence would be accessible to stromelysin 1. Such a position would readily fit in the active site of stromelysin 1, and its hydrolysis is obviously rapid as discerned from the turnover in the range of several seconds. The fact that this cleavage occurs so readily facilitates measurement of the hydrolysis rate of the second cleavage, which results in zymogen activation. In essence, the product of the first cleavage, which is inactive, serves as the substrate for the activation event. Our model predicts that the Arg^{106}-Phe^{107} peptide bond is less accessible than the Glu^{59}-Met^{60} bond (Fig. 5). The kinetics of pro-MMP-9 activation by stromelysin 1, measured in

this study, are for the slow cleavage step and follow an uncomplicated standard profile for a single saturation event. For the second cleavage to take place, a required relaxation of structure will have to occur. This would entail dissociation of Cys^{99} from coordination with the active site zinc ion (Fig. 5). It is necessary that after the formation of the pro-MMP-9/stromelysin 1 complex, pro-MMP-9 relaxes its secondary structure around the activation site, prior to its fitting into the active site of stromelysin 1 and hydrolysis of the peptide bond. This relaxation of structure should be the slow step in the catalytic turnover of pro-MMP-9.

The calculated $t_{1/2}$ for pro-MMP-9 turnover falls within the range of the length of time needed for larger scale motions of proteins, such as helix-coil transitions for example (51), which is consistent with our proposal for this local unfolding of the prodomain prior to its excision. It is also interesting to note that the pro-MMP-9_D is substantially more stable than the monomer form, based on the k_{cat} values that we have measured. This is explained intuitively by the observation that protein-protein interactions, in this case by dimerization, stabilize the protein making it more difficult to unfold. Thus, a possible, but yet unproven, explanation to the lower rate of dimer activation may be a reduced ability of the dimer to undergo the necessary relaxation of structure to permit the catalytic hydrolysis of the prodomain by stromelysin 1. The significance of the slower rate of activation of the pro-MMP-9 dimer by stromelysin 1 for MMP-9-dependent proteolysis is unclear. However, it is tempting to speculate that the existence of the slow activating dimer may provide an additional level of control during ECM degradation by MMP-9 species. Furthermore, fluctuations in the relative amounts of latent monomer and dimer secreted into the extracellular milieu may also play a role in the control of MMP-9-dependent proteolysis. The biochemical and cellular processes regulating dimerization of pro-MMP-9 remain to be determined.

Acknowledgment—We are indebted to Dr. Roger Poorman (Pharmacia-Upjohn, Kalamazoo, MI) for assistance with the use of the Fison Iasys™ instrument.

REFERENCES

1. Wilhelm, S. M., Collier, I. E., Marmer, B. L., Eisen, A. Z., Grant, G. A., and Goldberg, G. I. (1989) *J. Biol. Chem.* **264,** 17213–17221
2. Vu, T. H., and Werb, Z. (1998) in *Gelatinase B: Structure, Regulation and Function; Matrix Metalloproteinases* (Parks, W. C., and Mecham, R. P., eds) pp. 115–148, Academic Press, San Diego
3. Ahrens, D., Koch, A. E., Pope, R. M., Stein-Picarella, M., and Niedbala, M. J. (1996) *Arthritis Rheum.* **39,** 1576–1587
4. Li, Y. Y., Feldman, A. M., Sun, Y., and McTiernan, C. F. (1998) *Circulation* **98,** 1728–34
5. Tamarina, N. A., McMillan, W. D., Shively, V. P., and Pearce, W. H. (1997) *Surgery* **122,** 264–272
6. Himelstein, B. P., Canete-Soler, R., Bernhard, E. J., Dilks, D. W., and Muschel, R. J. (1994) *Invasion Metastasis* **14,** 246–258
7. Sehgal, G., Hua, J., Bernhard, E. J., Sehgal, I., Thompson, T. C., and Muschel, R. J. (1998) *Am. J. Pathol.* **152,** 591–596
8. Ohno, I., Ohtani, H., Nitta, Y., Suzuki, J., Hoshi, H., Honma, M., Isoyama, S., Tanno, Y., Tamura, G., Yamauchi, K., Nagura, H., and Shirato, K. (1997) *Am. J. Respir. Cell. Mol. Biol.* **16,** 212–219
9. Agren, M. S., Jorgensen, L. N., Andersen, M., Viljanto, J., and Gottrup, F. (1998) *Br. J. Surg.* **85,** 68–71
10. Moses, M. A., Marikovsky, M., Harper, J. W., Vogt, P., Eriksson, E., Klagsbrun, M., and Langer, R. (1996) *J. Cell. Biochem.* **60,** 379–386
11. Canete-Soler, R., Gui, Y. H., Linask, K. K., and Muschel, R. J. (1995) *Dev. Dyn.* **204,** 30–40
12. Vu, T. H., Shipley, J. M., Bergers, G., Berger, J. E., Helms, J. A., Hanahan, D., Shapiro, S. D., Senior, R. M., and Werb, Z. (1998) *Cell* **93,** 411–422
13. Massova, I., Kotra, L. P., Fridman, R., and Mobashery, S. (1998) *FASEB J.* **12,** 1075–1095
14. Murphy, G., and Crabbe, T. (1995) *Methods Enzymol* **248,** 470–484
15. Gomez, D. E., Alonso, D. F., Yoshiji, H., and Thorgeirsson, U. P. (1997) *Eur J. Cell Biol.* **74,** 111–122
16. Murphy, G., and Willenbrock, F. (1995) *Methods Enzymol.* **248,** 496–510
17. Goldberg, G. I., Marmer, B. L., Grant, G. A., Eisen, A. Z., Wilhelm, S., and He, C. S. (1989) *Proc. Natl. Acad. Sci. U. S. A.* **86,** 8207–8211
18. Bigg, H. F., Shi, Y. E., Liu, Y. E., Steffensen, B., and Overall, C. M. (1997) *J. Biol. Chem.* **272,** 15496–15500
19. Kjeldsen, L., Johnsen, A. H., Sengelov, H., and Borregaard, N. (1993) *J. Biol. Chem.* **268,** 10425–10432
20. Triebel, S., Blaser, J., Reinke, H., and Tschesche, H. (1992) *FEBS Lett.* **314,** 386–388
21. Toth, M., Gervasi, D. C., and Fridman, R. (1997) *Cancer Res.* **57,** 3159–3167
22. Moll, U. M., Youngleib, G. L., Rosinski, K. B., and Quigley, J. P. (1990) *Cancer Res.* **50,** 6162–6170
23. Vartio, T., and Baumann, M. (1989) *FEBS Lett.* **255,** 285–289
24. Mautino, G., Oliver, N., Chanez, P., Bousquet, J., and Capony, F. (1997) *Am. J. Respir. Cell. Mol. Biol.* **17,** 583–591
25. Upadhya, A. G., Harvey, R. P., Howard, T. K., Lowell, J. A., Shenoy, S., and Strasberg, S. M. (1997) *Hepatology* **26,** 922–928
26. Gonzalez-Avila, G., Iturria, C., Vadillo-Ortega, F., Ovalle, C., and Montano, M. (1998) *Pathobiology* **66,** 196–204
27. Goldberg, G. I., Strongin, A., Collier, I. E., Genrich, L. T., and Marmer, B. L. (1992) *J. Biol. Chem.* **267,** 4583–4591
28. Fridman, R., Fuerst, T. R., Bird, R. E., Hoyhtya, M., Oelkuct, M., Kraus, S., Komarek, D., Liotta, L. A., Berman, M. L., and Stetler-Stevenson, W. G. (1992) *J. Biol. Chem.* **267,** 15398–15405
29. Fridman, R., Toth, M., Pena, D., and Mobashery, S. (1995) *Cancer Res.* **55,** 2548–2555
30. Olson, M. W., Gervasi, D. C., Mobashery, S., and Fridman, R. (1997) *J. Biol. Chem.* **272,** 29975–29983
31. Gill, S. C., and von Hippel, P. H. (1989) *Anal. Biochem.* **182,** 319–326
32. Laemmli, U. K. (1970) *Nature* **227,** 680–685
33. Brown, P. D., Levy, A. T., Margulies, I. M., Liotta, L. A., and Stetler-Stevenson, W. G. (1990) *Cancer Res.* **50,** 6184–6191
34. Knight, C. G., Willenbrock, F., and Murphy, G. (1992) *FEBS Lett.* **296,** 263–266
35. Nagase, H., Fields, C. G., and Fields, G. B. (1994) *J. Biol. Chem.* **269,** 20952–20957
36. Knight, C. G. (1995) *Methods Enzymol.* **248,** 18–34
37. Morrison, J. F., and Walsh, C. T. (1988) *Adv. Enzymol. Relat. Areas Mol. Biol.* **61,** 201–301
38. Glick, B. R., Brubacher, L. J., and Leggett, D. J. (1978) *Can. J. Biochem.* **56,** 1055–1057
39. Libson, A. M., Gittis, A. G., Collier, I. E., Marmer, B. L., Goldberg, G. I., and Lattman, E. E. (1995) *Nat. Struct. Biol.* **2,** 938–942
40. Gohlke, U., Gomis-Ruth, F. X., Crabbe, T., Murphy, G., Docherty, A. J., and Bode, W. (1996) *FEBS Lett.* **378,** 126–130
41. Gomis-Ruth, F. X., Gohlke, U., Betz, M., Knauper, V., Murphy, G., Lopez-Otin, C., and Bode, W. (1996) *J. Mol. Biol.* **264,** 556–566
42. Pickford, A. R., Potts, J. R., Bright, J. R., Phan, I., and Campbell, I. D. (1997) *Structure* **5,** 359–370
43. Becker, J. W., Marcy, A. I., Rokosz, L. L., Axel, M. G., Burbaum, J. J., Fitzgerald, P. M., Cameron, P. M., Esser, C. K., Hagmann, W. K., Hermes, J. D., and Springer, J. P. (1995) *Protein Sci.* **4,** 1966–1976
44. O'Connell, J. P., Willenbrock, F., Docherty, A. J., Eaton, D., and Murphy, G. (1994) *J. Biol. Chem.* **269,** 14967–14973
45. Ogata, Y., Enghild, J. J., and Nagase, H. (1992) *J. Biol. Chem.* **267,** 3581–3584
46. Strongin, A. Y., Collier, I. E., Krasnov, P. A., Genrich, L. T., Marmer, B. L., and Goldberg, G. I. (1993) *Kidney Int.* **43,** 158–162
47. Mann, K. G., Nesheim, M. E., Church, W. R., Haley, P., and Krishnaswamy, S. (1990) *Blood* **76,** 1–16
48. Ramos-DeSimone, N., Hahn-Dantona, E., Sipley, J., Nagase, H., French, D. L., and Quigley, J. P. (1999) *J. Biol. Chem.* **274,** 13066–13076
49. Esser, C. K., Bugianesi, R. L., Caldwell, C. G., Chapman, K. T., Durette, P. L., Girotra, N. N., Kopka, I. E., Lanza, T. J., Levorse, D. A., MacCoss, M., Owens, K. A., Ponpipom, M. M., Simeone, J. P., Harrison, R. K., Niedzwiecki, L., Becker, J. W., Marcy, A. I., Axel, M. G., Christen, A. J., McDonnell, J., Moore, V. L., Olszewski, J. M., Saphos, C., Visco, D. M., Hagmann, W. K., *et al.* (1997) *J. Med. Chem.* **40,** 1026–1040
50. Finzel, B. C., Baldwin, E. T., Bryant, G. L., Jr., Hess, G. F., Wilks, J. W., Trepod, C. M., Mott, J. E., Marshall, V. P., Petzold, G. L., Poorman, R. A., O'Sullivan, T. J., Schostarez, H. J., and Mitchell, M. A. (1998) *Protein Sci.* **7,** 2118–2126
51. Brooks, C. L., Karpulus, M., and Pettitt, B. M. (1988) *A Theoretical Perspective of Dynamics, Structure, and Thermodynamics,* John Wiley & Sons, New York

Potent and Selective Mechanism-Based Inhibition of Gelatinases

Stephen Brown, M. Margarida Bernardo, Zhi-Hong Li, Lakshmi P. Kotra, Yasuhiro Tanaka, Rafael Fridman, and Shahriar Mobashery

Departments of Chemistry and Pathology, Wayne State University, Detroit, Michigan 48202-3489

JOURNAL OF THE AMERICAN CHEMICAL SOCIETY®

Reprinted from
Volume 122, Number 28, Pages 6799–6800

Potent and Selective Mechanism-Based Inhibition of Gelatinases

Stephen Brown,[§] M. Margarida Bernardo,[‡] Zhi-Hong Li,[§] Lakshmi P. Kotra,[§] Yasuhiro Tanaka,[§] Rafael Fridman,[‡] and Shahriar Mobashery*,[§]

Departments of Chemistry and Pathology
Wayne State University, Detroit, Michigan 48202-3489

Received April 27, 2000

Specific interactions of cells within the extracellular matrix are critical for the normal function of the organism. Alterations of the extracellular matrix are carried out by a family of zinc-dependent endopeptidases called matrix metalloproteinases (MMPs) in various cellular processes such as organ development, ovulation, fetus implantation in the uterus, embriogenesis, wound healing, and angiogenesis.[1,2] Gelatinases, collagenases, stromelysins, membrane-type MMPs, and matrilysin comprise the five major groups of MMPs, of which at least 26 members have been identified in humans to date. The activities of MMPs in physiological conditions are strictly regulated by a series of complicated zymogen activation processes and inhibition by the protein tissue inhibitors of metalloprotainases ("TIMPs").[2,3] Excessive MMP activity has been implicated in cancer growth, tumor metastasis and angiogenesis, arthritis, connective tissue diseases, inflammation, and cardiovascular and autoimmune diseases.[1,2,4] Due to the potential therapeutic value of MMP inhibitors for these conditions, synthetic inhibitors of MMPs are highly sought.[5,6] All the known inhibitors for MMPs take advantage of chelation to the active site zinc ion for inhibition of activity. The known MMP inhibitors usually suffer from toxicity to hosts.[5a,c,7] Besides the issue of undesirable side effects, the design of MMP inhibitors has been complicated by only low levels of specificity among members of the MMP family, which hampers our ability to target specific MMPs in each pathological condition. We describe herein the first mechanism-based inhibitor for MMPs, a novel concept for the selective inhibition of these enzymes. We show that our inhibitor rivals the action of TIMPs in its efficacy in inhibition of MMPs.

Increased level of activity for human gelatinases, MMP-2 and MMP-9, has been implicated in the process of tumor metastasis and angiogenesis.[8] As a result, we have been interested in the selective inhibition of these two key MMPs. For this purpose, we have resorted to the design of mechanism-based inhibitors

Scheme 1

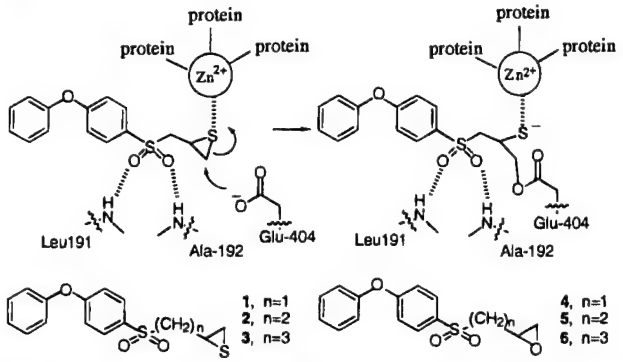

(also known as "k_{cat} inhibitors" or "suicide substrates"). This type of inhibitor has the potential to impart high selectivity in inhibition of closely related enzymes, such as MMPs.[9] Our strategy for mechanism-based inhibition of MMPs by compound **1** is depicted in Scheme 1. The strategy envisions that coordination of the thiirane with the active-site zinc ion would activate it for modification by a nucleophile in the enzyme active site. The biphenyl moiety in compounds **1**−**6** would fit in the $P_{1'}$ subsite of gelatinases, which is a deep hydrophobic pocket.[10,11] Energy-minimized complexes of MMP-2 and MMP-9[12] with compound **1** indicated that the biphenyl group would fit in the active site analogously to the same group in reversible inhibitors of MMP-2 and MMP-9.[6] This binding mode would bring the sulfur of the thiirane in **1** into the coordination sphere of the zinc ion. The models indicated that the thiirane moiety in compounds **2** and **3**, with longer carbon backbones, would not be able to coordinate with the zinc ion, but would fit in an extended conformation in the active site.

Scheme 2 shows the synthetic route for compounds **1**−**6**. 4-Phenoxythiophenol **10** was prepared from the commercially available 4-phenoxyphenol **7** via a three-step procedure described by Newman and Karnes for a related system.[13] Subsequent alkylation of **10** with allyl bromide, 4-bromo-1-butene, and 5-bromo-1-pentene, respectively, led to the sulfanyl compounds **11**−**13** in good yields. Epoxidation of **12** and **13** with mCPBA proceeded in 2−3 days, but that for **11** took 7 days and required an excess of mCPBA. Finally, conversion of the epoxides **4**−**6** to their corresponding thiirane derivatives **1**−**3**, respectively, was accomplished by the treatment of each epoxide with ammonium thiocyanate. Although the thiiranes **2** and **3** were isolated in high yields (93 and 85%, respectively), thiirane **1** could only be recovered in a poor 14% yield.

Compounds **1**−**6** were evaluated with MMPs.[14] Whereas inhibitors **2**−**6** showed either no inhibition or relatively poor

* Address correspondence to this author: Phone: 313-577-3924. FAX: 313-577-8822. E-mail:s om@chem.wayne.edu.
§ Department of Chemistry.
‡ Department of Pathology.

(1) Massova, I.; Kotra, L. P.; Fridman, R.; Mobashery, S. *FASEB J.* **1998**, *12*, 1075−1095.
(2) Forget, M.-A.; Desrosier, R. R.; Béliveau, R. *Can. J. Physiol. Pharmacol.* **1999**, *77*, 465−480.
(3) Brew, K.; Dinakarpandian, D.; Nagase, H. *Biochim. Biophys. Acta* **2000**, *1477*, 267−283. Westermarck, J.; Kahari, V. M. *FASEB J.* **1999**, *13*, 781−792.
(4) Nelson, A. R.; Fingleton, B.; Rothenberg, M. L.; Matrisian, L. M. *J. Clin. Oncol.* **2000**, *18*, 1135−1149.
(5) (a) Michaelides, M. R.; Curtin, M. L. *Curr. Pharm. Des.* **1999**, *5*, 787−819. (b) Beckett, R. P.; Davidson, A. H.; Drummond, A. H.; Huxley, P.; Whittaker, M. *Drug Discuss. Today* **1996**, *1*, 16−26. (c) Woessner, J. F., Jr. *Ann. N.Y. Acad. Sci.* **1999**, *878*, 388−403. (d) Skotnicki, J. S.; Zask, A.; Nelson, F. C.; Albright, J. D.; Levin, J. I. *Ann. N.Y. Acad. Sci.* **1999**, *878*, 61−72.
(6) Freskos, J. N.; Mischke B. V.; DeCrescenzo, G. A.; Heintz, R.; Getman, D. P.; Howard, S. C.; Kishore, N. N.; McDonald, J. J.; Munie, G. E.; Rangwala, S.; Swearingen, C. A.; Voliva, C.; Welsch, D. J. *Bioorg. Med. Chem. Lett.* **1999**, *9*, 943−948. Tamura, Y.; Watanabe, F.; Nakatani, T.; Yasui, K.; Fuji, M.; Komurasaki, T.; Tsuzuki, H.; Maekawa, R.; Yoshioka, T.; Kawada, K.; Sugita, K.; Ohtani, M. *J. Med. Chem.* **1998**, *41*, 640−649.
(7) Greenwald, R. A. *Ann. N.Y. Acad. Sci.* **1999**, *878*, 413−419.
(8) Dalberg, K.; Eriksson, E.; Enberg, U.; Kjellman, M.; Backdahl, M. *World J. Surg.* **2000**, *24*, 334−340. Salo, T.; Liotta, L. A.; Tryggvason, K. *J. Biol. Chem.* **1983**, *258*, 3058−3063. Pyke, C.; Ralfkiaer, E.; Huhtala, P.; Hurskainen, T.; Dano, K.; Tryggvason, K. *Cancer Res.* **1992**, *52*, 1336−1341. Dumas, V.; Kanitakis, J.; Charvat, S.; Euvrard, S.; Faure, M.; Claudy, A. *Anticancer Res.* **1999**, *19*, 2929−2938.
(9) The high specificity for a targeted enzyme with these inhibitors arises predominantly from a combination of the differentials in noncovalent interactions and those for the influences of microscopic rate constants for the incremental steps in the process of enzyme inhibition (Silverman, R. In *Mechanism-Based Enzyme Inactivation: Chemistry and Enzymology*; CRC Press: Boca Raton, FL, 1988).
(10) (a) Morgunova, E.; Tuuttila, A.; Bergmann, U.; Isupov, M.; Lindqvist, Y.; Schneider, G.; Tryggvason, K. *Science* **1999**, *284*, 1667−1670. (b) Massova, I.; Fridman, R.; Mobashery, S. *J. Mol. Mod.* **1997**, *3*, 17−34.
(11) Olson, M. W.; Bernardo, M. M.; Pietila, M.; Gervasi, D. C.; Toth, M.; Kotra, L. P.; Massova, I.; Mobashery, S.; Fridman, R. *J. Biol. Chem.* **2000**, *275*, 2661−2668.
(12) This enzyme has not been crystallized to date. However, a computational model based on three-dimensional homology modeling for this enzyme is at hand in our laboratory (see citations 10b and 11).
(13) Newman M. S.; Karnes H. A. *J. Org. Chem.* **1996**, *31*, 3980−3984.

10.1021/ja001461n CCC: $19.00
Published on Web 06/30/2000

Scheme 2

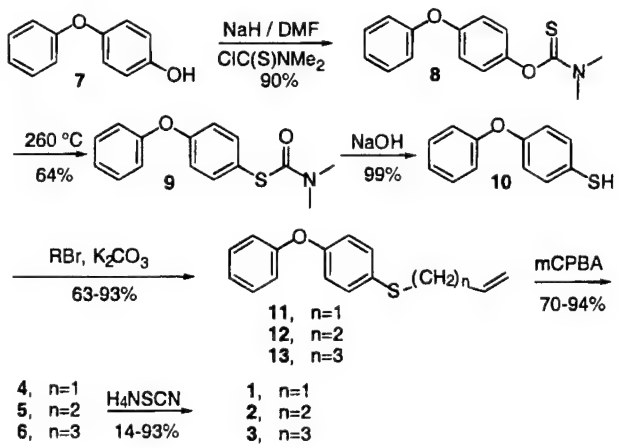

Table 1. Kinetic Parameters for Inhibition of MMPs by the Synthetic Inhibitor

	$10^{-4}k_{on}$ ($M^{-1}s^{-1}$)	$10^{3}k_{off}$ (s^{-1})	K_i (μM)
Inhibitor 1			
MMP-2	11 ± 1	1.8 ± 0.1	0.0139 ± 0.0004
MMP-9	1.4 ± 0.3	7.1 ± 0.5	0.6 ± 0.2
MMP-3	0.018 ± 0.004	5.5 ± 0.4	15 ± 6
MMP-7			96 ± 41
MMP-1			206 ± 60
TIMP-1[18]			
MMP-2	4.4 ± 0.1	1.3 ± 0.2	0.029 ± 0.005
MMP-9	5.2 ± 0.1	1.2 ± 0.2	0.024 ± 0.004
TIMP-2[18]			
MMP-2	3.3 ± 0.1	0.8 ± 0.1	0.023 ± 0.004
MMP-9	2.2 ± 0.1	1.3 ± 0.2	0.058 ± 0.007

inhibition of the MMPs (K_i values of micromolar at best; see Supporting Information), the behavior of inhibitor **1** was different. Inhibitor **1** showed a dual behavior. It served as a mechanism-based inhibitor with a partition ratio of 79 ± 10 (i.e., k_{cat}/k_{inact}) for MMP-2 and of 416 ± 63 for MMP-9.[15] Furthermore, it also behaved as a slow-binding inhibitor, for which the rate constants for the on-set of inhibition (k_{on}) and recovery of activity from inhibition (k_{off}) were evaluated (Table 1). It would appear that coordination of the thiirane with the zinc ion (as seen in the energy-minimized computational models; Scheme 1) would set in motion a conformational change, which is presumed from the slow-binding kinetic behavior. The kinetic data fit the model for slow-binding inhibition.[16] Covalent modification of the enzymes ensued this conformational change. We incubated inhibitor **1** with MMP-2 to the point that less than 5% activity remained. This inhibitor–enzyme complex was dialyzed over 3 days, which resulted in recovery of approximately 50% of the activity. This observation is consistent with modification of the active site Glu-404, via the formation of an ester bond, which is a relatively labile covalent linkage.[17]

We observe selectivity in inhibition of gelatinases by inhibitor **1**. The K_i values are 13.9 ± 0.4 and 600 ± 200 nM for MMP-2 and MMP-9, respectively. In contrast, the corresponding K_i values for the other MMPs tested, including MMP-3, which does show the slow-binding mechanism-based inhibition profile, are in the micromolar range. Interestingly, the values for k_{on} are 611- and 78-fold larger for MMP-2 and MMP-9, respectively, than that for MMP-3. Collectively, these kinetic parameters make inhibitor **1** a potent and selective inhibitor for both MMP-2 and MMP-9, more so for MMP-2. We have determined previously that two molecules of either TIMP-1 or TIMP-2 bind to activated MMP-2 and MMP-9.[18] One binding event is high affinity and would appear physiologically relevant, whereas the second binding event takes place with relatively lower affinity (micromolar).[18] Inhibition of MMP-2 and MMP-9 by TIMP-2 and TIMP-1, respectively, also follows slow-binding kinetics. The kinetic parameters for these interactions at the high affinity site are listed in Table 1. We find it noteworthy that the kinetic parameters for the slow-binding component of inhibition of MMP-2 and MMP-9 by inhibitor **1** (k_{on} and k_{off}) approach closely the same parameters for those of the TIMPs.[18]

We have outlined in this paper a novel example for potent inhibition of human gelatinases by the small-molecule inhibitor **1**, which follows both slow-binding and mechanism-based inhibition in its kinetic profile. This compound appears to behave similarly to TIMP-2 and TIMP-1 in the slow-binding component of inhibition. Furthermore, the inhibitor also exhibits a covalent mechanism-based behavior in inhibition of these enzymes. The selectivity that inhibitor **1** displays (in both affinities and the modes of inhibition) among the other structurally similar MMPs is noteworthy and should serve as a paradigm in the design of inhibitors for other closely related enzymes in the future.

Acknowledgment. This work was supported by grants DAMD17-97-1-7174 from the US Army (to S.M.) and CA-61986 and CA-82298 from the NIH (to R.F.). We are indebted to Dr. Paul Cannon and Dr. W. Parks for the gifts of human MMP-3 and MMP-1, respectively.

Supporting Information Available: Detailed procedures for syntheses and kinetic determinations are provided (PDF). This material is available free of charge via the Internet at http://pubs.acs.org.

JA001461N

(14) Homogeneous preparations of MMPs were used in our studies. Recombinant human MMP-2 and MMP-9 were prepared as described previously (see Supporting Information). Representative members of the other classes of MMPs, such as stromelysin 1 (MMP-3), matrilysin (MMP-7), and collagenase-1 (MMP-1), were used in our studies.

(15) The partition ratio indicates that there is turnover of the thiirane for each covalent inhibition of the enzyme. The partition ratios were relatively low, such that given the quantities of the enzymes available to us, we were not able to isolate and characterize the product of this turnover.

(16) Morrison, J. F. *Adv. Enzymol.* **1988**, *61*, 201–301.

(17) The time-dependent loss of activity is not merely due to the slow-binding behavior. For instance, for a k_{off} of 2×10^{-3} s^{-1} (the values are not very different from one another in Table 1) the half-time for recovery of activity ($t_{1/2}$) is calculated at just under 6 min. The fact that 50% of activity still did not recover after dialysis over 3 days strongly argues for the covalency of enzyme modification.

(18) Olson, M. W.; Gervasi, D. C.; Mobashery, S.; Fridman, R. *J. Biol. Chem.* **1997**, *272*, 29975–29983.

THE JOURNAL OF BIOLOGICAL CHEMISTRY
Vol. 275, No. 52, Issue of December 29, pp. 41415–41423, 2000
Printed in U.S.A.

Tissue Inhibitor of Metalloproteinase (TIMP)-2 Acts Synergistically with Synthetic Matrix Metalloproteinase (MMP) Inhibitors but Not with TIMP-4 to Enhance the (Membrane Type 1)-MMP-dependent Activation of Pro-MMP-2*

Received for publication, July 31, 2000, and in revised form, September 14, 2000
Published, JBC Papers in Press, September 20, 2000, DOI 10.1074/jbc.M006871200

Marta Toth‡, M. Margarida Bernardo‡, David C. Gervasi‡, Paul D. Soloway§, Zhiping Wang§, Heather F. Bigg¶, Christopher M. Overall¶, Yves A. DeClerck‖, Harald Tschesche, Michael L. Cher‡ ‡‡, Stephen Brown§, Shahriar Mobashery§§, and Rafael Fridman‡¶¶**

*From the ‡Departments of Pathology, ‡‡Urology and §§Chemistry, Wayne State University, Detroit, Michigan 48201, the §Department of Molecular and Cellular Biology, Roswell Park Cancer Institute, Buffalo, New York 14263, the ¶Department of Biochemistry and Molecular Biology, University of British Columbia, Vancouver, British Columbia V6T 1Z3, Canada, the ‖Division of Hematology-Oncology and Department of Pediatrics, Children's Hospital Los Angeles, University of Southern California, Los Angeles, California 90027, and the **Department of Biochemistry, Faculty of Chemistry, University of Bielefeld, W-4800 Bielefeld 1, Germany*

The membrane-type 1 matrix metalloproteinase (MT1-MMP) has been shown to be a key enzyme in tumor angiogenesis and metastasis. MT1-MMP hydrolyzes a variety of extracellular matrix components and is a physiological activator of pro-MMP-2, another MMP involved in malignancy. Pro-MMP-2 activation by MT1-MMP involves the formation of an MT1-MMP·tissue inhibitors of metalloproteinases 2 (TIMP-2)·pro-MMP-2 complex on the cell surface that promotes the hydrolysis of pro-MMP-2 by a neighboring TIMP-2-free MT1-MMP. The MT1-MMP·TIMP-2 complex also serves to reduce the intermolecular autocatalytic turnover of MT1-MMP, resulting in accumulation of active MT1-MMP (57 kDa) on the cell surface. Evidence shown here in *Timp2*-null cells demonstrates that pro-MMP-2 activation by MT1-MMP requires TIMP-2. In contrast, a C-terminally deleted TIMP-2 (Δ-TIMP-2), unable to form ternary complex, had no effect. However, Δ-TIMP-2 and certain synthetic MMP inhibitors, which inhibit MT1-MMP autocatalysis, can act synergistically with TIMP-2 in the promotion of pro-MMP-2 activation by MT1-MMP. In contrast, TIMP-4, an efficient MT1-MMP inhibitor, had no synergistic effect. These studies suggest that under certain conditions the pericellular activity of MT1-MMP in the presence of TIMP-2 can be modulated by synthetic and natural (TIMP-4) MMP inhibitors.

Proteolytic degradation of extracellular matrix (ECM)[1] is a fundamental aspect of cancer development and a key event in tumor-induced angiogenesis and tumor metastasis. A major group of enzymes responsible for ECM degradation in cancer tissue is the matrix metalloproteinase (MMP) family (1–4). The MMPs are zinc-dependent multidomain endopeptidases that, with few exceptions, share a basic structural organization comprising propeptide, catalytic, hinge, and C-terminal (hemopexin-like) domains (1, 5). All MMPs are produced in a latent form (pro-MMP) requiring activation for catalytic activity, a process that is usually accomplished by proteolytic removal of the propeptide domain. Once activated, all MMPs are specifically inhibited by a group of endogenous tissue inhibitors of metalloproteinases (TIMPs) that bind to the active site, inhibiting catalysis (1). Over the last 5 years, the MMP family has been expanded to include a new subfamily of membrane-tethered MMPs known as membrane-type MMPs (MT-MMPs), which to date includes six members (6–12). The MT-MMPs, with the exception of MT4-MMP, are unique because they are anchored to the plasma membrane by means of a hydrophobic stretch of approximately 20 amino acids, leaving the catalytic domain exposed to the extracellular space. This organization makes the MT-MMPs perfectly suited for regulation of pericellular proteolysis. MT1-MMP (MMP-14) was the first member of the MT-MMP family to be discovered and has been shown to be the major physiological activator of pro-MMP-2 (gelatinase A) on the cell surface (6, 12). The role of MT1-MMP in pericellular proteolysis is not restricted to pro-MMP-2 activation, since MT1-MMP is a multifunctional enzyme that can also degrade a variety of ECM components (13–16) and hence can play a direct role in ECM turnover. MT1-MMP has been recently shown to be the first member of the MMP family indispensable for normal growth and development, since mice deficient in MT1-MMP exhibit a variety of connective tissue pathologies and a short life span (17, 18). Furthermore, both MMP-2 (19) and MT1-MMP (20–26) have been associated with metastatic potential in many human cancers, angiogenesis (27), and enhanced tumor cell invasion in experimental systems (28–31). This has raised considerable interest in understanding the regulation of these MMPs because they represent an important target for development of novel drugs aimed at inhibiting tumor metastasis and angiogenesis (3, 32, 33).

Studies on the mechanism of activation of pro-MMP-2 by MT1-MMP revealed a complex role for TIMP-2 in this process. A model for the activation of pro-MMP-2 has been proposed in which the catalytic domain of MT1-MMP binds to the N-termi-

* This work was supported by National Institutes of Health Grant CA-61986-06 and Department of Defense Grant DAMD17-99-1-9440 (to R. F.). The costs of publication of this article were defrayed in part by the payment of page charges. This article must therefore be hereby marked "*advertisement*" in accordance with 18 U.S.C. Section 1734 solely to indicate this fact.

¶¶ To whom all correspondence should be addressed: Dept. of Pathology, Wayne State University, 540 E. Canfield Ave. Detroit, MI 48201. Tel.: 313-577-1218; Fax: 313-577-8180; E-mail: rfridman@med.wayne.edu.

[1] The abbreviations used are: ECM, extracellular matrix; MMP, matrix metalloproteinase; MT-MMP, membrane type MMP; MMPI, MMP inhibitor; TIMP, tissue inhibitor of metalloproteinase; PAGE, polyacrylamide gel electrophoresis; pAb, polyclonal antibody; pfu, plaque-forming units; DMEM, Dulbecco's modified Eagle's medium.

nal portion of TIMP-2, leaving the negatively charged C-terminal region of TIMP-2 available for the binding of the hemopexin-like domain of pro-MMP-2 (12, 34–38). This ternary complex has been suggested to cluster pro-MMP-2 at the cell surface near a residual TIMP-free active MT1-MMP molecule, which is thought to initiate activation of the bound pro-MMP-2. Pro-MMP-2 activation would occur only at low TIMP-2 concentrations relative to MT1-MMP, which would permit availability of active MT1-MMP to activate the pro-MMP-2 bound in the ternary complex (39). Thus, under restricted conditions, TIMP-2 is thought to promote the activation process by acting as a molecular link between MT1-MMP and pro-MMP-2. We have recently shown that TIMP-2, besides its role in ternary complex formation, has direct and critical effects on MT1-MMP processing, which influence the profile and spatial localization of MT1-MMP forms (40). Biochemical and cellular evidence showed that binding of TIMP-2 to active MT1-MMP (57 kDa) inhibits autocatalytic degradation, leading to accumulation of active MT1-MMP on the cell surface. In the absence of TIMP-2, MT1-MMP is rapidly processed to a 44-kDa membrane-bound inactive enzyme (40, 41). Thus, under controlled conditions, TIMP-2 may act as a positive regulator of MT1-MMP activity by promoting the availability of active MT1-MMP on the cell surface and consequently may support pericellular proteolysis. Since some of the effects of TIMP-2 on MT1-MMP activities are related to its inhibitory activity, we wished to examine the effects of synthetic and physiological MMP inhibitors (MMPIs) on MT1-MMP processing and its ability to promote pro-MMP-2 activation with TIMP-2. Although several types of MMPIs have been developed (3, 32, 33, 42–47), little is known about their effects on the processing and activity of membrane-tethered MMPs, which exhibit unique properties. Here we show for the first time that synthetic MMPIs and a C-terminally truncated TIMP-2 but not TIMP-4, which inhibit MT1-MMP activity, act synergistically with TIMP-2 to promote pro-MMP-2 activation by MT1-MMP. These studies demonstrate the complexity of MT1-MMP regulation and provide new insights into the roles of TIMP-2, TIMP-4, and MMPIs in this process.

EXPERIMENTAL PROCEDURES

Cell Culture—Nonmalignant monkey kidney epithelial BS-C-1 (CCL-26) and human fibrosarcoma HT-1080 (CCL-121) cells were obtained from the American Type Culture Collection (ATCC, Manassas, VA) and cultured in Dulbecco's modified Eagle's medium (DMEM) supplemented with 10% fetal bovine serum and antibiotics. HeLa S3 cells were obtained from ATCC (CCL-2.2) and grown in suspension in MEM Spinner medium (Quality Biologicals, Inc., Gaithersburg, MD) supplemented with 5% horse serum. All other tissue culture reagents were purchased from Life Technologies, Inc.

Isolation of Immortalized Timp2 Mutant Mouse Fibroblasts—Adult skin fibroblast cells were isolated from heterozygous (+/−) *Timp2* mutant mice and immortalized by retroviral infection using a Ha-*ras* and v-*myc*-producing, replication-defective retrovirus as described previously (48). A G418 selection protocol was used to select for homozygous *Timp2* (−/−) mutant cells from the immortalized (+/−) mutant clone as described (49). Detailed methods for the isolation and selection of the immortalized (+/−) and (−/−) isogenic cells will be reported elsewhere. The homozygous and heterozygous *Timp2* mutant cells were grown in DMEM supplemented with 10% fetal bovine serum and antibiotics.

Recombinant Vaccinia Viruses—The production of the recombinant vaccinia virus (vTF7–3) expressing bacteriophage T7 RNA polymerase has been described by Fuerst *et al.* (50). Recombinant vaccinia viruses expressing either human pro-MMP-2, TIMP-2, or MT1-MMP under control of the T7 promoter were obtained by homologous recombination as described previously (35, 40, 51).

Recombinant Proteins, Synthetic MMP Inhibitors, and Antibodies—Human recombinant pro-MMP-2, TIMP-2, and TIMP-1 were expressed in HeLa S3 cells infected with the appropriate recombinant vaccinia viruses and purified to homogeneity, as described previously (52). Human recombinant TIMP-4 was expressed in baby hamster kidney cells and purified from the conditioned medium by sequential application to Red Sepharose, phenyl-Sepharose, Q Sepharose, and Zn^{2+}-charged chelating Sepharose columns as described.[2] A C-terminally truncated human TIMP-2 ending at Cys^{126} (Δ-TIMP-2) was constructed and expressed in mammalian cells as described previously (53). The concentrations of TIMP-2 and Δ−TIMP-2 were determined by active-site titration with MMP-2. A Cys^{1} → Ala TIMP-2 mutant (Ala + TIMP-2) was kindly provided by Dr. W. G. Stetler-Stevenson (NCI, National Institutes of Health) (54). A recombinant catalytic domain of human MT1-MMP (MT1-MMP_{cat}) comprising residues Ile^{114} to Ile^{318} was expressed in *Escherichia coli*, purified, and characterized as described previously (55). The concentration of the MT1-MMP_{cat} enzyme was determined by active-site titration with recombinant TIMP-2 as described (56). Batimastat (BB-94) and marimastat (BB-2516), two hydroxamate-based MMP inhibitors (33, 45, 47), and BB-2116, a boronate-containing MMP inhibitor, were obtained from British Biotech (Annapolis, MD). The mechanism-based MMP inhibitor SB-3CT was synthesized and characterized as previously reported (42). Stock solutions of marimastat (1 mM), batimastat (1 mM), BB-2116 (20 mM), and SB-3CT (30 mM) were prepared in Me_2SO. The rabbit anti-TIMP-2 polyclonal antibody (pAb) and the anti-TIMP-2 monoclonal antibody CA-101 were previously described (57). The rabbit pAb 437 to MT1-MMP (40, 58) has been previously described. The rabbit pAb 160 to MT1-MMP (40, 59) and the rabbit pAb to human TIMP-4 were a generous gift from Dr. Amy Sang (Florida State University, Tallahassee, FL).

Expression of MT1-MMP by Vaccinia Infection—To express MT1-MMP, confluent cultures of BS-C-1 or *Timp2* mutant cells in 6- or 12-well plates were co-infected with 5–10 pfu/cell each of vTF7–3 and vT7-MT1 viruses for 45 min in infection medium (DMEM plus 2.5% fetal bovine serum and antibiotics) at 37 °C. As control, the cells were infected only with the vTF7–3 virus as described (40).

Natural and Synthetic Inhibitor Treatment and Pro-MMP-2 Activation—After infection, the media were aspirated, and the cells were rinsed with serum-free DMEM and replaced with fresh serum-free DMEM supplemented with or without various doses of purified human recombinant TIMP-2. After various times at 37 °C, the media were aspirated; the cells were rinsed with DMEM and then incubated (15–30 min, 37 °C) in fresh media supplemented with 10 nM pro-MMP-2. The media were then collected, and the cells were rinsed twice with cold phosphate-buffered saline and solubilized in cold lysis buffer (25 mM Tris-HCl (pH 7.5), 1% IGEPAL CA-630, 100 mM NaCl, 10 μg/ml aprotinin, 1 μg/ml leupeptin, 2 mM benzamidine, and 1 mM phenylmethylsulfonyl fluoride). The lysate fractions were analyzed for pro-MMP-2 activation by gelatin zymography and/or immunoblot analysis for assessment of MT1-MMP forms. To examine the effects of synthetic MMP inhibitors, Δ−TIMP-2, Ala + TIMP-2, and TIMP-4 on TIMP-2-dependent activation of pro-MMP-2, the MT1-MMP-infected cells were treated (16 h, 37 °C) with the appropriate MMP inhibitors (various doses) diluted in serum-free DMEM. Then the media were aspirated, and the cells were rinsed with DMEM. TIMP-2 (10 nM) was then added to the cells in serum-free DMEM for a 5–30-min incubation at 37 °C. The media were aspirated followed by a wash with DMEM to remove unbound TIMP-2. The cells were then incubated (15 min, 37 °C) with serum-free DMEM supplemented with 10 nM pro-MMP-2. Analysis of pro-MMP-2 activation and of the profile of MT1-MMP forms in the cell lysates were carried out as described below.

Gelatin Zymography and Immunoblot Analysis—Gelatin zymography was performed using 10% Tris-glycine SDS-polyacrylamide gels containing 0.1% gelatin. Briefly, samples of lysates or media were mixed with Laemmli sample buffer (60) without reducing agents and without heating and then subjected to SDS-polyacrylamide gel electrophoresis (SDS-PAGE) as described previously (61). For immunoblot analysis, the cell lysates were subjected to reducing SDS-PAGE following by transfer to a nitrocellulose membrane essentially as described (61). Detection of the immune complexes was performed using the enhanced chemiluminescence system (Pierce) according to the manufacturer's instructions.

Enzyme Inhibition Studies—MT1-MMP_{cat} activity was monitored with the fluorescence-quenched substrate $MOCAcPLGLA_2pr(Dnp)$-$AR-NH_2$ (62). Fluorescence was measured with a Photon Technology International (PTI) spectrofluorometer interfaced to a Pentium computer, equipped with the RatioMaster™ and FeliX™ hardware and software, respectively. The cuvette compartment was maintained at 25 °C. Excitation and emission passes of 1 and 3 nm, respectively, were used.

[2] Bigg, H. F., Morrison, C. J., Butler, G. S., Bogoyevitch, M.A., Wang, Z., Soloway, P. D., and Overall, C. M., submitted for publication.

Substrate hydrolysis was monitored at emission and excitation wavelengths of 328 and 393 nm, respectively. Fluorescence measurements were taken every 4 s. Less than 10% hydrolysis of the fluorogenic substrate was monitored, as described by Knight (62). For slow binding inhibition, progress curves were obtained by adding enzyme (0.5 nM) to a mixture of fluorogenic substrate (7 μM) and varying concentrations of inhibitor in buffer R (50 mM HEPES (pH 7.5), 150 mM NaCl, 5 mM $CaCl_2$, 0.01% Brij-35, and 1–5% Me_2SO; final volume 2 ml) in acrylic cuvettes with stirring and monitoring the increase in fluorescence with time for 15–30 min. The progress curves were nonlinear least squares fitted to Equation 1 (63),

$$F = v_s t + I(v_o - v_s)\,(1 - \exp(-kt))/k + F_0 \qquad \text{(Eq. 1)}$$

where v_0 represents the initial rate, v_s is the steady state rate, k is the apparent first order rate constant characterizing the formation of the steady-state enzyme-inhibitor complex, and F_0 is the initial fluorescence, using the program SCIENTIST (MicroMath Scientific Software, Salt Lake City, UT). The obtained k values, v_0, and v_s were further analyzed according to Equations 2 and 3 for a one-step association mechanism.

$$k = k_{off} + k_{on}\,[I]/(1 + [S]/K_m) \qquad \text{(Eq. 2)}$$

$$(v_o - v_s)/v_s = [I]/(K_i(1 + [S]/K_m)) \qquad \text{(Eq. 3)}$$

The K_m and k_{cat} values for the reaction of MT1-MMP$_{cat}$ with the fluorogenic substrate were determined to be 6.9 ± 0.6 μM and 0.67 ± 0.03 s^{-1}, respectively. Intercept and slope values, obtained by linear regression of the k *versus* inhibitor concentration plot (Equation 2), yielded the association and dissociation rate constants k_{on} and k_{off}, respectively, and the inhibition constant K_i (k_{off}/k_{on}). Alternatively, K_i was determined from the slope of the $(v_o - v_s)/v_s$ *versus* [I] plot according to Equation 3. The dissociation rate constant was determined independently from the enzyme activity recovered after dilution of a preformed enzyme-inhibitor complex. To this end, typically 50 nM of enzyme was incubated with 80 nM of inhibitor for a sufficient time to reach equilibrium (>45 min) at 25.0 °C. The complex was diluted 400-fold into 2 ml of buffer R containing fluorogenic substrate (10 μM final concentration). Recovery of enzyme activity was monitored for ~60 min. The fluorescence *versus* time trace was fitted, using the program SCIENTIST, to Equation 4,

$$F = v_s t + (v_o - v_s)\,(1 - \exp(-k_{off}t))/k_{off} + F_0 \qquad \text{(Eq. 4)}$$

where v_0 represents the initial rate (very small), v_s is the rate observed when the EI complex is completely dissociated, and k_{off} is the first order rate constant of EI dissociation. In light of the slow dissociation of the MT1-MMP$_{cat}$-TIMP-2 complex, the direct analysis of the k_{off} parameter for the wild type TIMP-2 was not possible and was estimated based on a 10-fold difference observed between the slopes of the linear portions of the dissociation curves for the complexes of MT1-MMP$_{cat}$ with Δ-TIMP-2 (steady state rate) and wild type TIMP-2. For competitive inhibition, initial rates were obtained by adding enzyme (0.5 nM) to a mixture of fluorogenic substrate (7 μM) and varying concentrations of inhibitor in buffer R (final volume 1 ml) in quartz semimicro cuvettes and monitoring the increase in fluorescence with time for 5–10 min. The initial velocities were determined by linear regression analysis of the fluorescence *versus* time traces using FeliX™. The initial rates were fitted to Equation 5 (64),

$$v_i/v_0 = (K_m + [S])/(K_m(1 + [I]/K_i) + [S]) \qquad \text{(Eq. 5)}$$

where v_i and v_0 represent the initial velocity in the presence and absence of inhibitor, respectively, using the program SCIENTIST.

RESULTS

Pro-MMP-2 Activation and MT1-MMP Processing in Timp2 Mutant Cells—Using a vaccinia expression system, we have recently shown that immortalized monkey kidney epithelial BS-C-1 cells infected to express MT1-MMP could activate pro-MMP-2 (40). Under these conditions, this process appeared to be independent of TIMP-2, since in infected BS-C-1 cells expression of the endogenous inhibitor was significantly suppressed (35, 40, 51). However, these studies were inconclusive in regard to the requirement of TIMP-2 for pro-MMP-2 activation, since a residual amount of endogenous inhibitor could not be ruled out. To establish the importance of TIMP-2 in the activation of pro-MMP-2 by MT1-MMP, we used homozygous (−/−) and heterozygous (+/−) *Timp2* mutant mouse fibroblasts (65) that were immortalized by retroviral infection. We tested the expression of TIMP-2 in both cell types by immunoblot analysis. As shown in Fig. 1*A*, TIMP-2 was only detected in the *Timp2* (+/−) mutant cells, as reported with the primary fibroblast cells (65). The cells were then tested for activation of exogenous pro-MMP-2 after treatment with concanavalin A (66), and neither cell variant activated pro-MMP-2 regardless of the presence of TIMP-2 (data not shown), suggesting a low level of endogenous MT1-MMP expression. We therefore infected the *Timp2* (+/−) and (−/−) mutant cells to express MT1-MMP using the recombinant vaccinia virus (vT7-MT1) and the T7 RNA polymerase virus (vTF7–3) (40). As control, the cells were infected with the vTF7–3 virus alone. MT1-MMP expression (60- and 44-kDa bands) was detected only in the cells infected to express MT1-MMP (Fig. 1*B*, *lane 2*) but not in the control-infected cells (Fig. 1*B*, *lane 1*) in both cell types (only the homozygous cells are shown in Fig. 1*B*).

The ability of the expressed MT1-MMP to promote pro-MMP-2 activation with or without TIMP-2 in this cellular system was examined by gelatin zymography of the lysate fraction. To this end, after infection, the cells were incubated with or without exogenous TIMP-2, washed to remove unbound inhibitor, and incubated with exogenous pro-MMP-2. The latter was added, since both the (+/−) and (−/−) *Timp2* mutant cells do not produce detectable pro-MMP-2 (Fig. 1*C*, *lanes 2* and *5*). As shown in Fig. 1*C*, the (−/−) *Timp2* mutant cells expressing MT1-MMP activated pro-MMP-2 only after the addition of exogenous TIMP-2 (Fig. 1*C*, *lane 7*). In contrast, the *Timp2* (+/−) mutant cells expressing MT1-MMP activated pro-MMP-2 regardless of exogenous TIMP-2 presence (Fig. 1*C*, *lane 6*, without TIMP-2; *lane 7*, with TIMP-2). Control-infected homozygous and heterozygous *Timp2* mutant cells consistently failed to activate pro-MMP-2 regardless of exogenous TIMP-2

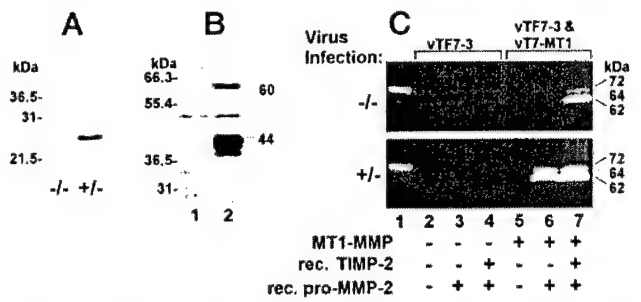

FIG. 1. **TIMP-2 expression and pro-MMP-2 activation in *Timp2* (+/−) and (−/−) mutant cells.** *A*, concentrated serum free-conditioned medium of −/− and +/− *Timp2* mutant cells was subjected to reducing 15% SDS-PAGE followed by immunoblot analysis using a specific pAb to TIMP-2. Detection of the antigen was performed by enhanced chemiluminescence. *B*, (−/−) *Timp2* mutant cells were infected with 10 pfu/cell of vTF7–3 (*lane 1*) or co-infected with 10 pfu/cell each of vTF7–3 and vT7-MT1 (*lane 2*) vaccinia viruses. Twenty-four hours postinfection, the cells were solubilized in lysis buffer and subjected to reducing 10% SDS-PAGE followed by immunoblot analysis using the pAb 437 to MT1-MMP. *C*, *Timp2* (−/−) and (+/−) mutant cells in six-well plates were infected with 10 pfu/cell of vTF7–3 (*lanes 2–4*) or coinfected with 10 pfu/cell each of vTF7–3 and vT7-MT1 (*lanes 5–7*) recombinant vaccinia viruses. After infection, the cells were incubated (16 h, 37 °C) with (+) or without (−) 10 nM recombinant TIMP-2 in serum-free DMEM (1 ml/well) followed by a gentle wash to remove unbound inhibitor. Then some wells received (*rec.*) 10 nM pro-MMP-2 (*lanes 3*, *4*, *6*, and *7*) in DMEM (1 ml/well) followed by a 30-min incubation at 37 °C. The cells were lysed in lysis buffer, and pro-MMP-2 activation was monitored by gelatin zymography. *Lane 1* in *C* shows the pro-MMP-2 added to the media. *72 kDa*, pro-MMP-2; *64 kDa*, intermediate form; *62 kDa*, active MMP-2.

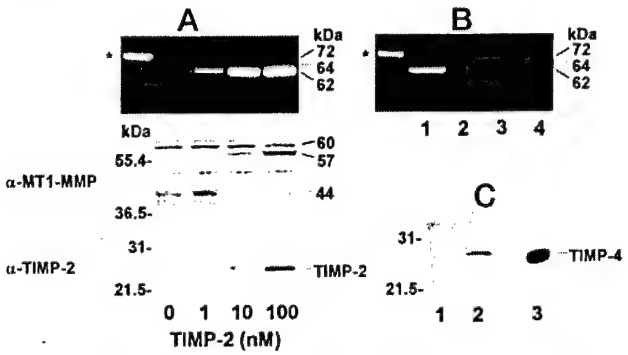

FIG. 2. **Effect of TIMP-2, Δ-TIMP-2, TIMP-4, and TIMP-1 on pro-MMP-2 activation in *Timp2* (−/−) mutant cells.** *A*, confluent *Timp2* (−/−) mutant cells were co-infected to express MT1-MMP as described in the legend to Fig. 1 and incubated (16 h, 37 °C) with TIMP-2 (0–100 nM). After a gentle wash, the cells were incubated with 10 nM pro-MMP-2 for 15 min at 37 °C. The lysates were subjected to gelatin zymography (nonreducing conditions) and reducing 10% and 15% SDS-PAGE for detection of MT1-MMP and TIMP-2, respectively, by immunoblot analysis with pAb 437 to MT1-MMP and monoclonal antibody CA-101 to TIMP-2 followed by detection with enhanced chemiluminescence. The ~50-kDa band is nonspecific. *B*, *Timp2* (−/−) mutant cells infected to express MT1-MMP were incubated (16 h, 37 °C) with 2.5 nM TIMP-2 (*lane 1*), 25 nM Δ-TIMP-2 (*lane 2*), 10 nM TIMP-4 (*lane 3*), or 25 nM TIMP-1 (*lane 4*). After the incubation, the media were aspirated, and the cells were washed with DMEM followed by the addition of serum-free DMEM containing 10 nM pro-MMP-2. After a 15-min incubation at 37 °C, pro-MMP-2 activation was determined in the cell lysate fraction by gelatin zymography. The *asterisks* show the pro-MMP-2 added to the media. *C*, *Timp2* (−/−) mutant cells infected to express MT1-MMP were incubated (16 h, 37 °C) without (*lane 1*) or with (*lane 2*) 10 nM exogenous recombinant TIMP-4. The cell lysates were subjected to reducing 10% SDS-PAGE followed by immunoblot analysis using a specific rabbit pAb to TIMP-4. *Lane 3* shows 10 ng of the purified recombinant TIMP-4.

presence (Fig. 1*C*, *lane 3*, without TIMP-2; *lane 4* with TIMP-2). Taken together, these studies establish the importance of TIMP-2 for the MT1-MMP-dependent activation of pro-MMP-2 and are in agreement with recent *in vitro* and *in vivo* studies (65, 67) with *Timp2* mutant fibroblasts and mice, respectively.

We have previously shown that TIMP-2 regulates the turnover of MT1-MMP on the cell surface by binding to the active form of the enzyme (40). This process induces the accumulation of active MT1-MMP (57 kDa) on the cell surface and concomitantly decreases the amount of a membrane-tethered 44-kDa form of MT1-MMP (40). N-terminal sequencing data demonstrated that the 57-kDa species starts at Tyr^{112} and the 44-kDa species starts at Gly^{285}; thus the latter represents an inactive enzyme form (40). To examine the relationship between pro-MMP-2 activation and MT1-MMP processing in the *Timp2*-null cell system, the homozygous *Timp2* mutant cells expressing MT1-MMP were analyzed for pro-MMP-2 activation and MT1-MMP forms as a function of TIMP-2 concentration. As shown in Fig. 2*A* (zymogram), as little as 1 nM TIMP-2 induced pro-MMP-2 activation as monitored in the cell lysate fraction. The lysates were also analyzed for MT1-MMP forms and TIMP-2 by immunoblot analyses (Fig. 2*A*, immunoblots). These studies show that overnight exposure to TIMP-2, at doses of >10 nM, induce a detectable accumulation of the 57-kDa species concomitantly with a reduction in the inactive 44-kDa form of MT1-MMP. Without TIMP-2 and at doses of 1 nM TIMP-2, the major species detected were the 60-kDa (pro-MT1-MMP) and the 44-kDa species. A minor 63-kDa protein represents the pro-MT1-MMP with the signal peptide,[3] and the ~50-kDa protein is a nonspecific band. TIMP-2 was also detected in the cell lysates (Fig. 2*A*, immunoblot α-TIMP-2) consistent with the association of the exogenous TIMP-2 with the MT1-MMP-expressing cells (38).

Importance of Ternary Complex on Pro-MMP-2 Activation by MT1-MMP in the Timp2-Null Cellular System—Previous studies demonstrated that the formation of an MT1-MMP·TIMP-2·pro-MMP-2 (ternary) complex on the cell surface is required for pro-MMP-2 activation (12, 36, 39). To demonstrate the importance of this complex in the *Timp2* null cellular system, we used a C-terminally truncated form of TIMP-2, Δ-TIMP-2, incapable of binding pro-MMP-2 (data not shown) and therefore unable to form the ternary complex (36, 53). In addition, we tested recombinant TIMP-4, known to bind to pro-MMP-2 (68). Due to their lower affinity for MT1-MMP, Δ-TIMP-2 (shown in Table I) and TIMP-1 (36, 69) were added to the homozygous cells at concentrations 10-fold higher than that of wild type TIMP-2. As shown in the zymogram of Fig. 2*B*, 2.5 nM TIMP-2 (Fig. 2*B*, *lane 1*) efficiently promoted pro-MMP-2 activation. In contrast, Δ-TIMP-2 (Fig. 2*B*, *lane 2*; 25 nM) and TIMP-1 (Fig. 2*B*, *lane 4*; 25 nM) failed to induce pro-MMP-2 activation. Interestingly, exogenous TIMP-4 also had no effect on activation (Fig. 2*B*, *lane 3*; 1–100 nM, only 10 nM shown), consistent with the results of Bigg *et al.*[2] In addition, co-expression of MT1-MMP with TIMP-4 in the (−/−) *Timp2* mutant cells using the vaccinia expression system had no effect on pro-MMP-2 activation.[4] Immunoblot analysis demonstrated the cell association of the exogenous TIMP-4 with (−/−) *Timp2* mutant cells expressing MT1-MMP (Fig. 2*C*, *lane 2*) suggesting the binding of TIMP-4 to MT1-MMP. Taken together, these results demonstrate that only full-length TIMP-2 can promote the MT1-MMP-dependent activation of pro-MMP-2 in a process that is dependent on ternary complex formation.

TIMP-2 and MMP Inhibitors Act Synergistically to Enhance Pro-MMP-2 Activation—Previous studies suggested that, in addition to ternary complex formation, the enhancing effect of TIMP-2 on pro-MMP-2 activation was the result of a specific inhibition of MT1-MMP autocatalytic turnover on the cell surface (40). Indeed, TIMP-2 induces the accumulation of the 57-kDa form of MT1-MMP (shown in Fig. 2*A*). It was hypothesized that at low inhibitor concentrations relative to MT1-MMP and continuous enzyme synthesis by the cells, this process would slow down enzyme turnover, generating a fraction of inhibitor-free active MT1-MMP and hence increase pericellular proteolysis (40). Since this effect is due to inhibition of MT1-MMP activity, we hypothesized that synthetic MMPIs may mimic TIMP-2 in its ability to reduce MT1-MMP turnover. We asked whether reduction of MT1-MMP autocatalytic turnover by MMPIs together with ternary complex formation by TIMP-2 would enhance pro-MMP-2 activation when compared with activation promoted by TIMP-2 alone.

To test this hypothesis, the *Timp2* (−/−) null cells were incubated overnight with a variety of synthetic and natural MMPIs to inhibit MT1-MMP autocatalysis and induce accumulation of the active 57-kDa species. The cells were then washed to remove excess unbound inhibitors and then exposed to TIMP-2 to generate the ternary complex. After a rinse to remove unbound TIMP-2, the cells received pro-MMP-2. We tested the effects of marimastat and batimastat, two hydroxamate-based inhibitors (33, 45, 47); SB-3CT, a mechanism-based inhibitor (42); and Δ-TIMP-2 (53). As shown in the zymogram of Fig. 3, administration of TIMP-2 alone for 5 min was sufficient to promote pro-MMP-2 activation, as expected (Fig. 3, *lane 2*). However, in the cells pretreated with a 1 μM concentration of either marimastat (Fig. 3, *lane 3*) or batimas-

[3] M. Toth, unpublished results.

[4] S. Hernandez-Barrantes, Y. Shimura, and R. Fridman, unpublished results.

TABLE I

Association, dissociation, and inhibition constants for MT1-MMP$_{cat}$ interactions with natural and synthetic MMP inhibitors

MT1-MMP$_{cat}$ (0.5 nM) was added to a solution of MOCAcPLGLA$_2$pr(Dnp)-AR-NH$_2$ (7 μM) and varying concentrations of inhibitor in buffer R at 25.0 °C. Substrate hydrolysis was monitored at excitation and emission wavelengths of 328 and 393 nm, respectively, for up to 30 min. To determine the dissociation rate constants, k_{off}, a mixture of enzyme (50 nM) and inhibitor (80 nM) in buffer R was incubated for ~1 h at 25 °C and diluted 400-fold in a solution of fluorogenic substrate (10 μM) in the same buffer containing 1% Me_2SO. Substrate hydrolysis was monitored for up to 1 h. The kinetic parameters were evaluated as described under "Experimental Procedures." Analogous results were obtained from at least two independent experiments.

Inhibitor	k_{on}	k_{off}	K_i
	$M^{-1}\ s^{-1}$	s^{-1}	nM
Wild type TIMP-2	$(2.74 \pm 0.14) \times 10^6$	2×10^{-4a}	0.07
Δ-TIMP-2	$(2.68 \pm 0.12) \times 10^6$	$(1.95 \pm 0.03) \times 10^{-3}$	0.73 ± 0.03
MARIMASTAT			2.1 ± 0.5
BATIMASTAT			3.4 ± 0.1
BB-2116			8 ± 1
SB-3CT			110 ± 11

[a] Estimated value based on a 10-fold difference between the slopes of the linear portions of the dissociation curves for the complexes of MT1-MMP$_{cat}$ with Δ-TIMP-2 (steady state rate) and wild type TIMP-2.

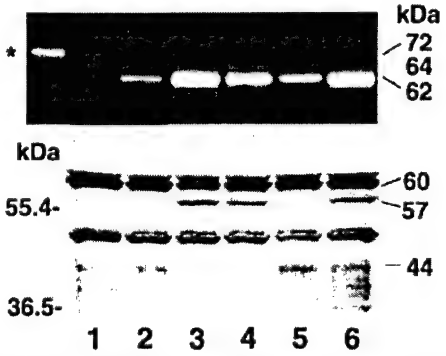

FIG. 3. **Synthetic MMPIs enhance pro-MMP-2 activation by MT1-MMP in the presence of TIMP-2.** The *Timp2* (−/−) mutant cells in 12-well plates were co-infected to express MT1-MMP as described in the legend to Fig. 1. After the infection, the media were aspirated and replaced with serum-free DMEM (1 ml/well) supplemented with 1 μM marimastat (*lane 3*), 1 μM batimastat (*lane 4*), 1 μM SB-3CT (*lane 5*), or 100 nM Δ-TIMP-2 (*lane 6*) followed by a 16-h incubation at 37 °C. Some wells received DMEM without inhibitors (*lanes 1* and *2*). The cells were washed once to remove excess inhibitors and then incubated with DMEM (1 ml/well) supplemented without (*lane 1*) or with (*lanes 2–6*) 10 nM TIMP-2 for 5 min at 37 °C. The media were then aspirated and replaced with fresh DMEM containing 10 nM pro-MMP-2. After 15 min at 37 °C, the cells were rinsed with phosphate-buffered saline and solubilized in lysis buffer. The lysates were analyzed for pro-MMP-2 activation and MT1-MMP forms by gelatin zymography and immunoblot analysis, respectively. The *asterisk* shows the pro-MMP-2 added to the media. The ~50-kDa band is nonspecific. This experiment was repeated at least three times with similar results.

tat (Fig. 3, *lane 4*) or 100 nM Δ-TIMP-2 (Fig. 3, *lane 6*), a significant increase in active MMP-2 was observed. SB-3CT at doses of 1 μM showed a modest effect (*lane 5*) when compared with the other synthetic MMPIs. Analysis of the lysate fractions for MT1-MMP forms by immunoblotting revealed accumulation of the 57-kDa species after treatment with marimastat, batimastat, and Δ-TIMP-2 (Fig. 3, *lanes 3*, *4*, and *6*, respectively) but not with SB-3CT (Fig. 3, *lane 5*). However, Δ-TIMP-2 was less efficient in inhibiting MT1-MMP conversion to the 44-kDa form (Fig. 3, *lane 6*, immunoblot). In the absence of TIMP-2, no activation was detected (Fig. 3, *lane 1*, zymogram).

Since the relationship between inhibition of MT1-MMP autocatalytic turnover and the existence of inhibitor-free MT1-MMP is dependent on the inhibitor concentration and affinity, we used inhibitor doses ranging from 0 to 500 nM to further examine the differential effects of marimastat and SB-3CT on pro-MMP-2 activation. We also tested BB-2116, a boronate-containing MMP inhibitor. In addition, we asked whether TIMP-4 would act synergistically with TIMP-2 in pro-MMP-2 activation by MT1-MMP. TIMP-4 inhibits MT1-MMP activity but cannot form a ternary complex with MT1-MMP and pro-MMP-2.[2] As shown in the zymogram of Fig. 4*A*, SB-3CT had no effect on pro-MMP-2 activation at doses of 4, 20, and 500 nM (Fig. 4*A*, *lanes 5* and *6*; only 20 and 500 nM, respectively, are shown). In contrast, as little as 20 nM marimastat (Fig. 4*A*, *lane 7*) had a noticeable effect on pro-MMP-2 activation when compared with TIMP-2 alone (Fig. 4*A*, *lane 2*). BB-2116 exhibited enhancing effects with TIMP-2 at doses of 500 nM (Fig. 4*A*, *lane 4*). Consistently, both marimastat (Fig. 4*A*, *lanes 7* and *8*) and BB-2116 (Fig. 4*A*, *lane 4*) induced accumulation of the 57-kDa form of MT1-MMP. Pretreatment of the cells with TIMP-4 (0–100 nM) followed by TIMP-2 addition, had no enhancing effect on pro-MMP-2 activation (Fig. 4*B*). Interestingly, TIMP-4 induced the accumulation of 57-kDa form of MT1-MMP consistent with its inhibitory activity. These results suggest that, with the exception of TIMP-4 and SB-3CT, certain synthetic MMPIs and Δ-TIMP-2, which inhibit MT1-MMP activity and consequently autocatalytic degradation, can enhance MT1-MMP-dependent pro-MMP-2 activation in the presence of TIMP-2.

The Enhancing Effect of MMPIs on Pro-MMP-2 Activation by MT1-MMP Requires TIMP-2 for Ternary Complex Formation—To examine the relationship between the effects of the MMPIs on pro-MMP-2 activation (inhibition of MT1-MMP autocatalysis) and ternary complex formation, the *Timp2* (−/−) mutant cells were pretreated with marimastat to accumulate the 57-kDa form of MT1-MMP and then were or were not exposed to TIMP-2, Δ-TIMP-2, or TIMP-1. As expected, marimastat pretreatment and the addition of TIMP-2 (Fig. 5, *lane 2*) resulted in a significant increase in pro-MMP-2 activation when compared with the activation observed with TIMP-2 alone (*lane 1*). In contrast, administration of either Δ-TIMP-2 (*lane 3*) or TIMP-1 (*lane 4*) after the marimastat treatment had no effect. Marimastat treatment alone had no effect on pro-MMP-2 activation (*lane 5*). Immunoblot analysis demonstrated the presence of the 57-kDa form of MT1-MMP after marimastat treatment, as expected (Fig. 5, immunoblot). Taken together, these results indicate that inhibition of MT1-MMP turnover alone is not sufficient to promote pro-MMP-2 activation, a process that requires ternary complex formation. However, both processes can act synergistically to enhance activation.

Effect of Δ-TIMP-2 and Synthetic MMPIs on MT1-MMP Activity—The results above indicated a differential inhibition of MT1-MMP autocatalytic turnover by various synthetic MMPIs and Δ-TIMP-2. In order to elucidate the inhibitor effects on MT1-MMP activity observed in the cells, the interactions of the catalytic domain of MT1-MMP (MT1-MMP$_{cat}$) with natural and synthetic inhibitors were characterized in a purified system. As depicted in Table I, both TIMP-2 and Δ−TIMP-2 exhibit slow binding kinetics with similar association rate constants of

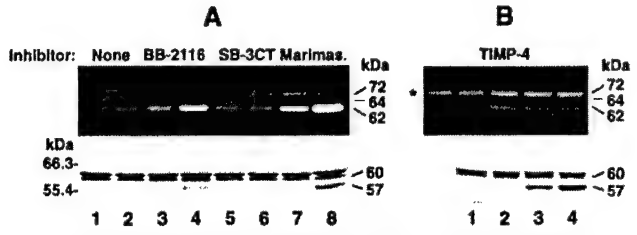

FIG. 4. **Synergistic effect of TIMP-2 with synthetic MMPIs and TIMP-4 on pro-MMP activation.** *A*, *Timp2* (−/−) mutant cells in 12-well plates were infected to express MT1-MMP as described in Fig. 1. After the infection, the media were aspirated and replaced with serum-free DMEM (1 ml/well) supplemented without (*lanes 1* and *2*) or with BB-2116 (*lane 3*, 20 nM; *lane 4*, 500 nM), SB-3CT (*lane 5*, 20 nM; *lane 6*, 500 nM) or marimastat (*lane 7*, 20 nM; *lane 8*, 500 nM). After a 16-h incubation at 37 °C, the media were aspirated, and the cells were washed with DMEM to remove excess inhibitors and then incubated with DMEM (1 ml/well) supplemented without (*lane 1*) or with (*lanes 2–8*) 10 nM TIMP-2 for 5 min at 37 °C. The media were then aspirated and replaced with DMEM containing 10 nM pro-MMP-2. After 15 min at 37 °C, the cells were solubilized in lysis buffer and analyzed for pro-MMP-2 activation and MT1-MMP forms by gelatin zymography and immunoblot analysis, respectively. *B*, *Timp2* (−/−) mutant cells in 12-well plates expressing MT1-MMP were incubated (16 h, 37 °C) without (*lane 1*) or with TIMP-4 (*lane 2*, 1 nM; *lane 3*, 10 nM; *lane 4*, 100 nM). After removal of the unbound TIMP-4, the cells received 10 nM TIMP-2 for a 5-min incubation at 37 °C followed by the addition of 10 nM pro-MMP-2 as described above. Analysis of pro-MMP-2 activation and MT1-MMP forms were monitored by gelatin zymography and immunoblot analysis, respectively.

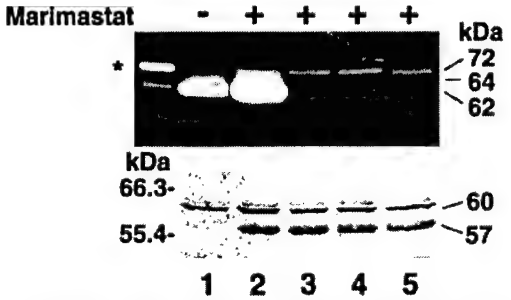

FIG. 5. **TIMP-2 is required for the enhancing effect of marimastat on pro-MMP-2 activation by MT1-MMP.** *Timp2* (−/−) mutant cells infected to express MT1-MMP in 12-well plates were treated (*lanes 2–5*) or not (*lane 1*) with 1 μM marimastat overnight at 37 °C. The medium was then aspirated and replaced with medium supplemented with either 10 nM TIMP-2 (*lanes 1* and *2*), Δ-TIMP-2 (*lane 3*), or TIMP-1 (*lane 4*) or medium without TIMPs (*lane 5*). After a 30-min incubation, the medium was aspirated, and the cells were rinsed with DMEM and incubated (30 min, 37 °C) with 10 nM pro-MMP-2. The cell lysates were analyzed for pro-MMP-2 activation and MT1-MMP forms by gelatin zymography and immunoblot analysis, respectively. The *asterisk* shows the pro-MMP-2 added to the medium.

$(2.74 \pm 0.14) \times 10^6$ and $(2.68 \pm 0.12) \times 10^6$ M^{-1} s^{-1}, respectively. The latter value is in agreement with that reported by Butler *et al.* (36) for the interaction of the (Δ128–194) TIMP-2 mutant with the catalytic domain of MT1-MMP ($2.80 \pm 0.45 \times 10^6$ M^{-1} s^{-1}). TIMP-2 bound with a picomolar K_i (0.07 nM) and showed significant inhibition at a concentration similar to that of the enzyme itself. Δ−TIMP-2 exhibits reduced affinity (K_i = 0.73 ± 0.03 nM) due to a 10-fold higher dissociation rate constant ($k_{off} = 1.95 \pm 0.03 \times 10^{-3}$ s^{-1}) relative to the value for the full-length TIMP-2. The synthetic MMP inhibitors marimastat, batimastat, BB-2116, and SB-3CT show competitive inhibition and, with the exception of SB-3CT, exhibit K_i values in the low nanomolar range. These data are in agreement with the IC_{50} values for marimastat and batimastat reported by Yamamoto *et al.* (70) for a mutant MT1-MMP lacking the transmembrane domain. In addition, the K_i value for marimastat with the $MT1\text{-}MMP_{cat}$ compares with IC_{50} values reported for the interaction of this inhibitor with the gelatinases (IC_{50} = 3–6 nM), fibroblast collagenase (IC_{50} = 5 nM), and matrylisin (IC_{50} = 16 nM) consistent with marimastat being a nonspecific (*i.e.* broad-spectrum) MMP inhibitor (33, 45, 47, 71). Interestingly, SB-3CT shows an ~10–1600-fold reduced affinity (K_i = 110 nM) for $MT1\text{-}MMP_{cat}$ compared with the other MMPIs, in agreement with its inability to induce accumulation of the 57-kDa species of MT1-MMP and pro-MMP-2 activation with TIMP-2.

Synergistic Effects of MMPI Inhibitors on Pro-MMP-2 Activation in a Background of Endogenous Expression of TIMP-2—To further examine the synergistic effects of MMPIs and TIMP-2 on pro-MMP-2 activation, we used BS-C-1 cells infected to express MT1-MMP. BS-C-1 cells produce low levels of endogenous TIMP-2, which are further suppressed but not completely eliminated upon viral infection (data not shown). Consistently, BS-C-1 cells infected to express MT1-MMP can activate pro-MMP-2 without the addition of exogenous TIMP-2 (40). Thus, we used BS-C-1 cells to examine the effects of MMPIs on pro-MMP-2 activation in a cellular system expressing a background level of endogenous TIMP-2. BS-C-1 cells infected to express MT1-MMP were incubated with increasing concentrations of TIMP-2 (0–20 nM), Δ-TIMP-2 (0–500 nM), SB-3CT (0–1 μM), or marimastat (0–10 μM) followed by the addition of pro-MMP-2. In addition, we tested the effects of Ala + TIMP-2 (0–100 nM), a mutant TIMP-2 devoid of inhibitory activity, as a negative control inhibition of MT1-MMP autocatalytic turnover. As shown in Fig. 6, pro-MMP-2 activation is greatly enhanced after administration of exogenous TIMP-2 (*TIMP-2 panel*). Both marimastat and Δ-TIMP-2 enhance pro-MMP-2 activation when compared with the basal activation detected in BS-C-1 cells in the absence of inhibitors (due to endogenous TIMP-2). Consistently, activation under these conditions is associated with accumulation of the 57-kDa species of MT1-MMP as shown in the immunoblots of Fig. 6. Both Ala + TIMP-2 and SB-3CT have no significant effects, suggesting that inhibition of the MT1-MMP autocatalytic turnover is required for the synergistic effect of the synthetic and natural MMPIs with the endogenous TIMP-2. Indeed, neither Ala + TIMP-2 nor SB-3CT induces a detectable accumulation of the 57-kDa form (Fig. 6, immunoblot). Taken together, these studies indicate that inhibition of MT1-MMP turnover (accumulation of 57-kDa form) by synthetic MMPIs can enhance the effect of the endogenous TIMP-2 in pro-MMP-2 activation in the BS-C-1 cell system.

DISCUSSION

The studies presented here provide conclusive evidence for the complex regulation of MT1-MMP activity by TIMP-2 and further demonstrate that some synthetic MMPIs might have the potential to promote MT1-MMP-dependent activation of pro-MMP-2. Our results clearly show that pro-MMP-2 activation requires the presence of TIMP-2, since the *Timp2*-null cells are unable to activate pro-MMP-2 even after expression of MT1-MMP. However, a short (5-min) incubation with exogenous TIMP-2 and a brief incubation (15 min) with pro-MMP-2 result in a significant conversion of pro-MMP-2 to its active form. This rapid activation of pro-MMP-2 is unprecedented in a cellular system and demonstrates the high catalytic efficiency of MT1-MMP for this substrate under optimal conditions. The dependence on TIMP-2 for activation is also evident from the results with the heterozygous *Timp2* (+/−) mutant cells and the BS-C-1 cells, both of which contain endogenous TIMP-2 and are able to activate pro-MMP-2 after expression of MT1-MMP without requirement of exogenous TIMP-2. Strongin *et al.* (12) proposed that the effect of TIMP-2 on activation is mediated by a ternary complex formed between active MT1-MMP, TIMP-2, and pro-MMP-2, where the C-terminal region of TIMP-2 binds

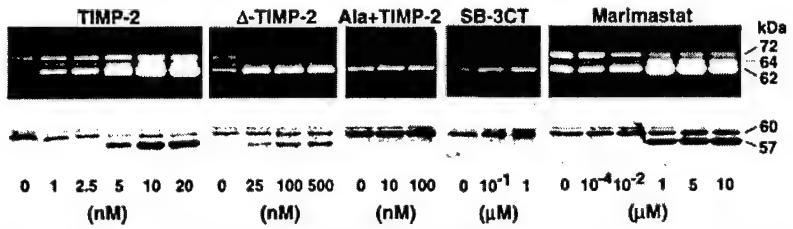

FIG. 6. **Effect of synthetic MMPIs on pro-MMP-2 activation in BS-C-1 cells expressing MT1-MMP and endogenous TIMP-2.** BS-C-1 cells were co-infected to express MT1-MMP as described previously (40). After infection, the media were aspirated and replaced with serum-free DMEM supplemented with various concentrations of TIMP-2, marimastat, Δ-TIMP-2, Ala + TIMP-2, or SB-3CT for a 16-h incubation at 37 °C. The media were then aspirated and replaced with DMEM containing 10 nM pro-MMP-2. After a 30-min incubation at 37 °C, the cells were rinsed with phosphate-buffered saline and then lysed in lysis buffer. The lysates were subjected to gelatin zymography and immunoblot analysis for assessment of pro-MMP-2 activation and generation of the 57-kDa form of MT1-MMP, respectively.

to pro-MMP-2 to anchor the zymogen to the cell surface. Although formation of such a complex was not directly demonstrated in the present study, the results with the Δ-TIMP-2, which lacks the C-terminal domain and failed to induce pro-MMP-2 activation in the *Timp2* (−/−) mutant cells, indirectly support the ternary complex model of pro-MMP-2 activation.

In addition to its role in ternary complex formation, TIMP-2 also influences the processing of MT1-MMP. We have recently shown that TIMP-2 prevents the autocatalytic conversion of active MT1-MMP (57 kDa) to its inactive 44-kDa species, and as a consequence the 57-kDa species accumulates on the cell surface (40). As shown here, a similar effect is induced by synthetic MMPIs (41) as well as by Δ-TIMP-2 and TIMP-4. We show for the first time that some synthetic MMPIs and Δ-TIMP-2 can enhance pro-MMP-2 activation by MT1-MMP in the presence of TIMP-2. This effect is due to the accumulation of the 57-kDa MT1-MMP species as a consequence of inhibition of MT1-MMP turnover. Our kinetic data suggest the possibility that the increase in MT1-MMP·TIMP-2 complexes may be a consequence of a displacement of the bound synthetic MMPI by TIMP-2 (K_i for TIMP-2 is approximately 1–2 orders of magnitude lower than that for the synthetic MMPI), a process that will generate more pro-MMP-2 "receptors." However, binding of small molecule inhibitors concurrently with TIMP-2 to active MT1-MMP cannot be ruled out. Regardless of the mechanism involved, pro-MMP-2 activation would require a "catalytic" quantity of the inhibitor-free MT1-MMP to hydrolyze the Asn^{37}-Leu^{38} bond of pro-MMP-2 as previously shown (69). It should be noted that the enhancing effects of the MMPIs on pro-MMP-2 activation in the *Timp2* null cells in the presence of TIMP-2 were evident only when the synthetic inhibitors (up to 10 μM to avoid toxic effects) were administered to the cells and removed from the system prior to the administration of the exogenous TIMP-2. Preincubation of the cells with the MMPIs was necessary to induce accumulation of the 57-kDa form of MT1-MMP, a fraction of which would be expected to be inhibitor-free, since the cells are continuously producing MT1-MMP. We postulate that these conditions (removal of excess synthetic inhibitor prior to the addition of TIMP-2 and pro-MMP-2 and continuous replenishment of MT1-MMP by the cells) generate sufficient catalytically active MT1-MMP to generate ternary complex and to process pro-MMP-2. In contrast, simultaneous administration of TIMP-2 with various doses of marimastat inhibits pro-MMP-2 activation in a dose-dependent manner (data not shown). This inhibitory effect is likely to be due to competition between TIMP-2 and marimastat for MT1-MMP binding, resulting in decreased ternary complex formation (38, 72). However, BS-C-1 cells, which contain low levels of endogenous TIMP-2, exhibit enhanced pro-MMP-2 activation upon administration of the MMPIs. In this case, enhanced activation is the result of the inhibition of MT1-MMP autocatalysis and ternary complex formation is not a limiting step. The result with the BS-C-1 cells also suggests that invasive tumor cells equipped with both MT1-MMP and TIMP-2 may be subject to similar synergistic effects of synthetic MMPIs on MT1-MMP activity under the right conditions.

The relationship between inhibition of MT1-MMP autocatalysis and ternary complex formation was also demonstrated in the experiments in which the *Timp2* (−/−) mutant cells were treated with marimastat followed by administration of Δ-TIMP-2 or TIMP-1, in which case pro-MMP-2 activation was not observed. Furthermore, the Ala + TIMP-2 mutant, devoid of inhibitory activity, failed to support pro-MMP-2 activation in the BS-C-1 cells in the presence of endogenous TIMP-2 due to its inability to inhibit MT1-MMP turnover. Likewise, pretreatment of the *Timp2* (−/−) cells with marimastat had no effect on pro-MMP-2 activation without subsequent addition of TIMP-2 revealing that accumulation of active MT1-MMP alone is not sufficient for pro-MMP-2 activation and requires a functional full-length TIMP-2 to generate the ternary complex. This was also demonstrated by the results with TIMP-4, which, despite its ability to inhibit MT1-MMP activity as found by Bigg *et al.*[2] and to bind pro-MMP-2 (68), was unable to promote MT1-MMP-dependent activation of pro-MMP-2 or to act synergistically with TIMP-2 in this process. Recent studies from Overall's laboratory[2] also show that TIMP-4 cannot form a ternary complex in a purified system and, if administered with TIMP-2, inhibits pro-MMP-2 activation by MT1-MMP in *Timp2* mutant cells. Here we have shown that TIMP-4, like other MMPIs, induces accumulation of the 57-kDa form of MT1-MMP, consistent with its inhibitory activity, but fails to act synergistically with TIMP-2 in the promotion of pro-MMP-2 activation. The reason for this puzzling result is yet unknown but may be related to differences in affinity between these inhibitors for MT1-MMP and pro-MMP-2. Indeed, TIMP-4 exhibits a lower affinity for pro-MMP-2 when compared with TIMP-2.[2] Also, a potential rapid internalization of the putative MT1-MMP·TIMP-4 complex, although yet unproven, may play a role. Further enzymatic and biochemical studies are required to understand the dynamics of TIMP-4 and TIMP-2 inhibitory activities in relation to MT1-MMP functions. Nevertheless, these studies suggest that the effects of TIMP-4 on TIMP-2 may represent a natural and unique regulatory mechanism of MMP-dependent proteolysis on the cell surface in which TIMP-4 may play a counter role to that of TIMP-2, physiologically, by binding to active MT1-MMP with high affinity. We therefore propose that the long held view of a balance between MMPs and TIMPs as a key determinant of proteolytic activity and tumor progression (73) may well include a balance of TIMP-2 and TIMP-4 as a major determining factor for MT1-MMP-dependent proteolysis in cancer tissues where both inhibitors may be present.

The results presented here demonstrate that pro-MMP-2 activation by MT1-MMP at the cell surface is the result of a

highly regulated enzymatic process that involves two independent events, which under certain conditions may work synergistically to enhance MT1-MMP-dependent activation of pro-MMP-2. It should be noted that this might not be the case in all circumstances or with different MT1-MMP substrates. For example, for pro-MMP-2, our data show that a short (5-min) exposure to TIMP-2 followed by a 15-min incubation with pro-MMP-2 was sufficient to rapidly activate pro-MMP-2 without detectable accumulation of active (57-kDa) MT1-MMP. The reason for the lack of detection of active enzyme under this conditions is unclear but may be related to the detection method (immunoblotting), rapid enzyme turnover, and/or the internalization and turnover of the MT1-MMP (57 kDa)·TIMP-2 complex as recently reported (72). Under conditions of substoichiometric TIMP-2 molar concentrations relative to MT1-MMP, the efficient binding of TIMP-2 and the catalytic efficiency of MT1-MMP for its substrate result in optimal pro-MMP-2 activation (39). Thus, while rapid bursts of TIMP-2 expression will be sufficient to generate ternary complex and consequently activate pro-MMP-2 in the absence of a significant and detectable accumulation of active MT1-MMP, chronic exposure to TIMP-2 or MMPIs would maintain a steady level of MT1-MMP on the cell surface due to inhibition of autocatalysis. For other MT1-MMP substrates such as ECM components, which do not require ternary complex formation to be hydrolyzed by MT1-MMP, sustained TIMP-2 expression and/or the presence of synthetic MMPIs may indirectly enhance catalytic activity, as demonstrated here using pro-MMP-2 as a target substrate.

Recent accomplishments in drug design have resulted in the generation of a variety of novel MMPIs with effective antitumor and anti-angiogenic activities in animal models of cancer (3, 4, 33, 46, 47). These encouraging results have brought some of these compounds, such as marimastat and batimastat, to human clinical trials. The majority of the compounds undergoing testing in humans, however, lack specificity toward the various MMP families. The hydroxamates, for instance, inhibit a wide spectrum of MMPs, including MT1-MMP as herein demonstrated, often with similar affinities (70, 71). The complex outcome of MT1-MMP inhibition on catalytic activity demonstrated here raises important issues regarding the potential consequences of inhibiting MT1-MMP. The intermolecular autocatalytic turnover of MT1-MMP on the cell surface may represent an important regulatory step aimed at controlling pericellular proteolysis, a process that is likely to be favored by lateral diffusion and clustering of MT1-MMP molecules in the cell surface (74, 75). Thus, reversible inhibition of MT1-MMP activity would play a role in preventing excessive enzyme clearance from the cell surface and indirectly favor proteolysis. Such an effect by synthetic MMPIs would depend on the spectrum of activity (K_i values) elicited by each particular inhibitor against the different members of the MMP family and on their pharmacokinetics and dosing regime. The MMPIs tested here exhibit different K_i values for the catalytic domain of MT1-MMP, which correlated well with their efficacy in promoting pro-MMP-2 activation with TIMP-2. We recently described the first example of a mechanism-based inhibitor for MMPs (42). This inhibitor, SB-3CT, is highly specific for inhibition of gelatinases, enzymes that were inhibited covalently by this inhibitor. SB-3CT does not pursue the metal chelation strategy for its inhibition, in contrast to the case of the existing inhibitors. We have shown here that SB-3CT is substantially less effective in inhibition of MT1-MMP, for which it was not designed, and simply behaves as a simple linear competitive inhibitor, in contrast to the case of gelatinases (42). Again in contrast to marimastat and batimastat, SB-3CT did not show any ability to stimulate activation of pro-MMP-2 induced by TIMP-2. Thus, the design of highly specific MMPIs will minimize potential adverse effects in conditions where inhibition of the MT1-MMP-MMP-2 system is a therapeutic goal.

The complex regulation of MT1-MMP activity by TIMP-2 may provide a biochemical framework for understanding several intriguing observations in human tumors and experimental models of metastasis using synthetic MMPIs. High levels of TIMP-2 expression were found in various human cancers, which positively correlated with metastasis and poor survival (21, 76–79). A recent study reported that treatment of tumor-bearing mice with batimastat significantly inhibited tumor growth but promoted tumor cell invasion into the liver of a variety of human cancer cells (80). However, the mechanism for such effect was not reported. Finally, recent tumorigenicity studies with the heterozygous and homozygous *Timp2* mutant cells indicate a higher incidence of tumor formation and metastasis in the heterozygous cells, suggesting a role for TIMP-2 in promotion of tumor progression.[5] Our findings disclosed in this report provide one plausible explanation for these observations, that by binding to active MT1-MMP, both natural and synthetic MMP inhibitors may produce a "pool" of active MT1-MMP available to degrade ECM components and to activate pro-MMP-2. While this may represent an undesired effect of some strategies for anti-MMP therapies in cancer that are being investigated, this effect may be beneficial in pathological conditions characterized by excessive deposition of collagen such as fibrosis and connective tissue disorders where increased MMP activity might be desired. These examples and the studies presented herein emphasize the importance of a rational approach for the design of specific MMP inhibitor, which should also be based on an understanding of the regulation of MT1-MMP and likely other members of the MT-MMP subfamily by TIMPs and MMPIs at the cell surface.

REFERENCES

1. Nagase, H., and Woessner, J. F., Jr. (1999) *J. Biol. Chem.* **274,** 21491–21494
2. Birkedal-Hansen, H., Moore, W. G., Bodden, M. K., Windsor, L. J., Birkedal-Hansen, B., DeCarlo, A., and Engler, J. A. (1993) *Crit. Rev. Oral Biol. Med.* **4,** 197–250
3. Stetler-Stevenson, W. G. (1999) *J. Clin. Invest.* **103,** 1237–1241
4. Nelson, A. R., Fingleton, B., Rothenberg, M. L., and Matrisian, L. M. (2000) *J. Clin. Oncol.* **18,** 1135–1149
5. Massova, I., Kotra, L. P., Fridman, R., and Mobashery, S. (1998) *FASEB J.* **12,** 1075–1095
6. Sato, H., Takino, T., Okada, Y., Cao, J., Shinagawa, A., Yamamoto, E., and Seiki, M. (1994) *Nature* **370,** 61–65
7. Puente, X. S., Pendas, A. M., Llano, E., Velasco, G., and Lopez-Otin, C. (1996) *Cancer Res.* **56,** 944–949
8. Pei, D. (1999) *J. Biol. Chem.* **274,** 8925–8932
9. Pei, D. (1999) *Cell Res.* **9,** 291–303
10. Velasco, G., Cal, S., Merlos-Suarez, A., Ferrando, A. A., Alvarez, S., Nakano, A., Arribas, J., and Lopez-Otin, C. (2000) *Cancer Res.* **60,** 877–882
11. Takino, T., Sato, H., Shinagawa, A., and Seiki, M. (1995) *J. Biol. Chem.* **270,** 23013–23020
12. Strongin, A. Y., Collier, I., Bannikov, G., Marmer, B. L., Grant, G. A., and Goldberg, G. I. (1995) *J. Biol. Chem.* **270,** 5331–5338
13. Pei, D., and Weiss, S. J. (1996) *J. Biol. Chem.* **271,** 9135–9140
14. d'Ortho, M. P., Stanton, H., Butler, M., Atkinson, S. J., Murphy, G., and Hembry, R. M. (1998) *FEBS Lett.* **421,** 159–164
15. d'Ortho, M. P., Will, H., Atkinson, S., Butler, G., Messent, A., Gavrilovic, J., Smith, B., Timpl, R., Zardi, L., and Murphy, G. (1997) *Eur. J. Biochem.* **250,** 751–757
16. Ohuchi, E., Imai, K., Fujii, Y., Sato, H., Seiki, M., and Okada, Y. (1997) *J. Biol. Chem.* **272,** 2446–2451
17. Zhou, Z., Apte, S. S., Soininen, R., Cao, R., Baaklini, G. Y., Rauser, R. W., Wang, J., Cao, Y., and Tryggvason, K. (2000) *Proc. Natl. Acad. Sci. U. S. A.* **97,** 4052–4057
18. Holmbeck, K., Bianco, P., Caterina, J., Yamada, S., Kromer, M., Kuznetsov, S. A., Mankani, M., Robey, P. G., Poole, A. R., Pidoux, I., Ward, J. M., and Birkedal-Hansen, H. (1999) *Cell* **99,** 81–92
19. Kleiner, D. E., and Stetler-Stevenson, W. G. (1999) *Cancer Chemother. Pharmacol.* **43,** (suppl.) 42–51
20. Jones, J. L., Glynn, P., and Walker, R. A. (1999) *J. Pathol.* **189,** 161–168
21. Davidson, B., Goldberg, I., Kopolovic, J., Lerner-Geva, L., Gotlieb, W. H., Ben-Baruch, G., and Reich, R. (1999) *Gynecol. Oncol.* **73,** 372–382

[5] P. Soloway, manuscript in preparation.

22. Kitagawa, Y., Kunimi, K., Ito, H., Sato, H., Uchibayashi, T., Okada, Y., Seiki, M., and Namiki, M. (1998) *J. Urol.* **160,** 1540–1545
23. Kurahara, S., Shinohara, M., Ikebe, T., Nakamura, S., Beppu, M., Hiraki, A., Takeuchi, H., and Shirasuna, K. (1999) *Head Neck* **21,** 627–638
24. Ueno, H., Nakamura, H., Inoue, M., Imai, K., Noguchi, M., Sato, H., Seiki, M., and Okada, Y. (1997) *Cancer Res.* **57,** 2055–2060
25. Yoshizaki, T., Sato, H., Maruyama, Y., Murono, S., Furukawa, M., Park, C. S., and Seiki, M. (1997) *Cancer* **79,** 139–144
26. Harada, T., Arii, S., Mise, M., Imamura, T., Higashitsuji, H., Furutani, M., Niwano, M., Ishigami, S., Fukumoto, M., Seiki, M., Sato, H., and Imamura, M. (1998) *J. Hepatol.* **28,** 231–239
27. Hiraoka, N., Allen, E., Apel, I. J., Gyetko, M. R., and Weiss, S. J. (1998) *Cell* **95,** 365–377
28. Rosenthal, E. L., Hotary, K., Bradford, C., and Weiss, S. J. (1999) *Otolaryngol. Head Neck Surg.* **121,** 337–343
29. Tsunezuka, Y., Kinoh, H., Takino, T., Watanabe, Y., Okada, Y., Shinagawa, A., Sato, H., and Seiki, M. (1996) *Cancer Res.* **56,** 5678–5683
30. Kadono, Y., Okada, Y., Namiki, M., Seiki, M., and Sato, H. (1998) *Cancer Res.* **58,** 2240–2244
31. Hotary, K., Allen, E., Punturieri, A., Yana, I., and Weiss, S. J. (2000) *J. Cell Biol.* **149,** 1309–1323
32. Yu, A. E., Hewitt, R. E., Connor, E. W., and Stetler-Stevenson, W. G. (1997) *Drugs Aging* **11,** 229–244
33. Rasmussen, H. S., and McCann, P. P. (1997) *Pharmacol. Ther.* **75,** 69–75
34. Overall, C. M., King, A. E., Bigg, H. F., McQuibban, A., Atherstone, J., Sam, D. K., Ong, A. D., Lau, T. T., Wallon, U. M., DeClerck, Y. A., and Tam, E. (1999) *Ann. N. Y. Acad. Sci.* **878,** 747–753
35. Fridman, R., Fuerst, T. R., Bird, R. E., Hoyhtya, M., Oelkuct, M., Kraus, S., Komarek, D., Liotta, L. A., Berman, M. L., and Stetler-Stevenson, W. G. (1992) *J. Biol. Chem.* **267,** 15398–15405
36. Butler, G. S., Butler, M. J., Atkinson, S. J., Will, H., Tamura, T., van Westrum, S. S., Crabbe, T., Clements, J., d'Ortho, M. P., and Murphy, G. (1998) *J. Biol. Chem.* **273,** 871–880
37. Fernandez-Catalan, C., Bode, W., Huber, R., Turk, D., Calvete, J. J., Lichte, A., Tschesche, H., and Maskos, K. (1998) *EMBO J.* **17,** 5238–5248
38. Zucker, S., Drews, M., Conner, C., Foda, H. D., DeClerck, Y. A., Langley, K. E., Bahou, W. F., Docherty, A. J., and Cao, J. (1998) *J. Biol. Chem.* **273,** 1216–1222
39. Jo, Y., Yeon, J., Kim, H. J., and Lee, S. T. (2000) *Biochem. J.* **345,** 511–519
40. Hernandez-Barrantes, S., Toth, M., Bernardo, M. M., Yurkova, M., Gervasi, D. C., Raz, Y., Sang, Q. A., and Fridman, R. (2000) *J. Biol. Chem.* **275,** 12080–12089
41. Stanton, H., Gavrilovic, J., Atkinson, S. J., d'Ortho, M. P., Yamada, K. M., Zardi, L., and Murphy, G. (1998) *J. Cell Sci.* **111,** 2789–2798
42. Brown, S., Bernardo, M. M., Zhi-Hong, L., Kotra, L. P., Tanaka, Y., Fridman, R., and Mobashery, S. (2000) *J. Am. Chem. Soc.* **122,** 6799–6780
43. Belotti, D., Paganoni, P., and Giavazzi, R. (1999) *Int. J. Biol. Markers* **14,** 232–238
44. Wojtowicz-Praga, S. (1999) *Drugs Res. Dev.* **1,** 117–129
45. Steward, W. P. (1999) *Cancer Chemother. Pharmacol.* **43,** (suppl.) 56–60
46. De, B., Natchus, M. G., Cheng, M., Pikul, S., Almstead, N. G., Taiwo, Y. O., Snider, C. E., Chen, L., Barnett, B., Gu, F., and Dowty, M. (1999) *Ann. N. Y. Acad. Sci.* **878,** 40–60
47. Brown, P. D. (1997) *Med. Oncol.* **14,** 1–10
48. Soloway, P. D., Alexander, C. M., Werb, Z., and Jaenisch, R. (1996) *Oncogene* **13,** 2307–2314
49. Mortensen, R. M., Conner, D. A., Chao, S., Geisterfer-Lowrance, A. A., and Seidman, J. G. (1992) *Mol. Cell. Biol.* **12,** 2391–2395
50. Fuerst, T. R., Earl, P. L., and Moss, B. (1987) *Mol. Cell. Biol.* **7,** 2538–2544
51. Fridman, R., Bird, R. E., Hoyhtya, M., Oelkuct, M., Komarek, D., Liang, C. M., Berman, M. L., Liotta, L. A., Stetler-Stevenson, W. G., and Fuerst, T. R. (1993) *Biochem. J.* **289,** 411–416
52. Olson, M. W., Gervasi, D. C., Mobashery, S., and Fridman, R. (1997) *J. Biol. Chem.* **272,** 29975–29983
53. Ko, Y. C., Langley, K. E., Mendiaz, E. A., Parker, V. P., Taylor, S. M., and DeClerck, Y. A. (1997) *Biochem. Cell Biol. Commun.* **236,** 100–105
54. Wingfield, P. T., Sax, J. K., Stahl, S. J., Kaufman, J., Palmer, I., Chung, V., Corcoran, M. L., Kleiner, D. E., and Stetler-Stevenson, W. G. (1999) *J. Biol. Chem.* **274,** 21362–21368
55. Lichte, A., Kolkenbrock, H., and Tschesche, H. (1996) *FEBS Lett.* **397,** 277–282
56. Olson, M. W., Bernardo, M. M., Pietila, M., Gervasi, D. C., Toth, M., Kotra, L. P., Massova, I., Mobashery, S., and Fridman, R. (2000) *J. Biol. Chem.* **275,** 2661–2668
57. Hoyhtya, M., Fridman, R., Komarek, D., Porter-Jordan, K., Stetler-Stevenson, W. G., Liotta, L. A., and Liang, C. M. (1994) *Int. J. Cancer* **56,** 500–505
58. Gervasi, D. C., Raz, A., Dehem, M., Yang, M., Kurkinen, M., and Fridman, R. (1996) *Biochem. Cell Biol. Commun.* **228,** 530–538
59. Li, H., Bauzon, D. E., Xu, X., Tschesche, H., Cao, J., and Sang, Q. A. (1998) *Mol. Carcinog.* **22,** 84–94
60. Laemmli, U. K. (1970) *Nature* **227,** 680–685
61. Toth, M., Gervasi, D. C., and Fridman, R. (1997) *Cancer Res.* **57,** 3159–3167
62. Knight, C. G. (1995) *Methods Enzymol.* **248,** 18–34
63. Muller-Steffner, H. M., Malver, O., Hosie, L., Oppenheimer, N. J., and Schuber, F. (1992) *J. Biol. Chem.* **267,** 9606–9611
64. Segel, I. H. (1993) *Enzyme Kinetics*, pp. 100–160 John Wiley & Sons, Inc., New York
65. Wang, Z., Juttermann, R., and Soloway, P. D. (2000) *J. Biol. Chem.* **275,** 26411–26415
66. Overall, C. M., and Sodek, J. (1990) *J. Biol. Chem.* **265,** 21141–21151
67. Caterina, J. J., Yamada, S., Caterina, N. C., Longenecker, G., Holmbäck, K., Shi, J., Yermovsky, A. E., Engler, J. A., and Birkedal-Hansen, H. (2000) *J. Biol. Chem.* **275,** 26416–26422
68. Bigg, H. F., Shi, Y. E., Liu, Y. E., Steffensen, B., and Overall, C. M. (1997) *J. Biol. Chem.* **272,** 15496–15500
69. Will, H., Atkinson, S. J., Butler, G. S., Smith, B., and Murphy, G. (1996) *J. Biol. Chem.* **271,** 17119–17123
70. Yamamoto, M., Tsujishita, H., Hori, N., Ohishi, Y., Inoue, S., Ikeda, S., and Okada, Y. (1998) *J. Med. Chem.* **41,** 1209–1217
71. Brown, P. D. (1999) *Apmis* **107,** 174–180
72. Maquoi, E., Frankenne, F., Baramova, E., Munaut, C., Sounni, N. E., Remacle, A., Noel, A., Murphy, G., and Foidart, J. M. (2000) *J. Biol. Chem.* **275,** 11368–11378
73. Liotta, L. A., Steeg, P. S., and Stetler-Stevenson, W. G. (1991) *Cell* **64,** 327–336
74. Nakahara, H., Howard, L., Thompson, E. W., Sato, H., Seiki, M., Yeh, Y., and Chen, W. T. (1997) *Proc. Natl. Acad. Sci. U. S. A.* **94,** 7959–7964
75. Nabeshima, K., Inoue, T., Shimao, Y., Okada, Y., Itoh, Y., Seiki, M., and Koono, M. (2000) *Cancer Res.* **60,** 3364–3369
76. Kanayama, H., Yokota, K., Kurokawa, Y., Murakami, Y., Nishitani, M., and Kagawa, S. (1998) *Cancer* **82,** 1359–1366
77. Murashige, M., Miyahara, M., Shiraishi, N., Saito, T., Kohno, K., and Kobayashi, M. (1996) *Jpn. J. Clin. Oncol.* **26,** 303–309
78. Ree, A. H., Florenes, V. A., Berg, J. P., Maelandsmo, G. M., Nesland, J. M., and Fodstad, O. (1997) *Clin. Cancer Res.* **3,** 1623–1628
79. Visscher, D. W., Hoyhtya, M., Ottosen, S. K., Liang, C. M., Sarkar, F. H., Crissman, J. D., and Fridman, R. (1994) *Int. J. Cancer* **59,** 339–344
80. Della Porta, P., Soeltl, R., Krell, H. W., Collins, K., O'Donoghue, M., Schmitt, M., and Kruger, A. (1999) *Anticancer Res.* **19,** 3809–3816

THE JOURNAL OF BIOLOGICAL CHEMISTRY
Vol. 276, No. 20, Issue of May 18, pp. 17125–17131, 2001
Printed in U.S.A.

X-ray Absorption Studies of Human Matrix Metalloproteinase-2 (MMP-2) Bound to a Highly Selective Mechanism-based Inhibitor

COMPARISON WITH THE LATENT AND ACTIVE FORMS OF THE ENZYME*

Received for publication, December 22, 2000
Published, JBC Papers in Press, January 30, 2001, DOI 10.1074/jbc.M011604200

Oded Kleifeld‡, Lakshmi P. Kotra§¶, David C. Gervasi§‖, Stephen Brown§¶, M. Margarida Bernardo§‖, Rafael Fridman§‖, Shahriar Mobashery§¶, and Irit Sagi‡**

From the ‡Department of Structural Biology, The Weizmann Institute of Science, Rehovot 76100, Israel and the §Institute for Drug Design, the ¶Department of Chemistry, Pharmacology and of Biochemistry and Molecular Biology, and the ‖Department of Pathology, Wayne State University, Detroit, Michigan 48202

Malignant tumors express high levels of zinc-dependent endopeptidases called matrix metalloproteinases (MMPs), which are thought to facilitate tumor metastasis and angiogenesis by hydrolyzing components of the extracellular matrix. Of these enzymes, gelatinases A (MMP-2) and B (MMP-9), have especially been implicated in malignant processes, and thus, they have been a target for drugs designed to block their activity. Therefore, understanding their molecular structure is key for a rational approach to inhibitor design. Here, we have conducted x-ray absorption spectroscopy of the full-length human MMP-2 in its latent, active, and inhibited states and report the structural changes at the zinc ion site upon enzyme activation and inhibition. We have also examined the molecular structure of MMP-2 in complex with SB-3CT, a recently reported novel mechanism-based synthetic inhibitor that was designed to be highly selective in gelatinases (1). It is shown that SB-3CT directly binds the catalytic zinc ion of MMP-2. Interestingly, the novel mode of binding of the inhibitor to the catalytic zinc reconstructs the conformational environment around the active site metal ion back to that of the proenzyme.

Zinc-dependent endopeptidases of the family of matrix metalloproteinases (MMPs)[1] serve important functions in tissue remodeling, organ development, ovulation, fetus implantation, embryogenesis, wound healing, and angiogenesis (2). Moreover, various members of the MMP family have been implicated in a number of pathological conditions, including cancer growth, tumor angiogenesis, metastasis and arthritis, connective tissue diseases, inflammation, and cardiovascular and autoimmune diseases (3). Due to the broad spectrum of pathological conditions associated with disregulation of MMP activity, synthetic MMP inhibitors are highly sought (1, 4–8). However, the molecular mechanisms of MMP activation and inhibition are still not fully understood (9, 10).

X-ray crystal structures are available for the catalytic domains of various MMPs (11, 12), including the full-length latent MMP-2 (pro-MMP-2) (13). In addition, structures of inhibitor-enzyme complexes are also available (14–19).

Structural analysis of MMP-inhibitor complexes has mainly focused on the study of the interactions of the catalytic domains of the enzyme with sulfonamide or hydroxamic acid derivatives as zinc-cheating ligands (7, 12, 17, 20). Most of the synthetic inhibitors are designed to provide a bidentate chelating ligand to the catalytic zinc ion. It is a general trend that these metal chelators largely lack selectivity in inhibition of MMPs. This complicates the possibility for targeting specific members of the MMP family in a particular pathological condition. A recent report by Brown *et al.* (1) described a novel concept for the selective inhibition of gelatinases (MMP-2 and MMP-9) by the design and synthesis of the first mechanism-based MMP inhibitor ("suicide substrate") for any MMP. This small molecule inhibitor, designated SB-3CT, provides a potent and highly selective inhibition of human gelatinases by the manifestation of both slow binding and mechanism-based inhibition behavior in its kinetic profile (1).

To gain insight into the mechanism of inhibition of MMP-2 by SB-3CT and the local structure around the catalytic zinc ion in latent, active, and inhibited MMP-2, the zinc ion coordination shell in all complexes was studied by x-ray absorption spectroscopy (XAS). Our results show that the catalytic zinc ion is directly coordinated to the sulfur atom of the bound inhibitor in a monodentate manner to form a tetrahedral coordination at the zinc ion. Interestingly, the inhibited enzyme retains the conformation of the latent MMP-2 around the zinc coordination shell, which may explain the remarkable selectivity of SB-3CT for gelatinases for which it was designed.

EXPERIMENTAL PROCEDURES

Human pro-MMP-2 was expressed in a recombinant vaccinia virus mammalian cell expression system, as described earlier (21). Pro-MMP-2 was purified to homogeneity from the media of infected HeLa cells by gelatin-agarose affinity chromatography, as described previously (21). The protein concentration of proMMP-2 was determined using the molar extinction coefficient of 122,800 M^{-1} cm^{-1} (22) and amino acid analysis. Pro-MMP-2 was activated by 1 mM *p*-aminophenylmercuric acetate (dissolved in 200 mM Tris) for 30 min at 37 °C. The protein concentration of the active MMP-2 was determined by titration with TIMP-2, as described previously (23).

The synthetic mechanism-based inhibitor was synthesized for these studies as described earlier (1). MMP-2 was inhibited for our studies according to the procedure that has been reported previously (1).

* This work was supported by Grants 6602/2 from the Binational Scientific Foundation and the Maurizio and Clotilde Pontecorvo Fund (to I. S.), Grant DAMD17-97-1-7174 from the United States Army (to S. M.), and Grants CA-61986 and CA-82298 from the National Institutes of Health (to R. F.). The costs of publication of this article were defrayed in part by the payment of page charges. This article must therefore be hereby marked "*advertisement*" in accordance with 18 U.S.C. Section 1734 solely to indicate this fact.

** To whom correspondence should be addressed: Dept. of Structural Biology, The Weizmann Institute of Science, Rehovot 76100, Israel. Tel./Fax: 972-8-934-2130; E-mail: irit.sagi@weizmann.ac.il.

[1] The abbreviations used are: MMP, matrix metalloproteinase; XAS, x-ray absorption spectroscopy; ICP-AES, inductively coupled plasma atomic emission spectroscopy; XANES, x-ray absorption near edge structure; EXAFS, extended x-ray absorption fine structure; TIMP, tissue inhibitor metalloproteinase.

Inductively Coupled Plasma Atomic Emission Spectroscopy (ICP-AES)

The metal content in MMP-2 samples was analyzed by inductively coupled plasma atomic emission spectroscopy using the ICP-AES model "Spectroflame" from Spectro (Kleve, Germany). Prior to measurement, the samples were digested with nitric acid, and the volume was adjusted to 6 ml (final concentration 10%). The zinc content in the protein samples was determined relative to an equivalent amount of the enzyme assay buffer.

XAS Studies

Sample Preparation—All enzyme samples were subjected to gelatin zymography before XAS data collection. The enzyme was concentrated by ultrafiltration using a Millipore Centricon-30 (Bedford, MA) device to make a final concentration of 10 mg/ml. Samples were loaded into copper sample holders (10 × 5 × 0.5 mm) covered with Mylar tape and were frozen immediately in liquid nitrogen. The frozen samples were then mounted inside a Displex closed-cycle helium cryostat, and the temperature was maintained at 30 K, to minimize the thermal disorder in the XAS data.

Data Collection—XAS data collection was performed at the National Synchrotron Light Source at Brookhaven National Laboratory, beam line X9B. The spectra were recorded at the zinc K-edge in fluorescence geometry at low temperature (30 K). The beam energy was defined using a flat Si(111) monochromator crystal. The incident beam intensity I_0 was recorded using an ionization chamber. The fluorescence intensity was recorded using a 13-element germanium detector. The transmission signal from a zinc foil was measured with a reference ion chamber simultaneously with fluorescence to calibrate the beam energy. Several scans of each sample were collected for a total of 1×10^6 counts across the edge. The samples were checked for burning marks after each scan, and the beam position on the sample was changed before each scan to minimize radiation damages.

Data Processing and Analysis—The average zinc K-edge absorption coefficient $\mu(E)$, which was obtained after 10–12 independent XAS measurements for each sample, was aligned using the first inflection point of a reference zinc metal foil XAS data (9659 eV). Subsequently, the absorption coefficients for different samples were shifted in x-ray energy until their first inflection points were aligned at the same energy.

The smooth atomic background was removed with the AUTOBK program of the UWXAFS data analysis package, developed at the University of Washington, Seattle (24). The same energy, E_0 = 9659 eV, was chosen for the purpose of background removal as the origin of the photoelectron energy. The R-space region for minimizing the signal below the first shell was chosen between 1.2 and 3 Å. After the removal of background, the useful k-range in the resultant k^2-weighted $\chi(k)$ was between 2.0 and 9 $Å^{-1}$. Model data for the fitting procedure were constructed by extracting the catalytic zinc site coordinates (in a radius of 6 Å from the crystallographic coordinates of gelatinase A (RCSB Protein Data Bank Code 1CK7). Using the computer code FEFF7 (25, 26), we calculated the theoretical photoelectron scattering amplitudes and phase shifts. Total theoretical $\chi(k)$ was constructed by adding the most important partial $\chi(k)$ values that contributed to the r-range of interest.

The theoretical XAFS signal was fitted to the experimental data using the nonlinear least squares method, implemented in the program FEFFIT (24) in R-space, by Fourier transforming both theory and data. Data and theory were weighted by k and multiplied by a Hanning window function in Fourier transforms.

Molecular Modeling

X-ray crystal structure of MMP-2 (RCSB Protein Data Bank Code 1CK7) was used to model the inhibitor in the active site of MMP-2 as well as to model the covalent complex between the inhibitor and MMP-2. The point charges on the inhibitor molecule were MNDO electrostatic potential charges, and the charge on the zinc was +1.62.[2] The same charge on the zinc ion was used in the covalent complex and the noncovalent complex. The inhibitor molecule was docked into the active site of MMP-2 by fitting the biphenyl moiety into the S1′ pocket. The complex, including crystallographic water molecules, was solvated using TIP3 water molecules in a box of 10-Å thicknesses from the surface of the enzyme. The entire complex was energy-minimized for 2500 iterations using AMBER 6.0 (28). In the case of the covalent complex, a bond between the zinc ion and the thiirane sulfur, and a bond between Glu^{404} and the methylene moiety of the thiirane ring, were defined. This complex was energy-minimized as described above. Only one enantiomer of the thiirane inhibitor is shown in Fig. 4, although we carried out energy minimizations with both stereoisomers.

[2] L. P. Kotra, Y. Shimura, R. Fridman, H. B. Schlegel, and S. Mobashery, unpublished results.

RESULTS

The Zinc Stoichiometry in the Full-length Recombinant Human MMP-2—Given the importance of the zinc ion in the proenzyme latency and in catalysis by the mature enzyme, quantitative analyses of the zinc stoichiometry in MMPs have given puzzling results (29–31). Direct measurements of the zinc ion content in various MMPs show variations between 1 and 2 equivalents of metal ions per enzyme. Studies by Willenbrock *et al.* (34), Springman *et al.* (33), and recently by Kleifeld *et al.* (32) suggest that full-length intact MMPs (for the ones tested) contain a single zinc ion, while truncated enzymes (lacking the C-terminal domain) contain two zinc ions. In addition, it was suggested that the zinc content in MMPs might be dependent on the procedure used for enzyme purification (32, 33). Nevertheless, the crystal structure of an inactive full-length pro-MMP-2 mutant clearly shows the presence of both structural and catalytic zinc ion sites (13).

The zinc content in our protein preparation has been determined by ICP-AES and XAS. The ICP-AES analysis gave a zinc stoichiometry of 1.93 ± 0.1 zinc ions per protein, as determined in four separate determinations.

The zinc-protein ratio was further investigated by XAS edge step analysis following previous procedures (32). Briefly, the edge step of the XAS coefficient should be proportional to the concentration of the absorbing element. Therefore, the number of zinc ions per protein can be determined by comparing the edge step intensity measured in the enzyme absorption coefficient data with an edge step calibration curve obtained for standard compounds, where the edge step is measured as a function of zinc concentration. This calibration curve is linear throughout its range where linearity in the lower concentrations of the calibration curve was obtained by extrapolating the line to zero. To obtain the estimated concentration of zinc ion in the enzyme as measured by XAS, we crossed the experimental edge step intensity value of recombinant human pro-MMP-2 with the calibration curve. The concentration of zinc ion obtained by this analysis was 1.75 ± 0.05 zinc ions per enzyme (data not shown).

The results obtained from the ICP-AES and XAS support the presence of two zinc ions per enzyme molecule. Similar ICP studies on the full-length recombinant pro-MMP-2 (purified from NSO mouse myeloma cells) showed a one-to-one ratio for zinc ion and protein (34), as opposed to two-to-one ratio reported by x-ray crystallography (13). Based on our studies of the natural human pro-MMP-9 (where only one zinc ion per protein was found), we cannot rule out the possibility that the zinc ion content in MMPs is dependent on the overall stability of the enzyme and the purification procedures. Nevertheless, we have treated our x-ray structural analysis with two zinc ions according to the stoichimetric ratio seen in the preparation used in this study.

X-ray Absorption Studies of the Latent, Activated, and Inhibited MMP-2—The active site structures of the catalytic zinc ion in the recombinant human MMP-2 in its latent, active, and inhibited states were studied by x-ray absorption near edge structure (XANES), and by XAFS spectroscopy. XAFS refers to modulations in x-ray absorption coefficient around an x-ray absorption edge of a given atom. XAFS is divided into EXAFS (extended x-ray absorption fine structure) and XANES that provide complementary information. EXAFS is a valuable technique for elucidating the structure of a variety of metal-binding

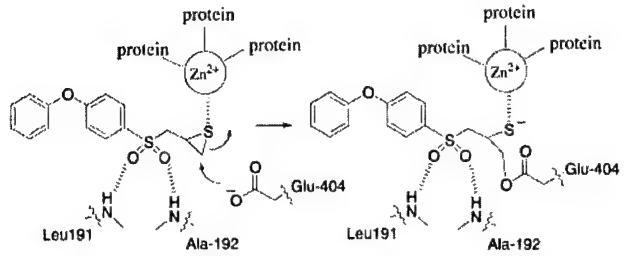

FIG. 1. **Proposed mode of MMPs inhibition by SB-3CT.** Schematic representation of the proposed binding of SB-3CT, a mechanism-based inhibitor, to the catalytic zinc ion in MMPs (adopted from Brown *et al.* (1)). The inhibitor is coordinated to the zinc ion via the thiolate of the thiirane group.

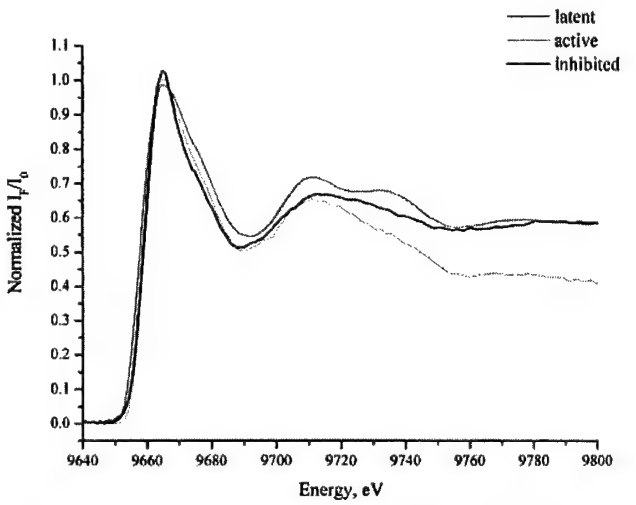

FIG. 2. **Edge spectra of pro, active, and inhibited forms of MMP-2.** Normalized raw XAS data in the zinc K-edge region of pro-MMP2 (*red*), active (*green*), and MMP-2-SB-3CT complex (*black*). The overall shape of the edge spectra of the pro and the active enzyme differs. The most distinct feature is the decrease in the peak at 9738 eV at the XANES region upon activation of the enzyme. Interestingly, this peak is restored in the inhibited MMP-2-SB-3CT complex.

sites in metalloproteins (36). Information available from XAFS includes average bond distances, mean square variation in distance, coordination numbers, and atomic species. Fig. 1 shows the proposed mechanism for inhibition of gelatinases by the mechanism-based inhibitor (adopted from Brown *et al.* (1)). Fig. 2 shows the normalized raw x-ray absorption edge spectra of recombinant human MMP-2 in the latent, active, and inhibited states of the enzyme. The proenzyme edge spectrum has three distinct peaks at 9665, 9710, and 9738 eV. Activation of MMP-2 results in a slight increase in peak intensity at 9665 eV and in drastic reduction in peak intensity at 9738 eV. The changes in the spectral features are consistent with the raw x-ray absorption spectra observed for the latent and active natural human MMP-9, respectively (32). Similar to the natural human MMP-9, a slight edge shift to a higher energy is observed upon activation. Interestingly, we observed that MMP-2 in complex with SB-3CT exhibited an edge spectrum similar to that observed with pro-MMP-2 alone with an increase in peak intensity at 9738 eV. In addition, the edge position is shifted back to lower energy and overlaps with the proenzyme edge position. This may indicate that the total atomic charge of the zinc ion in the inhibited enzyme is consistent with the atomic charge of the zinc ion in the proenzyme. Thus, in both the latent and the inhibited active form of the enzyme, a thiolate completes the coordination sphere. The great similarity in XAS features between natural MMP-9, which was shown to have one zinc ion (32), and MMP-2 points out to the near identity of the structure around the catalytic zinc ion in both enzymes. In addition, the binding of the inhibitor does not influence the backscattering contribution of the structural zinc. This observation is also supported by the MMP-2-SB-3CT binding ratio.

To further study the structure of the zinc site in the enzyme, we have performed a rigorous EXAFS analysis. EXAFS analyses of MMP-2, in its latent, active, and inhibited states, were conducted by fitting the data to theoretical phase shifts and amplitudes. Theoretical models of the proposed structural and catalytic zinc sites were constructed from the crystal structure of pro-MMP-2 (13). The crystal structure reports the presence of two zinc ions with proposed catalytic and structural functions. The catalytic zinc ion in pro-MMP-2 is bound to three histidines and one cysteine, whereas the structural zinc ion is bound to three histidines and one aspartate. The theoretical models that were constructed from these sites were used to modulate the catalytic and structural zinc sites of MMP-2 in the latent, active, and inhibited enzyme EXAFS data in our data analysis procedures. The conformational variations at the structural zinc (37) site were addressed by fitting the zinc site models obtained from the crystallographic data to the raw EXAFS data. Fig. 3, *a*—*c*, shows the best fitting results of the EXAFS analysis of the various structures. The fitting parameters and the quality of the fits are listed in Table I. The zinc sites in the various forms of the enzyme were fitted to the Zn-N, Zn-O, Zn-S, and Zn-C paths using different combinations of varied and constraint parameters. In addition, different initial conditions of distances, Debye-Waller factors, and ΔE_0 shifts were applied in the fitting procedure. To account for two zinc ions in our fitting procedures, we have used the following strategy. In the first stage, the EXAFS data were fitted to a relevant theoretical model containing only one zinc ion, and in the second stage, the fits were refined by constraining and fixing the structural zinc contributions in the fits and fitting the residual phases and amplitudes with the appropriate model. This procedure was repeated in an iterative way until a stable solution was achieved. Furthermore, final refinement of the data included the repeat of the second stage by fixing the catalytic zinc contributions. Using this fitting procedure allowed us to better estimate the goodness of the fits and to refine the final results. Stable and reproducible fits of pro-MMP-2 (Table IA, Fits 2–3) were consistent with a tetrahedral coordination of the zinc ion with three Zn-N(His) at 2.07 ± 0.03 Å, one Zn-S(Cys) at 2.30 ± 0.03 Å contributions (in the first coordination shell), and seven Zn-C contributions where three Zn-C at 2.87 ± 0.05 Å and four at 3.18 ± 0.04 Å (in the second coordination shell). The zinc-ligand distances derived from our EXAFS analysis for the proenzyme are in agreement (within the experimental error) with the crystal structure (13). Fitting the data to a one zinc site model resulted in a high χ^2 and unstable fits (Table IA, Fit 1).

EXAFS analysis of the active enzyme (Table IB, Fit 1) revealed three Zn-N(His) contributions at 1.97 ± 0.02 Å, one Zn-O contribution at 2.01 ± 0.05 Å and, five/six Zn-C contributions at 3.09 ± 0.03 Å. All attempts to successfully resolve a Zn-S phase and amplitude in the active enzyme data failed. The absence of a Zn-S(Cys) ligand at the zinc site indicates that a complete cleavage of the propeptide took place upon enzyme activation. In addition, good fits were obtained by using the "one zinc ion model," which means that the first coordination shell of both zinc ions in the active enzyme has similar atomic environments. The bond distances in this fit represent the average distances of both zinc centers. We have assigned the Zn-O contribution to the binding of a water molecule to the catalytic zinc ion. These results are consistent with the pro-

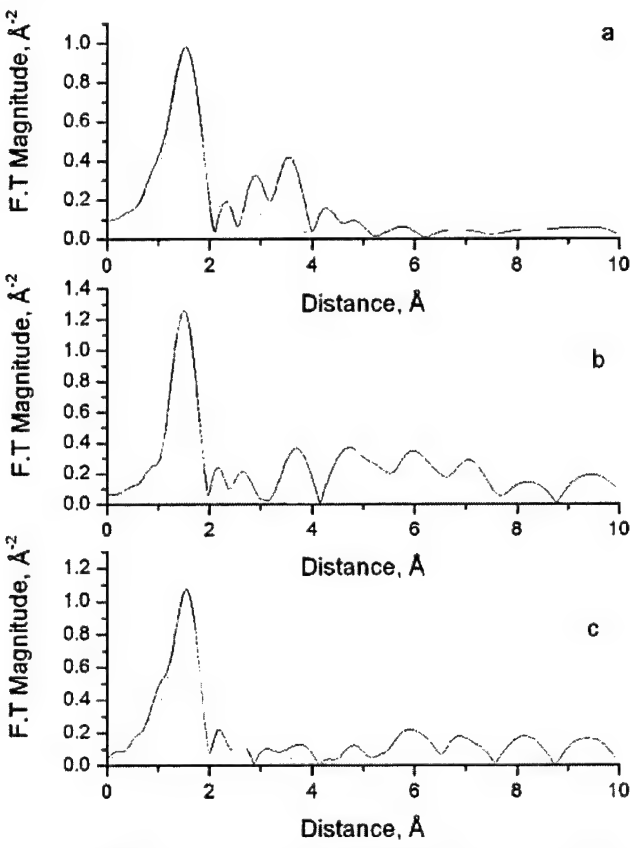

FIG. 3. **EXAFS fitting results for latent, active, and inhibited forms of MMP-2.** The results are presented in the R-space of the experimental data (*black*) to simulated theoretical zinc-ligand contributions (*red*). The experimental data were extracted and normalized using the UWXAFS analysis package. The theoretical XAFS signal was constructed based on the MMP-2 crystal structure code 1CK7 from Protein Data Bank and processed using FEFF7. The experimental data were fitted to the theoretical data using the nonlinear least squares method implemented in the program FEFFIT in R-space, by Fourier transforming both theory and data. *a*, best fit of pro-MMP-2 to 3 Zn-N, 1 Zn-O, and 7 Zn-C contributions. *b*, best fit of active MMP-2 to 3 Zn-N, 1 Zn-O, and 5/6 Zn-C contributions. *c*, best fit of the inhibited MMP-2-SB-3CT complex to 3 Zn-N, 1 Zn-S, and 7 Zn-C contributions. A great similarity in the Fourier-transformed features can be observed for pro-MMP-2, and inhibited enzyme can be observed. The structural zinc-ligand contributions were fixed in the fitting procedure in all fits. The fitting parameters for the various fits are listed in Table I.

posed "cysteine switch hypothesis" in MMPs (13, 38) where the intact propeptide maintains the latency of the proenzyme by shielding the active site from the milieu.

The EXAFS fitting results of the inhibited enzyme are in excellent agreement with its edge spectra. The first coordination shell of the inhibited enzyme is consistent with a tetrahedral coordination, which is similar in its type of ligation to the proenzyme. The zinc-ligand distances (Table IC, Fits 1–2) are consistent with three Zn-N(His) at 2.06 ± 0.03 Å, one Zn-S(inhibitor) at 2.22 ± 0.03 Å, and seven Zn-C contributions where three distances are at 3.05 ± 0.05 Å and four distances are at 3.31 ± 0.04 Å. These results are consistent with the reported molecular mechanical calculations (1), which predict a direct binding of the mechanism-based inhibitor to the catalytic zinc ion via the sulfur atom (Figs. 1 and 4). Interestingly, the EXAFS fitting analysis clearly shows that the Zn-S(SB-3CT) bond distance in the first coordination shell of the catalytic zinc atom in the inhibited enzyme is somewhat shorter than the Zn-S(Cys) in the proenzyme. This suggests that the mechanism-based inhibitor is bound to the catalytic zinc ion via a thiolate group. Essentially, initial coordination of the thioether group in the inhibitor has been transformed to that of the thiolate coordination, as would be expected for the mechanism of enzyme inhibition (Figs. 1 and 4).

The zinc ion coordination shell was found to be tetrahedral in the zymogenic, active, and inhibited enzymes. Attempts to fit additional Zn-O/N contribution resulted in high χ^2 values and high Debye-Waller factors. For the inhibited enzyme, these results suggest that the mechanism of inhibition of MMP-2 by SB-3CT includes a replacement of the Zn-O (water) at the catalytic zinc site with a monodentate ligation of a sulfur atom (from the inhibitor, see Fig. 1), as was anticipated in the design aspect of the inhibitor. The binding stoichiometry (*i.e.* a one-to-one ratio) of SB-3CT to MMP-2 provides us with the confidence that the differences observed in the mode of ligation in the XAFS spectra upon inhibition can be attributed to the catalytic zinc ion.

Inhibition of Recombinant Human MMP-2 by SB-3CT—Fig. 4 shows the modeling results of the binding of SB-3CT to the catalytic zinc ion in MMP-2. The design of the molecule commenced with the x-ray structure of MMP-2. The molecule was built based on the knowledge of binding of other inhibitors to the active site of the MMPs. The biphenyl group was designed to fit in the conserved hydrophobic P_1' pocket in gelatinases, and the thiirane group was intended to coordinate to the catalytic zinc ion. Fig. 4*A* depicts the energy-minimized complex for the MMP-2-inhibitor complex prior to covalent bond formation. This coordination would promote the thiirane for nucleophilic addition by the active-site glutamate, which results in irreversible enzyme inhibition. The energy-minimized model for the covalently modified MMP-2 is given as Fig. 4*B*. The irreversibly modified enzyme was predicted to have a thiolate coordinated to the catalytic zinc ion, and the inhibitor would be covalently tethered to the active-site glutamate (1).

DISCUSSION

In this work we present the local structure of the catalytic site zinc ions in MMP-2. The first and second coordination environments of the zinc ions were studied in the latent, active, and inhibited forms of MMP-2 using XANES, EXAFS spectroscopy, and modeling studies. Our EXAFS data analysis of the local structures around both the structural and catalytic zinc ions in pro-MMP2 is consistent with the reported crystal structure (13). The EXAFS fitting analysis of active MMP-2 shows that the Zn-S contribution at the catalytic zinc ion is replaced by Zn-O contribution. These results are consistent with the proposed "cysteine switch" mechanism where the propeptide cysteine residue is cleaved off the active site and substituted by a water molecule (13, 38).

Interestingly, great similarities in XANES and EXAFS features between pro-MMP-2 and inhibited MMP-2 can be observed (Figs. 2 and 3). The enzyme was inhibited with SB-3CT, which is a newly designed mechanism-based inhibitor of MMPs (Fig. 1) and highly selective for gelatinases (1). Overall, our results suggest that the molecular coordination at the catalytic zinc site in the presence of SB-3CT is similar in its type of ligation, coordination number, and conformation to the proenzyme structure. In addition, the XAS analysis of MMP2-SB-3CT is consistent with our modeling studies (Fig. 4) and the original proposed inhibition mechanism of MMPs by SB-3CT (1).

On the basis of these results, we suggest that the design of mechanism-based inhibitors provides a novel approach for MMP inhibition by imparting or re-establishing the proenzyme structural motifs. In essence, the covalently attached inhibitor mimics the binding of the propeptide segment in MMPs, which is coordinated via a cysteine residue to the catalytic zinc ion, by forming similar binding via the thiolate group. This fact, along with the provisions that incorporated excellent shape comple-

TABLE I

Curve fitting analysis of latent, active, and inhibited MMP-2

Results of EXAFS curve fitting analysis of pro-MMP-2, (A) active MMP-2 (B), and inhibited MMP-2 complex (C). The uncertainties are given in parentheses. The symbols F and V stand for "fixed" and "varied," respectively, and indicate how the respective parameter was treated in the fit model. R is distance of atoms from the zinc ion in Å. σ^2 is the Debye-Waller factor. Note: footnote A indicates that both σ^2s were treated as one.

A.Pro-MMP-2

	Path	ΔE_0	R (Å)	σ^2
Fit 1. One zinc site	1XZn-N x3	6.0 (F)	2.00±0.02 (V)	7.5E-3 (V)
	1XZn-S x1	6.0 (F)	2.29±0.04 (V)	1.0E-6 (V)
	1XZn-C x3	6.0 (F)	2.89±0.05 (V)	6.8E-4 (V)
	1XZn-C x4	6.0 (F)	3.15±0.04 (V)	6.8E-4 (V)
Fit 2. two zinc sites. Structural (F) and catalytic (V)	Structural zinc site			
	0.5XZn-N x3	6.5 (F)	1.95 (F)	5.0E-3 (F)
	0.5XZn-O x1	6.5 (F)	2.00 (F)	1.0E-6 (F)
	0.5XZn-C x3	6.5 (F)	2.92 (F)	5.0E-3 (F^A)
	0.5XZn-C x4	6.5 (F)	3.12 (F)	5.0E-3 (F^A)
	Catalytic zinc site			
	0.5XZn-N x3	6.0 (F)	2.07±0.03 (V)	5.0E-3 (V)
	0.5XZn-S x1	6.0 (F)	2.30±0.03 (V)	1.0E-6 (V)
	0.5XZn-C x3	6.0 (F)	2.87±0.05 (V)	1.0E-6 (V^A)
	0.5XZn-C x4	6.0 (F)	3.18±0.04 (V)	1.0E-6 (V^A)
Fit 3. Two zinc sites. Structural (V) and catalytic (F)	Structural zinc site			
	0.5XZn-N x3	6.0 (F)	1.94±0.03 (V)	3.0E-3 (V)
	0.5XZn-S x1	6.0 (F)	2.01±0.07 (V)	1.0E-6 (V)
	0.5XZn-C x3	6.0 (F)	2.91±0.06 (V)	3.0E-3 (V^A)
	0.5XZn-C x4	6.0 (F)	3.12±0.05 (V)	3.0E-3 (V^A)
	Catalytic zinc site			
	0.5XZn-N x3	6.0 (F)	2.07 (F)	5.0E-3 (F)
	0.5XZn-O x1	6.0 (F)	2.29 (F)	9.0E-6 (F)
	0.5XZn-C x3	6.0 (F)	2.88 (F)	1.0E-6 (F^A)
	0.5XZn-C x4	6.0 (F)	3.19 (F)	1.0E-6 (F^A)

B. Active MMP-2

	Path	ΔE_0	R (Å)	σ^2
Fit .1 One zinc site.	1XZn-N x3	-1.0 (F)	1.97±0.02 (V)	7.5E-3 (V)
	1XZn-O x1	-1.0 (F)	2.01±0.05 (V)	1.0E-6 (V)
	1XZn-C x5/6	-1.0 (F)	3.09±0.03 (V)	8.0E-3 (V)

C. MMP-2-SB-3CT

	Path	ΔE_0	R (Å)	σ^2
Fit 1. two zinc sites. Structural (F) and catalytic (V)	Structural zinc site			
	0.5XZn-N x3	2.5 (F)	1.95 (F)	3.4E-3 (F)
	0.5XZn-O x1	2.5 (F)	1.97 (F)	1.6E-4 (F)
	0.5XZn-C x3	2.5 (F)	2.88 (F)	1.0E-6 (F^A)
	0.5XZn-C x4	2.5 (F)	3.10 (F)	1.0E-6 (F^A)
	Catalytic zinc site			
	0.5XZn-N x3	-5.0 (F)	2.06±0.03 (V)	8.3E-4 (V)
	0.5XZn-S x1	-5.0 (F)	2.22±0.03 (V)	6.0E-4 (V)
	0.5XZn-C x3	-5.0 (F)	3.05±0.05 (V)	1.1E-3 (V^A)
	0.5XZn-C x4	-5.0 (F)	3.31±0.04 (V)	1.1E-3 (V^A)
Fit 2. Two zinc sites. Structural (V) and catalytic (F)	Structural zinc site			
	0.5XZn-N x3	1.8 (F)	1.94±0.03 (V)	3.3E-3 (V)
	0.5XZn-S x1	1.8 (F)	2.22±0.05 (V)	1.7E-5 (V)
	0.5XZn-C x3	1.8 (F)	2.83±0.03 (V)	1.0E-6 (V^A)
	0.5XZn-C x4	1.8 (F)	3.06±0.02 (V)	1.0E-6 (V^A)
	Catalytic zinc site			
	0.5XZn-N x3	-1.3 (F)	2.06 (F)	3.2E-3 (F)
	0.5XZn-O x1	-1.3 (F)	2.22 (F)	6.5E-4 (F)
	0.5XZn-C x3	-1.3 (F)	3.05 (F)	1.1E-4(F^A)
	0.5XZn-C x4	-1.3 (F)	3.31 (F)	1.1E-4(F^A)

mentarity for the enzyme to the active site during the design of the inhibitor, are important factors for the mimicry of the proenzyme metal coordination on the onset of inhibition by our inhibitor.

Detailed structures are available for the complexes between TIMP-1 and MMP-3 and TIMP-2 (16, 39, 40). These structures provide information about the critical residues involved in MMP inhibition by the natural inhibitors. Interestingly, the catalytic zinc ion in the MMP3-TIMP-1 complex is coordinated in a bidentate fashion to the Cys^1 residue of the TIMP molecule

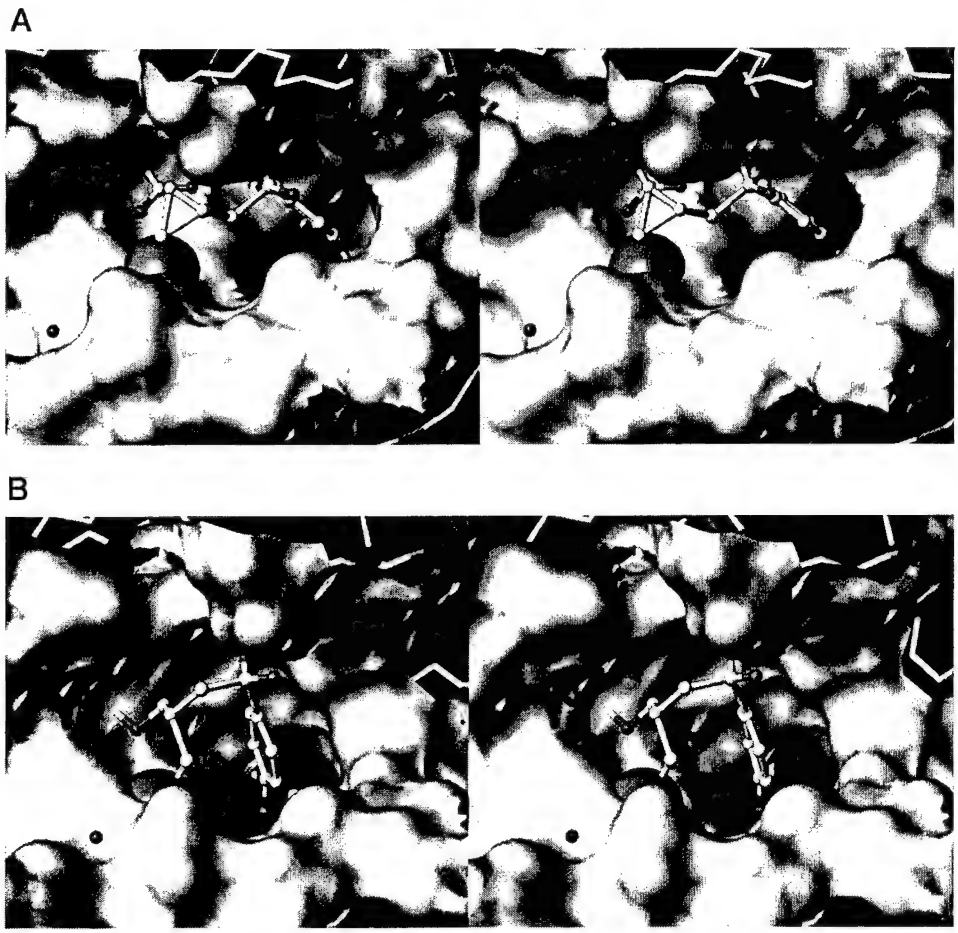

FIG. 4. **Modeling of the catalytic zinc ion in the MMP-2-SB-3CT complex.** Stereo views of the noncovalent (*A*) and covalent (*B*) complexes between the thiirane inhibitor and MMP-2. The active site is represented as a Connolly surface in *green*, and the catalytic zinc ion is shown in *orange* as a *sphere*. The inhibitor molecule and Glu^{404} are shown in *ball-and-stick* representation (carbon, *white*; oxygen, *red*; sulfur, *yellow*). Backbone of the enzyme is shown in *cyan* as a *capped-stick* representation.

via the N-terminal amino acid and the carbonyl group. The architectures of the inhibited active sites of these complexes have provided a model for the design of putative synthetic MMP inhibitors. The vast majority of these inhibitors utilize a hydroxamic acid to chelate the catalytic zinc ion by imposing a bidentate interaction between the zinc ion and the inhibitor hydroxamate group. A similar binding mode was proposed recently for thiol-based inhibitors (41).

In contrast, our EXAFS analysis shows that the binding of the mechanism-based inhibitor to the catalytic zinc ion via its sulfur atom is clearly monodentate. We recently reported that the kinetic profiles of MMP inhibition by SB-3CT and their natural protein inhibitors are similar. Specifically, we showed that the interaction of MMP-2 and MMP-9 with SB-3CT followed a slow binding pattern (42), which ultimately resulted in covalent modification of the enzyme in the active site. It is important to note that slow binding inhibition of gelatinases is also seen with TIMP-2 and TIMP-1 (43). Furthermore, it is most interesting that both the affinities of the inhibitor for the enzyme and the kinetic parameters for the onset of the slow binding inhibition by SB-3CT closely followed those for the binding of TIMPs at the high affinity site (43). The kinetic parameters for the inhibition showed a remarkable selectivity for both MMP-2 and MMP-9, since the molecule was specifically designed for gelatinases (1). The data presented here further indicate that inhibition of MMP-2 by SB-3CT restores the metal coordination environment to that seen for the zymogen form of the enzyme. These observations collectively argue for this inhibitor to be a nearly ideal inhibitor from the perspective of the design paradigms.

MMPs play an essential role in the turnover and remodeling of extracellular matrix on both normal and pathological processes (3, 27, 35). For example, MMP-2 has been shown to play a key role in tumor angiogenesis and metastasis. Therefore, MMP-2 represents an obvious target for the development of selective inhibitors that would block tumor cell invasion and tumor angiogenesis. Understanding the detailed molecular structures and the conformational changes of MMP-2 in its zymogen, active, and inhibited states can aid in the rational design of anti-cancer drugs. Here we define the mode of binding of a selective MMP inhibitor to the catalytic site of MMP-2 and provide insights on the basis for its exceptional properties in selective inhibition of gelatinases. In addition, we show that XAS can be used as a tool to screen and/or to design active site modifications in MMPs (in solution) upon binding to inhibitors via the catalytic zinc ion.

REFERENCES

1. Brown, S., Margarida, B., Li, Z., Korta, L. P., Tanaka, Y., Fridman, R., and Mobashery, S. (2000) *J. Am. Chem. Soc.* **122,** 6799–6800
2. Nagase, H., and Woessner, J. F. (1999) *J. Biol. Chem.* **274,** 21491–21494
3. Werb, Z. (1997) *Cell* **91,** 439–442
4. Abbruzzese, T. A., Guzman, R. J., Martin, R. L., Yee, C., Zarins, C. K., and Dalman, R. L. (1998) *Surgery* **124,** 328–335
5. Akizawa, T., Uratani, T., Matsukawa, M., Kunimatsu, A., Ito, Y., Itoh, M., Ohshiba, Y., Yamada, M., and Seiki, M. (1999) *Ann. N. Y. Acad. Sci.* **878,** 622–624
6. Almstead, N. G., Bradley, R. S., Pikul, S., De, B., Natchus, M. G., Taiwo, Y. O., Gu, F., Williams, L. E., Hynd, B. A., Janusz, M. J., Dunaway, C. M., and

Mieling, G. E. (1999) *J. Med. Chem.* **42,** 4547–4562
7. Betz, M., Huxley, P., Davies, S. J., Mushtaq, Y., Pieper, M., Tschesche, H., Bode, W., and Gomis-Ruth, F. X. (1997) *Eur. J. Biochem.* **247,** 356–363
8. Bigatel, D. A., Elmore, J. R., Carey, D. J., Cizmeci-Smith, G., Franklin, D. P., and Youkey, J. R. (1999) *J. Vasc. Surg.* **29,** 130–139
9. Tyagi, S. C., Kumar, S. G., Alla, S. R., Reddy, H. K., Voelker, D. J., and Janicki, J. S. (1996) *J. Cell. Physiol.* **167,** 137–147
10. Vallon, R., Muller, R., Moosmayer, D., Gerlach, E., and Angel, P. (1997) *Eur. J. Biochem.* **244,** 81–88
11. Lovejoy, B., Cleasby, A., Hassell, A. M., Longley, K., Luther, M. A., Weigl, D., McGeehan, G., McElroy, A. B., Drewry, D., Lambert, M. H., and *et al.* (1994) *Science* **263,** 375–377
12. Bode, W., Reinemer, P., Huber, R., Kleine, T., Schnierer, S., and Tschesche, H. (1994) *EMBO J.* **13,** 1263–1269
13. Morgunova, E., Tuuttila, A., Bergmann, U., Isupov, M., Lindqvist, Y., Schneider, G., and Tryggvason, K. (1999) *Science* **284,** 1667–1670
14. Becker, J. W., Marcy, A. I., Rokosz, L. L., Axel, M. G., Burbaum, J. J., Fitzgerald, P. M., Cameron, P. M. Esser, C. K., Hermes, J. D., and Springer, J. P. (1995) *Protein Sci.* **4,** 1966–1976
15. Lovejoy, B., Hassell, A. M., Luther, M. A., Weigl, D., and Jordan, S. R. (1994) *Biochemistry* **33,** 8207–8217
16. Gomis-Ruth, F. X., Maskos, K., Betz, M., Bergner, A., Huber, R., Suzuki, K., Yoshida, N., Nagase, H., Brew, K., Bourenkov, G. P., Bartunik, H., and Bode, W. (1997) *Nature* **389,** 77–81
17. Grams, F., Crimmin, M., Hinnes, L., Huxley, P., Pieper, M., Tschesche, H., and Bode, W. (1995) *Biochemistry* **34,** 14012–14020
18. Li, J., Brick, P., O'Hare, M. C., Skarzynski, T., Lloyd, L. F., Curry, V. A., Clark, I. M., Bigg, H. F., Hazleman, B. L., Cawston, T. E., *et al.* (1995) *Structure (Lond.)* **3,** 541–549
19. Bode, W., Fernandez-Catalan, C., Tschesche, H., Grams, F., Nagase, H., and Maskos, K. (1999) *Cell. Mol. Life Sci.* **55,** 639–652
20. Kiyama, R., Tamura, Y., Watanabe, F., Tsuzuki, H., Ohtani, M., and Yodo, M. (1999) *J. Med. Chem.* **42,** 1723–1738
21. Fridman, R., Furest, T. R., Bird, R. E., Hoyhtya, M., Oelkuct, M., Kraus, S., Komarek, D., Liotta, L. A., Berman, M. L., and Stetler-Stevenson, W. G. (1992) *J. Biol. Chem.* **267,** 15398–15405
22. Murphy, G., and Crabbet, T. (1995) *Methods Enzymol.* **248,** 470–484
23. Olson, M. W., Bernardo, M. M., Pietila, M., Gervasi, D. C., Kotra, L. P., Massova, I., Mobashery, S., and Fridman, R. (2000) *J. Biol. Chem.* **275,** 2661–2668
24. Stern, E. A., Newville, M., Ravel, B., Yacoby, Y., and Haskel, D. (1995) *Physica B* **208 & 209,** 117–122
25. Rehr, J. J., Mustre de leon, J., Zabinsky, S. I., and Albers, R. C. (1991) *J. Am. Chem. Soc.* **113,** 5135–5138
26. Zabinsky, S. I., Rehr, J. J., Ankudinov, A., Albers, R. C., and Eller, M. J. (1995) *Phys. Rev. B* **52,** 2995–2999
27. Birkedal-Hansen, H. (1995) *Curr. Opin. Cell. Biol.* **7,** 728–735
28. Case, D. A., Pearlman, D. A., Caldwell, J. W., Cheatham, T. E., III, Ross, W. S., Simmerling, C. L., Darden, T. A., Merz, K. M., Stanton, R. Cheng, R. V., Vincent, A. L., Crowley, J. J., Tsui, M., Radmer, V., Duan, R. J., Pitera, Y., Massova, J., Seibel, I., Singh, G. L., and Weiner, P. (1999) AMBER 6.0 computer program, University of California, San Francisco, CA
29. Salowe, S. P., Marcy, A. I., Cuca, G. C., Smith, C. K., Kopka, I. E., Hagmann, W. K., and Hermes, J. D. (1992) *Biochemistry* **31,** 4535–4540
30. Lowry, C. L., McGeehan, G., and LeVine, H. (1992) *Proteins Struct. Funct. Genet.* **12,** 42–48
31. Crabbe, T., Willenbrock, F., Eaton, D., Hynds, P., Carne, A. F., Murphy, G., and Docherty, A. J. P. (1992) *Biochemistry* **31,** 8500–8507
32. Kleifeld, O., Van den Steen, P., Frenkel, A., Cheng, F., Jiang, H., Opdenakker, G., and Sagi, I. (2000) *J. Biol. Chem.* **275,** 34335–34343
33. Springman, E. B., Nagase, H., Birkedal-Hansen, H., and Van Wart, H. E. (1995) *Biochemistry* **34,** 15713–15720
34. Willenbrock, F., Murphy, G., Phillips, I. R., and Brocklehurst, K. (1995) *FEBS Lett.* **358,** 189–192
35. McCawley, L. J., and Matrisian, L. M. (2000) *Mol. Med. Today* **6,** 149–156
36. Scott, R. A. (1985) *Methods Enzymol.* **117,** 414–458
37. Massova, I., Kotru, L. P., and Mobashery, S. (1998) *Bioorg. Med. Chem. Lett.* **8,** 853–858
38. Van Wart, H. E., and Birkedal-Hansen, H. (1990) *Proc. Natl. Acad. Sci. U. S. A.* **87,** 5578–5582
39. Fernandez-Catalan, C., Bode, W., Huber, R., Turk, D., Calvete, J. J., Lichte, A., Tschesche, H., and Maskos, K. (1998) *EMBO J.* **17,** 5238–5248
40. Muskett, F. W., Frenkiel, T. A., Feeney, J., Freedman, R. B., Carr, M. D., and Williamson, R. A. (1998) *J. Biol. Chem.* **273,** 21736–21743
41. Campbell, D. A., Xiao, X., Harris, D., Ida, S., Mortezaei, R., Ngu, K., Shi, L., Tien, D., Wang, Y., Navre, M., Patel, D. V., Sharr, M. A., DiJoseph, J. F., Killer, L. M., Leone, C. L., Levine, J. I., and Skotnicki, J. S. (1998) *Bioorg. Med. Chem. Lett.* **8,** 1157–1162
42. Morrison, J. F. (1988) *Adv. Enzymol.* **61,** 201–301
43. Olson, M. W., Gervasi, D. C., Mobashery, S., and Fridman, R. (1997) *J. Biol. Chem.* **272,** 29975–29983

BIBLIOGRAPHY OF ALL PUBLICATIONS

1. Massova, I. ; Fridman, R.; Mobashery, S. Structural Insights into the Catalytic Domains of Human Matrix Metalloprotease-2 and Human Matrix Metalloprotease-9: Implications for Substrate Specificities, *J. Mol. Mod.* **1997**, *3*, 17.

2. Olson, M. W.; Gervasi, D. C.; Mobashery, S.; Fridman, R. Kinetic Analysis for the Binding of the Latent and Active Forms of the Human Matrix metalloprotease-2 and -9 to TIMP-1 and TIMP-2, *J. Biol. Chem.* **1997**, *272*, 29975.

3. Massova, I.; Kotra, L. P.; Mobashery, S. Structural Insight into the Binding Motifs for Calcium Ion and the Non-Catalytic Zinc in Matrix Metalloproteases, *Bioorganic Med. Chem. Lett.* **1998**, *8*, 853.

4. Massova, I.; Kotra, L. P.; Fridman, R.; Mobashery, S. Matrix Metalloproteases: Structures, Evolution and Diversification, *FASEB J.* **1998**, *12*, 1075.

5. Olson, M. W.; Bernardo, M. M.; Pietila, M.; Gervasi, D. C.; Toth, M.; Kotra, L. P.; Massova, I.; Mobashery, S.; Fridman, R. Cahracterization of the Monomeric and Dimeric Forms of Latent and Active Matrix Metalloproteinase-9, *J. Biol. Chem.*, **2000**, *275*, 2661-2668.

6. Brown, S.; Bernardo, M.; Li, Z. H., Kotra, L. P.; Tanaka, Y.; Fridman, R.; Mobashery, S. Potent and Selective Mechanism-Based Inhibition of Gelatinases, *J. Am. Chem. Soc.* **2000** *122*, 6799-6800.

7. Toth, M.; Bernardo, M. M.; Gervasi, D. C.; Soloway, P. D.; Wang, Z.; Bigg, H. F.; Overall, C. M.; DeClerck, Y. A.; Tschesche, D.; Cher, M. L.; Brown, S.; Mobashery, S.; Fridman, R., TIMP-2 Acts Synergistically with Synthetic MMP Inhibitors but not with TIMP-4 to Enhance the MT1-MMP-Dependent Activation of Pro-MMP-2, *J. Biol. Chem.*, **2000**, *275*, 41415-41423.

8. Kleifeld, O.; Kotra, L. P.; Gervasi, D. C.; Brown, S.; Bernardo, M. M.; Fridman, R.; Mobashery, S.; Sagi, I. X-Ray Absorption Studies of Human Matrix Metalloproteinase-2 (MMP-2) Bound to a Highly Selective Mechanism-Based Inhibitor: Comparison to the Latent and Active Forms of the Enzyme, *J. Biol. Chem.*, **2001**, *276*, 17125-17131.

MEETING ABSTRACTS

1. Olson, M. W.; Mobashery, S.; Gervasi, D.; Poorman, R.; Ledbetter, S.; Fridman, R. Kinetics of Binding of Latent and Active Forms of MMP-2 and MMP-9 with TIMP-1 and TIMP-2 Reveal Low and High Affinity Interactions (poster), Inhibitors of Metalloproteinases in Development of Disease: TIMPS 1996, Banff, Canada, 1996.

2. Massova, I.; Mobashery, S. Structural Insight into the Catalytic Domains of Human Matrix Metalloprotease-2 and Human Matrix Metalloprotease-9: Implications for Substrate Specificity (poster), First Parke-Davis-WSU Poster Meeting, Detroit, MI, 1997.

3. Brown. S.; Bernardo, M.; Li, Z-H.; Kotra, L.P.; Tanaka, Y.; Fridman, R.; Mobashery, S. "Selective Mechanism-Based Inhibition of Matrix Metalloproteases", Era of Hope Meeting, Atlanta, Georgia, June 2000.

4. Brown. S.; Bernardo, M.; Li, Z-H.; Kotra, L.P.; Tanaka, Y.; Fridman, R.; Mobashery, S. "Selective Mechanism-Based Inhibition of Matrix Metalloproteases", Gordon Research Conferences, July 2000.

5. Brown. S.; Bernardo, M.; Li, Z-H.; Kotra, L.P.; Tanaka, Y.; Fridman, R.; Mobashery, S. "Selective Mechanism-Based Inhibition of Matrix Metalloproteases". Organic Chemistry Section, Pacifichem, Honolulu, Hawaii, December 14-19, 2000.

6. Mobashery, S.; Kotra, L.P.; Cross, J.; Schlegel, H. B. "Computational Studies on the Mechanism of Activation of Matrix Metalloproteases". Medicinal Chemistry Section, Pacifichem, Honolulu, Hawaii, December 14-19, 2000.

LIST OF PERSONNEL

1. Dr. Yasuhiro Tanaka has joined the Ajinomoto Company (Tokyo, Japan) as a Senior Scientist.

2. Dr. Zhi-Hong Li is currently a Senior Scientist with the Coulter Pharmaceutical Company (South San Francisco, CA).

3. Dr. Steven Brown is currently a member of the group.

4. Dr. Irina Massova has joined the Roche Pharmaceutical Company.

5. Dr. Lakshmi Kotra has joined the faculty of Pharmacy at the University of Toronto

6. Mr. Cosimo Fuda is currently a member of the group.